Nuclear Science
NEA/NSC/DOC (2010)

# VVER-1000 COOLANT TRANSIENT BENCHMARK

## Phase 2 (V1000CT-2)

Volume IV: Summary results of Exercise 2 on coupled 3D kinetics/core-vessel thermal hydraulics and Exercise 3 on core-plant MSLB simulation

*N.P.Kolev, I.Spasov, T.Tzanov*

INRNE, Bulgaria

*E. Royer*
INSTN, Saclay, France

**OECD 2010**

NUCLEAR ENERGY AGENCY
ORGANIZATION FOR ECONOMIC COOPERATION AND DEVELOPMENT

**ORGANISATION FOR ECONOMIC CO-OPERATION AND DEVELOPMENT**

Pursuant to Article 1 of the Convention signed in Paris on 14th December 1960, and which came into force on 30th September 1961, the Organisation for Economic Co-operation and Development (OECD) shall promote policies designed:

- to achieve the highest sustainable economic growth and employment and a rising standard of living in Member countries, while maintaining financial stability, and thus to contribute to the development of the world economy;
- to contribute to sound economic expansion in Member as well as non-member countries in the process of economic development; and
- to contribute to the expansion of world trade on a multilateral, non-discriminatory basis in accordance with international obligations.

The original Member countries of the OECD are Austria, Belgium, Canada, Denmark, France, Germany, Greece, Iceland, Ireland, Italy, Luxembourg, the Netherlands, Norway, Portugal, Spain, Sweden, Switzerland, Turkey, the United Kingdom and the United States. The following countries became Members subsequently through accession at the dates indicated hereafter; Japan (28th April 1964), Finland (28th January 1969), Australia (7th June 1971), New Zealand (29th May 1973), Mexico (18th May 1994), the Czech Republic (21st December 1995), Hungary (7th May 1996), Poland (22nd November 1996) and the Republic of Korea (12th December 1996). The Commission of the European Communities takes part in the work of the OECD (Article 13 of the OECD Convention).

***NUCLEAR ENERGY AGENCY***

*The OECD Nuclear Energy Agency (NEA) was established on 1st February 1958 under the name of OEEC European Nuclear Energy Agency. It received its present designation on 20th April 1972, when Japan became its first non-European full Member. NEA membership today consists of all OECD Member countries, except New Zealand and Poland. The Commission of the European Communities takes part in the work of the Agency.*

*The primary objective of the NEA is to promote co-operation among the governments of its participating countries in furthering the development of nuclear power as a safe, environmentally acceptable and economic energy source.*

*This is achieved by:*

- *encouraging harmonization of national regulatory policies and practices, with particular reference to the safety of nuclear installations, protection of man against ionising radiation and preservation of the environment, radioactive waste management, and nuclear third party liability and insurance;*
- *assessing the contribution of nuclear power to the overall energy supply by keeping under review the technical and economic aspects of nuclear power growth and forecasting demand and supply for the different phases of the nuclear fuel cycle;*
- *developing exchanges of scientific and technical information particularly through participation in common services;*
- *setting up international research and development programmes and joint undertakings.*

*In these and related tasks, the NEA works in close collaboration with the International Atomic Energy Agency in Vienna, with which it has concluded a Co-operation Agreement, as well as with other international organisations in the nuclear field.*

# Foreword

The OECD NEA has completed LWR benchmarks for coupled thermal-hydraulic/ neutron kinetics codes. In the course of these benchmarks, a systematic approach has been established to validate best estimate coupled codes. This approach employs a multi-level methodology that allows for consistent and comprehensive validation process and contributes to prepare a basis of licensing application of the coupled calculations for a specific reactor type.

The OECD VVER-1000 Coolant Transient Benchmark project started in 2002 with an overall objective to assess computer codes for safety analysis of VVER power plants, specifically for their use in reactivity transients. It consists of two phases. Phase 1, labeled V1000CT-1 and led by Pennsylvania State University (PSU) is a main coolant pump (MCP) start-up while three other MCP are in operation. Phase 2, labeled V1000CT-2 and led by the French Commissariat à l'Energie Atomique (CEA) includes calculation of coolant mixing experiments and a main steam line break (MSLB) analysis.

Coupled code benchmarks have identified the coolant mixing in the reactor vessel as an unresolved issue in the analysis of complex plant transients with reactivity insertion. In order to support the necessary development work, Phase 2 of the VVER-1000 Coolant Transient Benchmarks (V1000CT-2) was launched to provide a framework for:

- Assessment of single-phase vessel mixing models
- Assessment of coupled codes in MSLB simulations using validated mixing models

The V1000CT-2 benchmark consists of a computation of a plant experiment at Kozloduy-6 in Bulgaria and core-vessel and core-plant MSLB simulations for the same NPP unit. The testing process includes pure thermal-hydraulic and coupled calculations and allows code-to-experiment and code-to-code comparisons.

The V1000CT-2 benchmark team is from the Institute for Nuclear Research and Nuclear Energy (INRNE), Bulgaria and CEA and PSU. The V1000CT-2 benchmark sponsors are the OECD Nuclear Energy Agency (NEA) and CEA. The Kozloduy NPP is providing technical support and the AER Working Group D is collaborating in the benchmark activities.

The V1000CT-2 benchmark reports are being published by the NEA in four volumes. Volumes 1 and 2 provide the specifications of the VVER-1000 vessel mixing and MSLB benchmarks. In addition, the transient boundary conditions, cross section libraries and decay heat values as function of time are available on the NEA website and CD ROM.

Volume 3 summarizes the results of V1000CT-2 Exercise 1 and identifies the important issues of the single-phase vessel mixing modeling. The reference problem is a Kozlodyy-6 flow mixing experiment. The plant experiment is specially designed to have approximately separable thermal hydraulics and neutron kinetics. Plant data, including distributions are available for validation and assessment of the vessel thermal hydraulic models to be used for coupled code MSLB analysis.

The present Volume 4 summarizes the results of V1000CT-2 Exercises 2 and 3. Exercise 2 is a core-vessel coupled simulation with given MSLB vessel boundary

conditions. A realistic and a pessimistic scenario are considered. The main objective is to evaluate the response of the coupled 3D N/TH in code-to-code comparison. A specific objective is to provide an additional test of the vessel mixing models with MSLB boundary conditions, by comparing coarse-mesh solutions and reference CFD results for the core inlet distributions. Exercise 3 is a coupled full plant simulation.

Readers are kindly invited to note that the figures in the report were prepared in color. Color versions are available on the NEA website at 0Hwww.nea.fr/ html/science/ergslib/v1000ct/ .

*Acknowledgments*

This report is the sum of many efforts of the participants, the benchmark team and the funding agencies – the CEA France and OECD/NEA and their staff. Special thanks are due to D. Caruge and R. Lenain from CEA Saclay whose support and encouragement in establishing and preparing this benchmark are invaluable.

Particular appreciation goes to U. Bieder from CEA Grenoble who participated in the preparation of the specifications.

The authors would like to thank Prof. J. Aragones from Universidad Politecnica de Madrid – member of the NSC/NEA and Prof. F. d'Auria from the University of Pisa, member of the NEA Committee on the Safety of Nuclear Installations, for their support in establishing the OECD benchmark on VVER vessel mixing and MSLB.

Special thanks are due to the Kozloduy NPP personnel for providing plant data, simulator time and expertise. Of particular note is the support of J. Kostadinov, former Executive Director of KNPP.

The authors thank the V1000CT-2 Benchmark participants and the members of the AER Working groups D and C for their valuable support, comments and feedback.

Special appreciation goes to Dr. T. Hoehne from FZD who provided a supporting CFX transient solution for the vessel thermal hydraulics obtained with MSLB boundary conditions. This solution is taken as reference for coarse-mesh vessel mixing calculations.

The authors wish to express their sincere appreciation for the outstanding support offered by Dr. Enrico Sartori who provided efficient administration, organization and valuable technical recommendations.

The specifications of this benchmark were prepared with the CATHARE2 code, developed in a joint effort by CEA, IRSN, AREVA and EDF, and with the TRIO_U and CRONOS/FLICA codes developed by CEA.

# Table of contents

# List of tables

# List of figures

# List of abbreviations

| | |
|---|---|
| BOC | Beginning of Cycle |
| BOL | Beginning of Life |
| BPG | Best Practice Guidelines |
| BRU-K | Steam dump to condenser |
| BRU-SN | Steam dump to house needs |
| CEA | Commissariat à l'Energie Atomique |
| DTC | Doppler Temperature Coefficient |
| EFPD | Effective Full Power Days |
| FA | Fuel Assembly |
| FZD | Forschung Zentrum Dresden |
| FZK | Forschung Zentrum Karlsruhe (Karlsruhe Institut of Technology) |
| GRS | Geselschaft fur Reaktorsicherheit |
| HP | Hot Power |
| HRP | Highest Return to Power |
| HZP | Hot Zero Power |
| INRNE | Institute for Nuclear Research and Nuclear Energy |
| KI | Kurchatov Institute |
| KNPP | Kozloduy Nuclear Power Plant |
| LWR | Light Water Reactor |
| MCP | Main Coolant Pump |
| MSH | Main Steam Header |
| MSLB | Main Steam Line Break |
| NEA | Nuclear Energy Agency |
| NRC | Nuclear Regulatory Commission |
| OECD | Organization for Economic Cooperation and Development |
| PSU | Pennsylvania State University |
| PWR | Pressurizer Water Reactor |
| RCS | Reactor Coolant System |
| RPC | Reactor Power Controller |
| RPV | Reactor Pressure Vessel |
| SG | Steam Generator |
| SIV | Steam Isolation Valve |
| SST | Shear Stress Transport |
| TH | Thermal Hydraulics |
| UNIPI | University of Pisa |
| UPM | Universidad Politecnica de Madrid |
| 6N, 24N | 6 or 24 nodes/triangles per hexagon |

# Chapter 1: Introduction

Recently developed best-estimate computer code systems for modeling of 3D coupled neutronics/thermal hydraulic transients and for the coupling of core and system dynamics need to be validated against experimental results and compared against each other. International benchmark studies have been set up for this purpose.

Coupled code benchmarks identified the coolant mixing as an unresolved issue in the analysis of complex plant transients with reactivity insertion. In order to support the necessary development work, Phase 2 of the OECD/NEA VVER-1000 Coolant Transient Benchmarks (V1000CT-2) was defined (Kolev et al, 2004; 2006). The objective is to provide a framework for

- Assessment of single-phase vessel mixing models
- Assessment of coupled codes in MSLB simulations using validated mixing models.

The benchmark includes a complete set of input data and consists of three exercises as summarized below. In addition to the definition of the benchmark exercises, technical specifications including CFD grade thermal-hydraulics data as well as neutronics and secondary circuit data are given in Volumes 1 and 2.

## 1.1 Exercise 1 – Computation of a vessel mixing experiment

The vessel mixing problem (Kolev et al, 2004; Bieder et al, 2005) is based on VVER-1000 plant experiments at Kozloduy Unit 6 in Bulgaria (Topalov and Popov, 2004). The objective is to test the capability of the reactor vessel thermal-hydraulic models to represent single-phase flow mixing. The reference problem is a coolant transient initiated by steam generator isolation at low power, considered as a pure thermal hydraulic problem. The available plant data permit code validation on different scales:

- Separate effects
- Component level (reactor pressure vessel)
- System level

For CFD codes, the task is to assess the ability of CFD to reproduce the experimentally observed angular turn of the loop flow centres (swirl) and the assembly inlet temperatures given the vessel boundary conditions and the pressure above the core. The calculation of the vessel outlet parameters (loop-to-loop mixing) is an option.

For system codes, the task is to assess the ability of coarse-3D models and multi-1D vessel models with cross flow to reproduce the swirl and the assembly inlet temperatures as well as the vessel outlet temperatures. Given vessel boundary conditions or full plant simulation can be used.

## 1.2 Exercise 2 – Computation of a VVER-1000 MSLB transient with given vessel boundary conditions

The task is to model the core and the vessel only, using the validated coolant mixing models and pre-calculated vessel MSLB boundary conditions. A realistic and a

pessimistic scenario are considered. The overall objective is to evaluate the response of the coupled 3D neutronics/core-vessel thermal hydraulics in code-to-code comparison. A specific objective is to provide an additional test of the vessel mixing models with MSLB boundary conditions, by comparing coarse-mesh and CFD results for the core inlet distributions. For this purpose, a CFX transient solution for the down-comer and core inlet parameters was made available by FZD (Hoehne, 2007). Supplementary plant estimated data from the Kozloduy-6 mixing experiments (Popov, Topalov, 2004) can also be used for qualitative comparison of the disturbed sector formation and the angular turn of the loop flows.

### 1.3 Exercise 3 – Best-estimate coupled core-plant MSLB simulation

This exercise is an extension of Exercise 2 to core-vessel-plant simulation. It is a best-estimate analysis of the transient in its entirety, for a realistic and a pessimistic scenario.

### 1.4 Benchmark documentation

Background information on this benchmark with complete list of participants can be found in the summaries of the seven V1000CT workshops held in Saclay, France [NEA/NSC/DOC(2003)6]; Sofia, Bulgaria [NEA/NSC/DOC(2004)9]; Garching, Germany [NEA/NSC/DOC(2005)1]; Avignon, France [NEA/NSC/DOC(2005)18]; Pisa, Italy [NEA/NSC/DOC(2006)7]; Vancouver, BC, Canada [NEA/NSC/DOC(2006)21] and Paris, France [NEA/NSC/DOC(2007)5].

The V1000CT-2 benchmark is documented in four volumes. Volumes 1 and 2 contain the specifications of the vessel mixing problem and the VVER MSLB problem respectively. Volume 3 summarizes the comparative analysis of the submitted results for Exercise 1 on vessel mixing simulation.

The present Volume 4 contains summary results of Exercises 2 and 3 on MSLB simulation. There are seven submitted solutions for Exercise 2 and three results for Exercise 3, see Tables 1.1 and 1.2 below. The list includes recently obtained COBAYA and COBAYA/COBRA3 solutions (Spasov et al, 2009), (Spasov et al, 2010).

Chapter 2 of this report gives a summary description of Exercises 2 and 3. Chapter 3 discusses the methodology of comparison of the results. Chapter 4 presents additional tests of the coarse-mesh mixing models (once validated in Exercise 1), in comparison with support CFD results obtained using MSLB boundary conditions (Hoehne, 2007). Chapter 5 shows the results of coupled core-vessel calculation with vessel boundary conditions. Chapter 6 presents results of the full plant simulation. Appendices A and B contain results of the steady state HZP and HFP calculations. Appendix C presents results of Exercise 2 Scenario 1. Appendix D shows results from Exercise 2 Scenario 2. Appendix E presents results from Exercise 3. Appendix F describes the codes and Appendix G contains the participant provided calculation details.

**Table 1.1: List of participants in V1000CT-2 Exercise 2**

| Organisation | Country | Code | Type |
|---|---|---|---|
| FZD | Germany | DYN3D/ATHLET | System |
| FZK | Germany | PARCS/TRACE | System |
| GRS/KI | Germany/Russia | BIPR8/ATHLET | System |
| INRNE/CEA | Bulgaria/France | CRONOS/FLICA | Core |
| INRNE/UPM | Bulgaria/Spain | COBAYA/COBRA | Core |
| VTT | Finland | HEXTRAN/SMABRE | System |
| UNIPI | Italy | NEM/RELAP3D | System |
| Supplementary solutions | | | |
| FZD | Germany | CFX | CFD |
| INRNE | Bulgaria | CATHARE2 – Vessel | System |

**Table 1.2: List of participants in V1000CT-2 Exercise 3**

| Organisation | Country | Code | Type |
|---|---|---|---|
| GRS/KI | Germany/Russia | BIPR8/ATHLET | System |
| VTT | Finland | HEXTRAN/SMABRE | System |
| UNIPI | Italy | NEM/RELAP3D | System |

# Chapter 2: VVER-1000 MSLB benchmark problem

The analyzed transient is initiated by a main steam line break in a VVER-1000 between the steam generator (SG) and the steam isolation valve (SIV), outside the containment. This event is characterized by significant space-time effects in the core caused by asymmetric cooling and assumed stuck-out control rods after scram. One of the major concerns for this case is the possible return to power and criticality after scram, due to overcooling. Because of this concern, the main objective of the study is to clarify the local 3-D feedback effects depending on the vessel mixing.

A burnt core with three-year fuel loading is considered. The reference plant is Kozloduy-6, at Cycle 8. The reactor is at the end of cycle (EOC) and at hot full power (HFP). The SG water inventory is about the possible maximum at HFP. The break is assumed to occur in Main Steam Line 4 (MSL-4).

Two scenarios are considered. The first is close to the current licensing practice. The second is a pessimistic one, derived from Scenario 1 by assuming that all MCP remain in operation and by reducing the tripped rods worth. The purpose of Scenario 2 is to enhance the code-to-code comparison.

The specification of the VVER-1000 MSLB benchmark in V1000CT-2 Volume 2 (Kolev et al, 2010a) completely defines Exercises 2 and 3.

## 2.1 MSLB Scenario 1

Following the break and the scram signal, one of the most reactive peripheral control rod assemblies remains stuck out of the core and is assumed to be close to the location of maximum overcooling (not necessarily in the faulted loop sector). The MCP in the faulted loop trips to mitigate the overcooling, with a coast down time of 55s. Starting from a symmetric initial state, the reactor cooling system makes a transition to reversed flow in one loop and three MCP running normally during the transient.

A mechanical failure of the large feed water control valve in the broken line is assumed. At the time of the break the valve starts to open from about 70% to 100% and then remains stuck in the open position. The main feed water flow to the faulted SG is terminated by closure of the feed water block valve in 52s. The mass of feed water in the piping between the isolation valve and the affected SG, estimated to about 7 500 kg, also contributes to the overcooling. The intact SG feed water temperature after the reactor trip varies from 220°C to about 164°C during the transient. The FW temperature to the faulted SG varies from 220°C to about 130°C in the first 160s of the transient. For the purposes of this benchmark the temperature is conservatively fixed to 160°C to the broken SG and 170°C to the intact ones.

The steam isolation valve in line #4 starts to close and the check valve in the broken line closes to isolate the MSH from the break. Turbine stop valves close on protection signal 10 s after scram. The turbine bypass to condenser starts to open and switches to MSH pressure control mode. Secondary circuit controllers and off-site electric power are assumed to be available. Overcooling of about 50 K relative to the initial state occurs in loop #1 next to the faulted loop and the corresponding core sector. A part of this coolant reaches the inlet of some fuel assemblies practically unmixed.

## 2.2 MSLB Scenario 2

This is a pessimistic case derived from Scenario 1. The MCP in the faulted loop fails to trip on signal and all MCP remain in operation. The tripped rods worth is reduced (through adjustment of the cross-sections). The maximum overcooling is approximately 80 K and occurs in the faulted loop.

From a thermal-hydraulic viewpoint this test problem is similar to the vessel mixing experiments: asymmetric temperature and flow disturbance with sector formation.

## 2.3 Core neutronics and cross-section library

The problem is to be solved in 2-group diffusion approximation, with six delayed neutron groups. The ANS-79 decay heat standard is the recommended decay heat model. A decay heat table is provided to the participants as an option. Twenty-eight assembly types (see Figure 1.1) axially discretized to 30 nodes define the core geometry by 840 un-rodded and 330 rodded compositions.

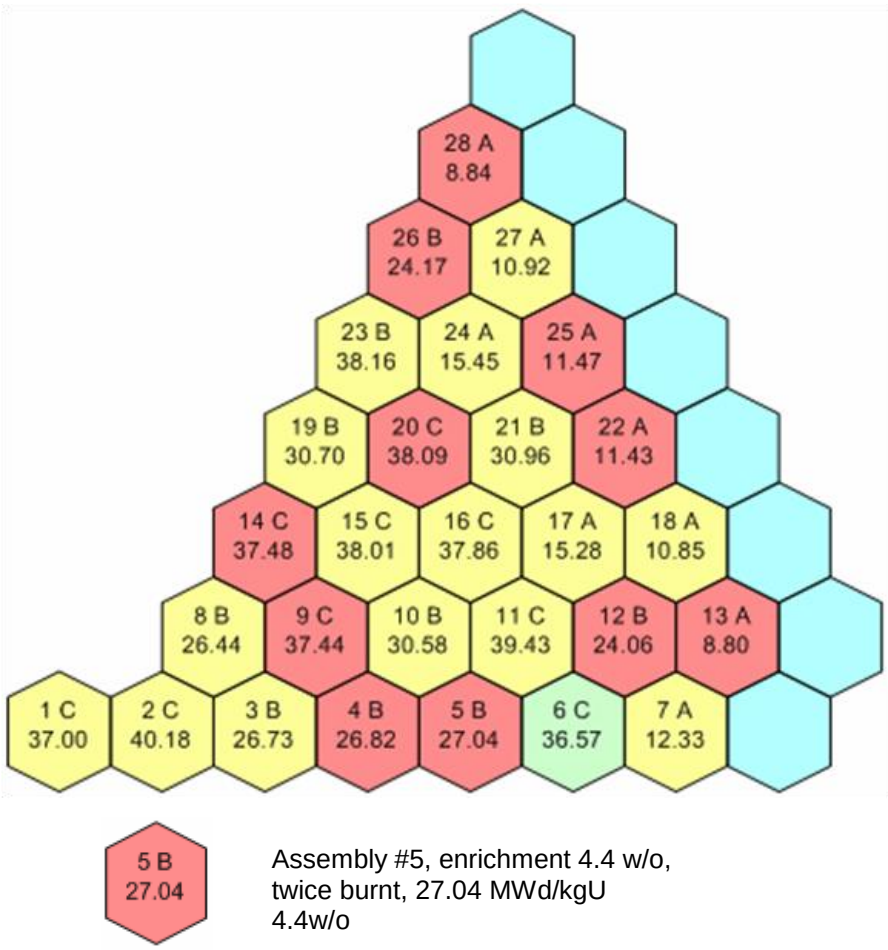


**Figure 2.1: Reference core of Kozloduy-6 at the end of Cycle 8**

A HELIOS1.9 generated wide-range XS library in the NEMTAB format is provided (Ivanov et al, 2006). Burn-up dependence is a vector of (Tmod, Den_mod, T_dopp, exposure). The boron concentration is constant and equal to 53ppm. For each composition, the benchmark defines a set of cross-sections, diffusion coefficients, inverse velocity and kinetic parameters. The cross-sections implicitly include the assembly discontinuity factors (ADF). Sufficiently wide parameter range is considered. The dependence on the state parameters is modeled through a table look-up. For details, see the MSLB benchmark specification in V1000CT-2 Volume 2 (Kolev et al, 2010a).

### 2.4 Steady state conditions

The reactor is at the end of the cycle (EOC) with an average core exposure of 270.4 Effective Full Power Days (26.18 MWd/kgU) and boron concentration of 53 ppm and equilibrium Xe and Sm concentrations. Control rods groups from 1 to 9 are completely withdrawn. Group 10 is 80% withdrawn (283.2cm from the bottom of the core).

### 2.5 Transient calculation

Exercise 2 is a vessel boundary condition problem with pre-calculated MSLB thermal-hydraulic boundary conditions. In Scenario1, involving pump trip in the faulted loop, the application points of the boundary conditions for loop #4 reverse with the flow reversal. For this purpose the hot leg #4 temperature and cold leg #4 pressure boundary conditions are also given. The use of boundary conditions after flow reversal may require small adjustment (regulation) of the loop #4 singular losses so that the computed reversed cold leg#4 flow matches the mass flow boundary condition to the hot leg #4.

For a detailed description of the modeling conventions, see the benchmark specification in V1000CT-2 Volume 2.

The expected sequence of events is as described in Tables 2.1 and 2.2.

**Table 2.1: Expected sequence of major events in Scenario 1**

| Time, s | Event | Hardware Action |
|---|---|---|
| 0 | HFP state at EOC | |
| | Break opens | FW regulation valves to SG-4 starts to open to 100% due to mechanical failure |
| | $Ts_1 - Ts_2 > 75^0C$ for SG-4 | |
| | S4.P49T&DT:<br>P2 < 4.9MPa and $Ts_1 - Ts_2 > 75^0C$<br>and T primary > $200^0C$ (for MSL-4) | Start of HPI pumps (TQ3, TQ4)<br>(no injection by TQ3 before<br>P above core < 10.75MPa) |
| | Signal to close SIV-4<br>on S4.P49T&DT | SIV-4 starts to close |
| | S4.P44T&DT:<br>P2 < 4.4MPa and $Ts_1 - Ts_2 > 75^0C$<br>and T primary > $200^0C$ | |
| | MCP-4 trip signal on P44T&DT | MCP-4 trips |
| | Switchover signal to BRU-SN<br>on MCP-4 trip and P_MSH > 5.5MPa | Bypass to House Consumption Header<br>(BRU-SN) starts to open |
| | Signal to close FW-4 isolation valve<br>on P44T&DT | FW isolation valve to SG-4 starts to close |
| | SCRAM signal<br>on S4.P49T&DT | Start of SCRAM with 0.3s delay<br>Stuck rod: (a) in FA#90 of 1/4 Sector #1<br>(b) in FA#63 of 1/4 Sector #4 |
| | | Check valve of the broken MSL is closed |
| | Low pressure above the core | PRZ heaters ON |
| | | Control rods fully inserted |
| | | SIV-4 closes |
| | Protection signal: TSV↓ 10 s after scram | Turbine Stop Valves start to close |
| | | TSV closed |
| | | BRU-K switches to pressure control mode |
| | Intact SG-1,2,3 level ↓ 100 mm | Auxiliary FW pumps start to feed |
| | P_MSH > 6.67MPa | BRU-K starts to open with 15s opening time |
| | Terminated forced FW flow<br>to the broken SG | Block valve in FW line #4 closes |
| | PRZ Level < 4.2 m | PRZ heaters OFF |
| | Terminated main FW flow to intact SG | Main FW Pumps in bypass mode |
| | P_MSH < 5.79MPa | BRU-K closes, P_MSH recovers a few minutes<br>and is stabilized by the controller |
| | Max overcooling at core inlet | |
| | IF (P above core < 10.75MPa) | HPIS begins to inject<br>(No credit taken for boron reactivity insertion) |
| | PMSH < 5.297MPa and Reactor tripped<br>and TSV closed | BRU-SN valves start to close |
| | | BRU-SN valves closed |
| | Transient ends | |

**Table 2.2: Expected sequence of major events in Scenario 2**

| Time, s | Event | Hardware Action |
|---|---|---|
| 0 | HFP state at EOC | |
| | Break opens | FW regulation valves to SG-4 start to open to100% due to mechanical failure |
| | P-S4.DTS75:<br>$Ts_1 - Ts_2 > 75^0C$ for SG-4 | |
| | S4.P49T&DT:<br>P2 < 4.9MPa and $Ts_1 - Ts_2 > 75^0C$<br>and T primary > 200oC (for MSL-4) | Start of HPI pumps (TQ3, TQ4)<br>(no injection by TQ3 before<br>P above core < 10.75MPa) |
| | Signal to close SIV-4<br>on S4.P49T&DT | SIV-4 starts to close<br>with 0.3s delay |
| | S4.P44T&DT:<br>P2 < 4.4Mpa and Ts1 – Ts2 > 75oC<br>and Primary temperature > 200oC | |
| | MCP-4 trip signal on P44T&DT | MCP-4 does not trip (Sc2 assumption) |
| | Signal to close FW-4 isolation valve<br>on P44T&DT | FW isolation valve to SG-4 starts to close |
| | SCRAM signal<br>on S4.P49T&DT | Start of SCRAM with 0.3s delay<br>Stuck rod: (a) in FA #140 of 1/4 Sector #4<br>(b) in FA #140 and #117 |
| | | Check valve of the broken MSL is closed |
| | Low pressure above the core | PRZ heaters ON |
| | | Control rods fully inserted |
| | | SIV-4 closes |
| | Protection signal: TSV↓ 10 s after scram | Turbine Stop Valves start to close |
| | | TSV closed |
| | | Bypass to condenser (BRU-K)<br>switches to pressure control mode |
| | Switchover signal to BRU-SN<br>on Closing 2 of 4 Turbine Stop Valves<br>(BRU-SN algorithm in load following | Bypass to House Consumption Header<br>(BRU-SN) starts to open |
| | Intact SG-1,2,3 level ↓ 100 mm | Auxiliary FW pumps start to feed |
| | P_MSH > 6.67MPa | BRU-K starts to open with 15s opening time |
| | P_MSH < 6.67MPa | BRU-K maintains P_MSH < 6.28MPa |
| | PRZ Level < 4.2 m | PRZ heaters OFF |
| | Terminated forced FW flow<br>to the broken SG | Block valve in FW line #4 closes |
| | Max local overcooling at core inlet | |
| | Min pressure above the core | |
| | Maximal total core power | |
| | Terminated main FW flow to intact SG | Main FW Pumps switch to bypass mode |
| | PRZ Level > 4.2 m | PRZ heaters ON |
| | Transient ends | |

# Chapter 3: Methodology of comparison

The MSLB situation target analysis presented here comprises three scales:

- separate effects (mixing in the down-comer and the lower plenum; neutronics)
- component scale (core and core-vessel)
- system scale

The following comparisons are considered:

- system code vs. CFD vessel mixing calculations with MSLB vessel BC
- code-to-code comparison of vessel TH and coupled core-vessel N/TH solutions
- code vs. mean results of all codes

In accordance with the Best Practice Guidelines (Mahaffy et al, 2007), the ability of the validated vessel thermal-hydraulic models in system codes to reproduce main flow features was tested vs. plant data and CFD results. For this purpose, supplementary plant data for loop #4 from the Kozloduy-6 vessel mixing experiments and a transient CFX-5 calculation (Hoehne, 2007) with MSLB vessel boundary conditions were used as reference. The domain of the CFD solution is from the vessel inlet to the core inlet. Plant data were used in a qualitative manner only - to assess the disturbed sector formation and the angular turn of the loop #4 flow centre.

The following target variables are chosen for comparison: integral parameters and their time history as well as 1D power profiles, and 2D distributions of power, temperature and flow rates. The applied metrics is discussed below.

### 3.1 Integral parameters

The statistical criteria used are as follows:

*Mean value:* $$\overline{x_{ref}} = \frac{\sum_i^N x_i}{N} \tag{3.1}$$

*Standard deviation:* $$\sigma = \pm\sqrt{\frac{\sum\left(x_i - x_{ref}\right)^2}{N-1}} \tag{3.2}$$

*Relative deviation:* $$e_i = x_i - x_{ref} \tag{3.3}$$

*Figure of merit:* $$\Phi_i = \frac{e_i}{\sigma} \tag{3.4}$$

### 3.2 One-dimensional (1D) distributions

*Mean value:* $$\overline{x_{ref}} = \frac{\sum_i^N x_i}{N} \tag{3.5}$$

*Standard deviation:* $\sigma = \pm\sqrt{\frac{\sum\left(x_i - x_{ref}\right)^2}{N-1}}$ (3.6)

### 3.3 Two-dimensional (2D) distributions

The criteria used are as follows:

1. *Mean error (ME):* $ME = \frac{1}{N}\left\{\sum_{i=1}^{N}(x_i - x_{i,ref})\right\}$ (3.7)

2. *Maximum in modulus error:* $e_{i,\max} = \max\left|x_i - x_{i,ref}\right|$ (3.8)

   where $e_{i,max}$ is the absolute value of the maximum difference of computed datum $x_i$ to the reference value $x_{i,ref}$

3. *Average in modulus error ($ME_{ABS}$):* $ME_{ABS} = \frac{1}{N}\left\{\sum_{i=1}^{N}\left|\left(x_i - x_{i,ref}\right)\right|\right\}$ (3.9)

   where $ME_{ABS}$ is the average of the absolute values of the deviations from the reference.

For the assessment of vessel mixing models, $x_{i,ref}$ is a CFX result with MSLB vessel BC, in a computational domain from the vessel inlet to the core inlet.

For benchmarking standalone neutronics solvers, because of the observed clustering of the results in two groups, we consider two comparisons, where:

(a) "reference" is the mean of all codes solutions

$x_{i,ref} = \bar{x}_i$ and

(b) "reference" is the mean of PARCS, DYN3D, CRONOS and COBAYA solutions. A CRONOS 2nd order FEM solution with 24 triangles per hexagon (24N) also serves as reference.

For coupled code solutions, "reference" is the mean of five coupled codes: PARCS/TRACE, DYN3D/ATHLET, CRONOS/FLICA, COBAYA/COBRA and HEXTRAN/SMABRE

$x_{i,ref} = \bar{x}_i$

# Chapter 4: Assessment of vessel mixing models in MSLB calculations

This chapter presents results from the assessment of coarse-mesh vessel mixing models against CFD calculations with MSLB vessel boundary conditions. The objective is to analyze the modeling of separate effects - flow mixing in the down-comer and the lower plenum. A transient CFX solution (Hoehne, 2007) serves as reference. It has been obtained with the SST turbulence model, unstructured mesh with 4 700 000 cells and the upwind advection scheme. The domain of solution is from the reactor inlet to the core inlet. The task is to calculate the flow parameters in the down-comer and at the core inlet, given the vessel boundary conditions and the pressure above the core. The boundary conditions correspond to MSLB Scenario 2, with all MCP in operation.

The vessel mixing models (coarse-mesh and CFD) used in this comparison have been validated against plant data in Exercise 1 of this benchmark - see the V1000CT-2 Volume 3 (Kolev et al, 2010b). The considered calculation with MSLB boundary conditions is an additional test of the validated models. It requires modeling of a different configuration where the faulted loop is #4 and the temperature and flow disturbances are much stronger.

It is worth noting that the main coolant loops of a VVER-1000 are asymmetrically connected to the vessel. There is an experimentally observed counter clockwise swirl in the vessel, looking from the top. The azimuthal turn of loop #4 flow is app. +8 degrees ± 20% clockwise (estimated from loop heat-up experiments), while for loop #1 the shift is -26 degrees counter clockwise (Topalov and Popov, 2004), (Kolev et al, 2009). Since the hypothetical MSLB overcooling transient with all pumps in operation features single-phase flow and high Reynolds numbers, the plant data from loop heat-up experiments could be used to assess the ability of the model to reproduce the disturbed sector formation as well as the angular shift of the loop flow.

For the present study, the analysis includes:

- coarse-mesh to CFD comparison of the flow parameters in selected points in the down-comer and at fuel assembly inlets
- qualitative code-to-experiment comparison of the predicted azimuthal turn of loop #4 flow centre with respect to the cold leg axis.

The CFX solution is used as an approximate reference, keeping in mind the following uncertainties:

- it has been obtained with ATHLET calculated vessel boundary conditions which are slightly different from the CATHARE calculated ones (Kolev et al, 2005)
- it is a first post-test calculation and tends to overestimate the clockwise angular turn of loop #4 flow centre - see Figures 4.9 and 4.10 below and the results in V1000CT-2 Volume 3

Table 4.1 summarizes the coarse-mesh r,θ vessel discretization used in each code for this comparison.

**Table 4.1: Participants' codes and meshing of the down-comer and lower plenum**

| Organisation | Code | Vessel model | Nodalization |
|---|---|---|---|
| FZD | ATHLET/ DYN3D | Multi-1D | 4 sectors in the vessel<br>2 axial nodes in the DC<br>2 axial nodes in the LP |
| FZK (KIT) | TRACE/ PARCS | Coarse-3D | 6 sectors in the DC and LP<br>3 radial rings in the LP<br>4 axial nodes in the DC<br>2 axial nodes in the LP |
| INRNE | CATHARE2 | Multi-1D | 24 sectors in the vessel<br>12 axial nodes in the DC<br>2 axial nodes in the LP |
| VTT | SMABRE/ HEXTRAN | Multi-1D | 6 sectors in the vessel<br>2 axial nodes in the DC<br>2 axial nodes in the LP |
| UNIPI | RELAP3D/ NEM | Coarse-3D | 20 sectors in the DC<br>60 sectors in the upper LP<br>8 radial rings in the upper LP<br>20 axial nodes in the DC<br>4 axial nodes in the LP |

### 4.1 The vessel mixing models

In this study, the coarse-3D models used 3D modeling without turbulence. The TRACE user model had 6 sectors in the vessel and 3 radial rings in the lower plenum. The RELAP3D model of UNIPI had 20 sectors in the down-comer and variable r,θ-meshing of the lower plenum depending on the elevation: three axial layers in the lower plenum with up to 60 sectors and 8 radial rings at the core inlet.

The multi-channel models with cross-flow used lower vessel nodalization as follows:

- ATHLET: 4 sectors in the vessel. A sector formation model is tuned to fit CFD results

- SMABRE: 6 sectors in the vessel, one radial node and two axial nodes in the lower plenum. Parallel channels with cross flow and aproximate turbulence modeling

- CATHARE2: 24 sectors in the vessel, one radial node and two axial nodes in the lower plenum. Parallel channels with cross flow governed by the local pressure drops, without turbulence

The CFX-5 simulation used the SST turbulence model and unstructured mesh with 4 700 000 cells and upwind advection scheme.

For details, see Appendix F of this report and V1000CT-2 Volume 3 (Kolev et al, 2010b).

## 4.2 Coarse-mesh vs. CFD calculations

*Down-comer flow parameters*

*Scenario 1*: Figures 4.1 and 4.2 show a code-to-code comparison of the computed down-comer temperature distribution at elevations 5800 mm and 2500 mm, in the moment of max overcooling (166 s). The MCP #4 trips and the other three pumps are in operation. The flow in the faulted loop #4 reverses and because of the cross-flow in the outlet ring of the reactor vessel, the maximum overcooling (43 K) occurs in loop #1. The results show a reasonable agreement of the coarse-mesh predictions when using 24-60 azimuth meshes. At the same time, the 6-sector coarse-3D model solution illustrates the limitations of the too coarse mesh.

*Scenario 2*: Figures 4.3 and 4.4 show the comparison of coarse-mesh vs. CFX computed down-comer temperature distributions at elevation 5800 mm and 2500 mm from the bottom of the reactor vessel, in the moment of maximum overcooling (app. 69s). All main coolant pumps are in operation. The temperature of the faulted loop #4 is 74 K lower than that in the initial state. The results show a good overall agreement with the CFX prediction. Larger discrepancies can be seen at the borders of the disturbed sector depending on the spatial resolution and the predicted azimuthal turn of loop #4 flow. Figures 4.5 and 4.6 illustrate the corresponding down-comer velocity distributions. The coarse-mesh models without turbulence cannot reproduce the detailed velocity distribution and the predicted values are near the average ones.

*Assembly inlet flow parameters*

Figures 4.7, 4.12, 4.15, 4.18 and 4.21 show the computed assembly-by-assembly core inlet temperatures, in comparison with the CFX results at time of highest return to power. The core maps in Figures 4.13, 4.16, 4.19 and 4.22 show the corresponding differences to CFD results. The maximum deviation varies from a few K (for 60 azimuth meshes) to 14K (for 24 meshes) or 25K (for 6 meshes). The results of the V1000CT-2 Exercise 1 on vessel mixing simulation suggest that the actual maximum deviations can be a little smaller than those observed here, in view of the uncertainty in the first CFX solutions.

Note that the very good agreement of RELAP3D and CFD results can be associated with a similar sector formation and similar overestimation of the angular turn of the loop flow, observed in V1000CT-2 Exercise 1. The CATHARE predicted disturbed sector is rather similar to that of CFX, with some quantitative differences in the angular turn of the main loop flow and in the transitional (border) regions.

The coarse-mesh solutions show a reasonable agreement with the CFX results in the regions of strong or very weak disturbances, for all models. At the borders of the disturbed sector, which are transitional regions, the coarse-mesh resolution is acceptable when using at least 16-24 sectors in the down-comer and the lower plenum.

The results with 4- and 6-sector models illustrate the limitations in local resolution of the too coarse azimuth meshes.

## 4.3 Qualitative comparison with plant data

Figure 4.9 shows the experimentally observed azimuth shift of loop #4 flow centre relative to the cold leg axis, see the V1000CT-2 Exercise 1 specification (Kolev et al, 2009). It is +8° ±20% clockwise and opposite to that of -26 degrees observed for loop #1. The plant data is used for qualitative comparison with the MSLB Scenario 2 results, assuming all MCP in operation during the transient.

Figure 4.10 illustrates the CFX results at time of maximum overcooling (highest return to power). The CFD solution shows an overestimation of the angular turn that may cause larger discrepancies at the disturbed sector borders, if the solution is used as reference. This should be kept in mind when comparing with other code solutions.

Figures 4.11, 4.14, 4.17 and 4.20 illustrate the angular turn of the loop flow as predicted by the coarse-mesh user models. It is defined as the centerline of the zone of minimum mixing. The disturbed sector is estimated in terms of temperature differences between the assembly inlets and the cold leg. The zone of minimal difference (dark blue) is the zone of minimal mixing. In this test, the CATHARE and SMABRE results are in reasonable agreement with the plant data, while the RELAP3D and FZD ATHLET solutions overestimate the angular turn.

### 4.4 Conclusions

Coarse-3D and multi-1D vessel thermal-hydraulic models with cross-flow, validated against coolant mixing experiments and CFD calculations, can produce acceptable accuracy in MSLB transient calculations, provided that a sufficiently fine azimuthal mesh is used.

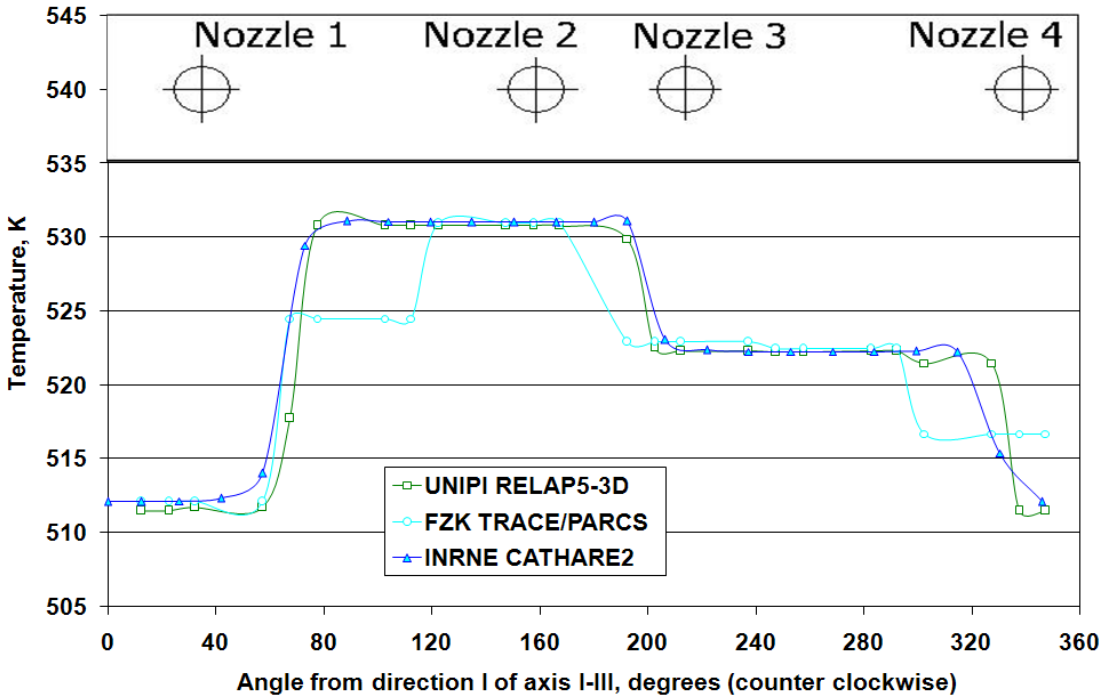


**Figure 4.1: MSLB Scenario 1, time of maximum overcooling (166s): Temperature distribution in the down-comer at elevation 5800 mm**

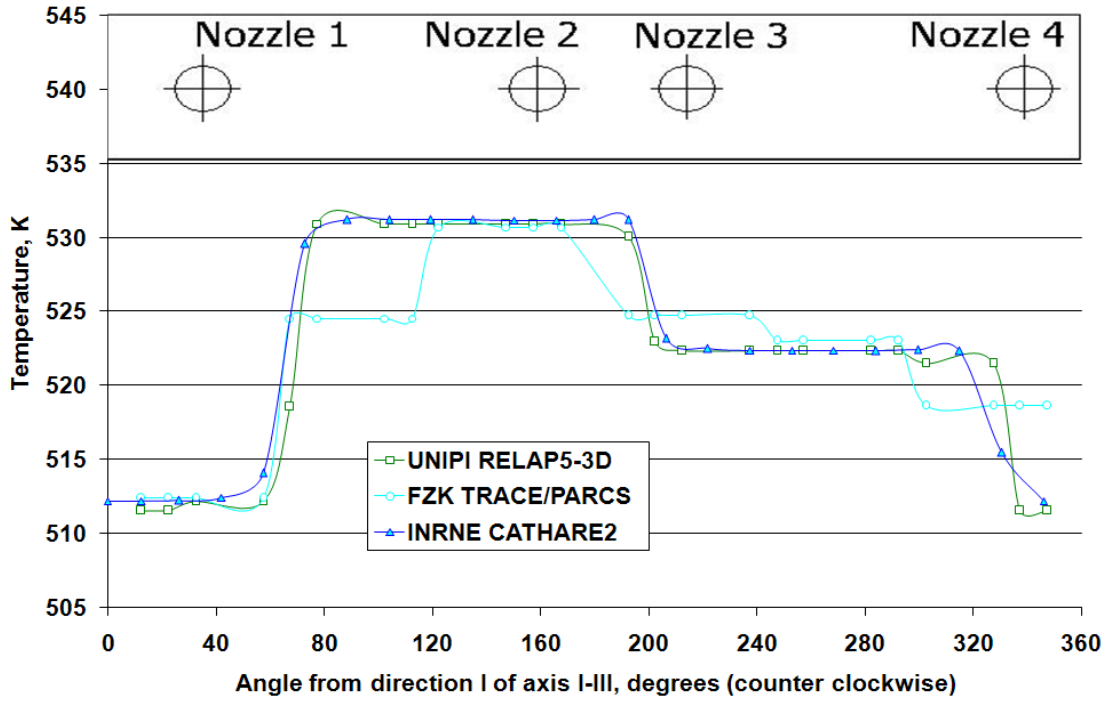


**Figure 4.2: MSLB Scenario 1, time of maximum overcooling (166s): Temperature distribution in the down-comer at elevation 2500 mm**

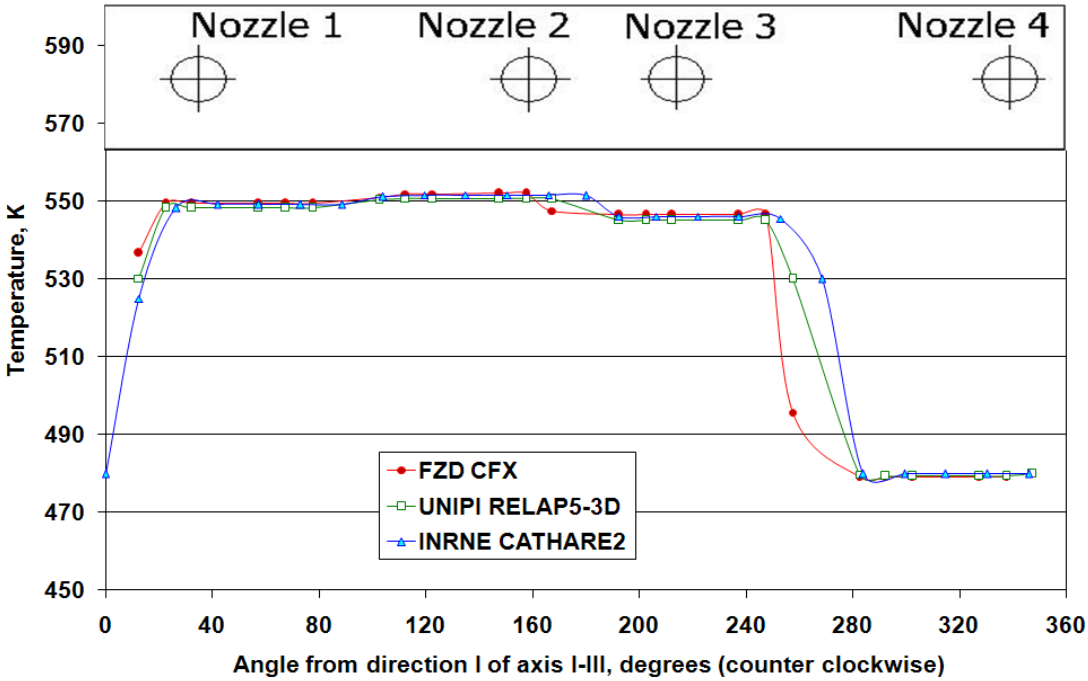


**Figure 4.3: MSLB Scenario 2, time of maximum overcooling (69s): Azimuthal temperature distribution in the down-comer at elevation 5800 mm**

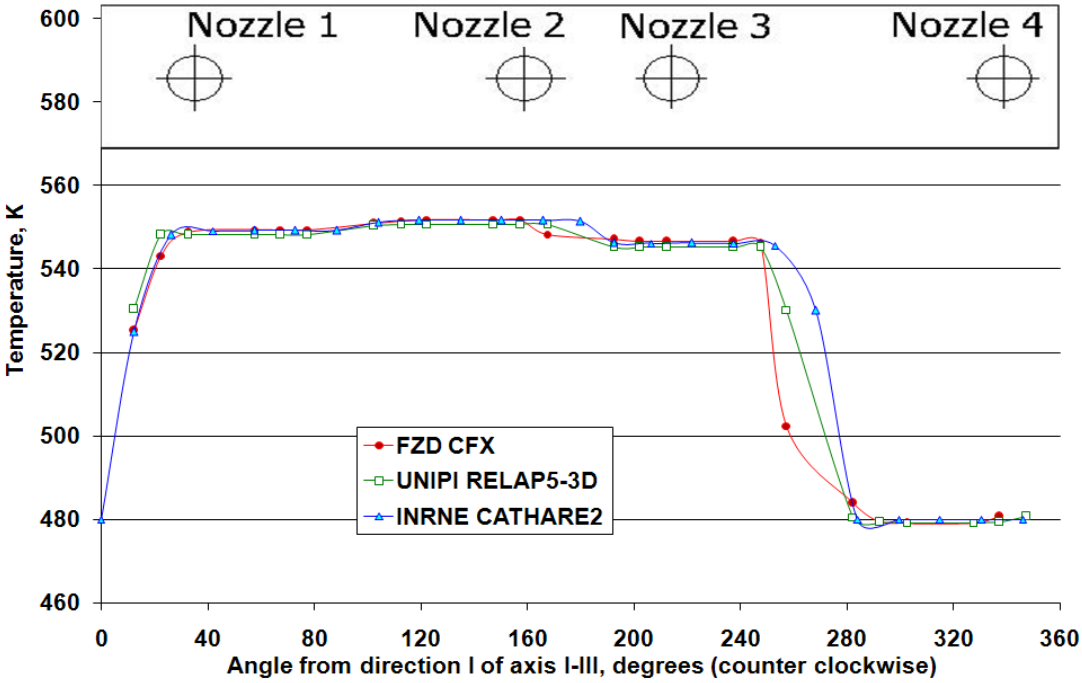


**Figure 4.4: MSLB Scenario 2, time of maximum overcooling (69s): Azimuthal temperature distribution in the down-comer at elevation 2500 mm**

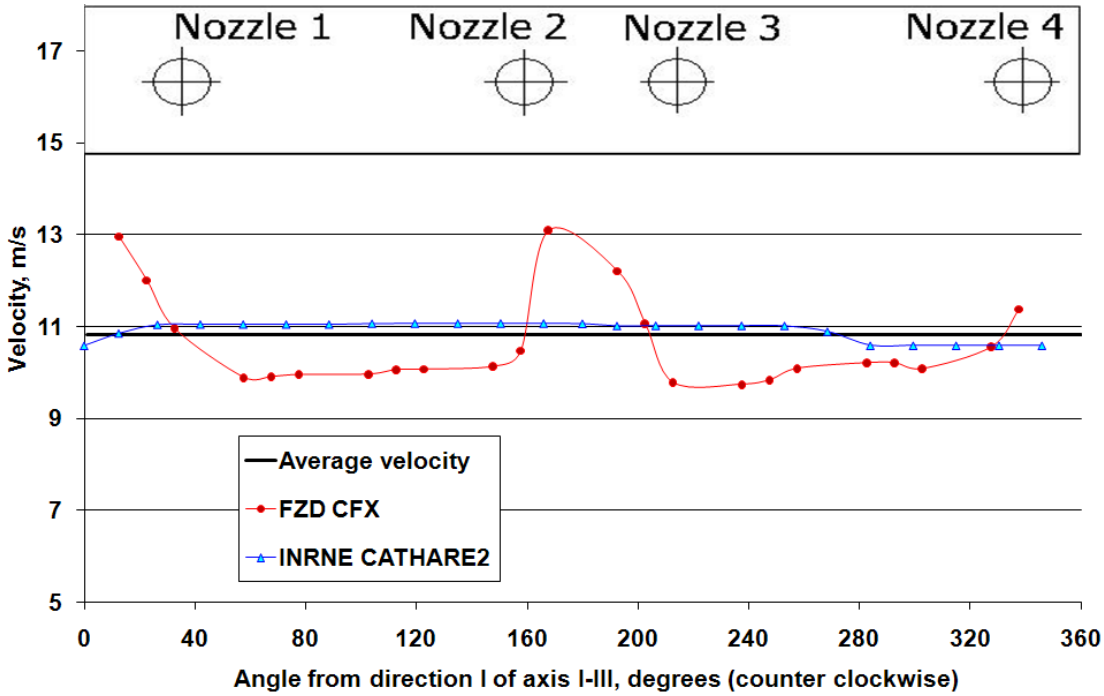


**Figure 4.5: MSLB Scenario 2, time of maximum overcooling: Azimuthal velocity distribution in the down-comer at elevation 5800 mm**

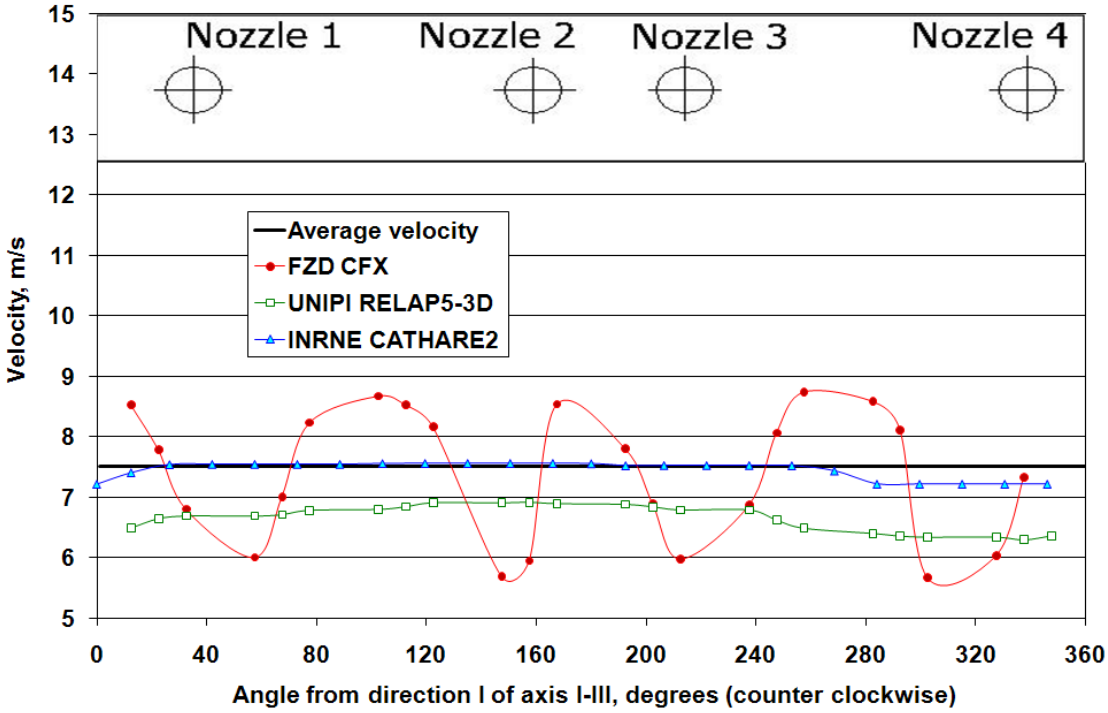


**Figure 4.6: MSLB Scenario 2, time of maximum overcooling: Azimuthal velocity distribution in the down-comer at elevation 2500 mm**

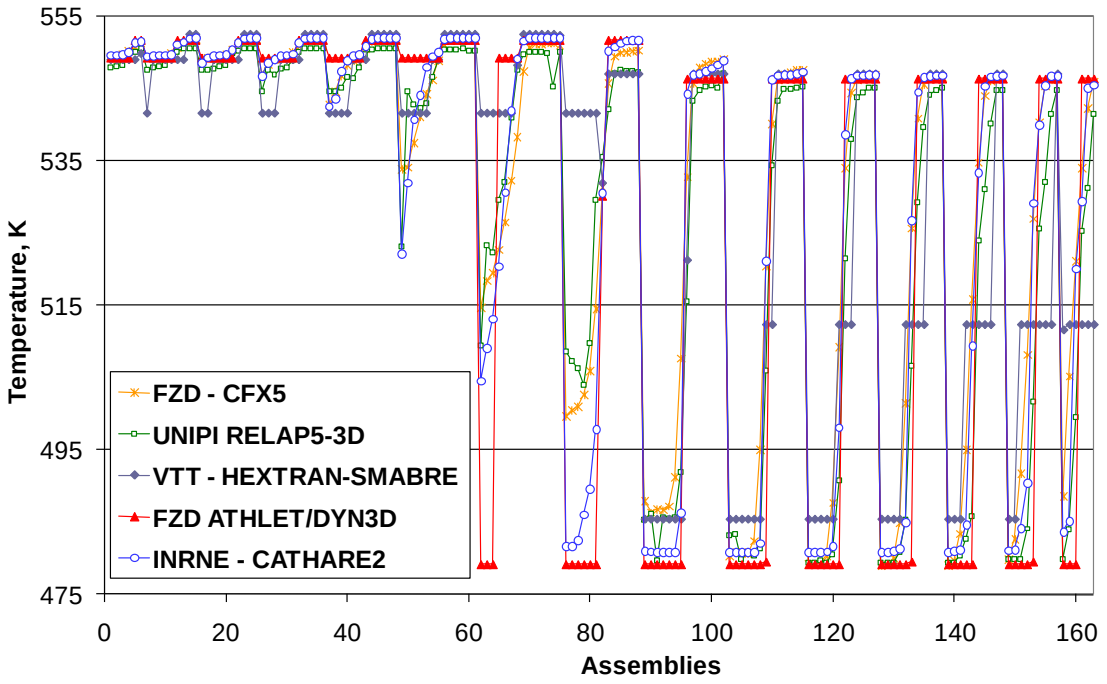


**Figure 4.7: Assembly-by-assembly core inlet temperatures at highest return to power**

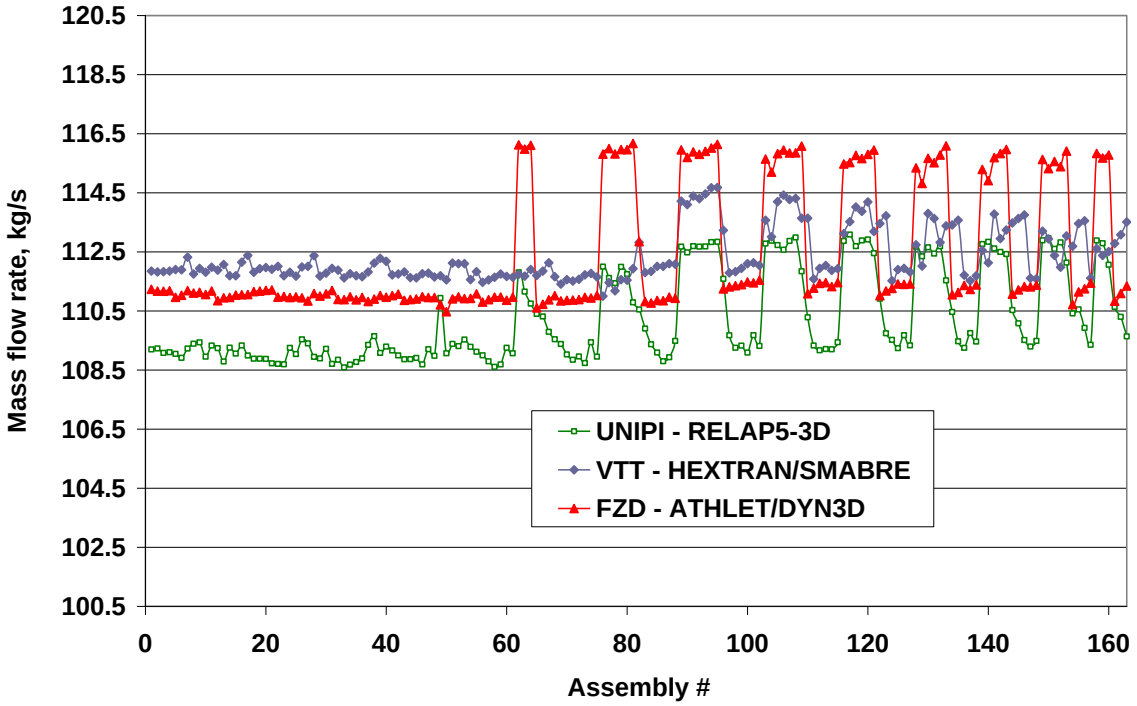


**Figure 4.8: Assembly-by-assembly core inlet mass flow rates at highest return to power**

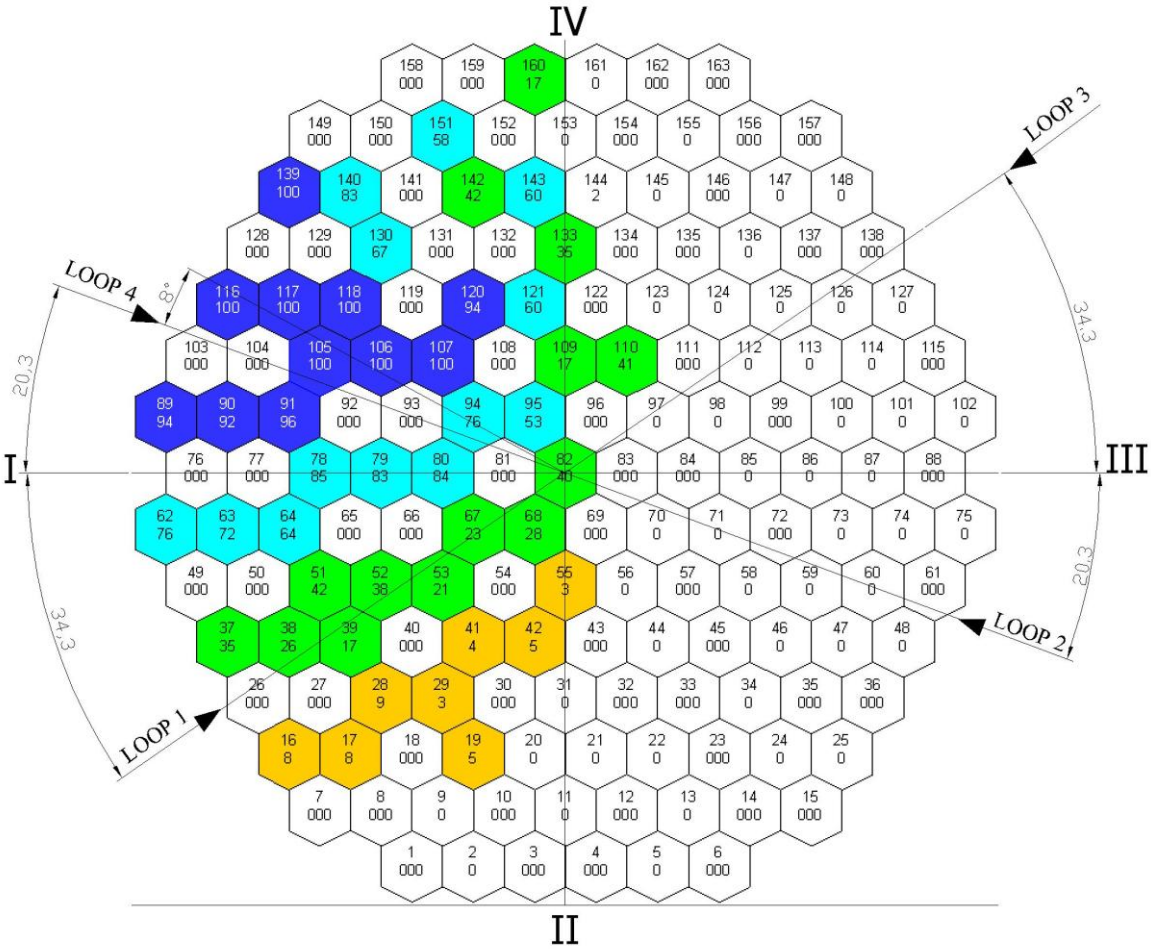


**Figure 4.9: Plant data from the Kozloduy-6 vessel mixing experiments: Disturbed sector and azimuthal turn of the loop #4 flow centre. Blue color corresponds to loop-to-assembly mixing coefficients of 92-100% or**
**$\Delta Ti = Tin,i - Tcold\ leg\ 4 < 1.5$ K, i =1,163**

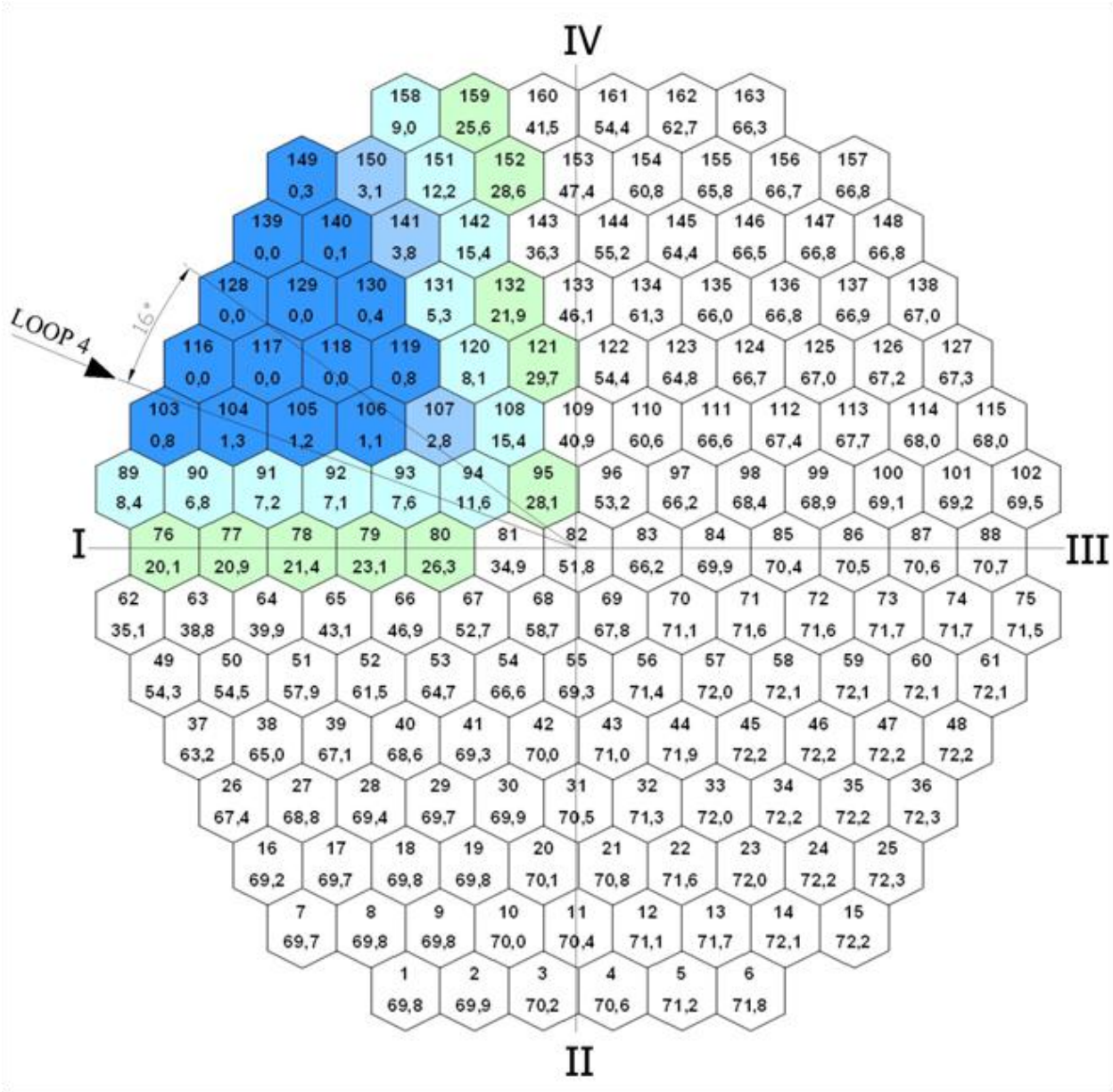


**Figure 4.10: MSLB Scenario 2 at time of max overcooling, with stuck rods in #117 and #140: CFX computed disturbed sector and angular turn of loop #4 flow centre, in terms of temperature differences between the assembly inlets and cold leg #4 (ΔTi = Tin, i – T cold leg 4, i =1,...,163)**

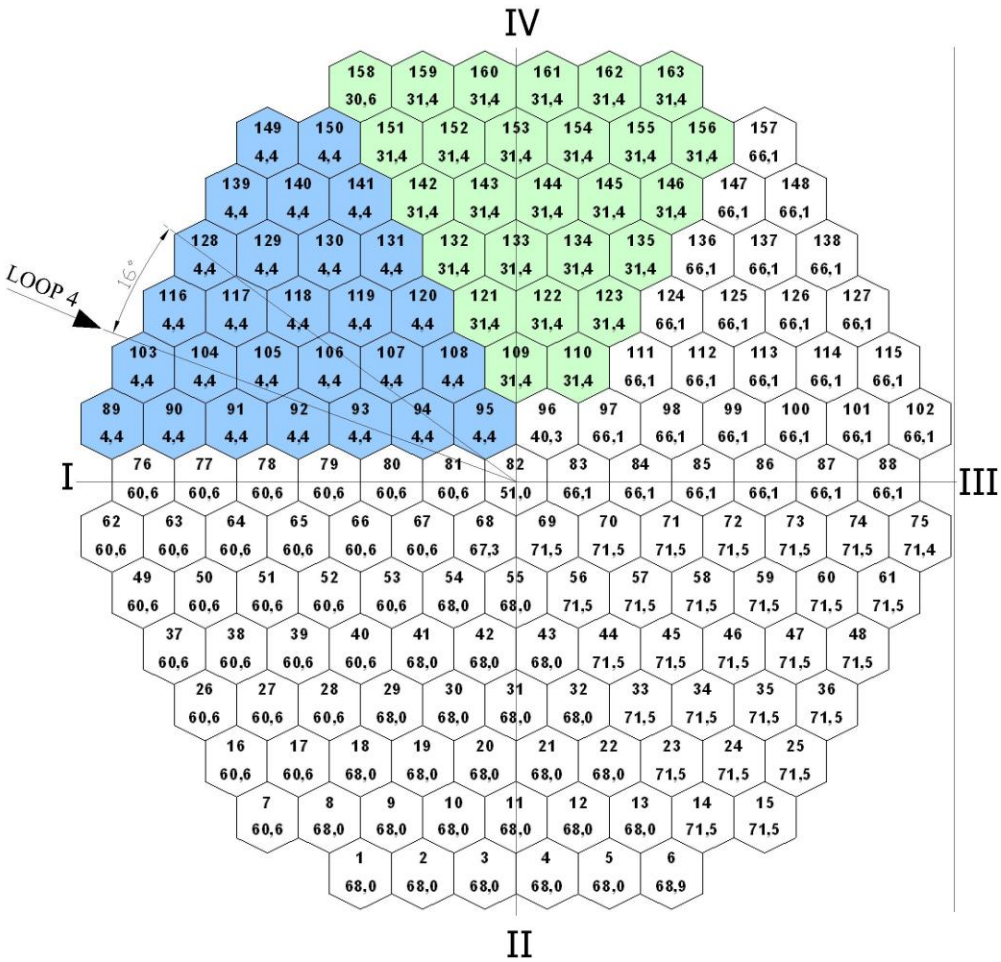


**Figure 4.11: Scenario 2 at time of max overcooling, with stuck rods in #117 and #140: SMABRE/HEXTRAN computed disturbed sector and azimuthal shift of the loop#4 flow centre (ΔTi = Tin, i - Tcold leg 4, i =1,...,163)**

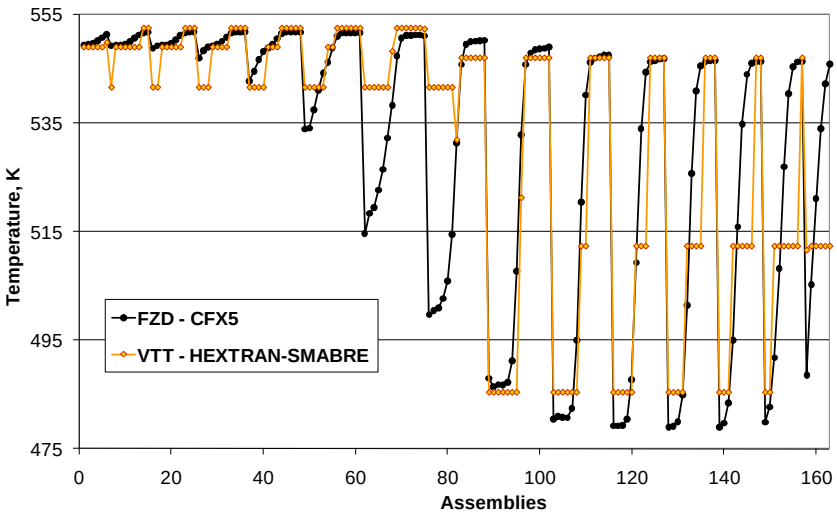


**Figure 4.12: Scenario 2 at time of max overcooling, with stuck rods in #117 and #140: HEXTRAN/SMABRE vs. CFX computed assembly-by-assembly core inlet temperatures**

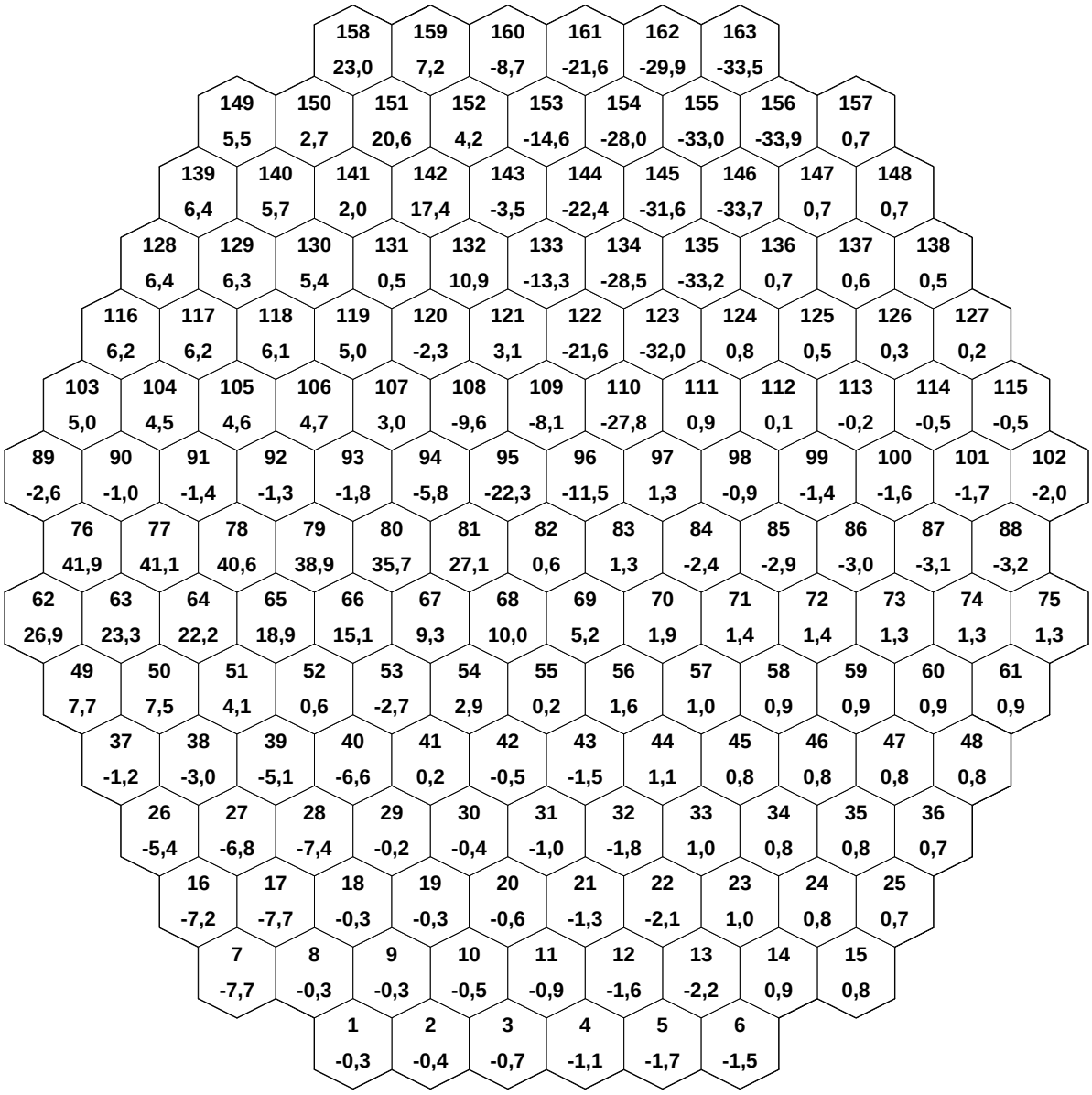


**Figure 4. 13: Scenario 2 at time of max overcooling, with stuck rods in #117 and #140: Differences between the HEXTRAN-SMABRE and CFX predicted assembly inlet temperatures ($\Delta T$ = Tin – Tin, ref)**

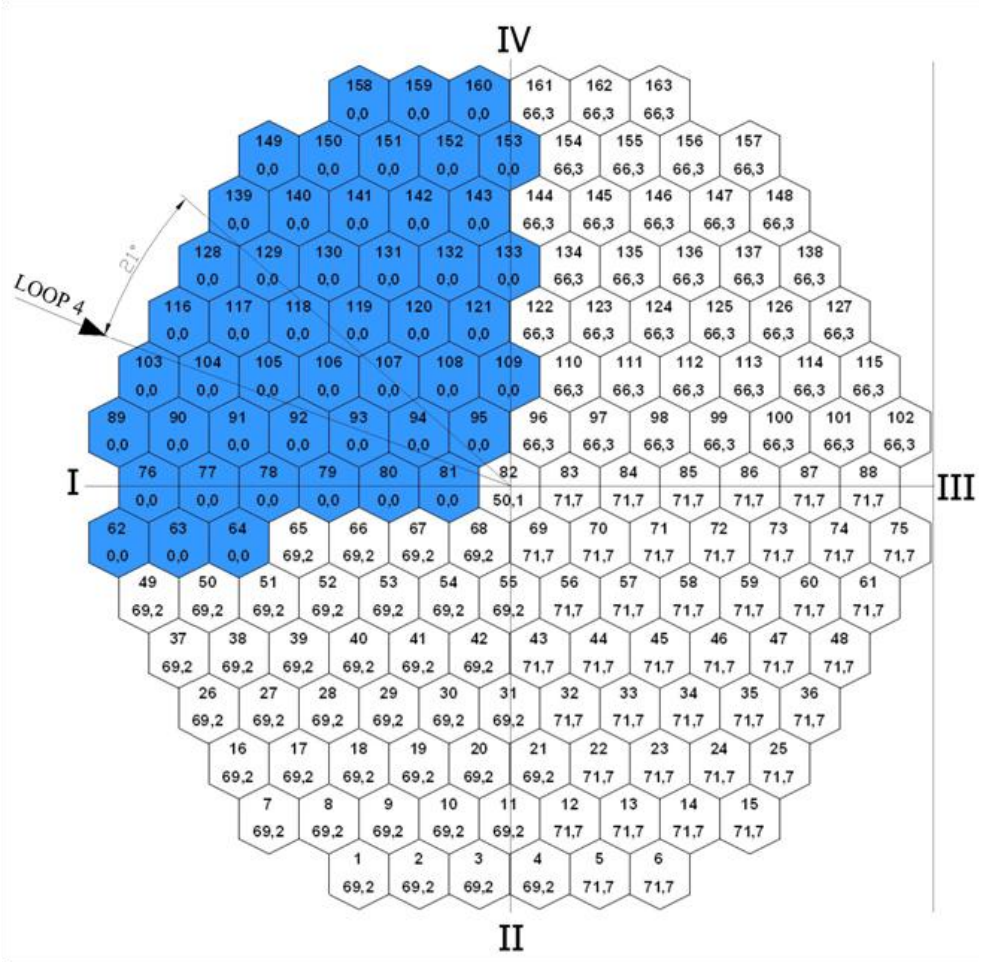


**Figure 4.14: Scenario 2 at time of max overcooling, with stuck rods in #117 and #140: ATHLET/DYN3D computed disturbed sector and angular turn of loop#4 flow centre**
**(ΔTi = Tin, i – T cold leg 4, i =1,...,163)**

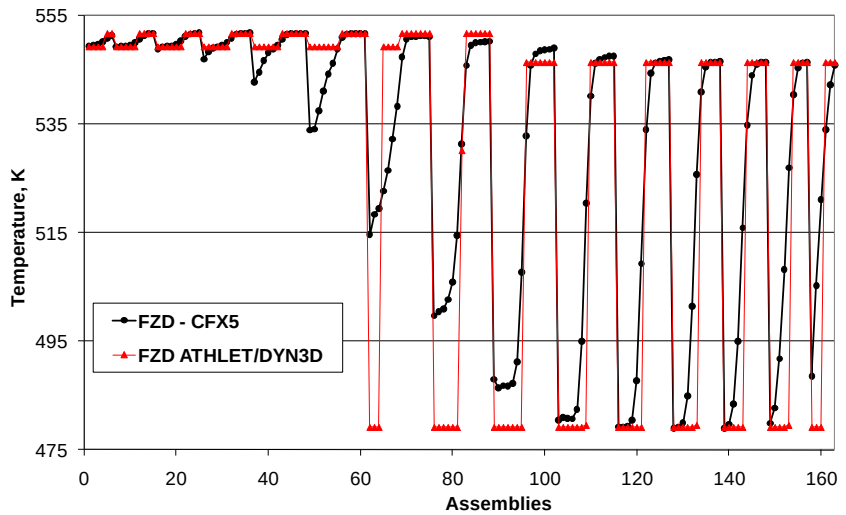


**Figure 4.15: Scenario 2 at time of max overcooling, with stuck rods in #117 and #140: HEXTRAN/SMABRE vs. CFX calculated assembly-by-assembly core inlet temperatures**

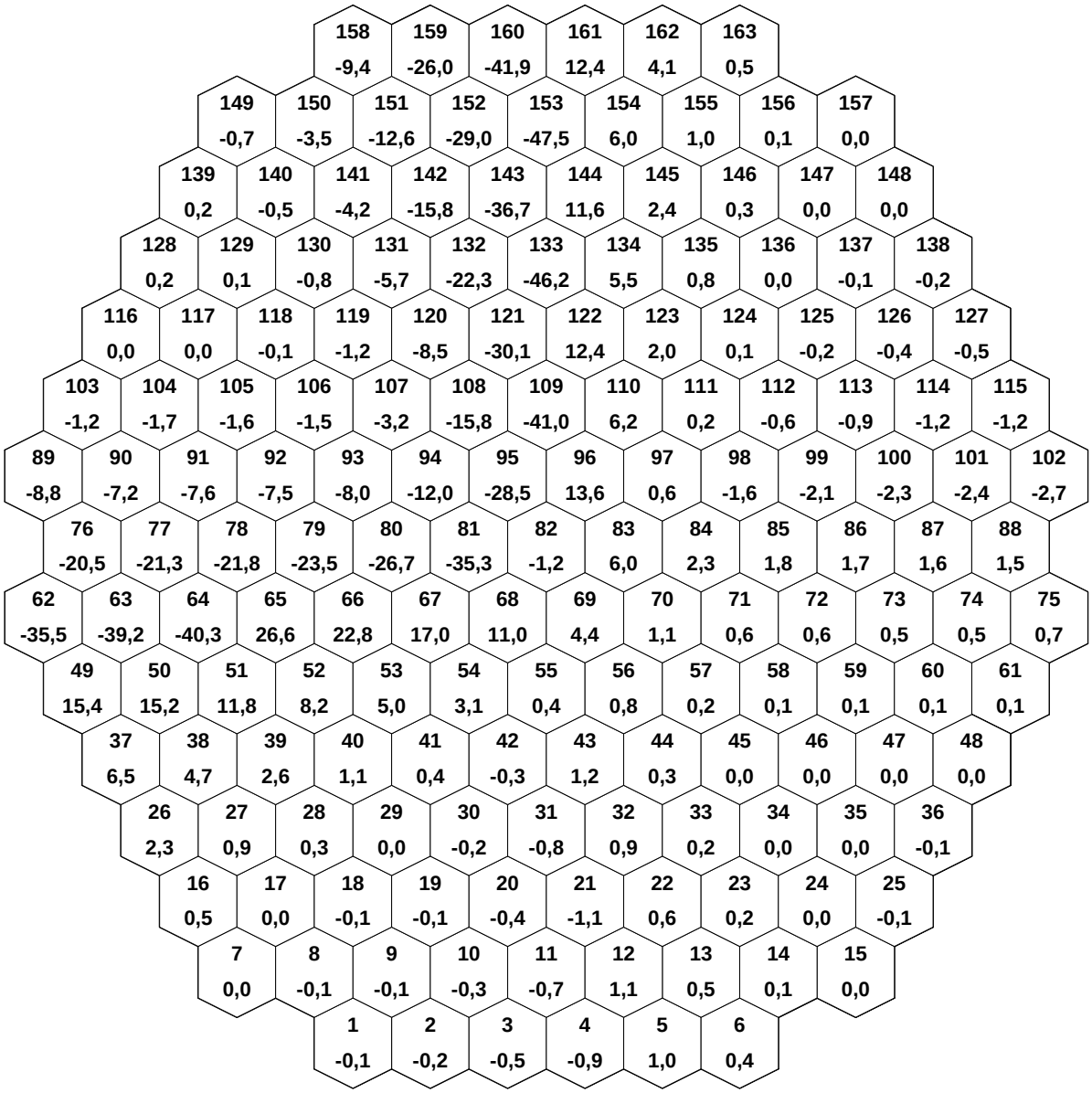


**Figure 4.16: Scenario 2 at time of max overcooling, with stuck rods in #117 and #140: Differences between ATHLET/DYN3D and CFX predicted assembly inlet temperatures (ΔT = Tin – Tin, ref)**

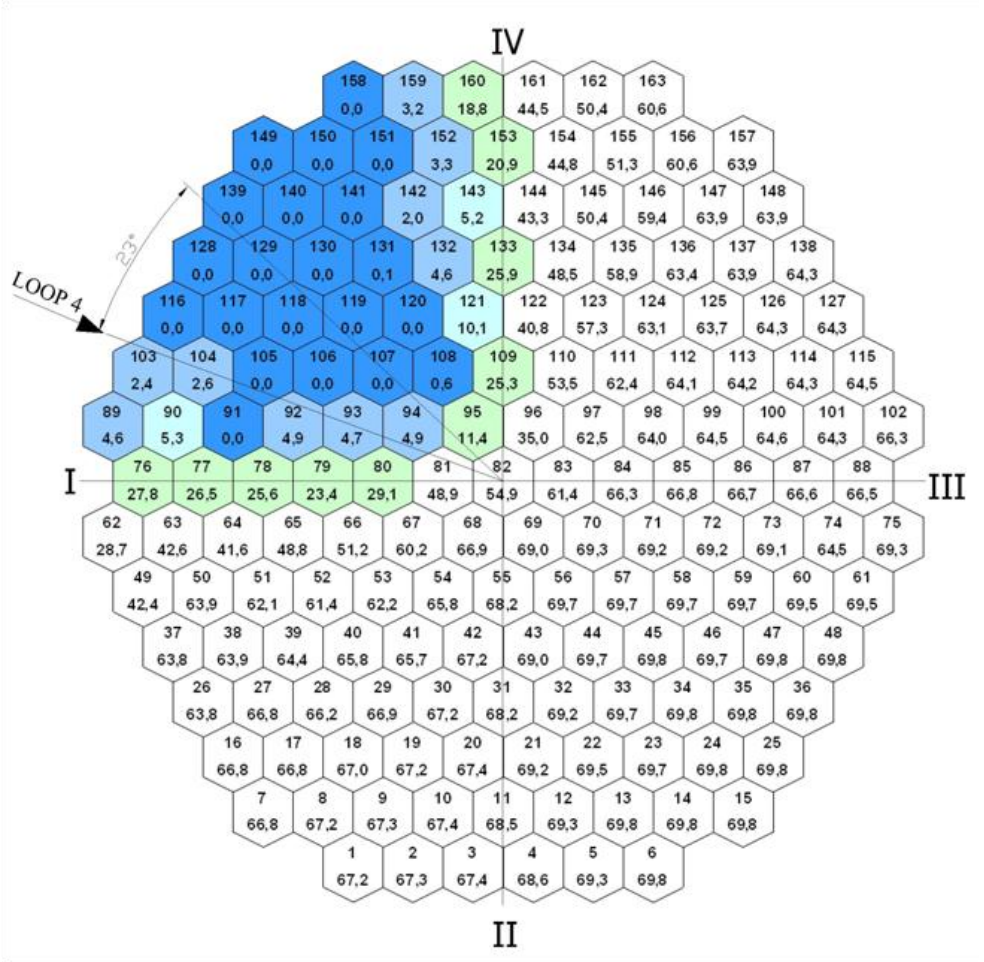


**Figure 4.17: Scenario 2 at time of max overcooling, with stuck rods in #117 and #140: RELAP3D/NEM predicted disturbed sector and angular turn of loop #4 flow centre (ΔTi = Tin, i – T cold leg 4, i =1,...,163)**

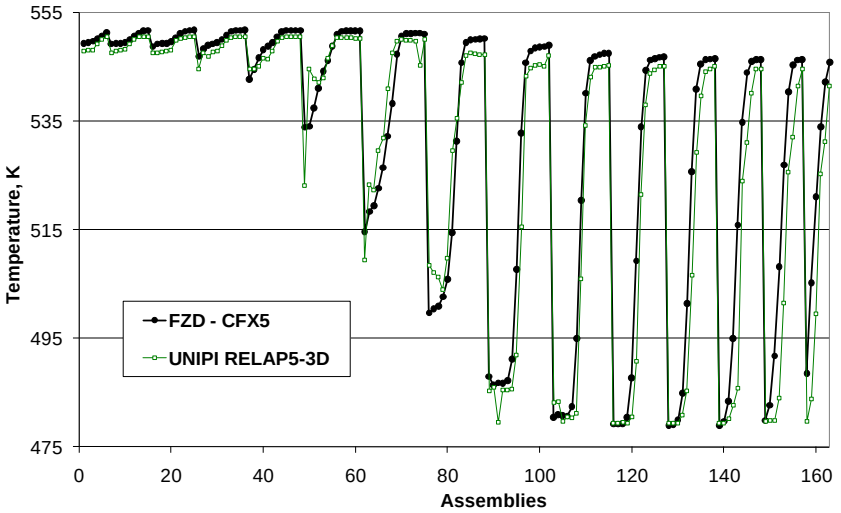


**Figure 4.18: Scenario 2 at time of max overcooling, with stuck rods in #117 and #140: RELAP3D/NEM vs. CFX calculated assembly-by-assembly core inlet temperatures**

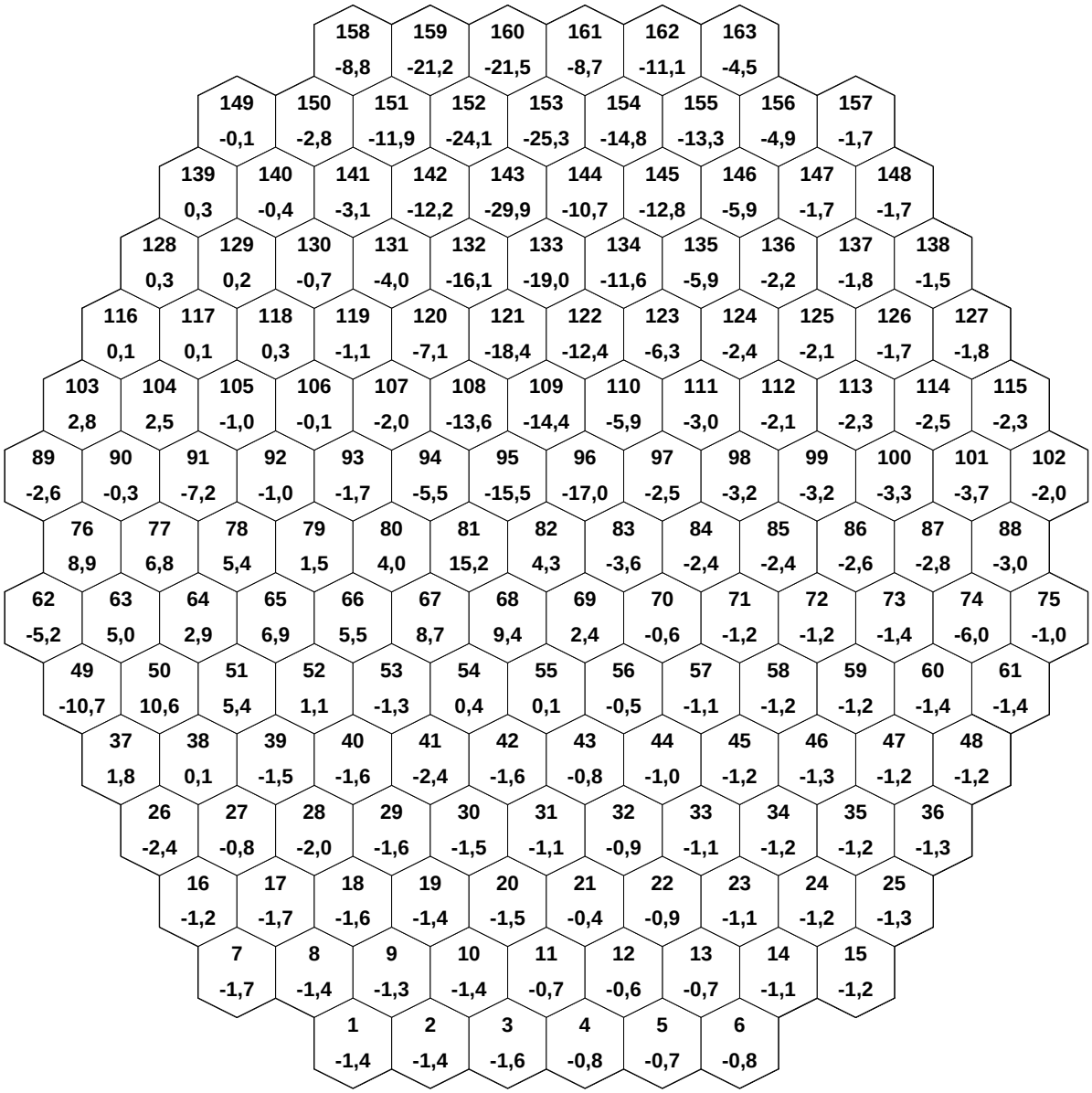


**Figure 4.19: MSLB Scenario 2 at time of max overcooling, with stuck rods in #117 and #140: Differences between the RELAP3D/NEM and CFX predicted assembly inlet temperatures (ΔT = Tin – Tin, ref)**

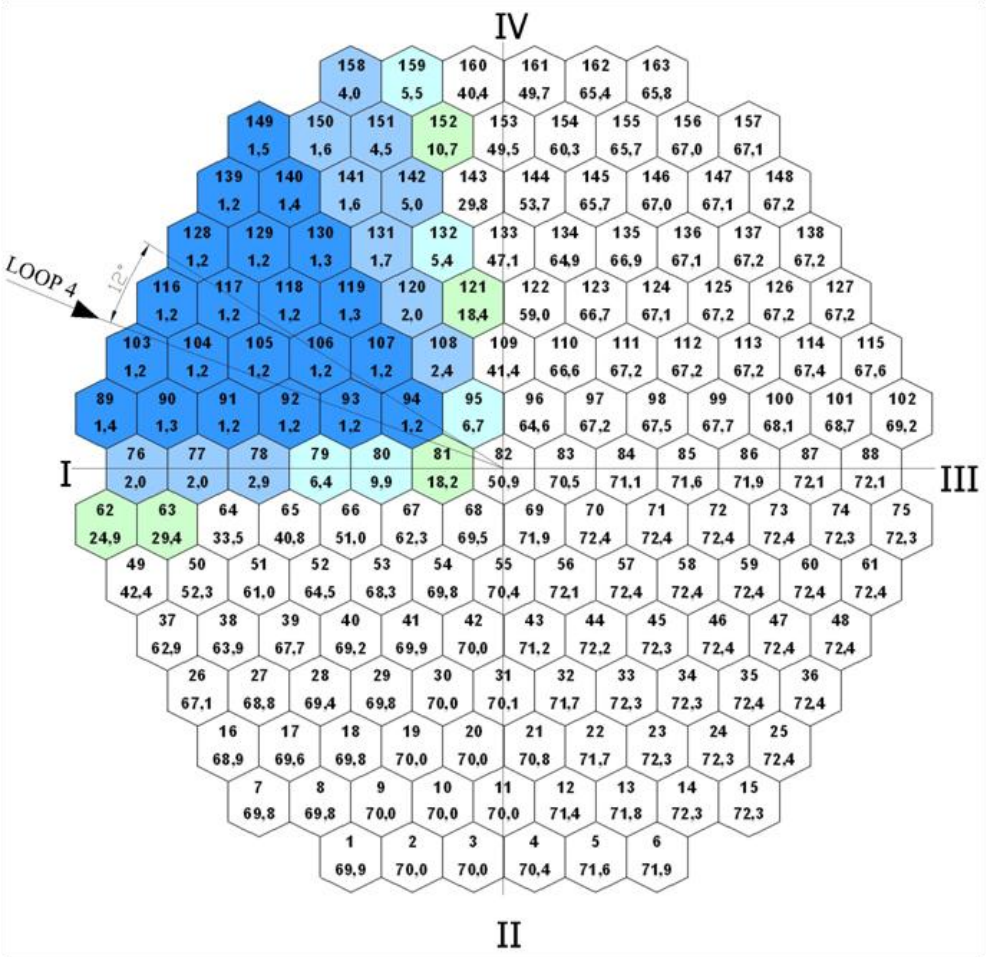


**Figure 4.20: Scenario 2 at time of max overcooling, with stuck rods in #117 and #140: CATHARE2/PKin predicted disturbed sector and angular turn of loop#4 flow centre (ΔTi = Tin, i – T cold leg 4, i =1,...,163)**

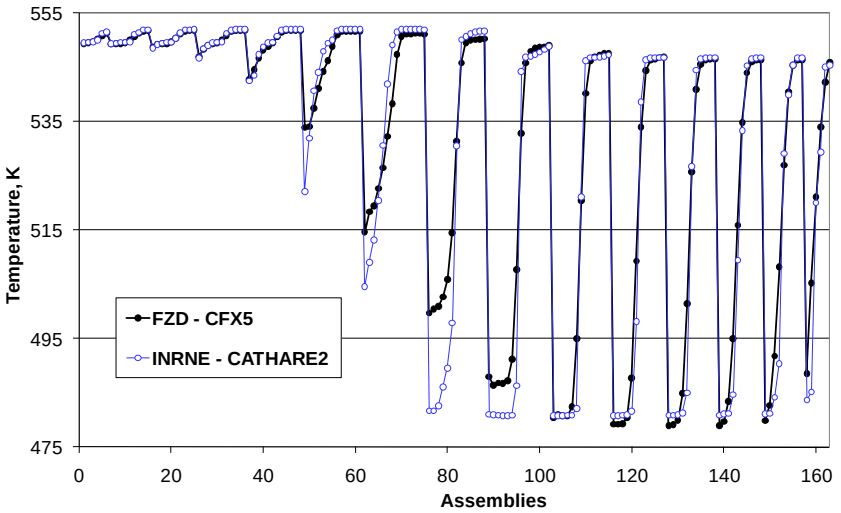


**Figure 4.21: Scenario 2 at time of max overcooling, with stuck rods in #117 and #140: CATHARE2 vs. CFX calculated assembly-by-assembly core inlet temperatures. CATHARE 24-sector vessel model used**

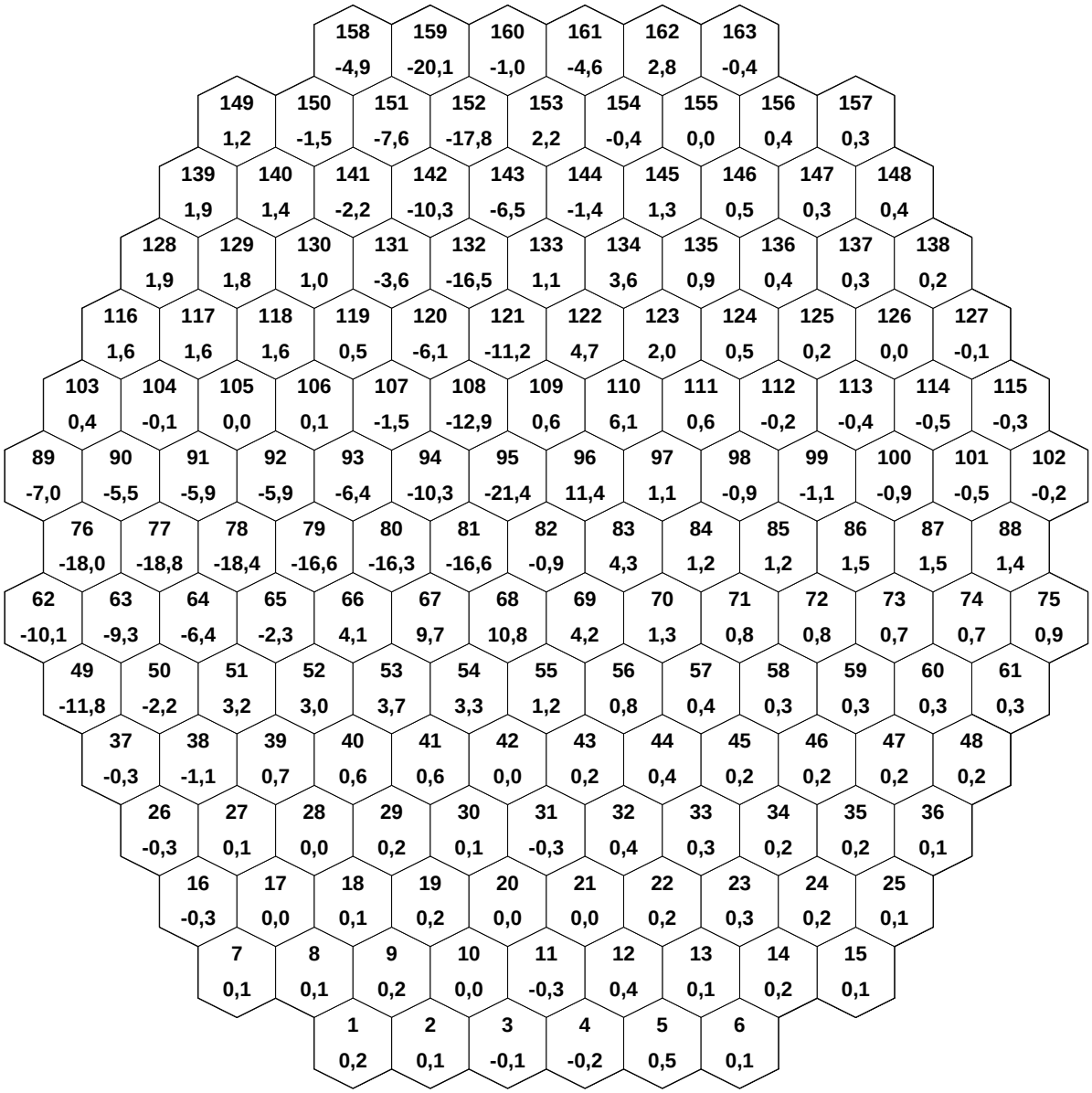


**Figure 4.22: MSLB Scenario 2 at time of max overcooling, with stuck rods in #117 and #140: Differences between the CATHARE and CFX predicted assembly inlet temperatures (ΔT = Tin – Tin, ref)**

# Chapter 5: Results of Exercise 2

This chapter presents the results of Exercise 2 of the VVER-1000 MSLB Benchmark. The coupled 3D neutronics/TH codes were tested in the following sequence of calculations:

- Hot zero power (HZP) states, as defined in Section 5.1
- Initial hot full power (HFP) steady state
- Transient

The steady state problems allow all standard steady state nodal calculations, from clean tests to simple coupled N/TH calculations.

Six complete solutions and additional partial solutions for separate steps were submitted. Section 5.1 shows HZP results of the evaluation of standalone nodal neutronics models and solvers. Section 5.2 shows HFP results from coupled calculations. Section 5.3 presents the transient results.

## 5.1 HZP results

Table 5.1 shows the steady states to be calculated. The parameters of the zero power states are as follows: total power of 300 kW, fuel/moderator temperature of 279.15°C (552.15 K) and moderator density of 766.5 kg/m$^3$.

This section discusses the comparison of Keff, rod worth, peaking factors and axial core power distributions. Appendix A illustrates the two-dimensional distributions and their deviations from the mean.

**Table 5.1: Definition of the steady states**

| State no. | TH conditions | Control rod positions | Scenario |
|---|---|---|---|
| 0 | HZP | Groups 1-10 ARO$^+$ | 1 |
| 1a | HZP (near critical) | Groups 1-5 out, 6 - 81% wd, 7-10 in | 1 |
| 1b | HZP | Groups 1-10 ARI | 1 |
| 2 | HFP | Groups 1-9 ARO Group 10 is 80% wd | 1 |
| 3 | HZP | Groups 1-10 ARI, #90 is 100% wd | 1 |
| 4 | HZP | Groups 1-10 ARI, #63 is 100% wd | 1 |
| 5 | HZP | Groups 1-10 ARI, #140 is 100% wd | 2 |
| 6 | HZP | Groups 1-10 ARI, #140 and #117 100% wd | 2 |

ARO – all rods out, ARI – all rods in

The comparison in the sequel shows that the submitted HZP results cluster in two groups: one including DYN3D, PARCS, CRONOS2 and COBAYA3 results, and another consisting of NEM and HEXTRAN results. The two groups differ in Keff and the core power distributions, the differences being of systematic nature, with maximal discrepancies of up to 13-15%. Similar clustering appears in the results of V1000CT-1

benchmark (Ivanov et al, 2006b). It is due to the properties of the considered nodal flux approximations. NEM and HEXTRAN solvers use polynomial nodal expansion methods without node subdivision. The results indicate that they need some improvements to produce converged solutions for large hexagonal nodes and regions of steep gradients.

Because of this clustering, we consider two comparisons: (a) with the mean of all codes results used as 'reference' solution, and (b) with the mean of DYN3D, PARCS, CRONOS and COBAYA solutions as reference. CRONOS $2^{nd}$-order finite-element solutions with 24 nodes/triangles per hexagon (24N) also serve as reference.

In the discussion to follow, reference is the mean result of all codes unless explicitly stated otherwise.

*HZP state 0*

All control rod groups are out of the core (ARO).

Tables 5.2 and 5.3 show the computed Keff and peaking factors, along with the deviations from the mean. The finer-mesh CRONOS 24N and COBAYA 24N results tend to converge to the same solution. The coarse-mesh results are in good agreement and are close to the mean and the 24N solutions.

Figure 5.1 shows the computed axial power distributions. The results of DYN3D, PARCS, CRONOS and COBAYA are in excellent agreement. The NEM and HEXTRAN results show certain deviations, which are larger in the upper part of the core. The relative deviation in Fz is +6% for HEXTRAN and -5.5% for NEM. These discrepancies are due to differences in the reflector modeling and the neutronics models as applied to large hexagonal nodes.

Figure 5.2 presents the mean of all codes solutions and the standard deviations.

Figures A.1-A.6 in Appendix A show 2D maps with the computed radial power distribution vs. mean of DYN3D, PARCS, CRONOS 6N and COBAYA 6N solutions. The individual DYN3D, PARCS, CRONOS 6N and COBAYA 6N results are in very good agreement with the mean values (max relative deviation of 0.6%, PARCS). The finer-mesh CRONOS 24N and COBAYA 24N solutions tend to converge to the same solution.

The maximal systematic deviation in the NEM computed radial power distribution is 13% and that of the HEXTRAN solution is up to 15%.

*HZP state 1a*

The reactor is near critical. Control rod groups 1-5 are fully withdrawn. Group number 6 is 81% withdrawn and groups 7-10 are fully inserted. The rodded assemblies are marked in blue in the core maps (see Figures A.7 - A.12).

Tables 5.4 and 5.5 show the participants results for $K_{eff}$ and the peaking factors, in comparison with the mean. HEXTRAN results are not available because of incorrectly filled submittal template.

The peaking factors predicted by DYN3D, PARCS, CRONOS 6N and COBAYA 6N are in very good agreement with the mean. The NEM computed Fxy differs by 3.4%.

Figure 5.3 shows a very good agreement of the predicted core average axial power distributions for all codes, except the NEM solution for which the relative difference in Fz to the mean of all codes is 4.6%.

*HZP state 1b*

All control rod groups are fully inserted (ARI).

Tables 5.6 and 5.7 show the comparison of the computed Keff and peaking factors. The results of DYN3D, PARCS, CRONOS and COBAYA are in very good agreement. The NEM results differ from the mean of the above four codes by -216 pcm in Keff, 8.24% in Fxy and – 10.57% in Fz.

Figure 5.5 shows a good agreement of the axial core power distributions for DYN3D, PARCS, CRONOS and COBAYA.

Figures A.13-A.18 in Appendix A show 2D maps with the computed radial power distribution vs. mean of DYN3D, PARCS, CRONOS 6N and COBAYA 6N solutions. The individual DYN3D, PARCS, CRONOS 6N and COBAYA 6N results are in very good agreement with the mean.

*HZP state 3*

HZP states 3 and 4 are similar stuck rods states with different locations of the stuck rods. For this analysis, we consider only HZP state 3. All control rods are fully inserted except the one in assembly #90 which is fully withdrawn.

Table 5.8 presents the results for Keff and the peaking factors compared with the mean value of DYN3D, PARCS, CRONOS 6N and COBAYA 6N solutions. Table 5.9 gives the deviations from the mean of all codes results. Table 5.10 shows the tripped and stuck rods worth in comparison with the CRONOS 24N solution.

Figure 5.7 shows the computed axial power distributions. Figures A.19-A.23 in Appendix A show 2D maps with the computed radial power distribution vs. mean of DYN3D, PARCS, CRONOS 6N and COBAYA 6N solutions.

The comparison shows that the results of DYN3D, PARCS, CRONOS 6N and COBAYA 6N are in very good agreement, and those of NEM have systematic deviations. The NEM result differs from the mean by -99 pcm in Keff, 6.46% in Fxy and -8.9% in Fz.

*HZP state 5*

All control rods are fully inserted, except the rod in #140 which is fully withdrawn. This calculation uses the XS library for Scenario 2.

Table 5.11 shows the computed Keff and peaking factors and the deviations from the reference. Figure 5.9 illustrates the computed axial power distributions. Figure A.29 in Appendix A shows a comparison CRONOS 6N and COBAYA 6N solutions.

The coarse-mesh COBAYA and CRONOS results are in very good agreement – with each other and with the reference. The NEM results differ from the mean by -251 pcm in Keff, 7.3% in Fxy and -6% in Fz.

*HZP state 6*

All control rods are fully inserted except the rods in #117 and #140 which are fully withdrawn. This analysis includes calculations with the XS libraries for Scenario 1 and 2.

The results in Tables 5.12 and 5.13, and Figure 5.11, obtained with the XS library for the realistic Scenario 1 show a very good code-to-code agreement for DYN3D, PARCS, COBAYA3 and CRONOS2 results.

Table 5.14 gives a comparison of the computed Keff and peaking factors, using XS library for Scenario 2. The COBAYA and CRONOS results are close to each other and in good agreement with the mean.

Figure 5.12 presents the predicted core averaged axial power distributions and the standard deviation. The CRONOS and COBAYA solutions are in good agreement with the reference. The NEM solution shows certain deviations, similar to those observed in the other calculated states.

Figure A.30 shows a code-to-code CRONOS and COBAYA comparison of the computed radial power distributions. The solutions are in good agreement, with a maximum deviation in the order of 3% in the vicinity of stuck rods.

**Table 5.2: Computed parameters in HZP state 0 and deviations from the mean of four codes**

| Code/Parameter | $k_{eff}$ | $\delta k_{eff}$, pcm | $F_{xy}$ | $\delta F_{xy}$,% | $F_z$ | $\delta F_z$,% | AO |
|---|---|---|---|---|---|---|---|
| **VTT HEXTRAN** | 1.03480 | 474 | 1.258 | -6.08 | 3.071 | 3.94 | 0.820 |
| **FZD DYN3D** | 1.02988 | -4 | 1.337 | -0.19 | 2.949 | -0.19 | 0.803 |
| **UNIPI NEM** | 1.02821 | -166 | 1.284 | -4.14 | 2.786 | -5.70 | 0.772 |
| **FZK PARCS** | 1.02986 | -6 | 1.341 | 0.11 | 2.957 | 0.08 | 0.805 |
| **INRNE CRONOS 6N** | 1.02989 | -3 | 1.341 | 0.11 | 2.954 | -0.02 | N/A |
| **INRNE CRONOS 24N** | 1.02996 | 4 | 1.339 | -0.04 | 2.951 | -0.12 | N/A |
| **INRNE/UPM COBAYA 6N** | 1.03006 | 13 | 1.339 | -0.04 | 2.958 | 0.12 | 0.805 |
| **INRNE/UPM COBAYA 24N** | 1.03003 | 10 | 1.340 | 0.04 | 2.962 | 0.25 | 0.806 |
| **Reference*** | 1.02992 | | 1.340 | | 2.955 | | N/A |

**Reference* = mean of PARCS, DYN3D, CRONOS 6N and COBAYA 6N**

**Table 5.3: Computed parameters in HZP state 0 and deviations from the mean of all codes**

| Code/Parameter | $k_{eff}$ | $\delta k_{eff}$, pcm | $F_{xy}$ | $\delta F_{xy}$,% | $F_z$ | $\delta F_z$,% | AO |
|---|---|---|---|---|---|---|---|
| **VTT HEXTRAN** | 1.03480 | 433 | 1.258 | -4.87 | 3.071 | 4.15 | 0.820 |
| **FZD DYN3D** | 1.02988 | -44 | 1.337 | 1.11 | 2.949 | 0.02 | 0.803 |
| **UNIPI NEM** | 1.02821 | -206 | 1.284 | -2.9 | 2.786 | -5.51 | 0.772 |
| **FZK PARCS** | 1.02986 | -46 | 1.341 | 1.41 | 2.957 | 0.29 | 0.805 |
| **INRNE CRONOS 6N** | 1.02989 | -43 | 1.341 | 1.41 | 2.954 | 0.19 | N/A |
| **INRNE CRONOS 24N** | 1.02996 | -37 | 1.339 | 1.26 | 2.951 | 0.08 | N/A |
| **INRNE/UPM COBAYA 6N** | 1.03006 | -27 | 1.339 | 1.26 | 2.958 | 0.32 | 0.805 |
| **INRNE/UPM COBAYA 24N** | 1.03003 | -30 | 1.340 | 1.33 | 2.962 | 0.46 | 0.806 |
| **Reference** | 1.03034 | | 1.322 | | 2.949 | | N/A |
| **Standard deviation** | 0.00190 | | 0.03249 | | 0.07727 | | N/A |

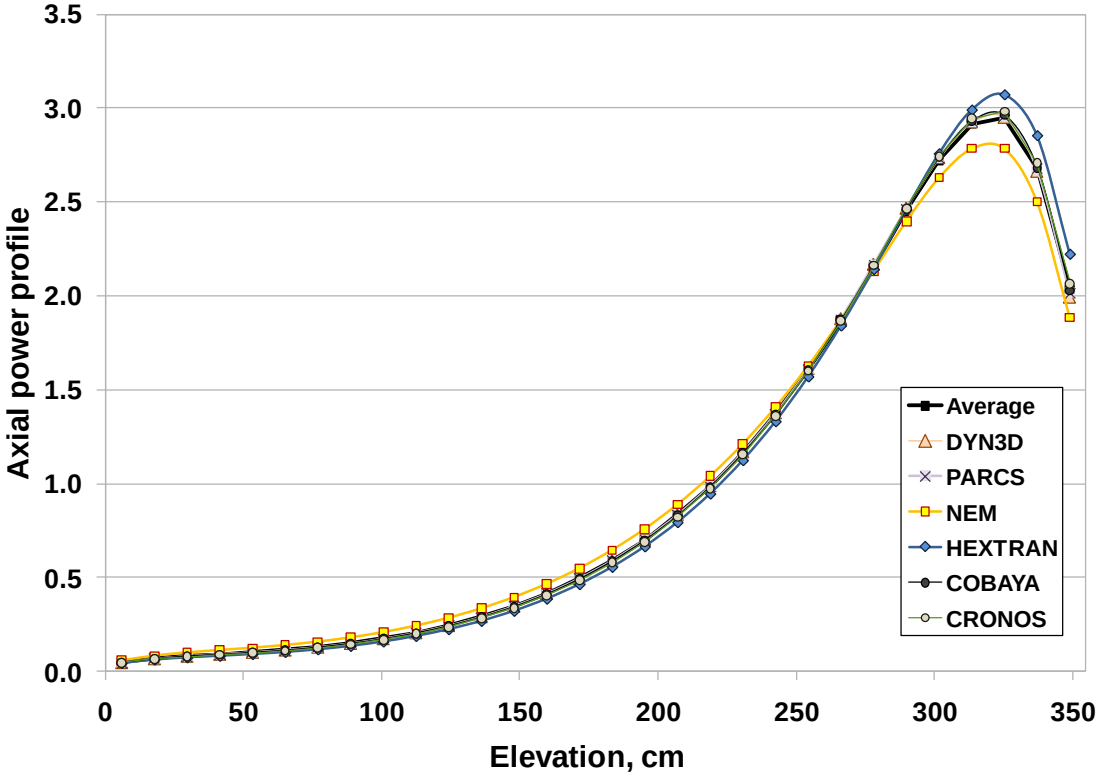


**Figure 5.1: Core-averaged axial power distribution in HZP state 0**

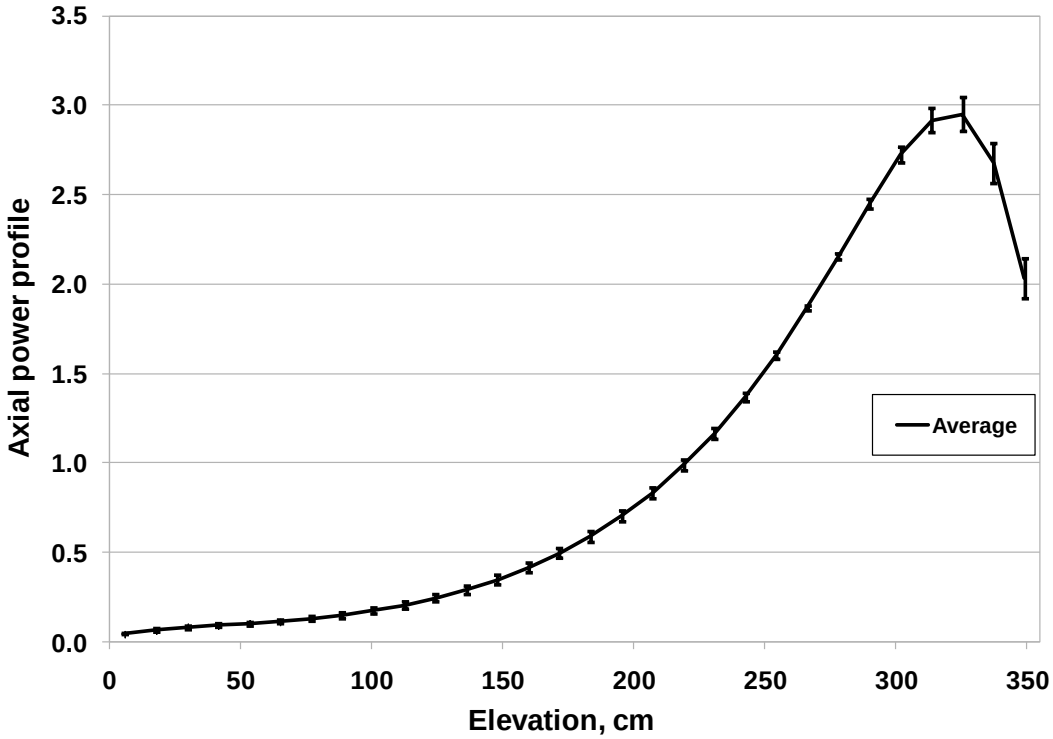


**Figure 5.2: Core-averaged axial power distribution in HZP state 0 (mean of all codes and standard deviation)**

**Table 5.4: Computed parameters in HZP state 1a and deviations from the mean of four codes**

| Code/Parameter | $k_{eff}$ | $\delta k_{eff}$, pcm | $F_{xy}$ | $\delta F_{xy}$,% | $F_z$ | $\delta F_z$,% | AO |
|---|---|---|---|---|---|---|---|
| **FZD DYN3D** | 0.99755 | 1 | 1.416 | 0.11 | 1.863 | -0.25 | 0.481 |
| **UNIPI NEM** | 0.99665 | -90 | 1.463 | 3.43 | 1.791 | -4.11 | 0.455 |
| **FZK PARCS** | 0.99745 | -10 | 1.414 | -0.04 | 1.874 | 0.33 | 0.488 |
| **INRNE CRONOS 6N** | 0.99745 | -10 | 1.410 | -0.32 | 1.863 | -0.25 | N/A |
| **INRNE CRONOS 24N** | 0.99761 | 7 | 1.414 | -0.04 | 1.865 | -0.15 | N/A |
| **INRNE/UPM COBAYA 6N** | 0.99773 | 19 | 1.418 | 0.25 | 1.871 | 0.17 | 0.487 |
| **INRNE/UPM COBAYA 24N** | 0.99764 | 10 | 1.415 | 0.04 | 1.873 | 0.28 | 0.488 |
| **Reference*** | 0.99755 | | 1.415 | | 1.868 | | N/A |

*** Reference = mean of PARCS, DYN3D, CRONOS 6N and COBAYA 6N**

**Table 5.5: Computed parameters in HZP state 1a and deviations from the mean of all codes**

| Code/Parameter | $k_{eff}$ | $\delta k_{eff}$, pcm | $F_{xy}$ | $\delta F_{xy}$,% | $F_z$ | $\delta F_z$,% | AO |
|---|---|---|---|---|---|---|---|
| **FZD DYN3D** | 0.99755 | 11 | 1.416 | -0.38 | 1.863 | 0.32 | 0.481 |
| **UNIPI NEM** | 0.99665 | -79 | 1.463 | 2.92 | 1.791 | -3.56 | 0.455 |
| **FZK PARCS** | 0.99745 | 1 | 1.414 | -0.52 | 1.874 | 0.91 | 0.488 |
| **INRNE CRONOS 6N** | 0.99745 | 1 | 1.410 | -0.80 | 1.863 | 0.32 | N/A |
| **INRNE CRONOS 24N** | 0.99761 | 17 | 1.414 | -0.52 | 1.865 | 0.42 | N/A |
| **INRNE/UPM COBAYA 6N** | 0.99773 | 29 | 1.418 | -0.24 | 1.871 | 0.75 | 0.487 |
| **INRNE/UPM COBAYA 24N** | 0.99764 | 20 | 1.415 | -0.45 | 1.873 | 0.85 | 0.488 |
| **Reference** | 0.99744 | | 1.421 | | 1.857 | | N/A |
| **Standard deviation** | 0.00036 | | 0.01849 | | 0.02953 | | N/A |

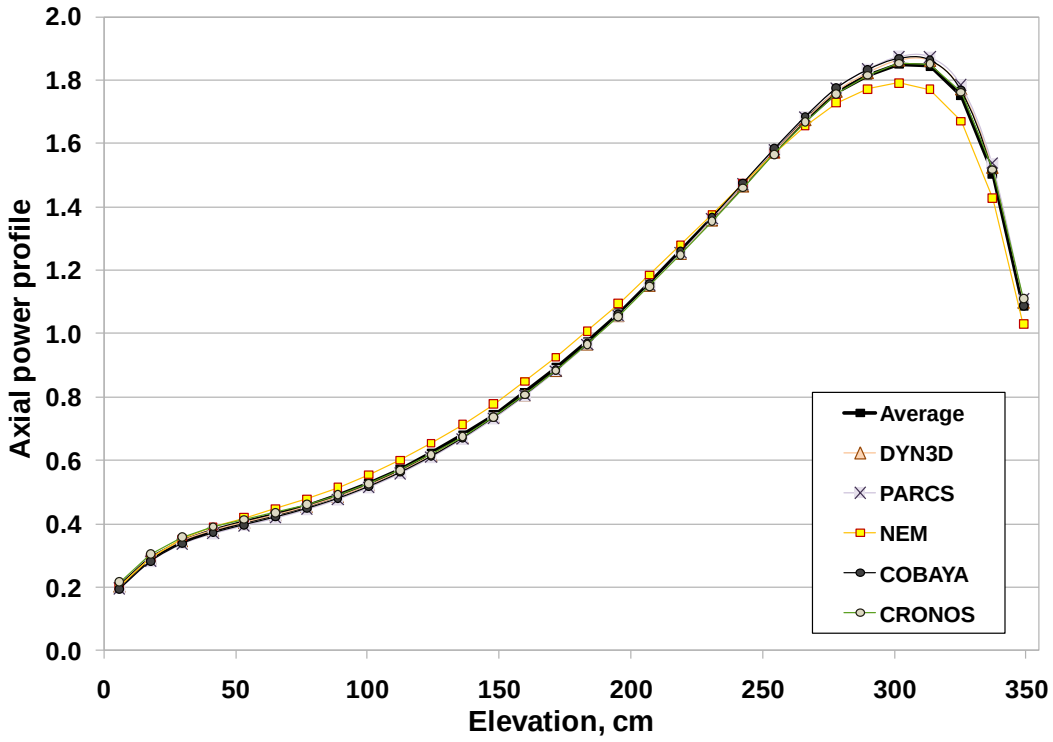


**Figure 5.3: Core-averaged axial power distribution in HZP state 1a**

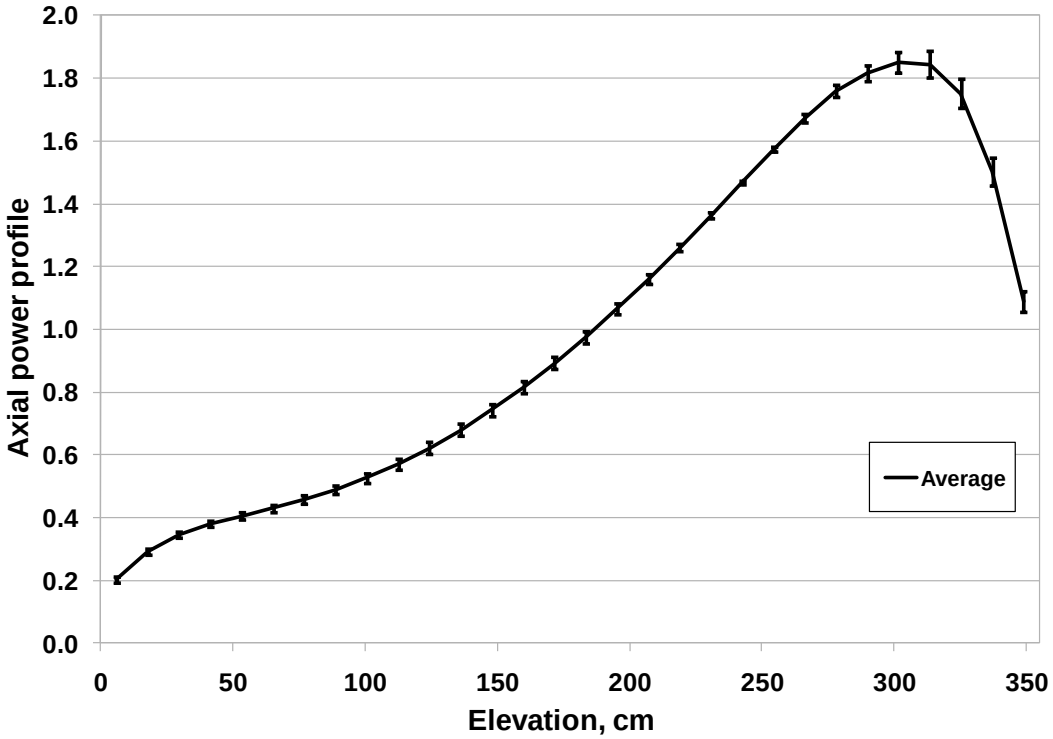


**Figure 5.4: Core-averaged axial power distribution in HZP state 1a: (mean of all codes and standard deviation)**

**Table 5.6: Computed parameters in HZP state 1b and deviations from the mean of four codes**

| Code/Parameter | $k_{eff}$ | $\delta k_{eff}$, pcm | $F_{xy}$ | $\delta F_{xy}$,% | $F_z$ | $\delta F_z$,% | AO |
|---|---|---|---|---|---|---|---|
| **FZD DYN3D** | 0.96213 | 8 | 1.383 | -0.07 | 2.342 | 0.35 | 0.481 |
| **UNIPI NEM** | 0.95997 | -216 | 1.498 | 8.24 | 2.087 | -10.57 | 0.455 |
| **FZK PARCS** | 0.96192 | -14 | 1.387 | 0.22 | 2.338 | 0.18 | 0.488 |
| **INRNE CRONOS 6N** | 0.96192 | -14 | 1.378 | -0.43 | 2.33 | -0.16 | N/A |
| **INRNE CRONOS 24N** | 0.96210 | 5 | 1.384 | 0.00 | 2.322 | -0.50 | N/A |
| **INRNE/UPM COBAYA 6N** | 0.96223 | 19 | 1.388 | 0.29 | 2.325 | -0.37 | 0.487 |
| **INRNE/UPM COBAYA 24N** | 0.96216 | 11 | 1.383 | -0.07 | 2.334 | 0.01 | 0.488 |
| **Reference*** | 0.96205 | | 1.384 | | 2.334 | | N/A |

*** Reference = mean of PARCS, DYN3D, CRONOS 6N and COBAYA 6N**

**Table 5.7: Computed parameters in HZP state 1b and deviations from the mean of all codes**

| Code/Parameter | $k_{eff}$ | $\delta k_{eff}$, pcm | $F_{xy}$ | $\delta F_{xy}$,% | $F_z$ | $\delta F_z$,% | AO |
|---|---|---|---|---|---|---|---|
| **FZD DYN3D** | 0.96213 | 37 | 1.383 | -1.22 | 2.342 | 4.51 | 0.481 |
| **UNIPI NEM** | 0.95997 | -188 | 1.498 | 6.99 | 2.087 | -20.99 | 0.455 |
| **FZK PARCS** | 0.96192 | 15 | 1.387 | -0.94 | 2.338 | 4.11 | 0.488 |
| **INRNE CRONOS 6N** | 0.96192 | 15 | 1.378 | -1.58 | 2.33 | 3.31 | N/A |
| **INRNE CRONOS 24N** | 0.96210 | 34 | 1.384 | -1.15 | 2.322 | 2.51 | N/A |
| **INRNE/UPM COBAYA 6N** | 0.96223 | 47 | 1.388 | -0.87 | 2.325 | 2.81 | 0.487 |
| **INRNE/UPM COBAYA 24N** | 0.96216 | 40 | 1.383 | -1.22 | 2.334 | 3.71 | 0.488 |
| **Reference** | 0.96178 | | 1.400 | | 2.297 | | N/A |
| **Standard deviation** | 0.00080 | | 0.04327 | | 0.09280 | | N/A |

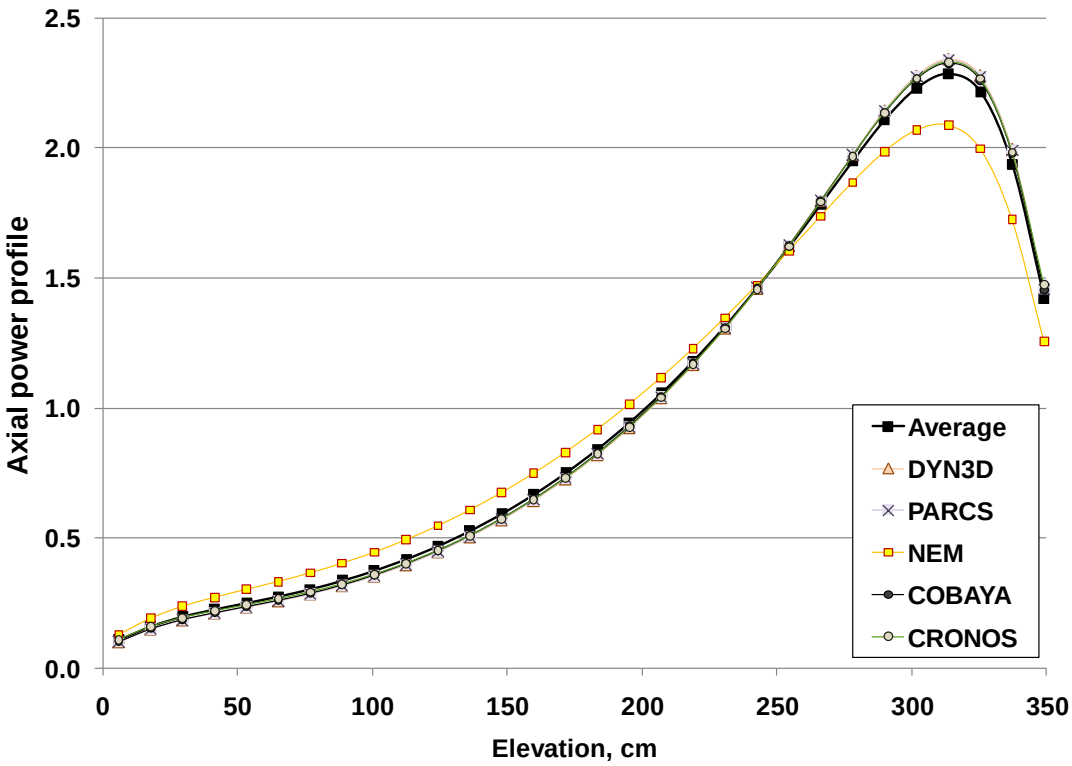


**Figure 5.5: Core-averaged axial power distribution in HZP state 1b**

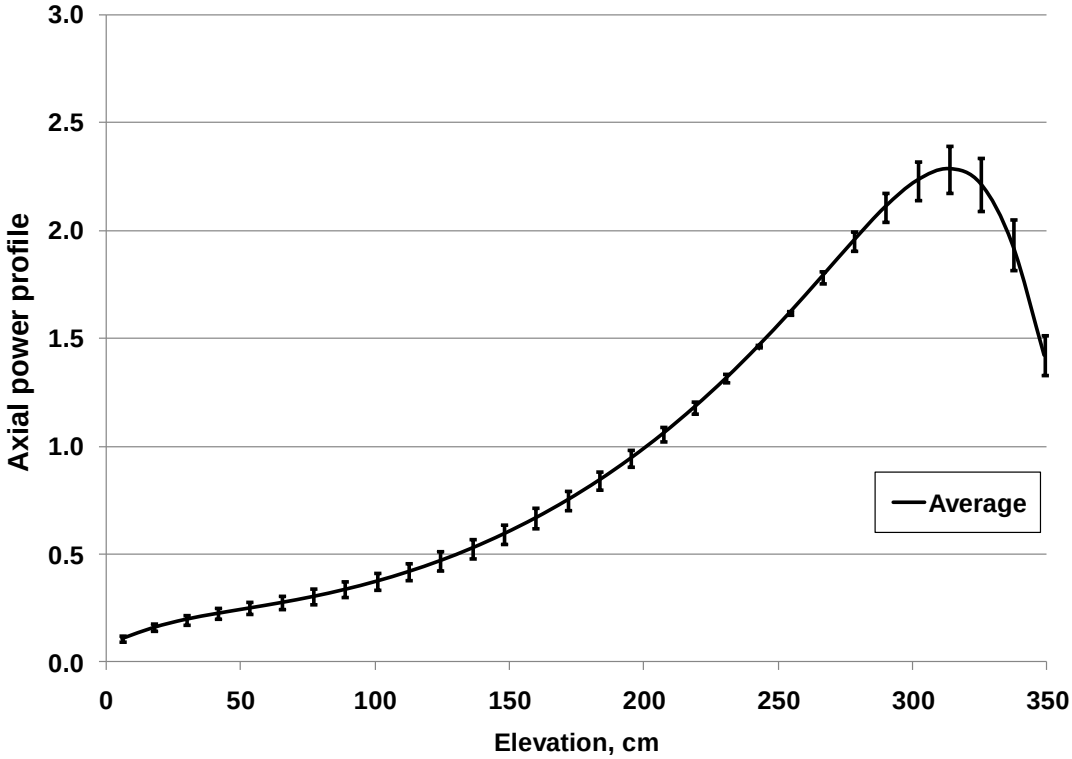


**Figure 5.6: Core-averaged axial power distribution (mean of all codes and standard deviation)**

**Table 5.8: Computed parameters in HZP state 3 and deviations from the mean of four codes. XS library for Scenario 1**

| Code/Parameter | $k_{eff}$ | $\delta k_{eff}$, pcm | $F_{xy}$ | $\delta F_{xy}$,% | $F_z$ | $\delta F_z$,% | AO |
|---|---|---|---|---|---|---|---|
| **FZD DYN3D** | 0.96866 | 7 | 6.470 | -0.32 | 2.12 | 0.49 | 0.481 |
| **UNIPI NEM** | 0.96763 | -99 | 6.910 | 6.46 | 1.922 | -8.90 | 0.455 |
| **FZK PARCS** | 0.96843 | -16 | 6.486 | -0.07 | 2.114 | 0.20 | 0.488 |
| **INRNE//UPM COBAYA 6N** | 0.96884 | 25 | 6.543 | 0.80 | 2.099 | -0.51 | 0.487 |
| **INRNE//UPM COBAYA 24N** | 0.96869 | 10 | 6.490 | -0.01 | 2.108 | -0.08 | 0.488 |
| **INRNE CRONOS 6N** | 0.96843 | -16 | 6.464 | -0.41 | 2.106 | -0.18 | N/A |
| **INRNE CRONOS 24N** | 0.96867 | 8 | 6.501 | 0.16 | 2.098 | -0.56 | N/A |
| **Reference*** | 0.96859 | | 6.491 | | 2.110 | | N/A |

*** Reference = mean of PARCS, DYN3D, CRONOS 6N and COBAYA 6N**

**Table 5.9: Computed parameters in HZP state 3 and deviation from the mean of all codes**

| Code/Parameter | $k_{eff}$ | $\delta k_{eff}$, pcm | $F_{xy}$ | $\delta F_{xy}$,% | $F_z$ | $\delta F_z$,% | AO |
|---|---|---|---|---|---|---|---|
| **FZD DYN3D** | 0.96866 | 19 | 6.47 | -1.25 | 2.12 | 1.87 | 0.481 |
| **UNIPI NEM** | 0.96763 | -88 | 6.91 | 5.46 | 1.922 | -7.64 | 0.455 |
| **FZK PARCS** | 0.96843 | -5 | 6.486 | -1.01 | 2.114 | 1.59 | 0.488 |
| **INRNE/UPM COBAYA 6N** | 0.96884 | 37 | 6.543 | -0.14 | 2.099 | 0.86 | 0.487 |
| **INRNE//UPM COBAYA 24N** | 0.96869 | 22 | 6.49 | -0.95 | 2.108 | 1.30 | 0.488 |
| **CEA CRONOS 6N** | 0.96843 | -5 | 6.464 | -1.34 | 2.106 | 1.20 | N/A |
| **CEA CRONOS 24N** | 0.96867 | 20 | 6.501 | -0.78 | 2.098 | 0.82 | N/A |
| **Reference** | 0.96848 | | 6.552 | | 2.081 | | N/A |
| **Standard deviation** | 0.00040 | | 0.14809 | | 0.06531 | | N/A |

**Table 5.10: Tripped and stuck rods worth. Reference is the CRONOS 24N solution**

| Parameters | Tripped RW, pcm | Scram W, pcm | Stuck RW, pcm |
|---|---|---|---|
| **FZD DYN3D** | -6509 | -6837 | -328 |
| **UNIPI NEM** | -6437 | -6914 | -476 |
| **FZK PARCS** | -6533 | -6858 | -326 |
| **INRNE/UPM COBAYA 6N** | -6509 | -6844 | -335 |
| **INRNE//UPM COBAYA 24N** | -6522 | -6848 | -326 |
| **CEA CRONOS 6N** | -6536 | -6861 | -325 |
| **CEA CRONOS 24N** | -6517 | -6848 | -331 |

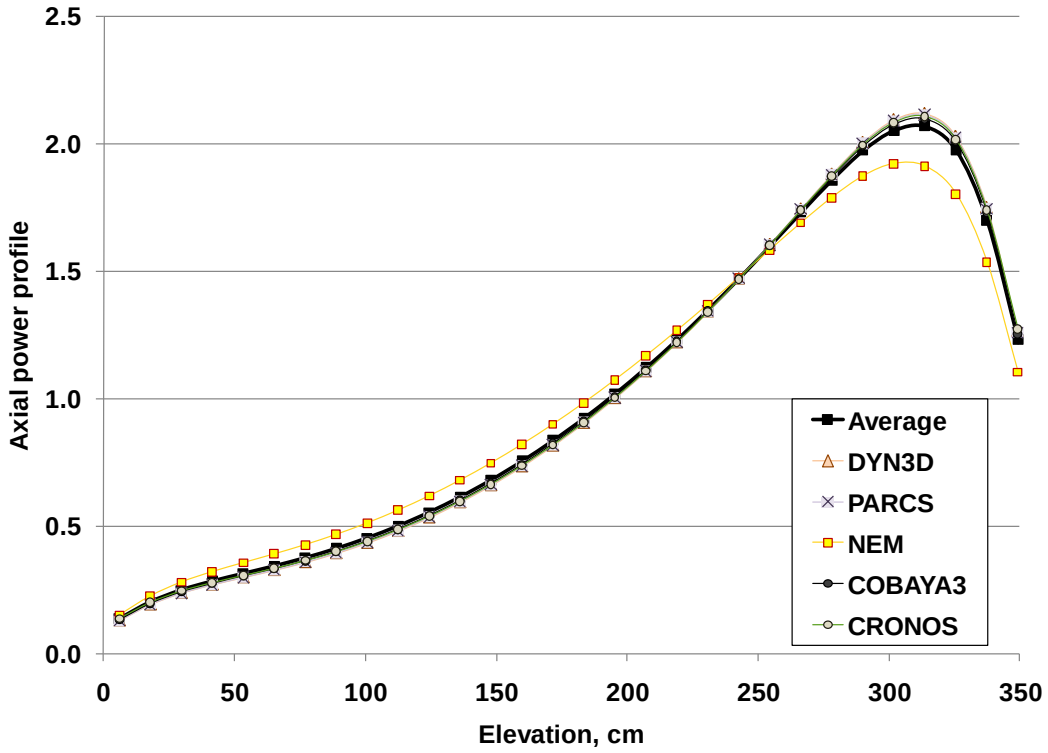


**Figure 5.7: Core-averaged axial power distribution in HZP state 3**

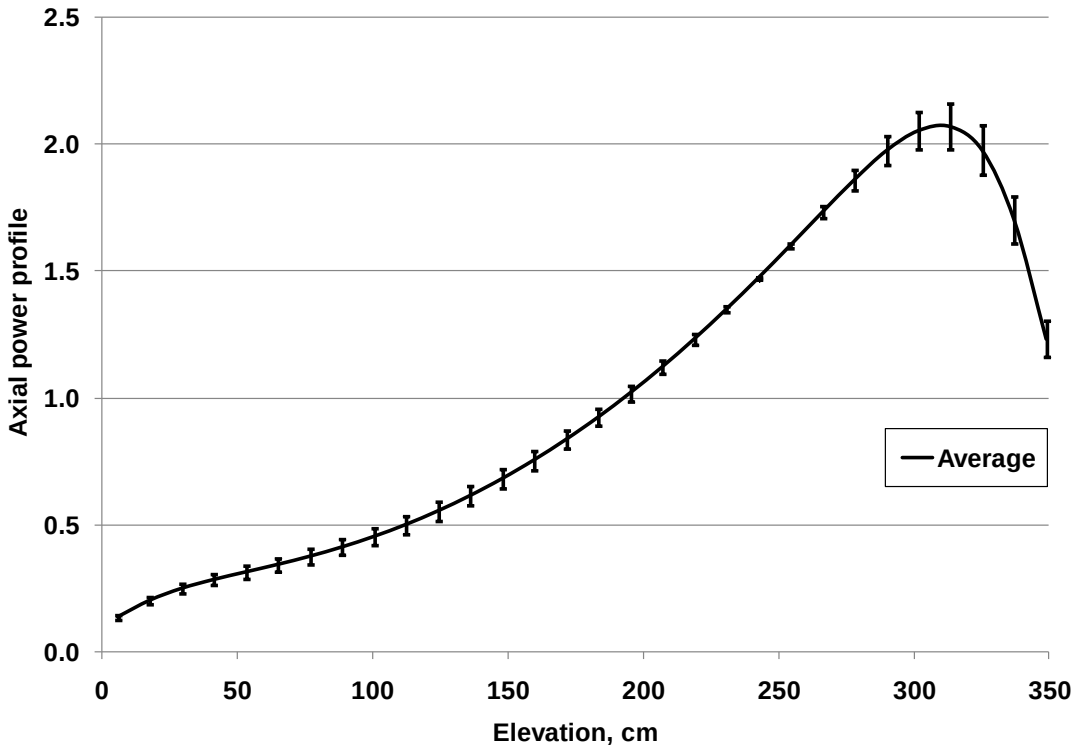


**Figure 5.8: Core-averaged axial power distribution in HZP state 3 (mean of all codes and standard deviation)**

**Table 5.11: Computed parameters in HZP state 5 and deviation from the mean of all codes (XS library for Scenario 2)**

| Code/Parameter | $k_{eff}$ | $\delta k_{eff}$, pcm | $\delta F_{xy}$, | $\delta F_{xy}$,% | $F_z$ | $\delta F_z$,% | AO | Tripped RW, pcm |
|---|---|---|---|---|---|---|---|---|
| UNIPI NEM | 0.99635 | -251 | 2.37 | 7.29 | 2.15 | -6.04 | 0.58 | -3110 |
| INRNE/UPM COBAYA 6N | 0.99977 | 91 | 2.159 | -2.26 | 2.34 | 2.26 | 0.639 | -2922 |
| INRNE/UPM COBAYA 24N | 0.99960 | 74 | 2.148 | -2.76 | 2.334 | 2.00 | N/A | -2958 |
| INRNE CRONOS 6N | 0.99972 | 86 | 2.159 | -2.26 | 2.329 | 1.78 | N/A | -2943 |
| Average | 0.99886 | | 2.209 | | 2.288 | | N/A | |
| Standard deviation | 0.00167 | | 0.10746 | | 0.09228 | | N/A | |

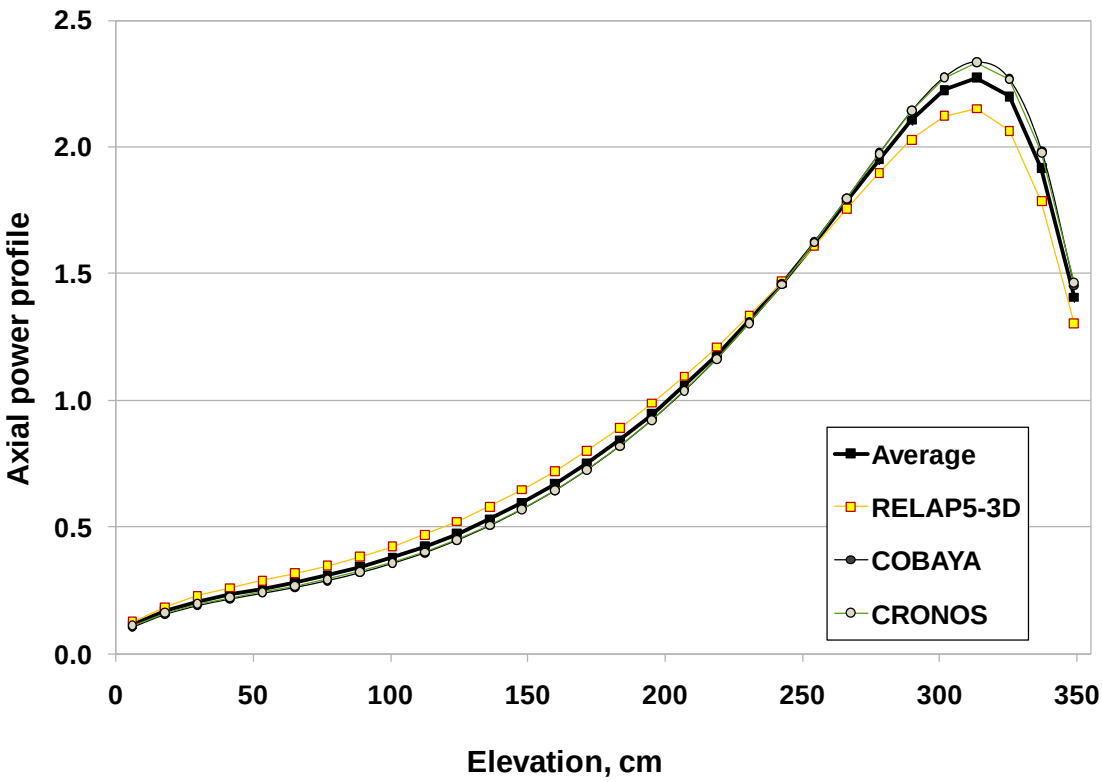


**Figure 5.9: Core averaged axial power distribution in HZP state 5**

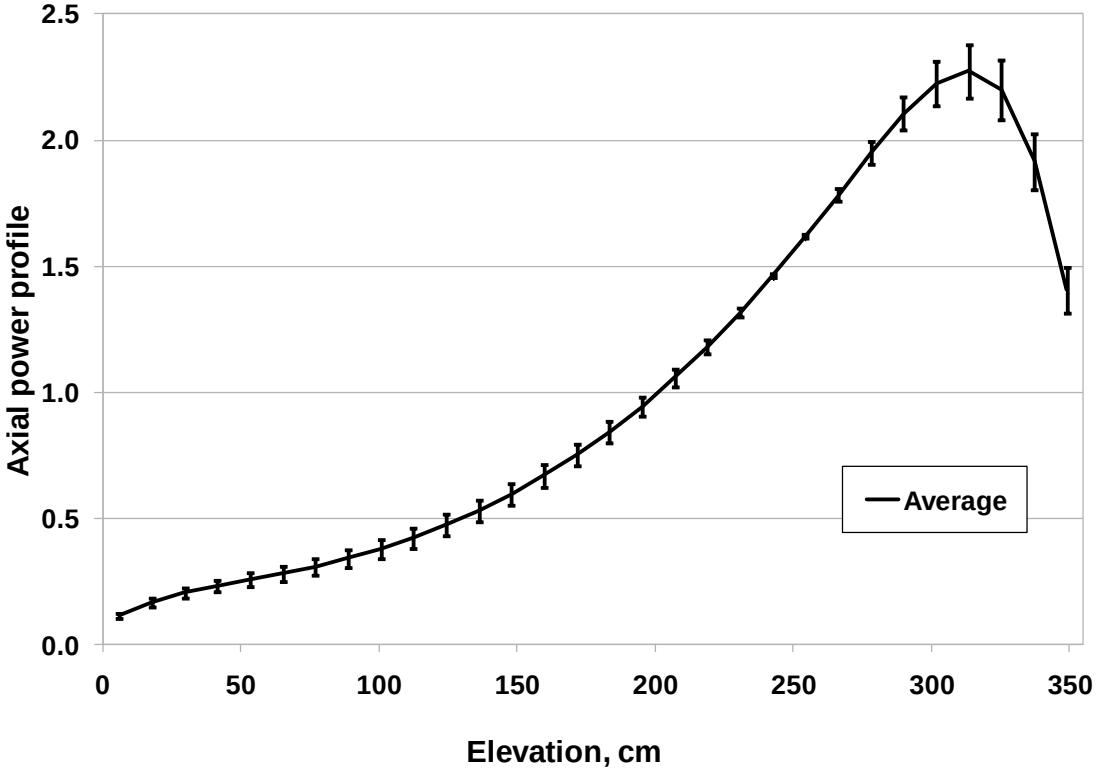


**Figure 5.10: Core averaged axial power distribution in HZP state 5 (mean of all codes and standard deviation)**

**Table 5.12: Computed parameters in HZP state 6 and deviations from the mean of all codes (XS library for Scenario 1)**

| Code/Parameter | $k_{eff}$ | $\delta k_{eff}$, pcm | $F_{xy}$ | $\delta F_{xy}$,% | $F_z$ | $\delta F_z$,% | AO |
|---|---|---|---|---|---|---|---|
| **FZD DYN3D** | 0.97691 | -3 | 8.542 | -0.16 | 2.003 | 0.15 | 0.535 |
| **FZK PARCS** | 0.97667 | -27 | 8.568 | 0.14 | 2.004 | 0.20 | 0.537 |
| **INRNE/UPM COBAYA 6N** | 0.97717 | 24 | 8.575 | 0.22 | 1.993 | -0.35 | 0.533 |
| **INRNE/UPM COBAYA 24N** | 0.97700 | 6 | 8.539 | -0.20 | 2.000 | 0.00 | 0.536 |
| **Mean** | 0.97694 | | 8.556 | | 2.000 | | N/A |
| **Standard deviation** | 0.00021 | | 0.01817 | | 0.00497 | | N/A |

**Table 5.13: Tripped and stuck rods worth (XS library for Scenario 1) Reference is the COBAYA 24N solution**

| Code/Parameter | Tripped RW, pcm | Scram W, pcm | Stuck RW, pcm |
|---|---|---|---|
| **FZD DYN3D** | -5584 | -6837 | -1253 |
| **FZK PARCS** | -5609 | -6858 | -1249 |
| **INRNE/UPM COBAYA 6N** | -5575 | -6844 | -1268 |
| **INRNE/UPM COBAYA 24N** | -5591 | -6848 | -1257 |

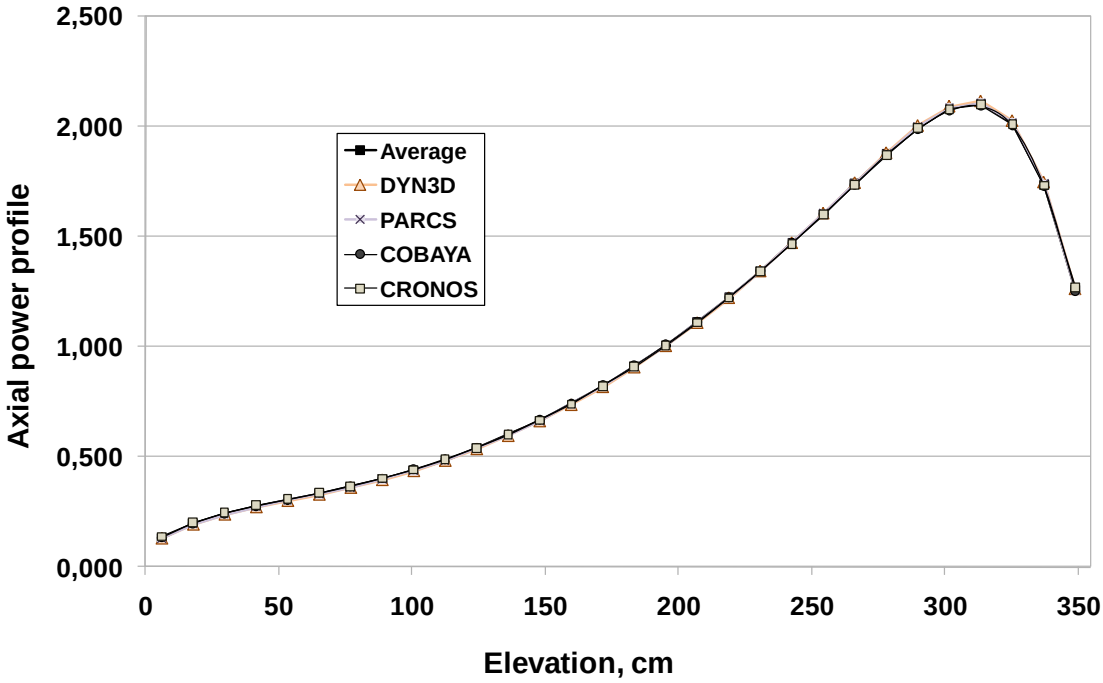


**Figure 5.11: Core averaged axial power distribution in HZP state 6 (XS lib for Sc1)**

**Table 5.14: Computed parameters in HZP state 6 (XS library for Scenario 2)**

| Code/Parameter | $k_{eff}$ | $\delta k_{eff}$, pcm | $\delta F_{xy}$,% | $\delta F_{xy}$ | $F_z$ | $\delta F_z$,% | AO | Tripped RW, pcm |
|---|---|---|---|---|---|---|---|---|
| **UNIPI NEM** | 0.99830 | -220 | 3.535 | 9.51 | 2.124 | -6.15 | 0.572 | -2913 |
| **INRNE/UPM COBAYA 6N** | 1.00133 | 83 | 3.132 | -2.97 | 2.315 | 2.29 | 0.632 | -2783 |
| **INRNE/UPM COBAYA 24N** | 1.00111 | 61 | 3.114 | -3.53 | 2.31 | 2.07 | N/A | -2791 |
| **INRNE CRONOS 6N** | 1.00125 | 75 | 3.131 | -3.00 | 2.304 | 1.80 | N/A | -2784 |
| **Mean** | 1.00050 | | 3.228 | | 2.263 | | N/A | |
| **Standard deviation** | 0.00147 | | 0.20483 | | 0.09294 | | N/A | |

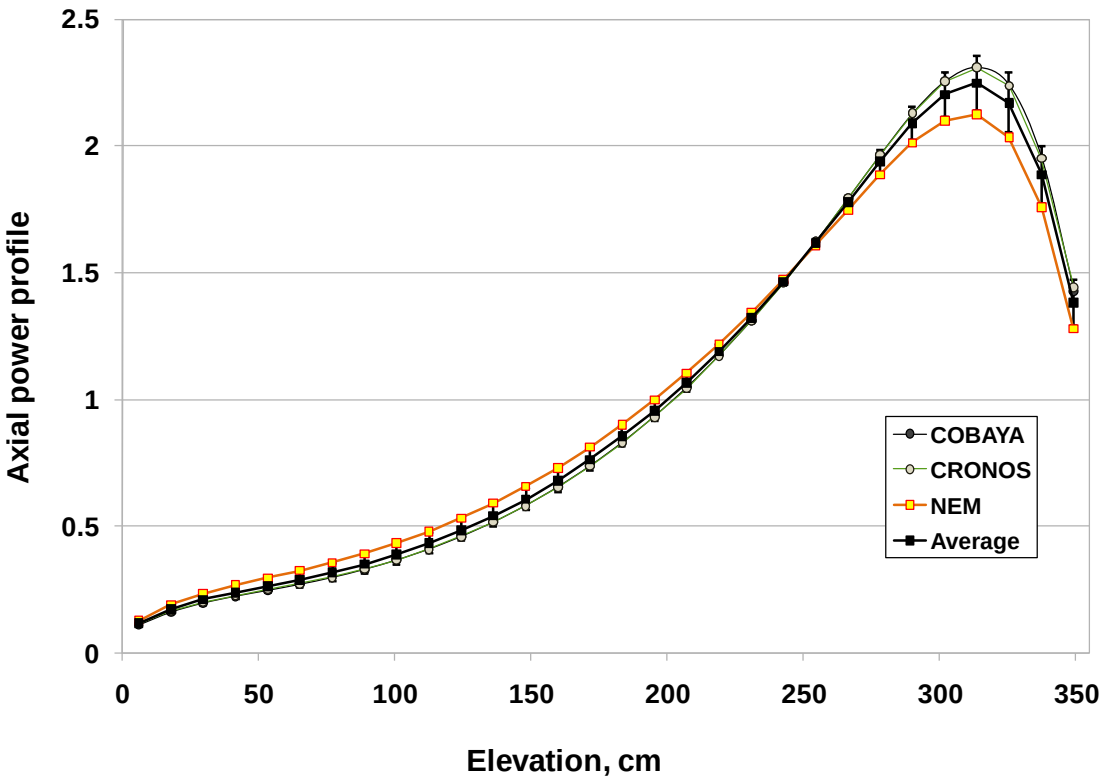


**Figure 5.12: Core-averaged axial power distribution in HZP state 6 (XS lib for Sc2)**

## 5.2 Initial HFP state results

The HFP steady state core parameters are as given in the V1000CT-2 Exercise 2 specification (Kolev et al, 2006). The cross-section library for Scenario 1 is used.

Table 5.15 and Figure 5.13 show a code-to-code comparison of the computed core parameters. The results have been obtained with DYN3D/ATHLET (FZD), CRONOS2/ FLICA4 (INRNE/CEA), COBAYA3/COBRA3 (INRNE/UPM), NEM/RELAP3D (UNIPI) and HEXTRAN/SMABRE (VTT) codes, using modeling assumptions as described in Appendix G. Reference is the mean result of all codes.

The CRONOS and COBAYA nodal flux solvers used subdivision to 6 triangles/nodes per hexagon. FLICA4 and COBRA3 used one point per hexagon. CATHARE2 calculated thermal-hydraulic boundary conditions were imposed on the core, using a 24-sector mapping scheme.

The DYN3D, NEM and HEXTRAN nodal solvers used one point per hexagon. In the NEM/RELAP3D calculation the core boundary conditions were obtained through a detailed mapping scheme with 60 channels in the upper part of the lower plenum. In the HEXTRAN/SMABRE and DYN3D/ATHLET calculations, coarse-mesh mapping schemes were used.

The CRONOS/FLICA, COBAYA/COBRA and NEM/RELAP3D results for Keff are in good agreement with the reference. The HEXTRAN/SMABRE result differs by + 380 pcm and the DYN3D/ATHLET result shows a difference of -351 pcm, most of which can be attributed to the fuel gap conductance model and the spatial N/TH coupling.

The maximum difference in Fxy and Fz (to the mean of all codes) is -1.36% and -3.02% respectively. The discrepancies are mainly due to differences in the core and the vessel thermal hydraulic models, leading to differences in the temperatures at the core inlet and in the core.

Figures 5.15-5.19 present the coupled code computed relative assembly powers, in comparison with the mean. The DYN3D/ATHLET and COBAYA/COBRA3 solutions are close to each other despite the differences in the spatial coupling. In these solutions, the differences in fuel Doppler temperature (see Appendix B) are relatively uniform and affect mainly Keff (see T|able 5.15). Because of the observed clustering of the solutions, there is a significant spread around the mean of all codes: up to 7.2% for HEXTRAN/SMABRE and up to 4.9% for the other codes.

Appendix B documents details of the code-to-code comparison of 2D maps and graphs displaying the assembly-by-assembly Doppler temperatures and core inlet parameters.

In order to separate the effects, the benchmark team performed a systematic code-to-code comparison using the same core inlet BC for each pair of codes. The COBAYA3/COBRA3 solution served as reference. The results in Tables 5.16 and 5.17, and Figures B.5, B.7 and B.11-B.13 show that

- CRONOS2/FLICA4 and PSU PARCS/TRACE results are in good agreement with the COBAYA3/COBRA3 results
- DYN3D/ATHLET and HEXTRAN/SMABRE results are in good agreement with the COBAYA3/COBRA3 predicted peaking factors, but give a δk of 320-410 pcm due to differences in the neutronics solver and the computed Doppler temperature

**Table 5.15: Computed HFP state parameters**

| Code/Parameter | Keff | Δk, pcm | $F_{xy}$ | $\delta F_{xy}$,% | $F_z$ | $\delta F_z$,% | AO |
|---|---|---|---|---|---|---|---|
| VTT HEXTRAN/SMABRE | 1.00210 | 380 | 1.303 | 1.04 | 1.187 | 1.78 | N/A |
| FZD DYN3D/ATHLET | 0.99481 | -351 | 1.283 | -0.96 | 1.18 | 1.08 | -0.050 |
| UNIPI NEM/RELAP3D | 0.99800 | -31 | 1.303 | 1.04 | 1.139 | -3.02 | -0.028 |
| INRNE/UPM COBAYA/COBRA | 0.99823 | -8 | 1.279 | -1.36 | 1.177 | 0.78 | -0.048 |
| INRNE/CEA CRONOS/FLICA | 0.99841 | 10 | 1.295 | 0.24 | 1.163 | -0.62 | N/A |
| Reference | 0.99831 | | 1.293 | | 1.169 | | |
| Standard deviation | 0.0026 | | 0.0112 | | 0.0190 | | |

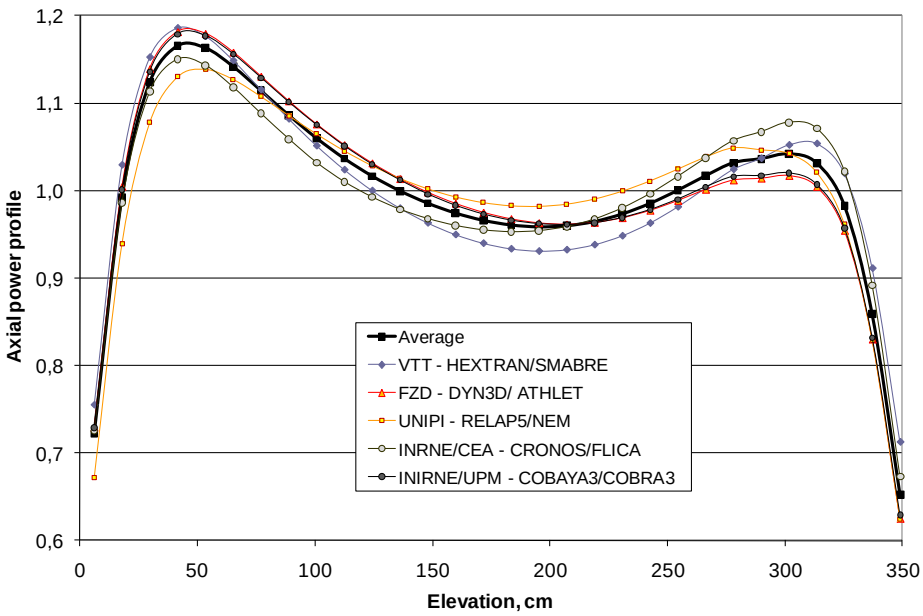


**Figure 5.13: Computed core average axial power distributions in the HFP state**

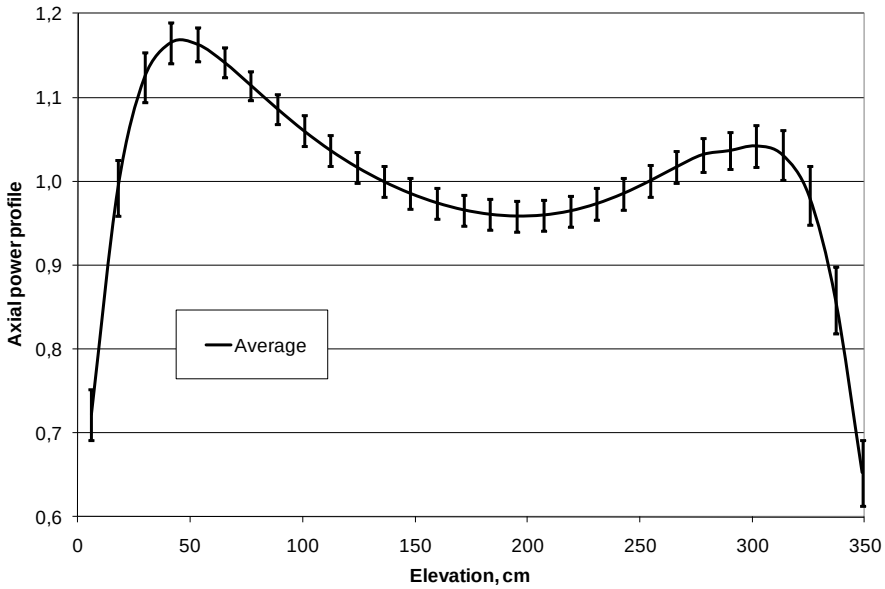


**Figure 5.14: Computed core average axial power distributions in the initial HFP steady state (mean of all codes and standard deviation)**

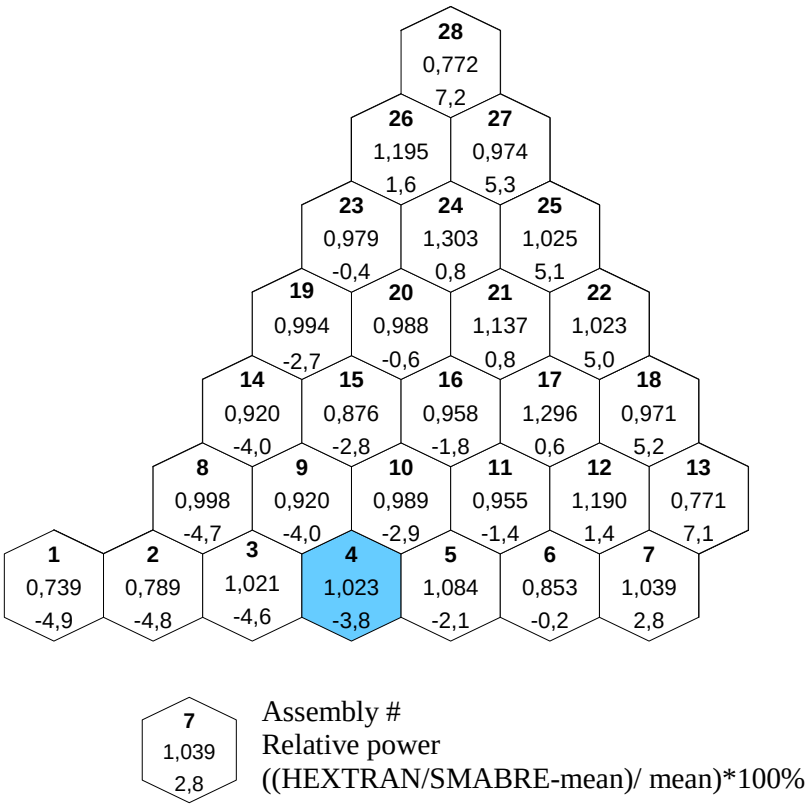


**Figure 5.15: HEXTRAN/SMABRE computed assembly powers vs. mean of all codes in the initial HFP state**

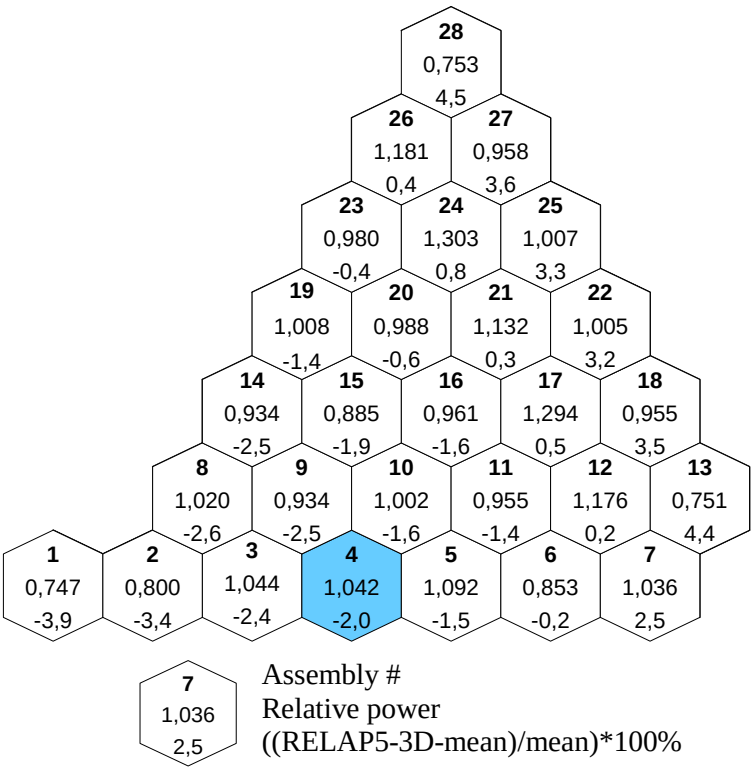


**Figure 5.16: NEM/RELAP3D computed assembly powers vs. mean of all codes in the initial HFP state**

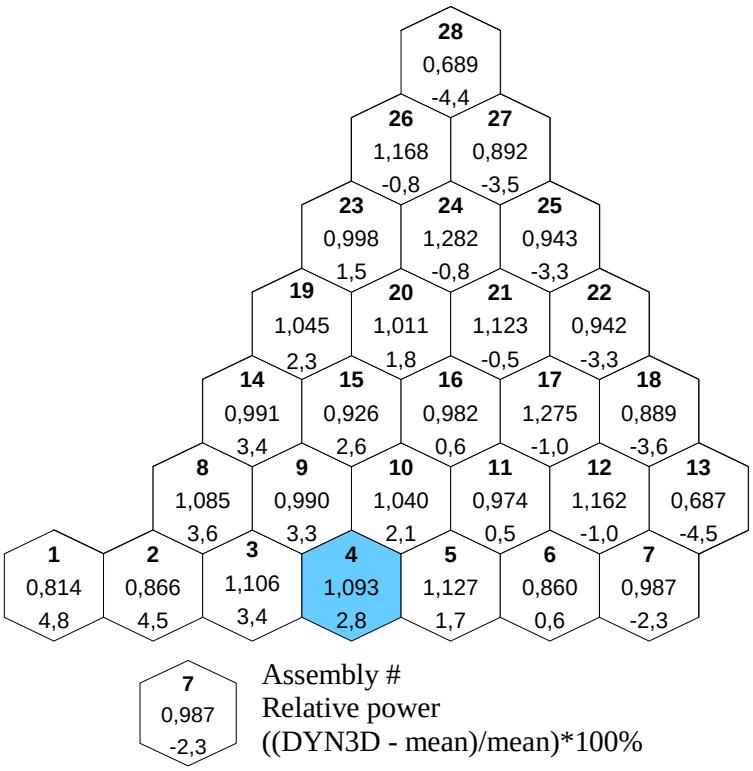


**Figure 5.17: DYN3D/ATHLET computed radial power distribution vs. mean of all codes in the initial HFP state**

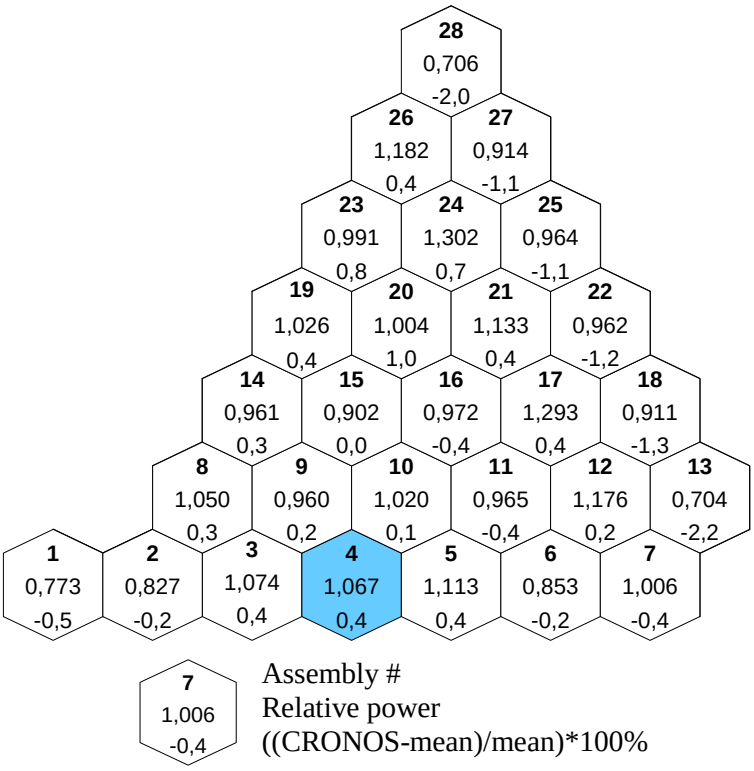


**Figure 5.18: CRONOS/FLICA4 computed radial power distribution vs. mean of all codes in the initial HFP state. CRONOS/FLICA used flat core inlet BC**

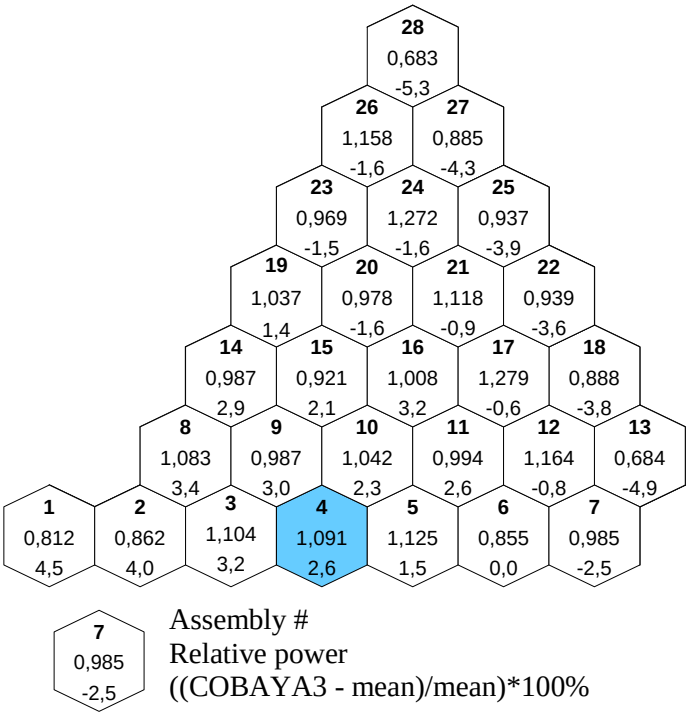


**Figure 5.19: COBAYA3/COBRA3 computed radial power distribution vs. mean of all codes in the initial HFP state. COBAYA3/COBRA3 used CATHARE2 calculated core BC**

**Table 5.16: Comparison of HFP results using core inlet BC as obtained from the considered system code. Reference is the COBAYA3/COBRA3 result**

| | DYN3D/ATHLET | COBAYA3/COBRA3 | Abs. deviation |
|---|---|---|---|
| **Keff** | 0.99481 | 0.99810 | -329 pcm |
| **Fxy** | 1.283 | 1.284 | -0.001 |
| **Fz** | 1.180 | 1.178 | 0.002 |
| **Axial offset** | -0.050 | -0.048 | -0.002 |

| | HEXTRAN/SMABRE | COBAYA3/COBRA3 | Abs. deviation |
|---|---|---|---|
| **Keff** | 1.00210 | 0.99796 | +414 pcm |
| **Fxy** | 1.303 | 1.278 | 0.025 |
| **Fz** | | 1.170 | |

| | NEM/RELAP3D | COBAYA3/COBRA3 | Abs. deviation |
|---|---|---|---|
| **Keff** | 0.99844 | 0.99696 | +148 pcm |
| **Fxy** | 1.303 | 1.276 | 0.027 |
| **Fz** | 1.139 | 1.204 | -0.066 |

**Table 5.17: Comparison of HFP state simulations with flat core inlet BCs**

| Flat BCs at the core inlet | PSU PARCS/TRACE | COBAYA3/COBRA3 | Abs. deviation |
|---|---|---|---|
| **Keff** | 0.99759 | 0.99823 | -64 pcm |
| **Fxy** | 1.293 | 1.279 | 0.016 |
| **Fz** | 1.170 | 1.177 | -0.007 |

| Flat BCs at the core inlet | CRONOS/FLICA* | COBAYA3/COBRA3 | Abs. deviation |
|---|---|---|---|
| **Keff** | 0.99750 | 0.99823 | -73 pcm |
| **Fxy** | 1.295 | 1.279 | 0.014 |
| **Fz** | 1.163 | 1.177 | -0.014 |

* The compared CRONOS/FLICA* solution is not sufficiently converged

## 5.3 Transient results

Two transient scenarios are considered which differ in the

- worth of negative tripped rod reactivity inserted during the scram
- sequence of events

### 5.3.1 Scenario 1

The task is to calculate the core-vessel MSLB transient with imposed vessel boundary conditions, corresponding to the realistic Scenario 1. This scenario is more complex for thermal-hydraulic simulation because the MCP in the faulted loop trips and the loop flow reverses. On the other hand, the total power after the reactor trip is at the level of decay heat. The main objective is to test the improved vessel thermal-hydraulic modeling in a coolant transient involving asymmetric loop cool-down and pump trip.

*Time histories*

Figures 5.20-5.28 show the time histories of main reactor parameters, such as temperatures, coolant density, pressure, total power, total reactivity, power peaking factor and the average and maximum nodal Doppler temperature. The results are compared code-to-code and the figures graphically illustrate the agreement or disagreement of participant's predictions.

In this scenario, the tripped rods reactivity is sufficient to prevent return to power after scram. The power of the tripped reactor is at the level of decay heat. The differences in the predicted hot leg temperatures are mainly due to the vessel thermal hydraulic models.

The RELAP3D solution shown in Figure 5.23 has been obtained with a 60-sector, coarse-3D model of the uppermost layer of the lower plenum. However, the modeling of the upper plenum is 1D which smears the response in reactor outlet temperatures. The result indicates that this simulation does not take into account the reversal in the boundary condition for the faulted loop.

The PARCS/TRACE solution in Figure 5.23 has been obtained with a coarse-3D, six-sector, 18-channel model throughout the vessel.

The HEXTRAN/SMABRE result has been obtained with a 6-sector, multi-channel vessel model using approximate turbulence modeling.

The DYN3D/ATHLET solution has been obtained with a 4-sector, multi-channel vessel model. The lower plenum mixing is described by an empirical model tuned to fit CFX calculation results for the flow re-distribution in case of pump trips. There is no mixing in the upper plenum.

The UNIPI and FZD results in Figure 5.23 show significant discrepancies to the VTT and INRNE solutions, which indicate a difference in the modeling of the reversal in the boundary condition for the faulted loop. The rips in the ATHLET results seem to be due to the controller used to fit the imposed boundary condition.

The CATHARE2 solution is supplementary, with point kinetics. It is possible to compare the results with the coupled code solutions because the total power is at the level of decay heat. The vessel thermal hydraulics is described with a 24-sector multi-channel model with cross flow governed by the local pressure drops.

Figure 5.29 illustrates the evolution of Fxyz as predicted by COBAYA3/COBRA3 and DYN3D/ATHLET. In this simulation, COBAYA/COBRA used CATHARE2 calculated core BCs. The observed difference is significant and is mainly due to differences in the spatial coupling.

*Snapshots*

Figures 5.30 and 5.32 show the comparison of the computed core-average axial power distributions at time of maximum overcooling (166s) and at the end of transient (600s). The results indicate a grouping consistent with that in HZP states. PARCS/TRACE and DYN3D/ATLET results are close to each other, independently of the different detail in vessel thermal-hydraulic models.

Figures 5.34 and 5.36 show the comparison of the computed axial power distributions in the position of stuck rod, at time of maximum overcooling (166s) and at the end of transient (600s). The observed grouping of the results is consistent with that in HZP states.

Figures 5.38 and 5.39 illustrate the resulting core power distribution at time of maximum overcooling, as predicted with DYN3D/ATHLET and PARCS/TRACE.

For more details of the core inlet distributions, see Appendix C.

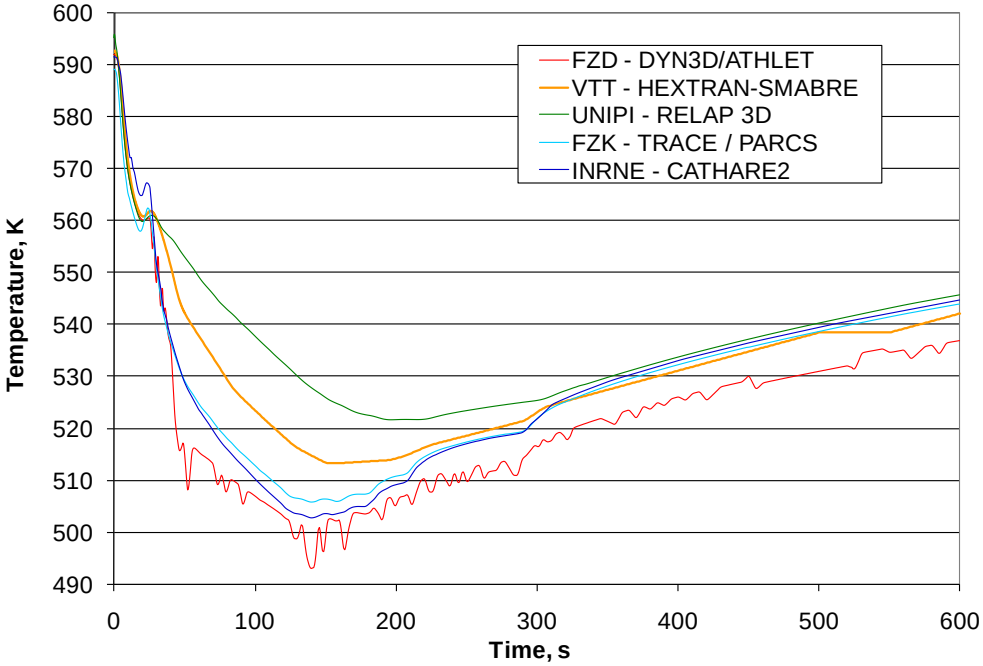


**Figure 5.20: Time history of hot leg 1 temperature in Scenario 1**

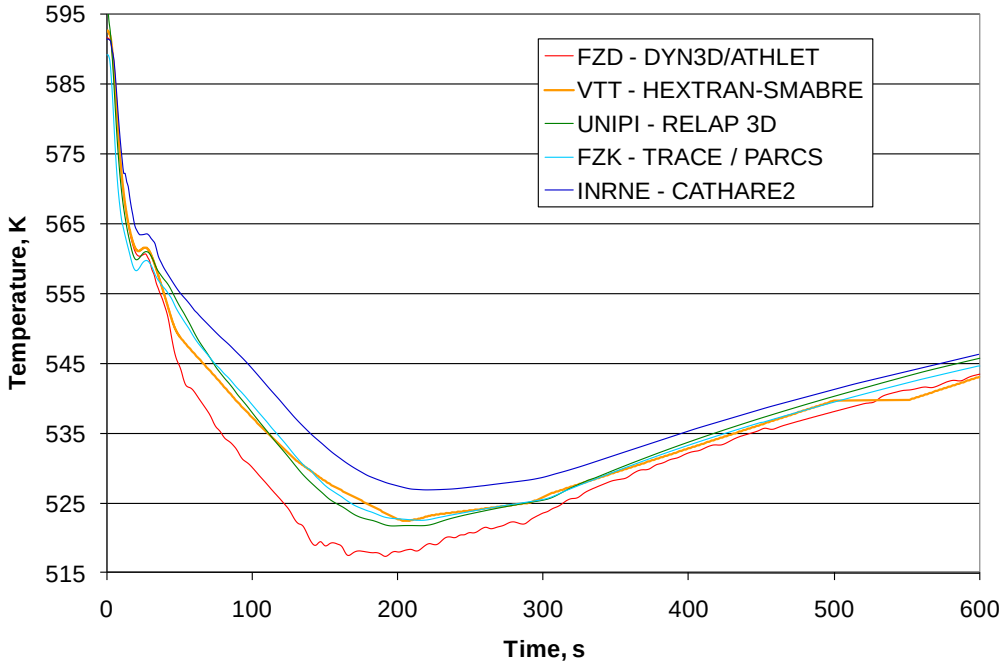


**Figure 5.21: Time history of hot leg 2 temperature in Scenario 1**

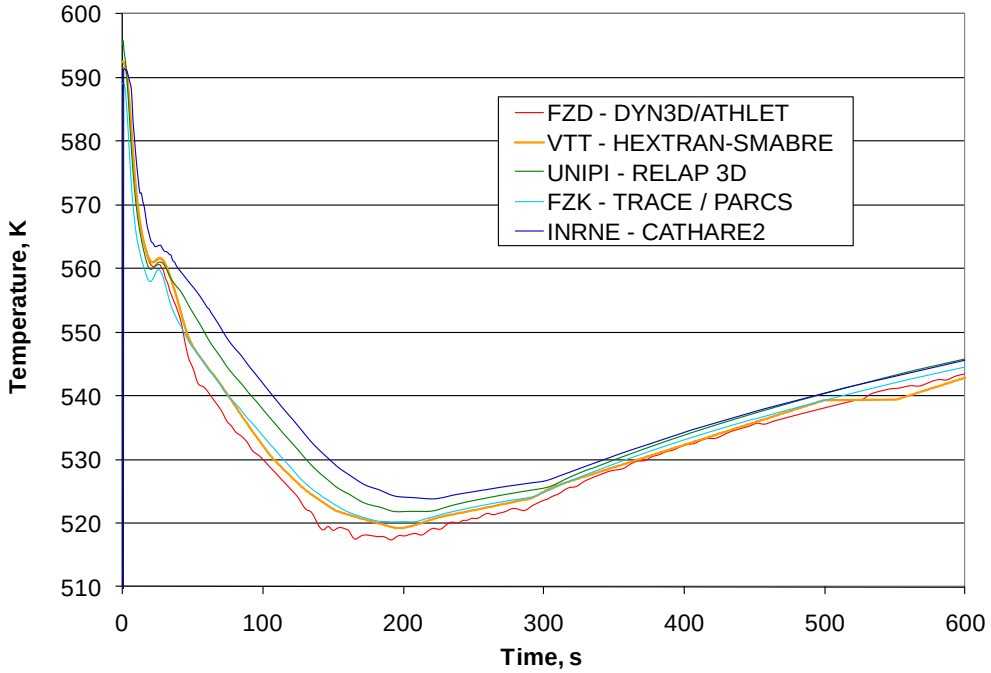


**Figure 5.22: Time history of hot leg 3 temperature in Scenario 1**

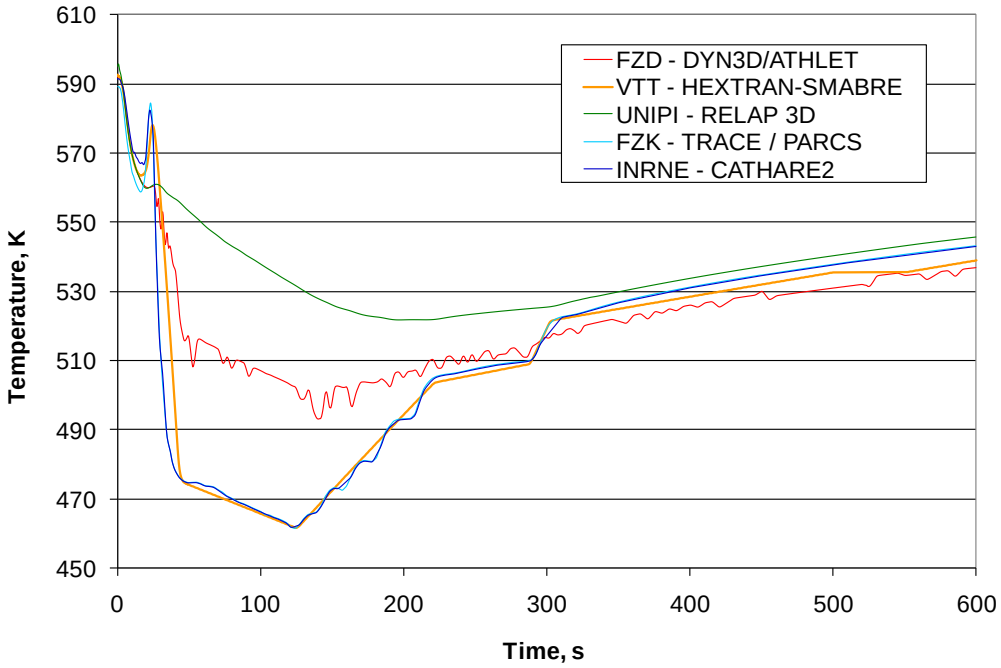


**1**

**Figure 5.23: Time history of hot leg 4 temperature in Scenario 1**

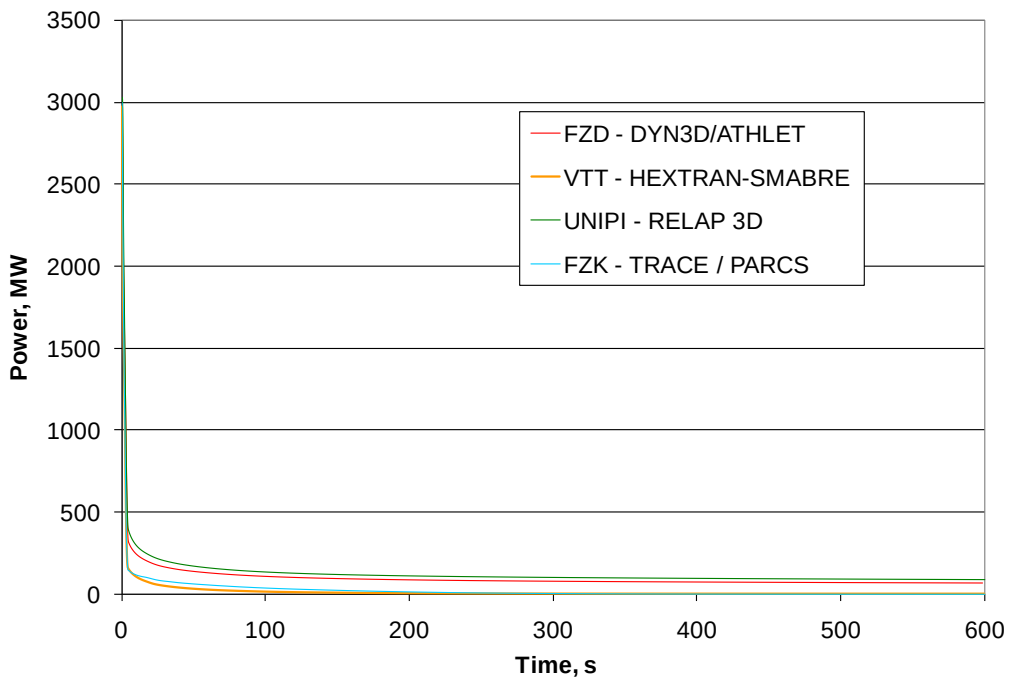


**Figure 5.24: Time history of the total power (or fission power for VTT and FZK solutions) in Scenario 1**

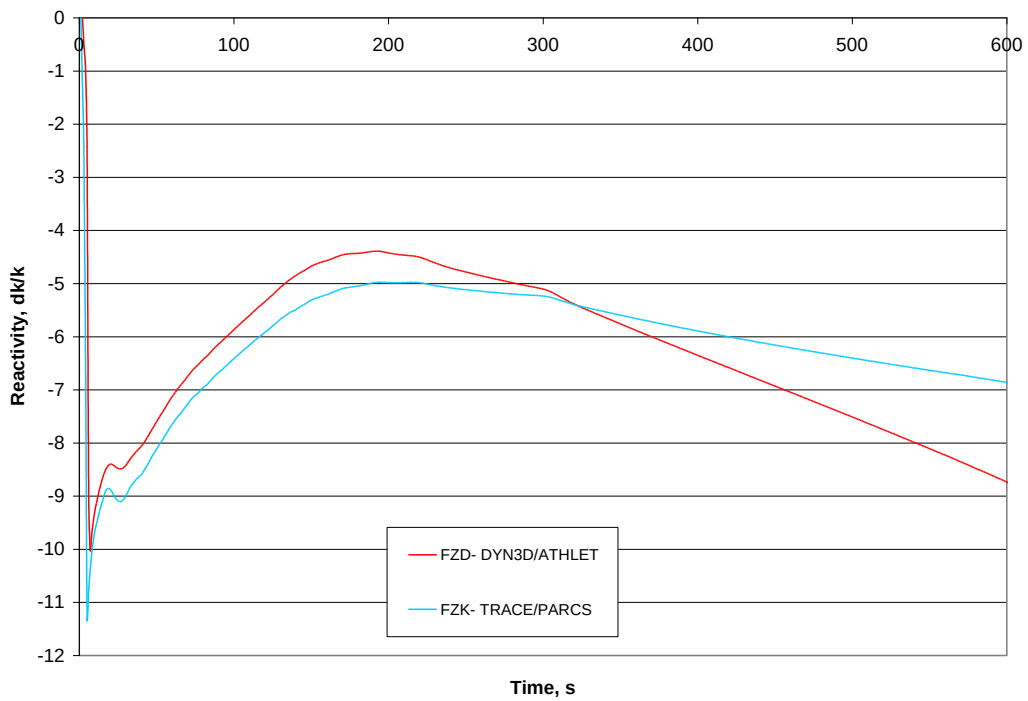


**Figure 5.25: Time history of the total reactivity in Scenario 1**

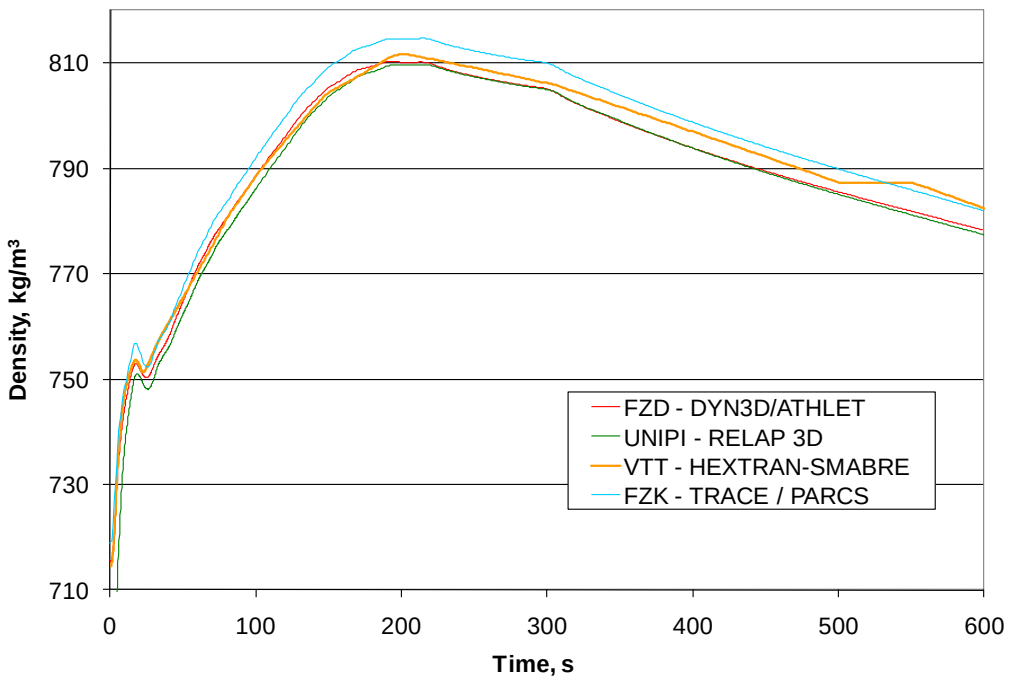


**Figure 5.26: Time history of the core average moderator density in Scenario 1**

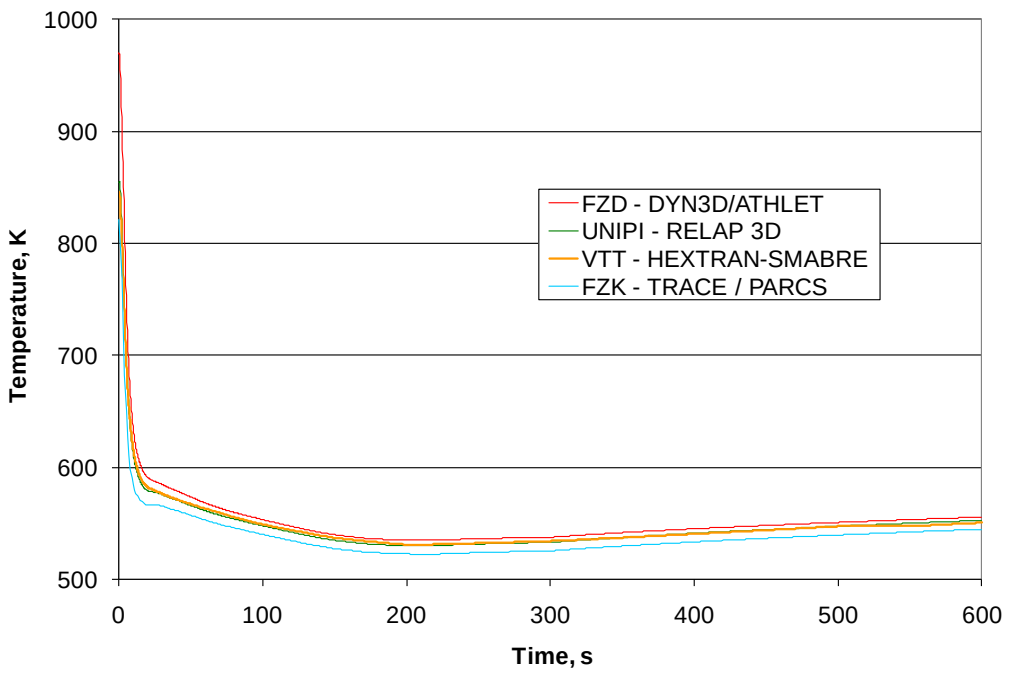


**Figure 5.27: Time history of the core average Doppler temperature in Scenario 1**

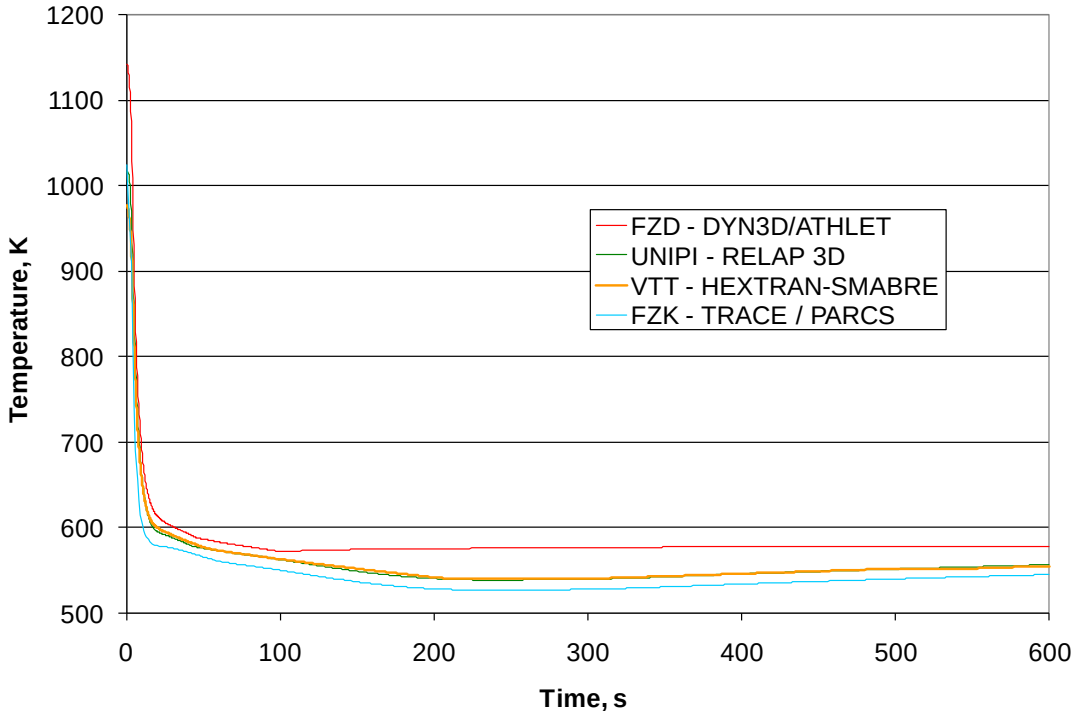


**Figure 5.28: Time history of the max nodal Doppler temperature in Scenario 1**

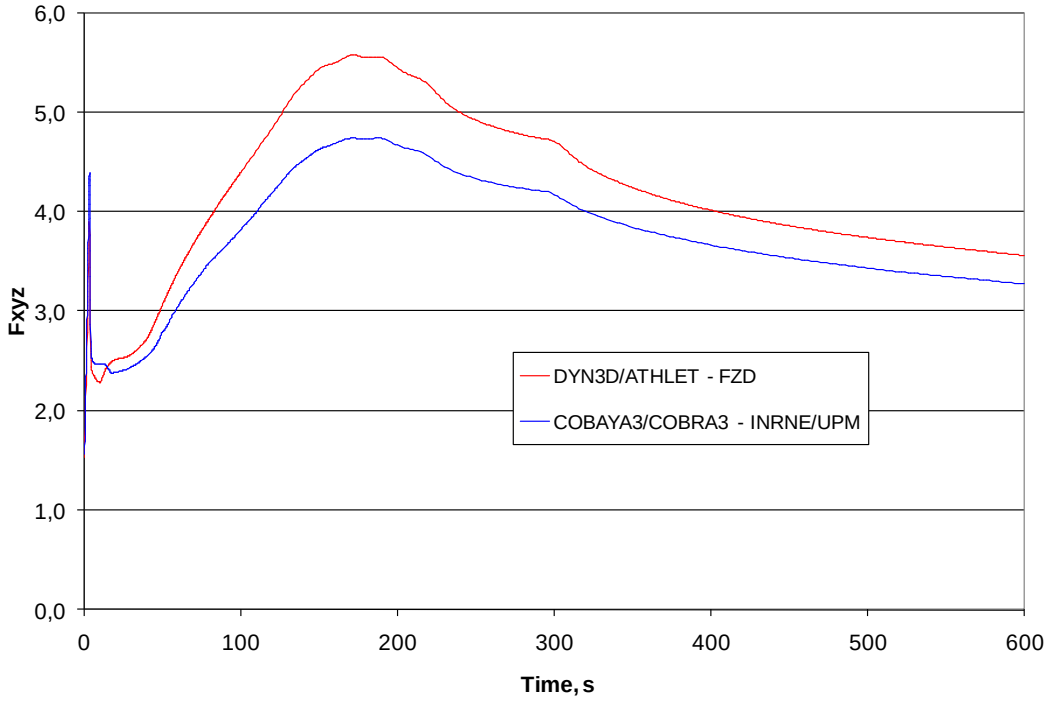


**Figure 5.29: Time history of Fxyz in Scenario 1**

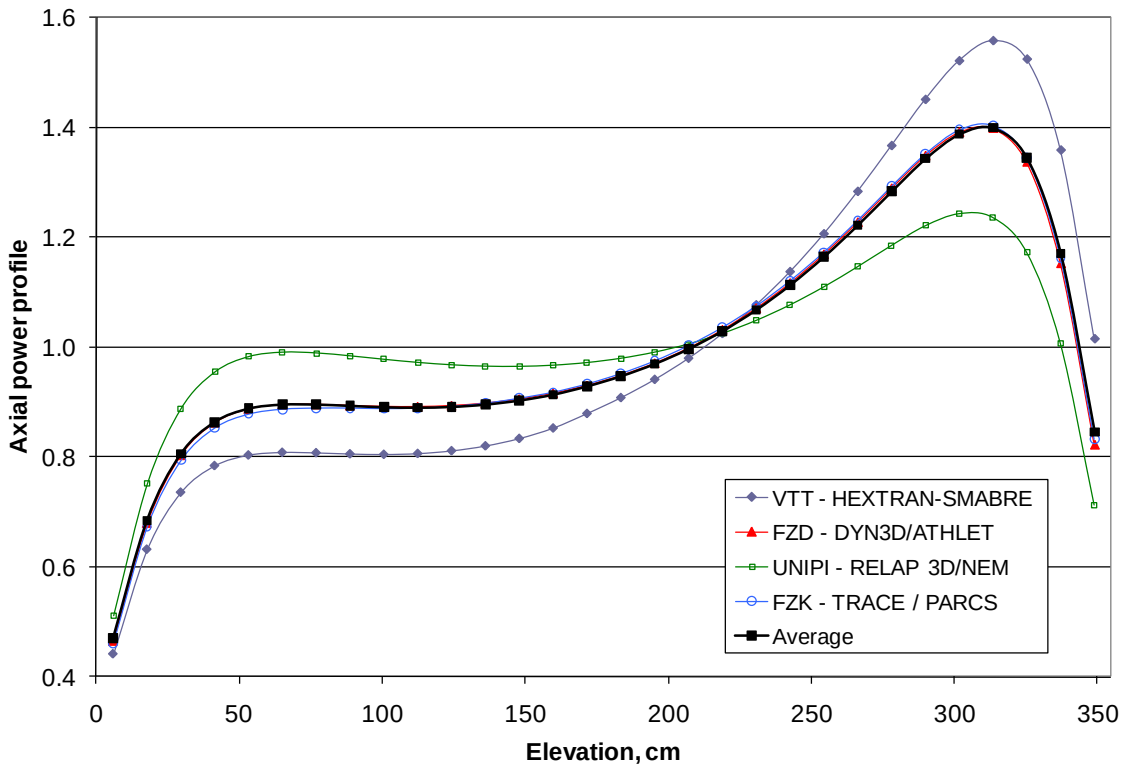


**Figure 5.30: Scenario 1 with stuck rod in #90. Core-average axial power distribution at time of maximum overcooling (166s)**

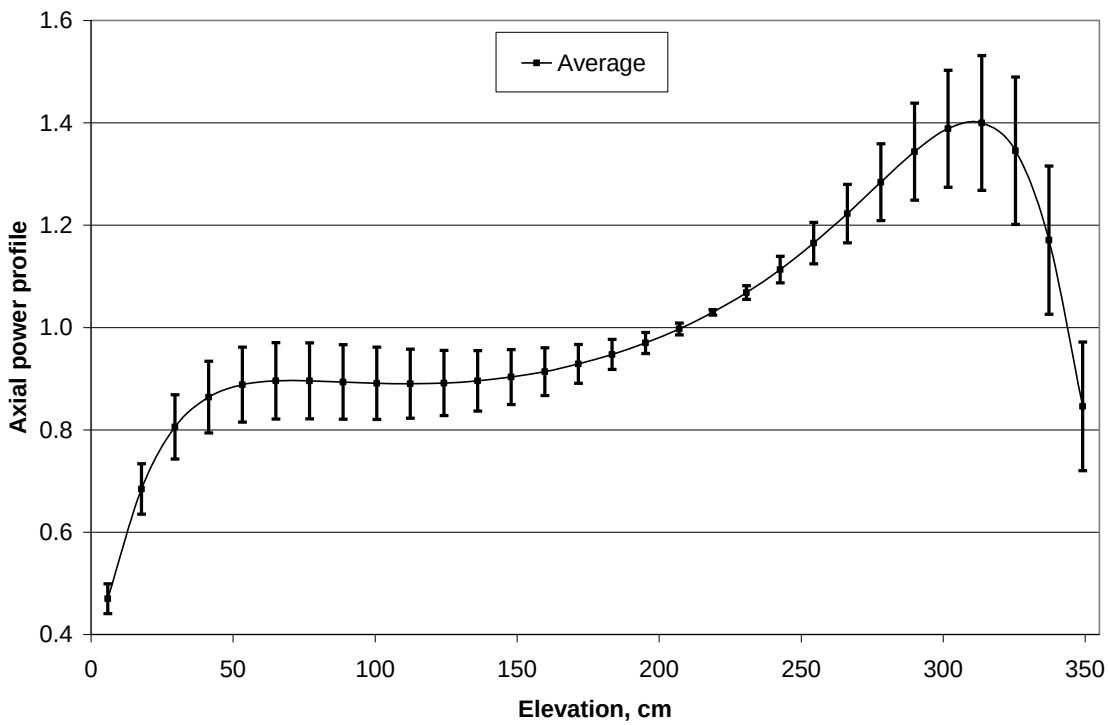


**Figure 5.31: Scenario 1 with stuck rod in #90. Core-average axial power distribution at time of maximum overcooling (166s) - mean and standard deviation**

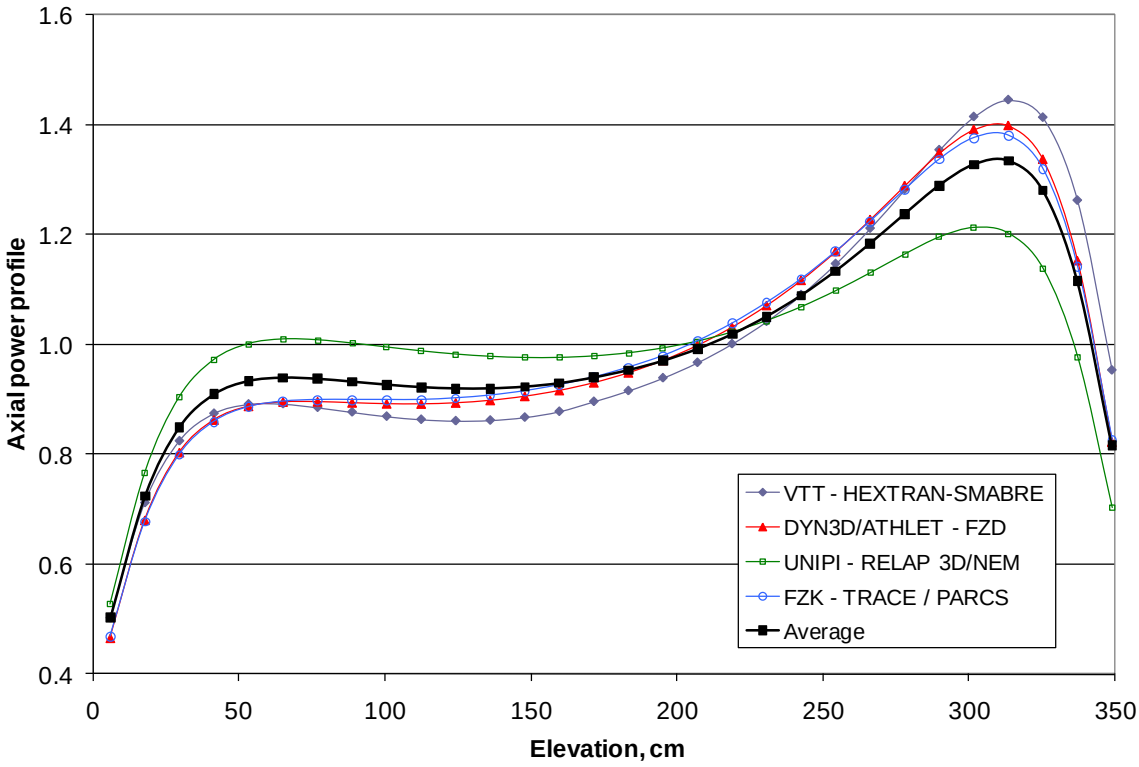


**Figure 5.32: Scenario 1 with stuck rod in #90. Core-average axial power distribution at 600s**

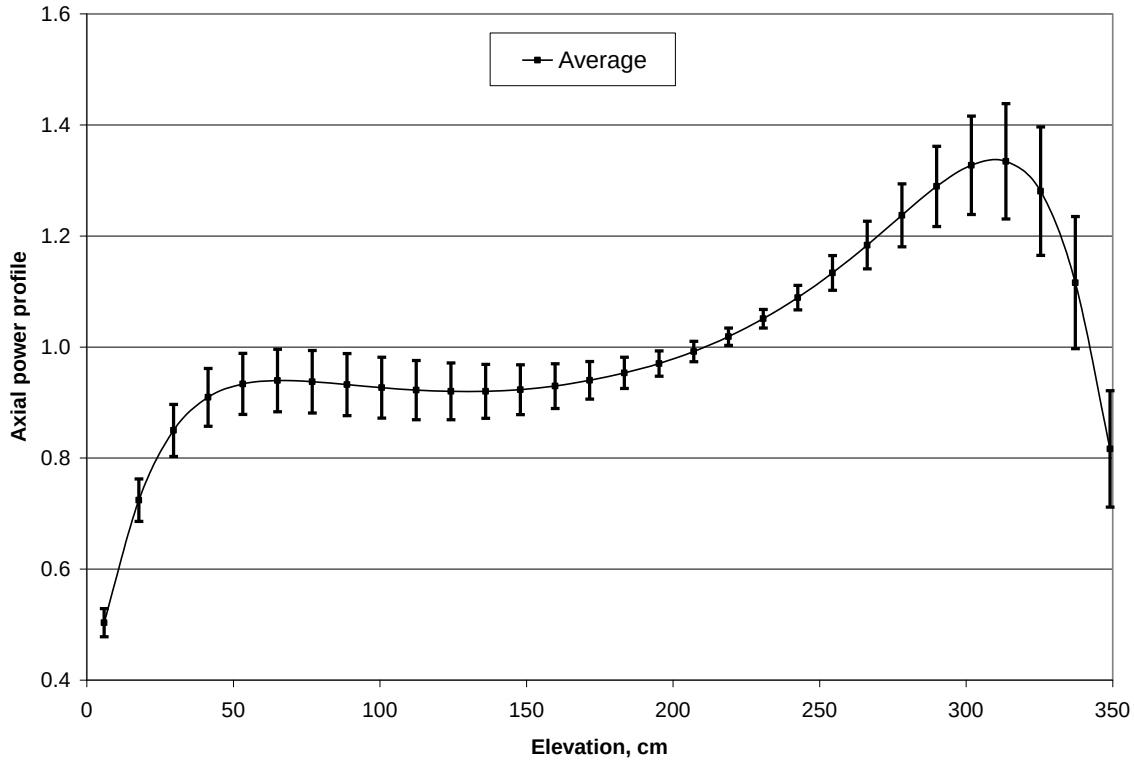


**Figure 5.33: Scenario 1 with stuck rod in #90. Core-average axial power distribution at 600s - mean and standard deviation**

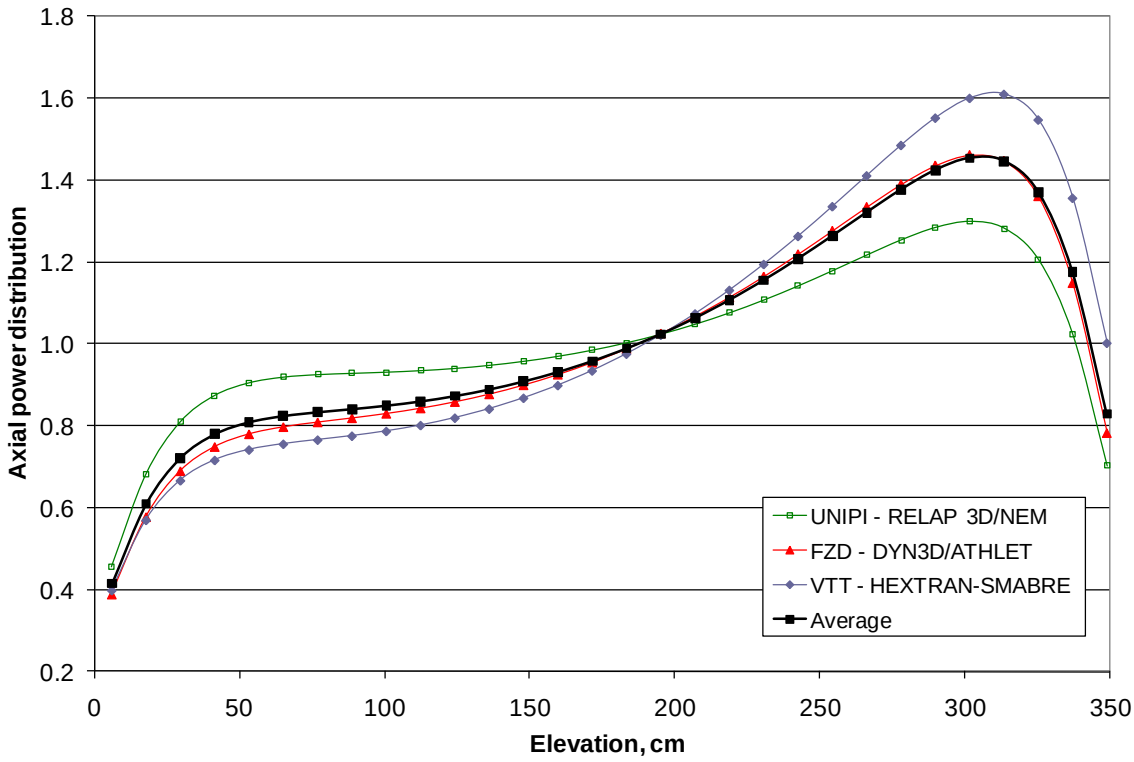


**Figure 5.34: Scenario 1 with stuck rod in #90. Axial power distribution in the stuck rod assembly at 166s**

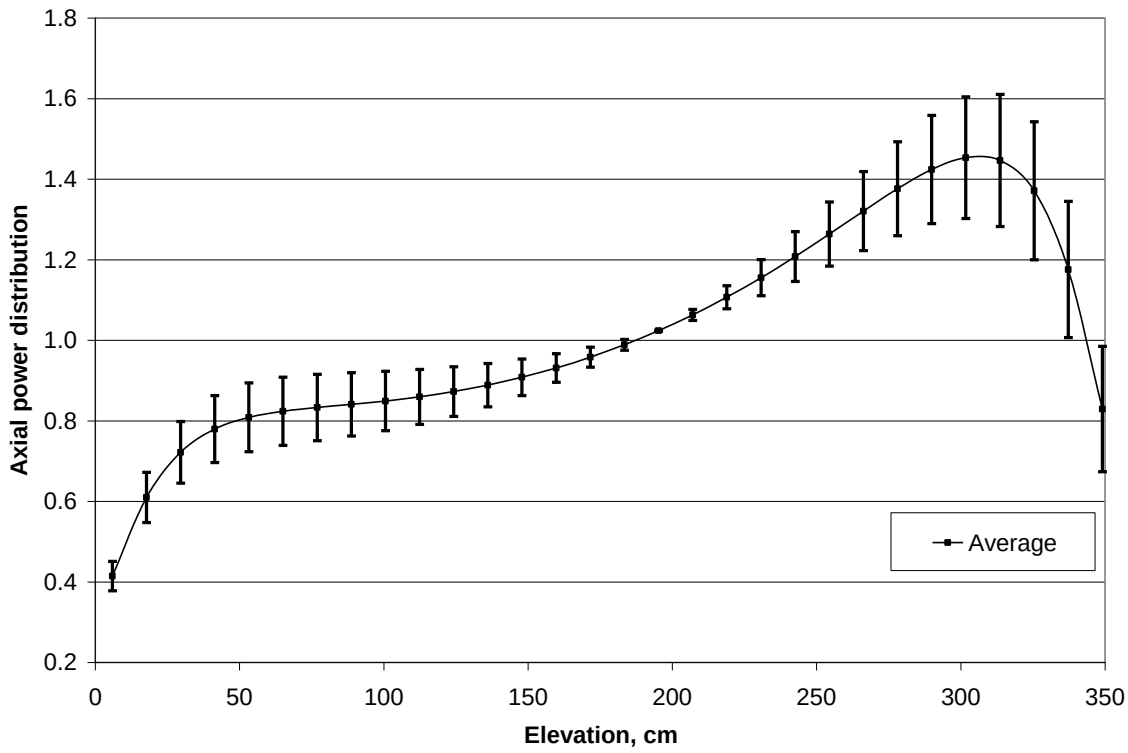


**Figure 5.35: Scenario 1 with stuck rod in #90. Axial power distribution in the stuck rod assembly at 166s - mean and standard deviation**

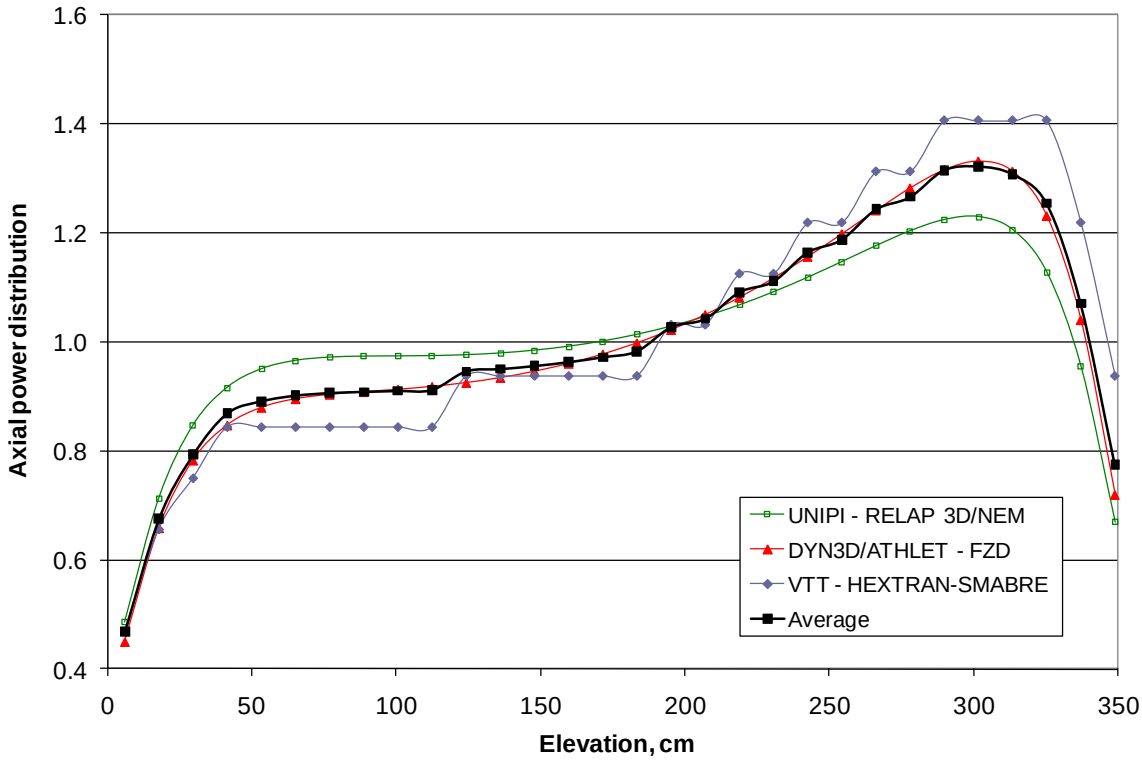


**Figure 5.36: Scenario 1 with stuck rod in #90. Axial power distribution in the stuck rod assembly #90 at 600s**

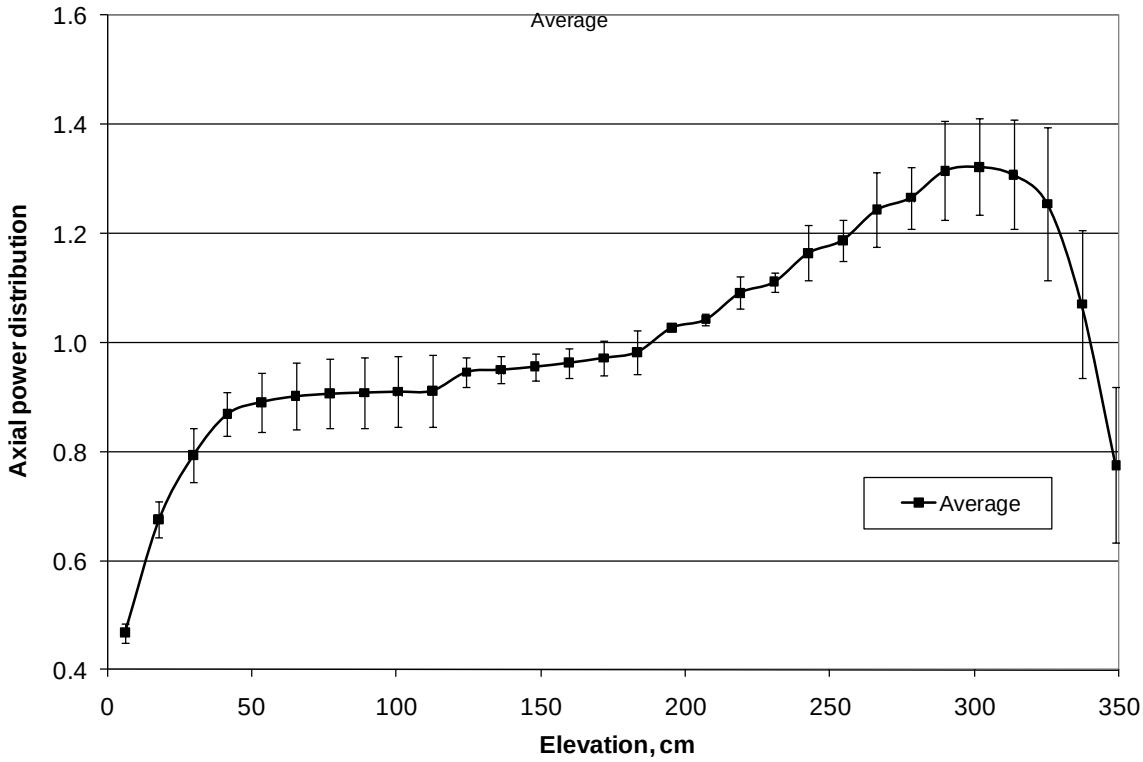


**Figure 5.37: Scenario 1 with stuck rod in #90. Axial power distribution in the stuck rod assembly #90 at 600s - mean and standard deviation**

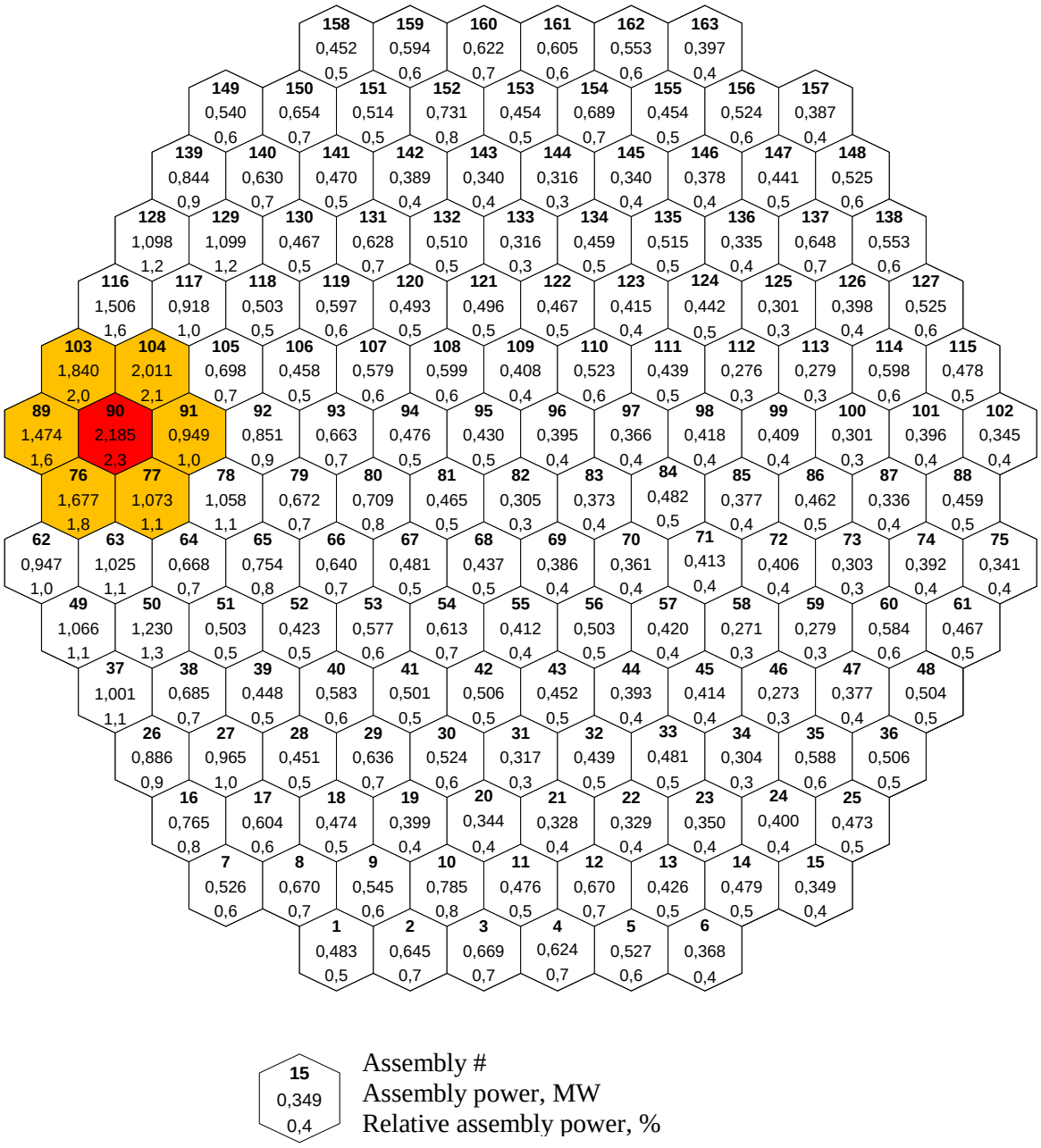


**Figure 5.38: Scenario 1 with stuck rod in #90. DYN3D/ATHLET computed radial power distribution at 166s**

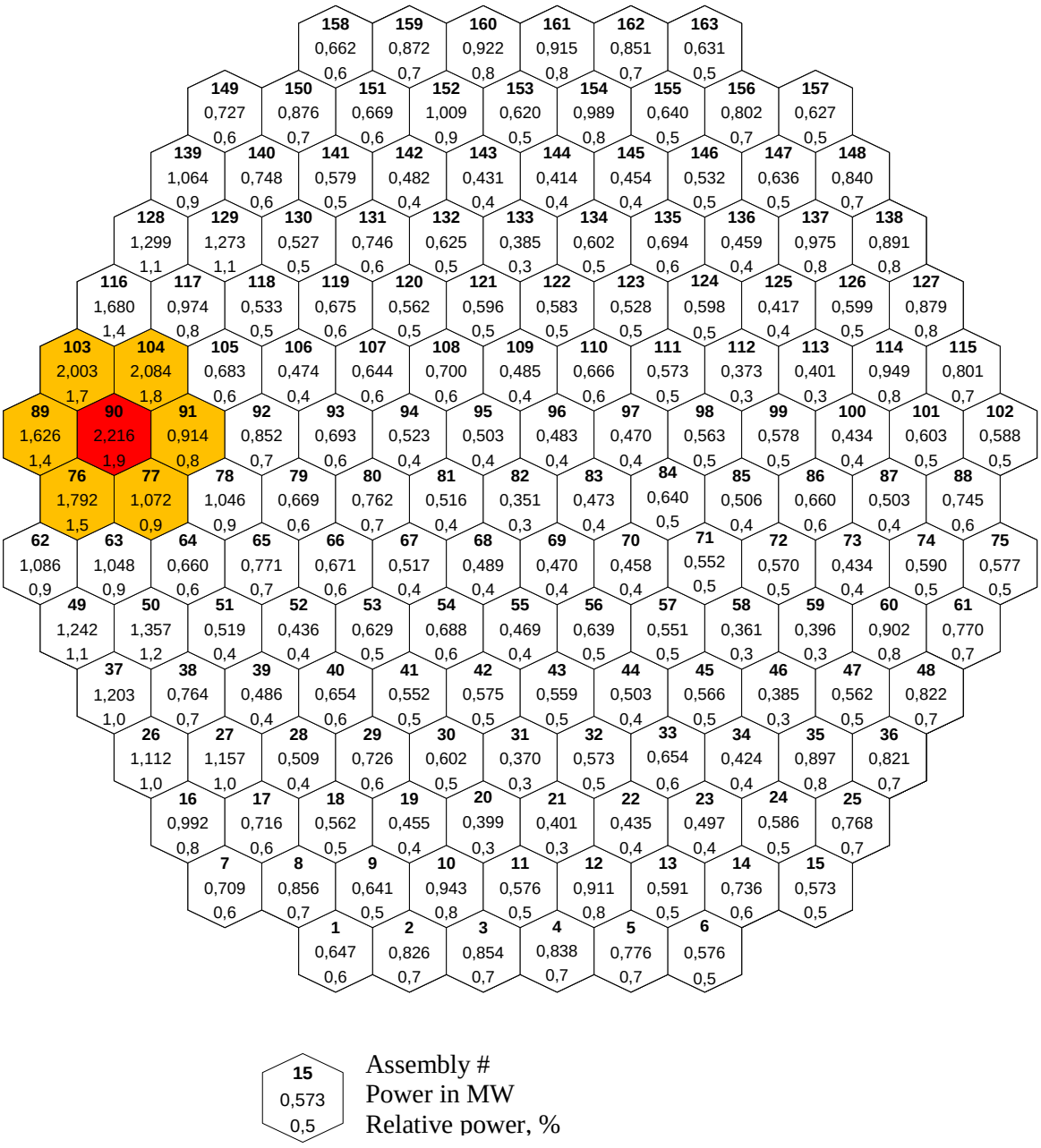


**Figure 5.39: Scenario 1 with stuck rod in #90. RELAP3D/NEM computed radial power distribution at 166s**

### 5.3.2 Scenario 2

The task is to calculate the core-vessel MSLB transient with imposed vessel boundary conditions, corresponding to the pessimistic Scenario 2. In this scenario the MCP in the faulted loop fails to trip on MSLB signal and all MCP remain in operation. In order to enhance the testing of the coupled codes, the cross sections are adjusted so that the scram reactivity is about a half of the real one. A significant return to power after scram is expected.

This scenario is of particular interest for the testing of vessel mixing models and 3D N/TH coupling schemes. In the analysis to follow, we consider the case with stuck rods in assemblies #117 and #140.

*Time histories*

Figures 5.40-5.43 show the computed hot leg temperatures at the reactor outlet.

The NEM/RELAP3D solution was obtained with a 3D 60-sector model of the lower plenum and 1D model of the upper plenum, which explains the deviations from the other codes results.

The HEXTRAN/SMABRE and DYN3D/ATHLET results are in reasonable agreement for the undisturbed loops and show a significant difference for the faulted loop. As the predicted total powers and total reactivities are close to each other (see Figures 5.44 and 5.46), the loop differences can be attributed to the combined effect of:

- mixing models in the down-comer and the lower plenum
- spatial N/TH coupling in terms of number of TH channels
- mixing models in the upper plenum (weak mixing in SMABRE and no mixing in the ATHLET user model)

The results in Figures 5.45, 5.47 and 5.52 present a sensitivity study with COBAYA3/COBRA3 to illustrate the impact of using finer mesh in the flow-mixing model.

Figures 5.49 and 5.50 show the computed time histories of the maximum nodal fuel temperatures and the core average Doppler temperatures. The dynamic gap conductance model used in DYN3D/ATHLET predicts a considerably higher fuel temperature compared to that of HEXTRAN/SMABRE and NEM/RELAP3D. This has an impact on the total power dynamics, compensated in part by other mesh related effects.

The predicted time history of Fxy and Fxyz is shown in Figures 5.51 and 5.52. The COBAYA/COBRA results were obtained from a coupled N/TH solution, with CATHARE2 multi-1D calculated core inlet BCs using 6-, 12- and 24-sector azimuth meshing. The results provide insight of the sensitivity of the 3D peaking factor to modeling refinements in the vessel and the core.

In the overall, since the predicted integral core parameters in the considered simulations are relatively close to each other (except the Doppler temperature), and the same vessel boundary conditions are used, the main difference in the participants solutions comes from the different modeling of local 3D effects in the vessel and the core. The observed differences require further attention.

*Snapshots*

The computed peaking factors at time 0 s (HFP), 69 s (HRP) and 200 s are shown in Tables 5.19 and 5.20. The results show that Fxy and Fz are sensitive to mesh refinement in the vessel mixing models and in spatial coupling.

Figures 5.53-5.56 present the participants computed core-averaged axial power distributions. The analysis shows that they are sensitive to refinement of the vessel mixing models, the spatial coupling schemes and the decay heat distribution during the transient. It is interesting to note that in Figure 5.54 the difference between COBAYA/COBRA results with 24- and 6-sector BC is in the order of magnitude of the difference between COBAYA/COBRA 24-sector BC and HEXTRAN/SMABRE with 6-sector BC in Figure 5.53.

Figures 5.57-5.64 show snapshots of the computed axial power distributions in the stuck rod positions. They are sensitive to angular mesh refinement in the vessel mixing models and to the spatial coupling.

The radial core power distributions in Figures 5.65 and 5.66 illustrate coarse-mesh coupling results obtained with multi-1D thermal-hydraulic models: DYN3D/ATHLET with 4 sectors in the vessel and HEXTRAN/SMABRE with 6 sectors. The results of the two codes are similar, with the 6-sector modeling being closer to the results produced by finer spatial coupling (see Figures 5.66 and 5.67).

The radial core power distributions in Figures 5.67 and 5.68 illustrate the effect of finer spatial coupling. The results were obtained with COBAYA3/COBRA3 using one point per hexagon in COBRA3 and core BC from CATHARE2 12-sector and 24-sector vessel calculations.

Tables 5.24 and 5.25, and Figures 5.52, 5.54, 5.58 and 5.60 illustrate the impact of spatial mesh and spatial coupling. The peaking factors are sensitive to spatial mesh and spatial coupling, especially in case of steep flux gradients.

Appendix D shows additional snapshots of core inlet distributions and the assembly-by-assembly fuel Doppler temperatures.

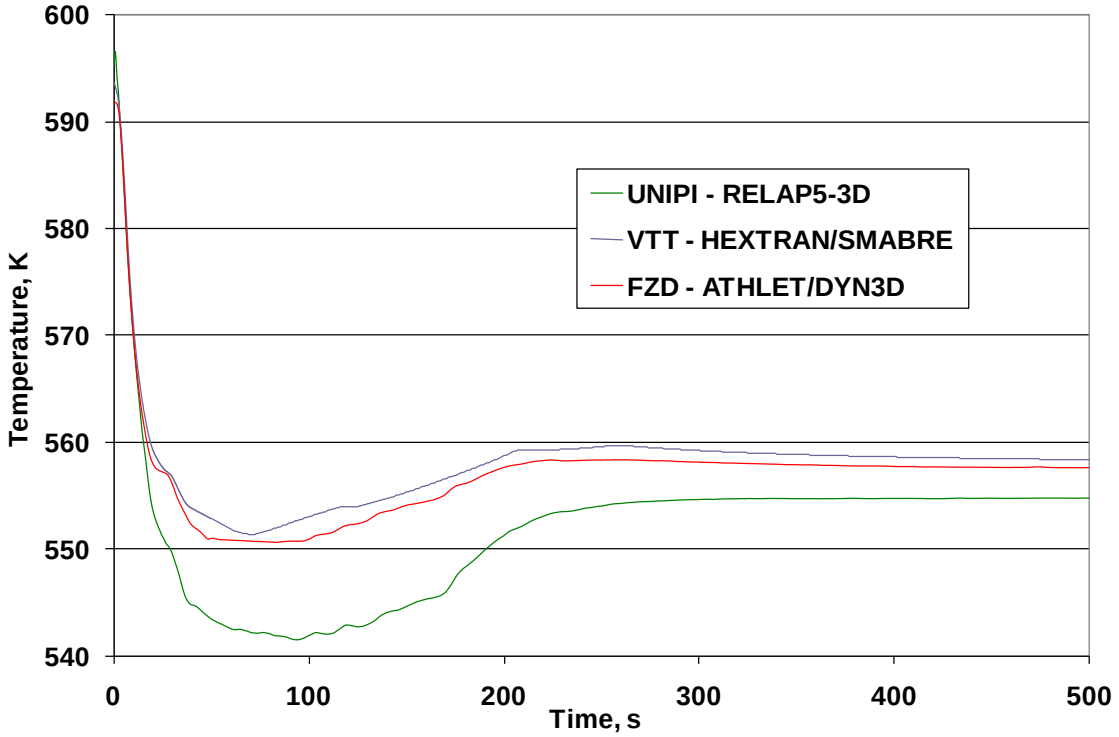


**Figure 5.40: Hot leg 1 temperature**

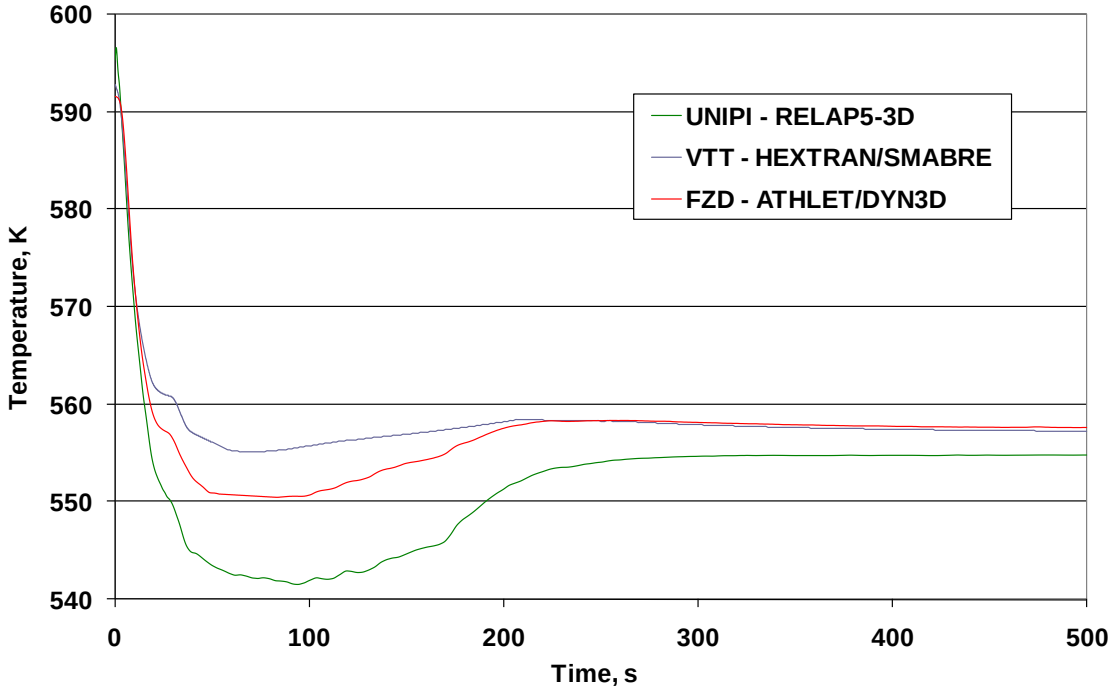


**Figure 5.41: Hot leg 2 temperature**

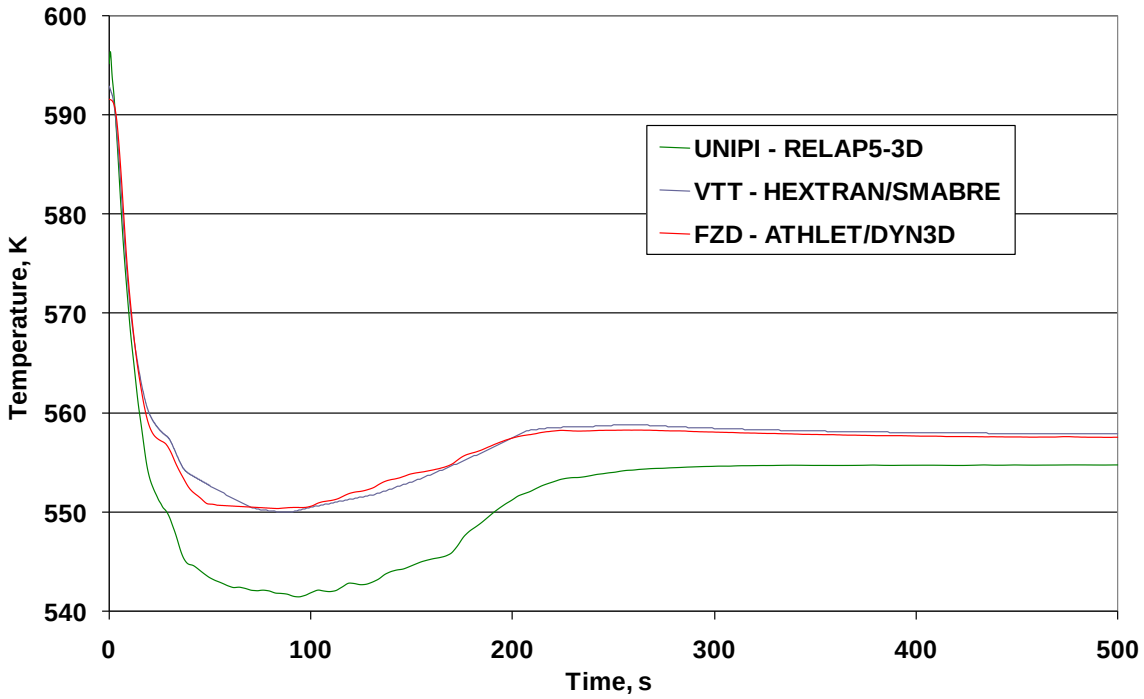


**Figure 5.42: Hot leg 3 temperature**

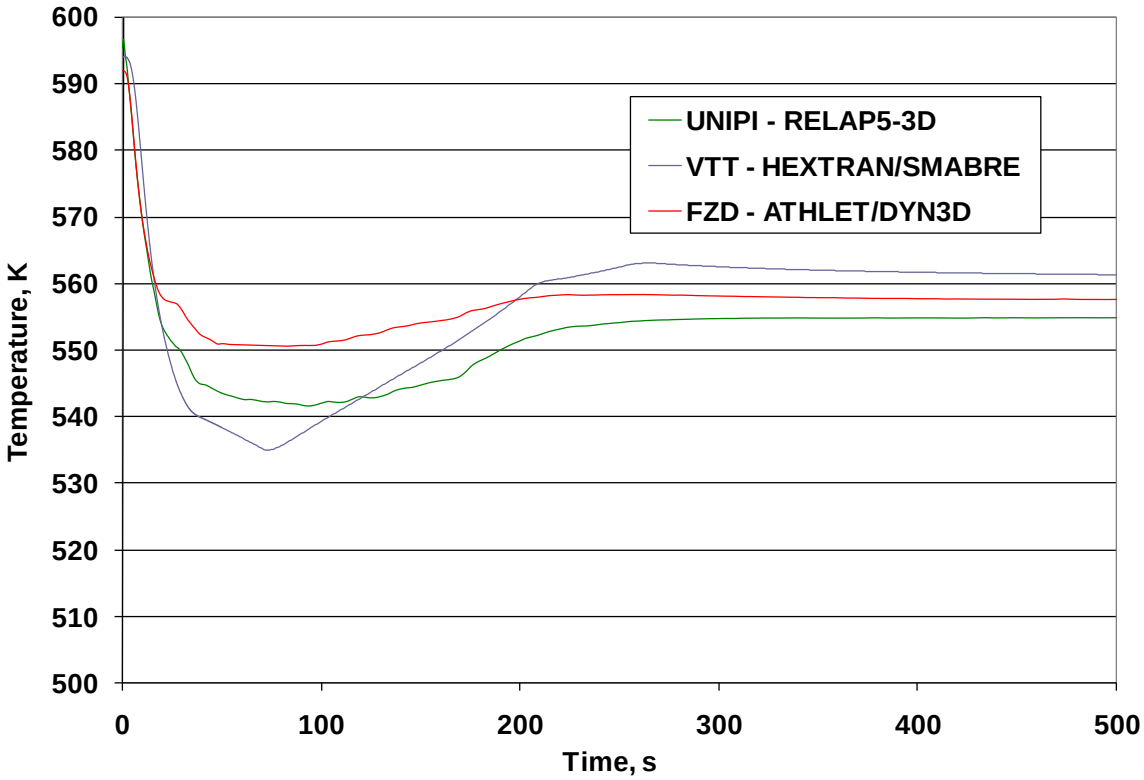


**Figure 5.43: Hot leg 4 temperature**

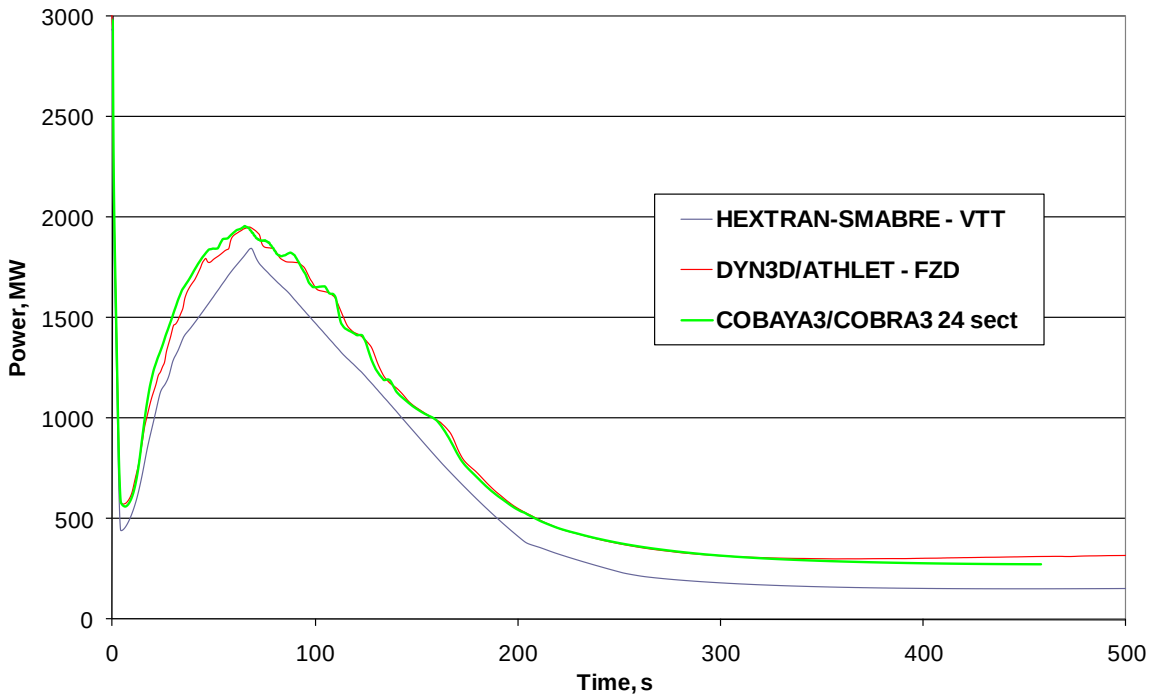


**Figure 5.44: Total power**

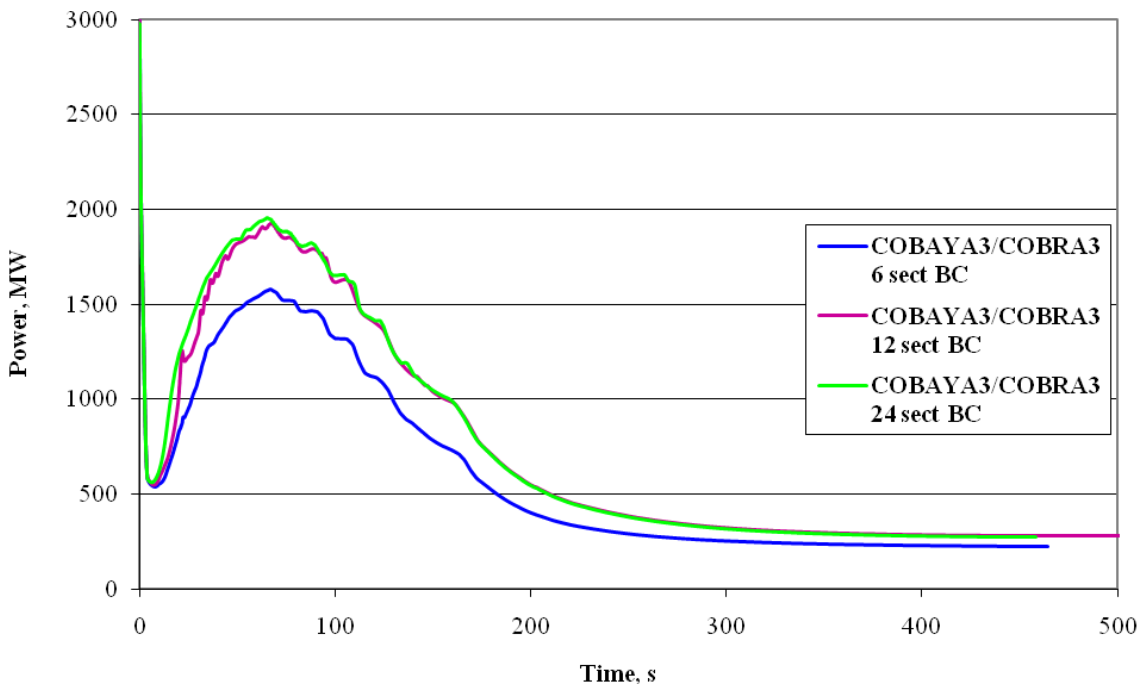


**Figure 5.45: Total power. Impact of the meshing in the vessel mixing model**

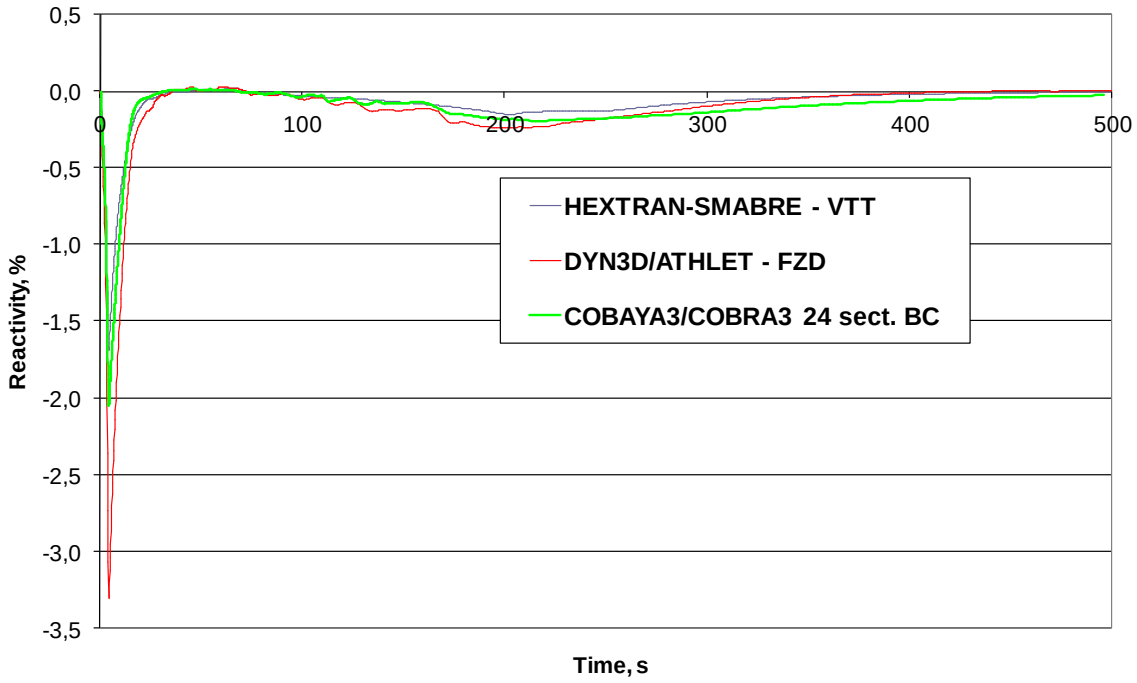


**Figure 5.46: Total reactivity**

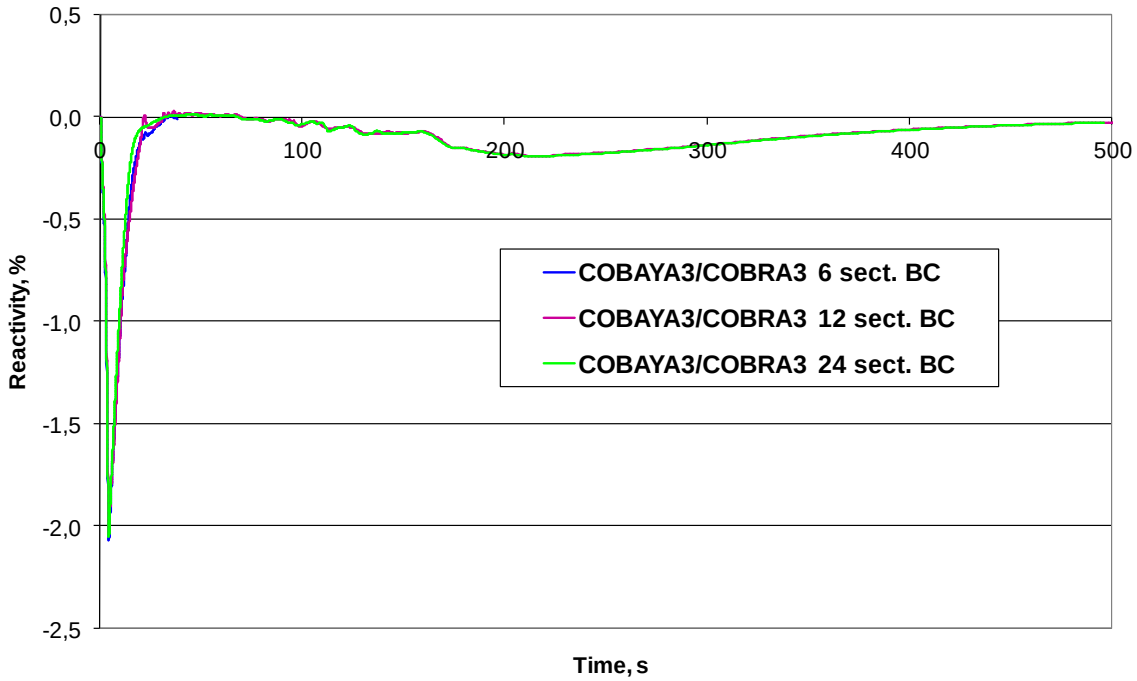


**Figure 5.47: Total reactivity. Impact of the vessel mixing model meshing**

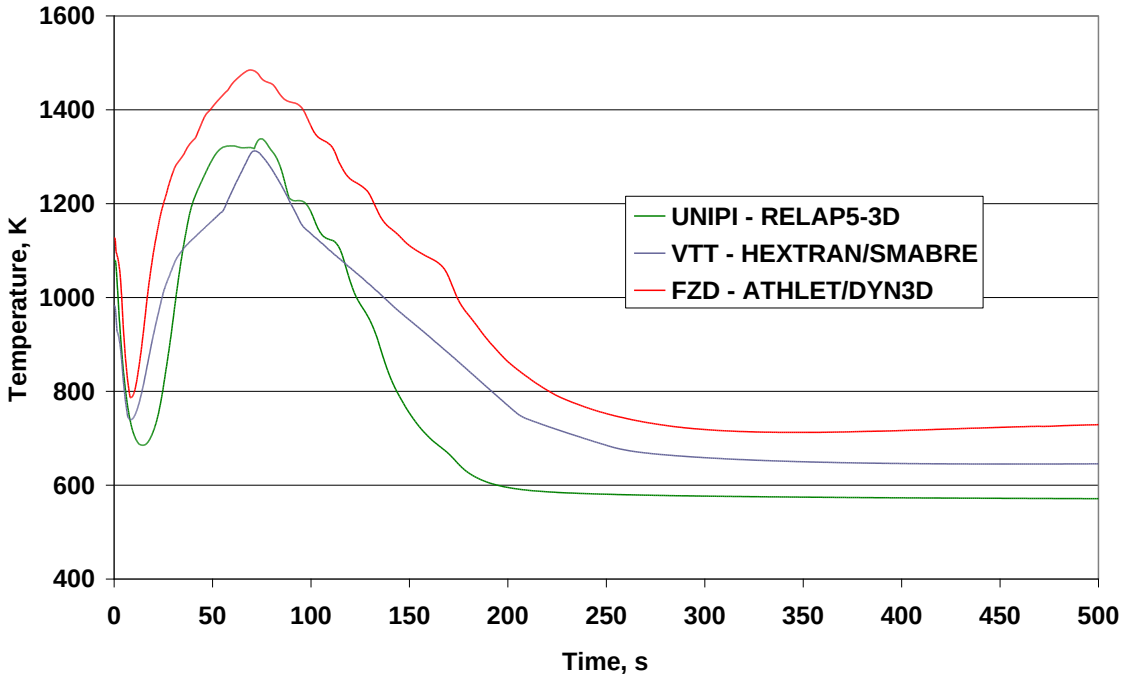


**Figure 5.48: Maximum nodal fuel temperature**

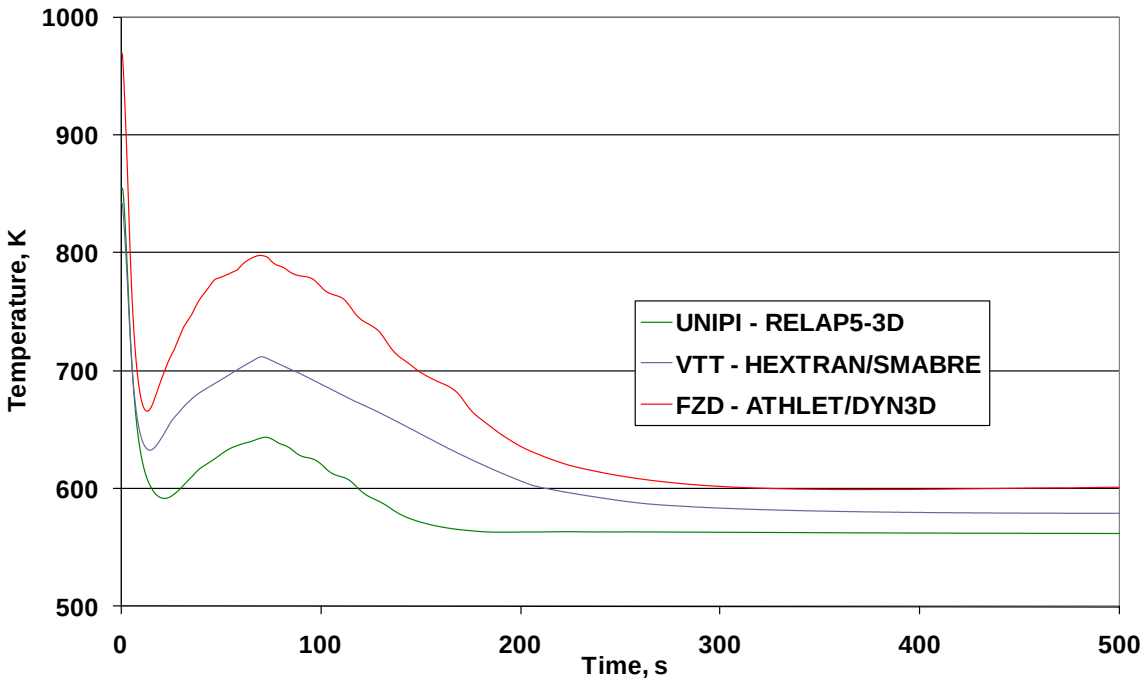


**Figure 5.49: Core average Doppler temperature**

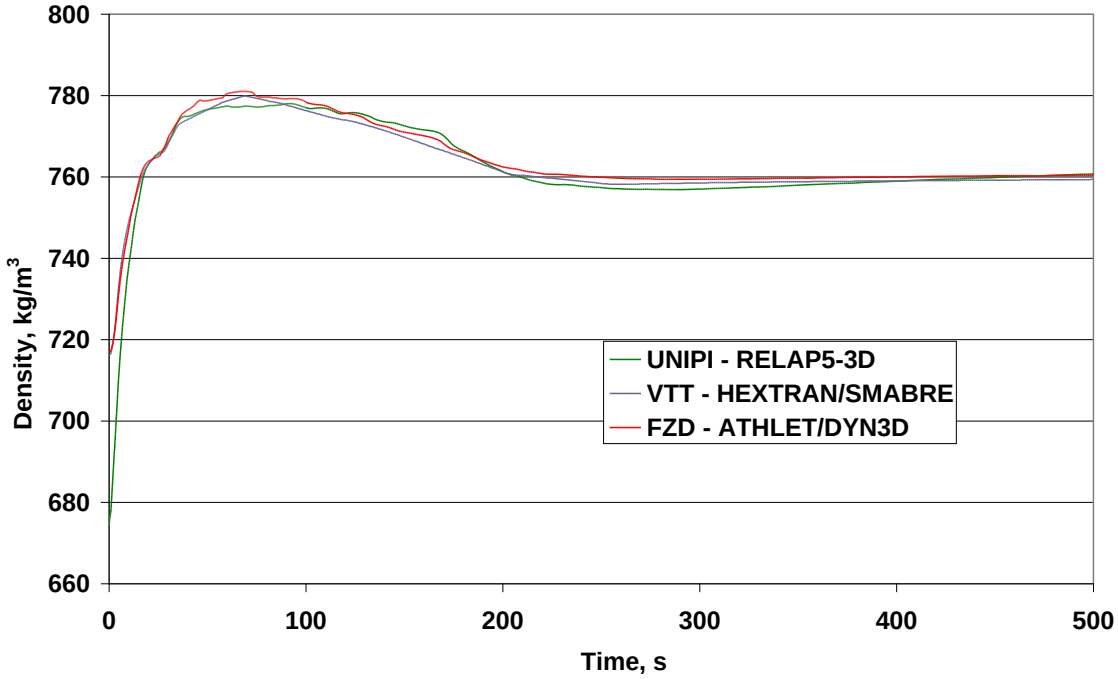


**Figure 5.50: Core average coolant density**

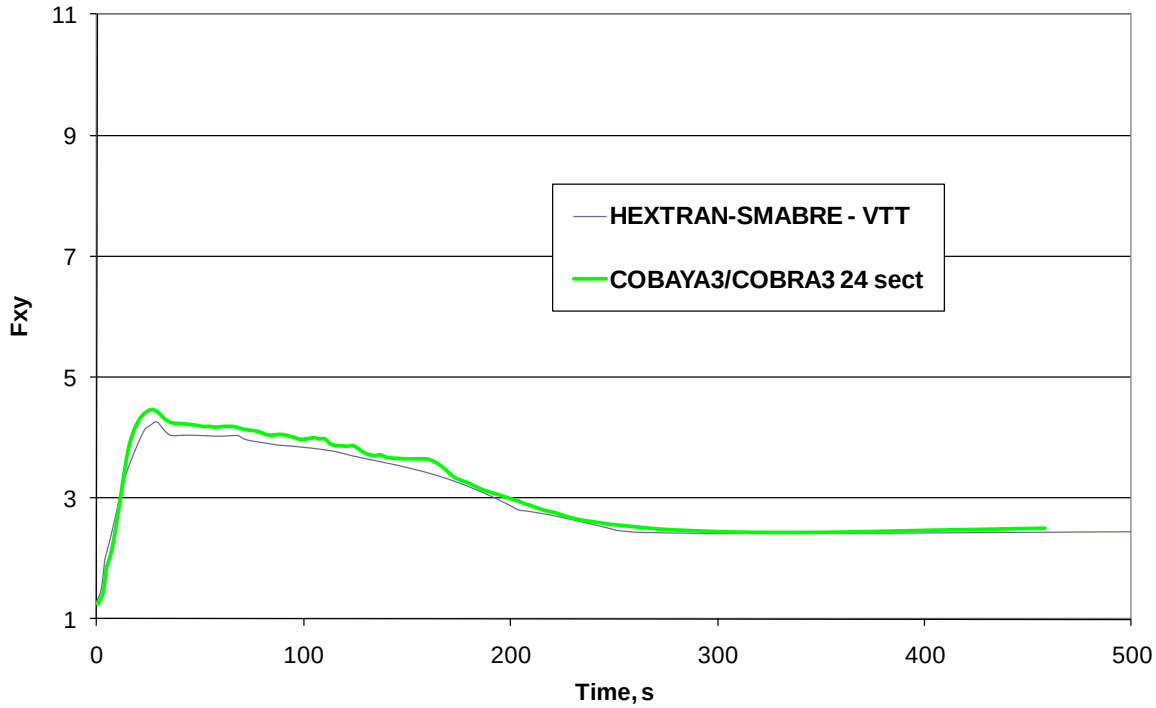


**Figure 5.51: Scenario 2 with stuck rods in #117&140: Time history of Fxy Core inlet conditions for COBAYA/COBRA from a CATHARE 24-sector vessel calculation**

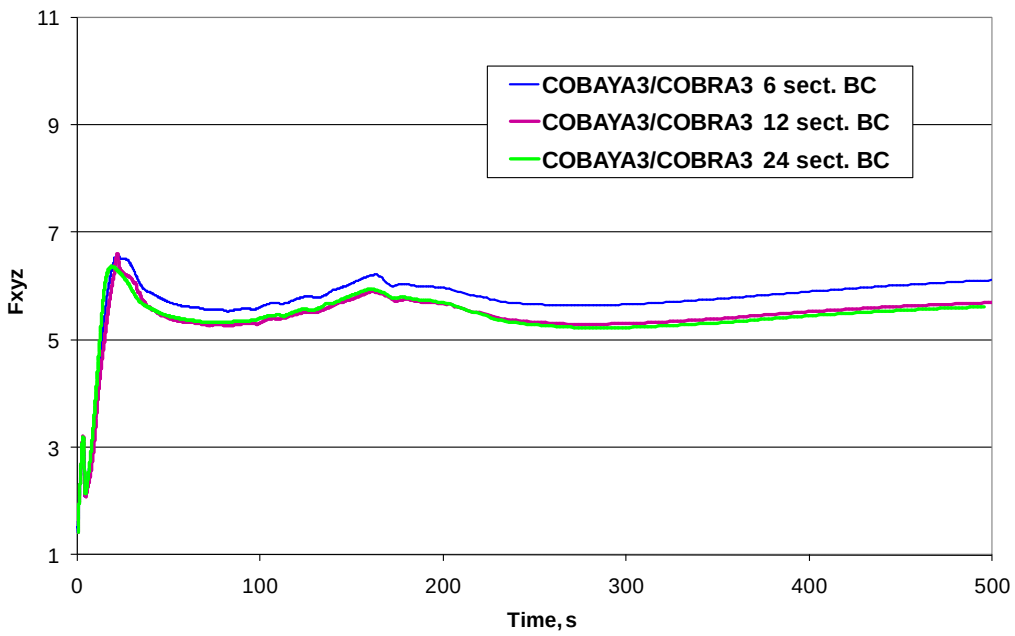


**Figure 5.52: Scenario 2, stuck rods in #117&140. Time history of Fxyz**
**Impact of the meshing in the vessel mixing model**

**Table 5.18: Comparison of $F_{xy}$ and $F_z$**

| | DYN3D/ATHLET | HEXTRAN/SMABRE | COBAYA/COBRA |
|---|---|---|---|
| **Fxy-HFP** | 1.283 | 1.303 | 1.279 |
| **Fxy-HRP*** | 4.051 | 4.011 | 3.937 |
| **Fxy-200s** | 2.816 | 2.878 | 2.575 |
| **Fz-HFP** | 1.180 | 1.187 | 1.151 |
| **Fz-HRP** | 1.272 | 1.400 | 1.268 |
| **Fz-200s** | 1.815 | 2.043 | 1.722 |
| **$Fz_{\#140}$-HRP** | 1.213 | 1.160 | 1.184 |
| **$Fz_{\#140}$-200s** | 1.552 | 1.799 | 1.592 |
| **$Fz_{\#117}$-HRP** | 1.195 | 1.180 | 1.171 |
| **$Fz_{\#117}$-200s** | 1.554 | 1.763 | 1.588 |

**Table 5.19: COBAYA results: Comparison of $F_{xy}$ and $F_z$**

| | COBAYA 6sect. | COBAYA 12sect. | COBAYA 24 sect. |
|---|---|---|---|
| **Fxy-HFP** | | 1.279 | |
| **Fxy-HRP** | 3.534 | 3.854 | 3.937 |
| **Fxy-200s** | 2.531 | 2.561 | 2.575 |
| **Fz-HFP** | | | |
| **Fz-HRP** | 1.439 | 1.282 | 1.268 |
| **Fz-200s** | 1.735 | 1.725 | 1.722 |
| **$Fz_{\#140}$-HFP** | | | |
| **$Fz_{\#140}$-HRP** | 1.263 | 1.166 | 1.184 |
| **$Fz_{\#140}$-200s** | 1.641 | 1.597 | 1.592 |
| **$Fz_{\#117}$-HFP** | | | |
| **$Fz_{\#117}$-HRP** | 1.21 | 1.154 | 1.171 |
| **$Fz_{\#117}$-200s** | 1.635 | 1.592 | 1.588 |

* HRP – at highest return to power

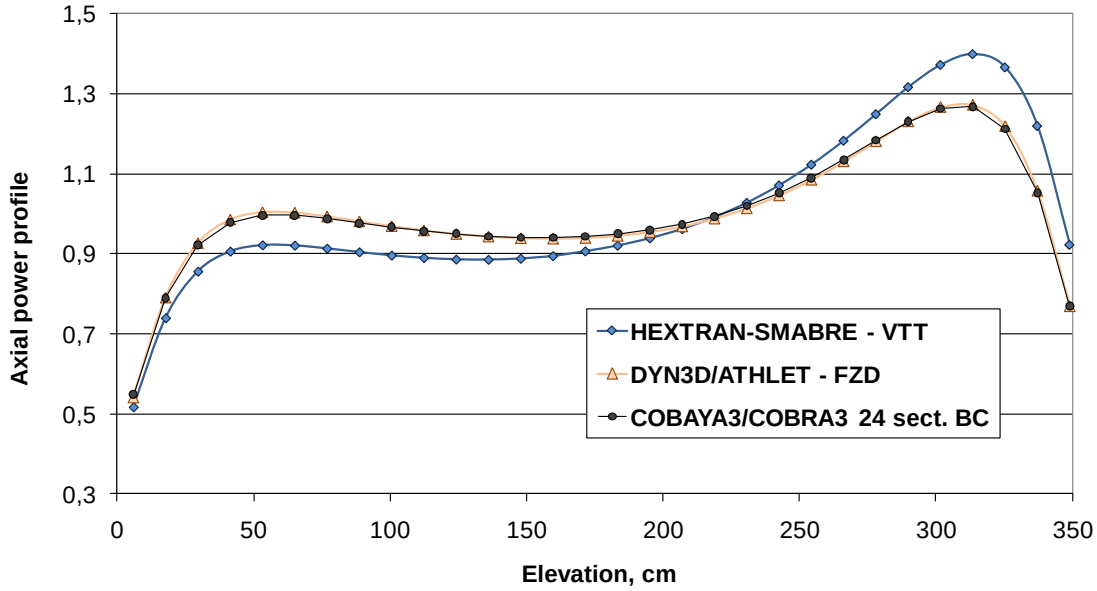


**Figure 5.53: Core-average axial power distribution at time of maximum overcooling (69s), for Scenario 2 with stuck rods in #117&#140**

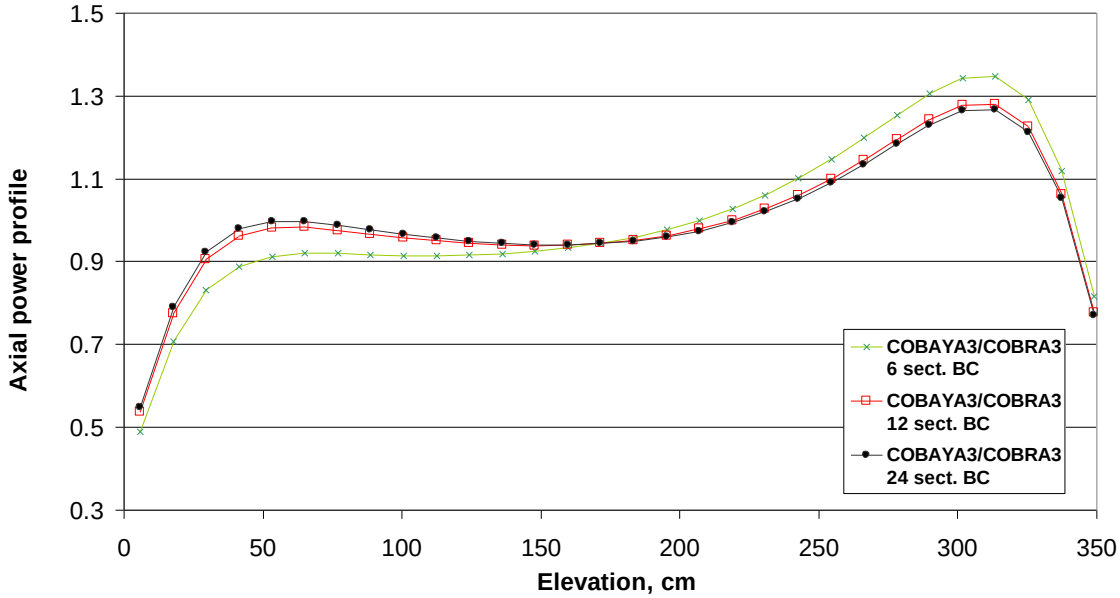


**Figure 5.54: Impact of the vessel mixing model on the core-average axial power distribution at 69s, for Scenario 2 with stuck rods in #117&#140**

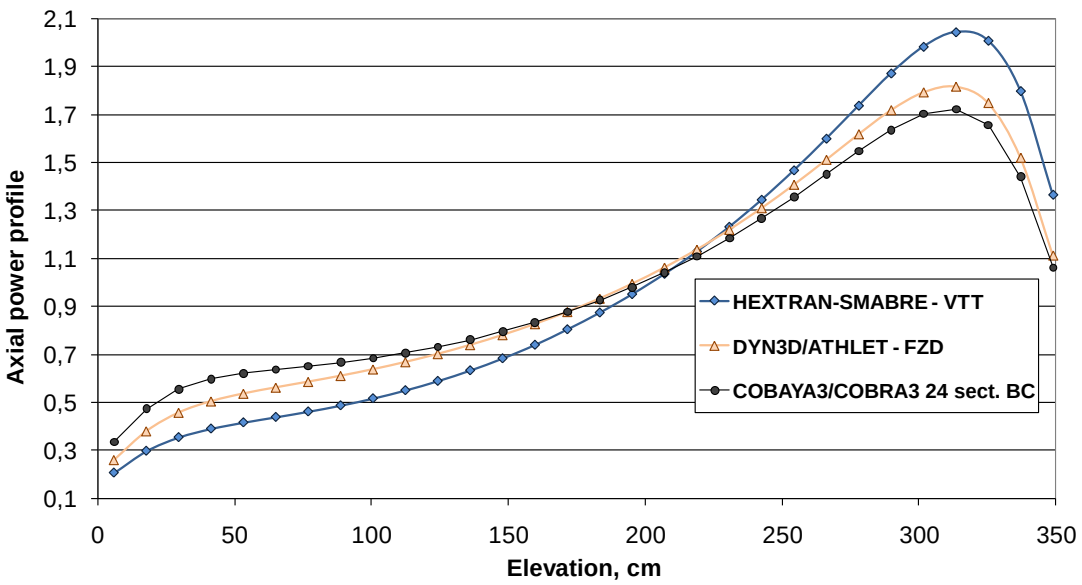


**Figure 5.55: Core-average axial power distribution at 200s, for Scenario 2 with stuck rods in #117&#140**

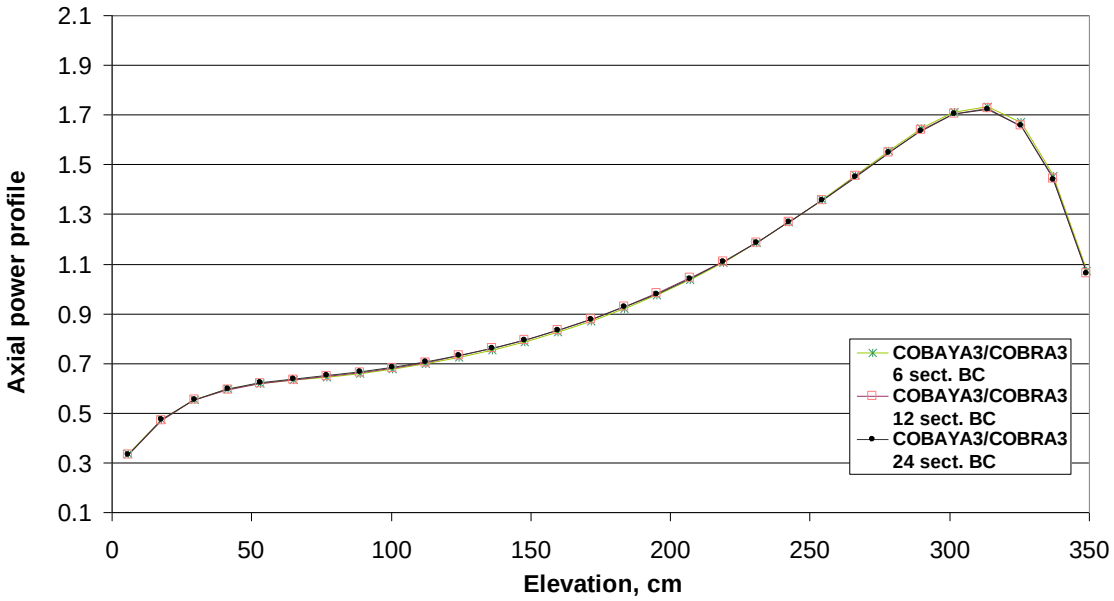


**Figure 5.56: Impact of the meshing in the vessel mixing model on the core average axial power distribution at 200s, for Scenario 2 with stuck rods in #117&#140**

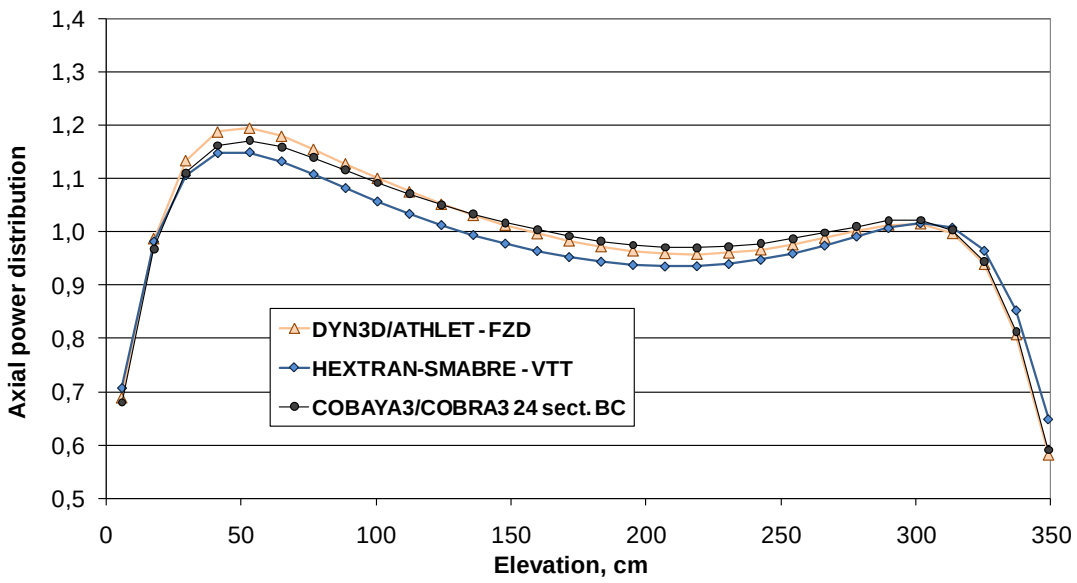


**Figure 5.57: Axial power distribution in stuck rod position #117 at 69s, for Scenario 2 with stuck rods in #117&#140**

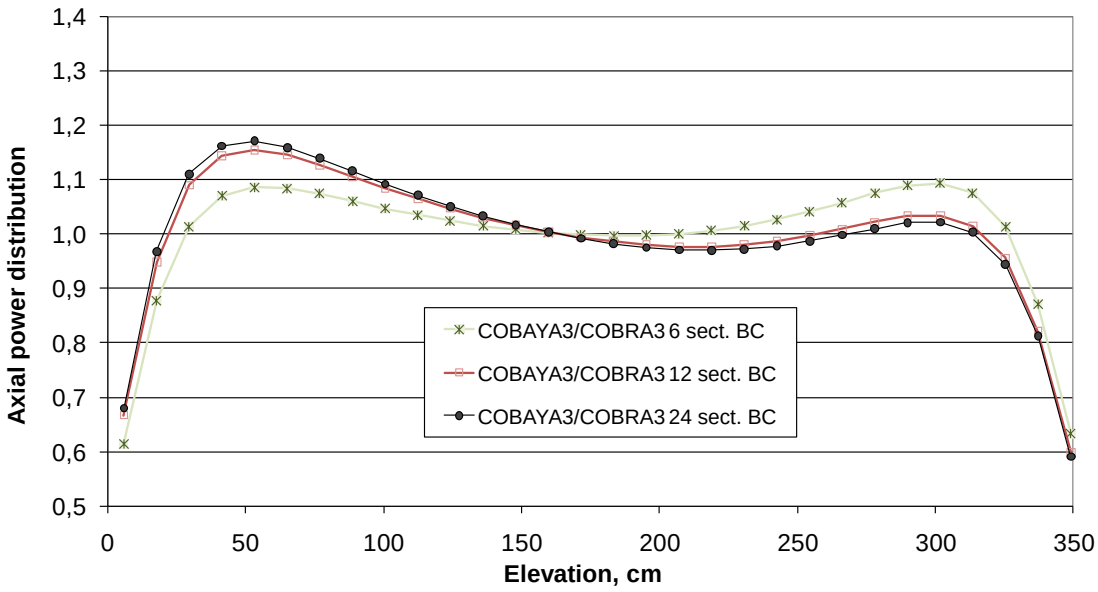


**Figure 5.58: Scenario 2 with stuck rods in #117&#140. Impact of the mixing model meshing on the axial power distribution in stuck rod position #117 at 69 s**

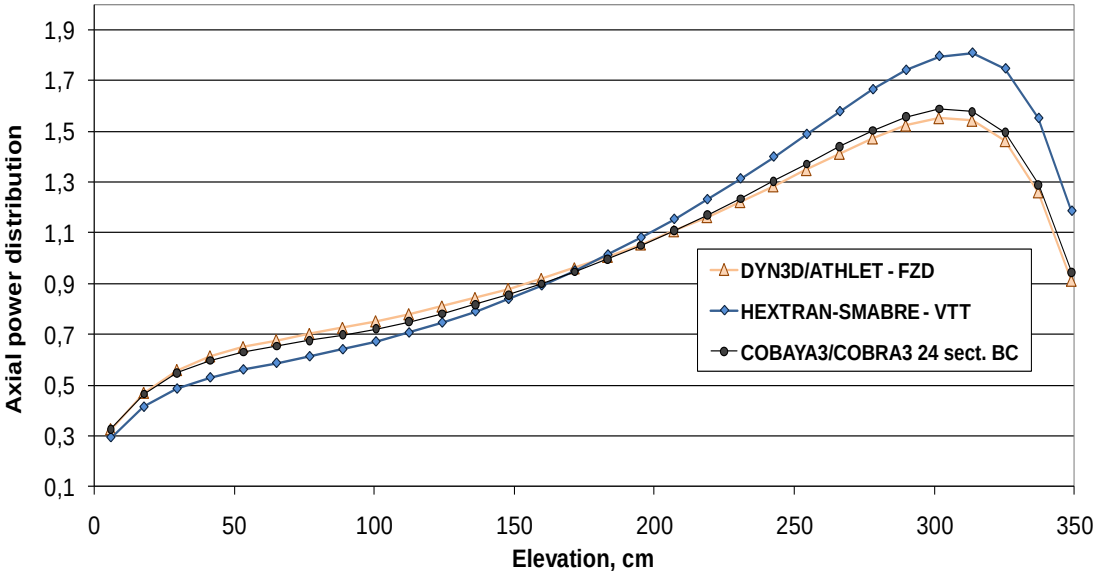


**Figure 5.59: Scenario 2 with stuck rods in #117&#140. Axial power distribution in stuck rod position #117 at 200s**

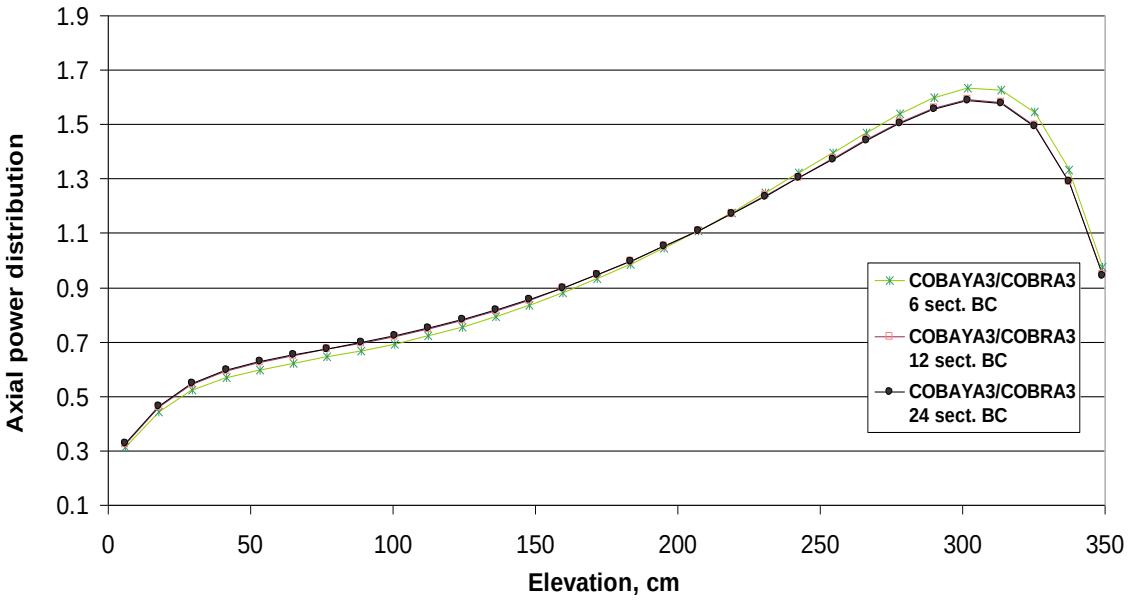


**Figure 5.60: Scenario 2 with stuck rods in #117&#140. Impact of the mixing model meshing on the axial power distribution in stuck rod position #117 at 200s**

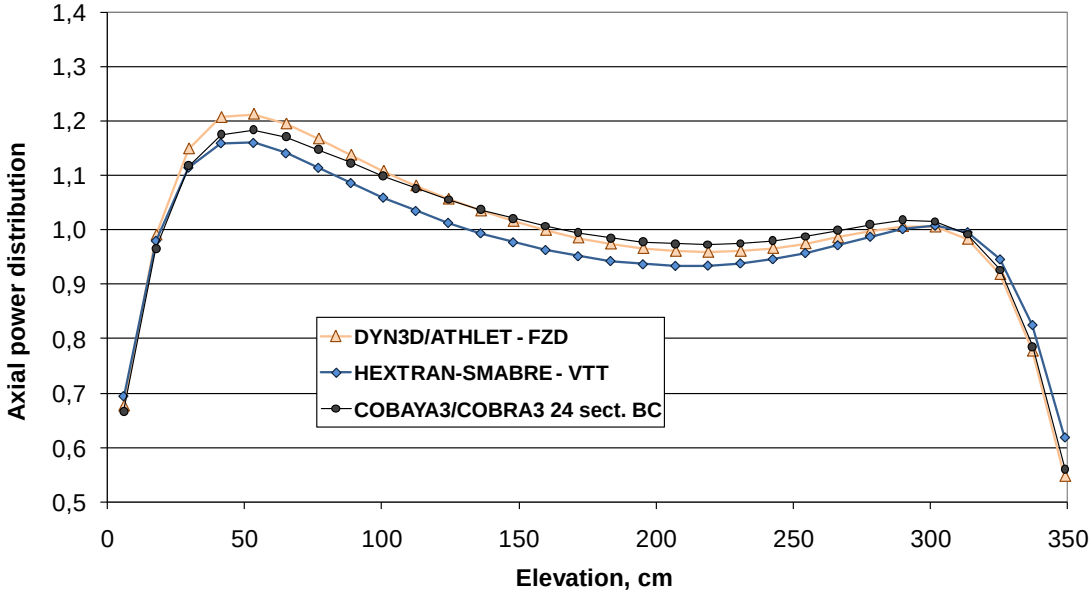


**Figure 5.61: Scenario 2 with stuck rods in #117&#140. Axial power distribution in stuck rod position #140 at 69s**

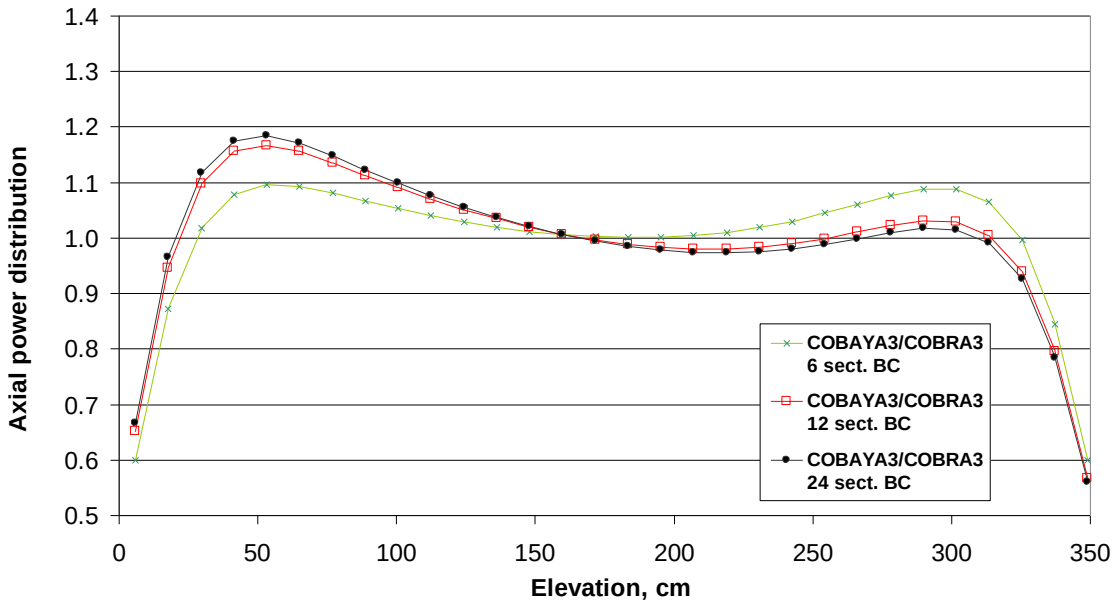


**Figure 5.62: Scenario 2 with stuck rods in #117&#140. Impact of the mixing model meshing on the axial power distribution in stuck rod position #140 at 69s**

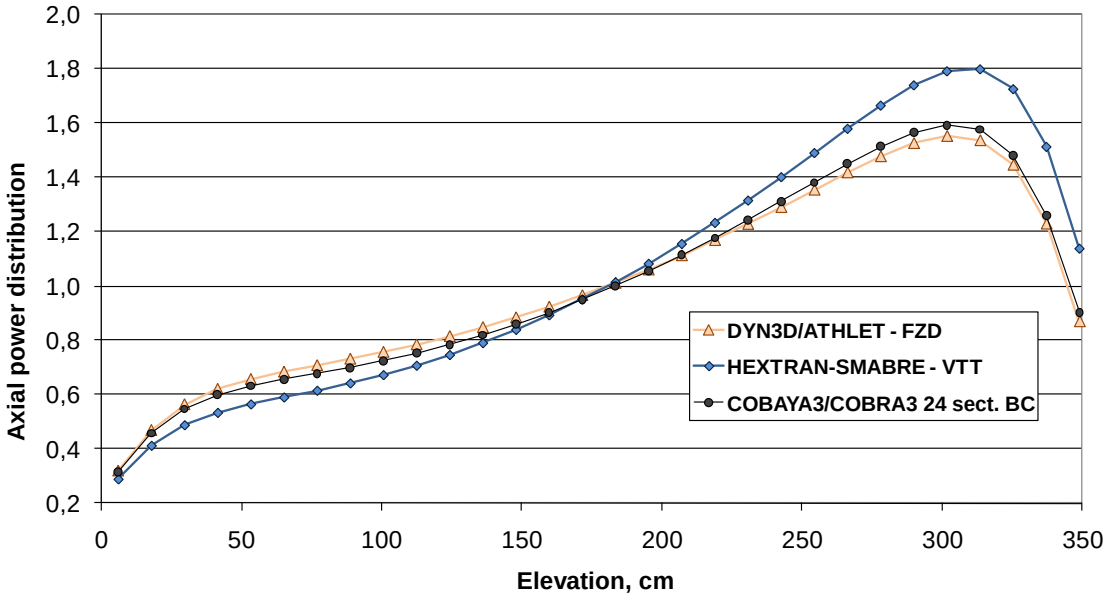


**Figure 5.63**: **Scenario 2 with stuck rods in #117&#140. Axial power distribution in stuck rod position #140 at 200s**

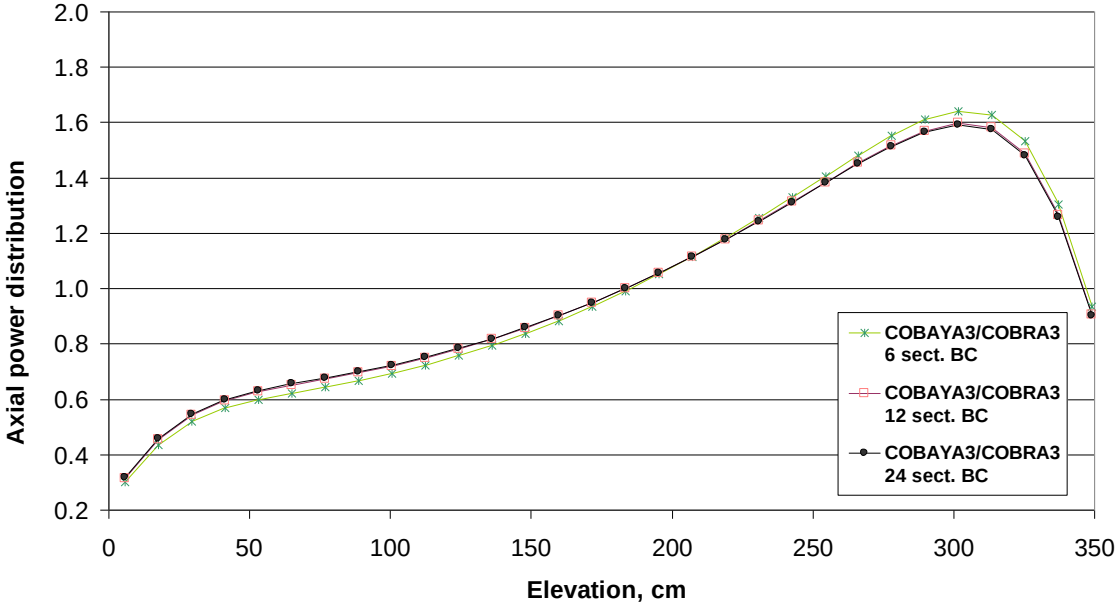


**Figure 5.64: Scenario 2 with stuck rods in #117&#140. Impact of the mixing model meshing on the axial power distribution in stuck rod position #140 at 200s**

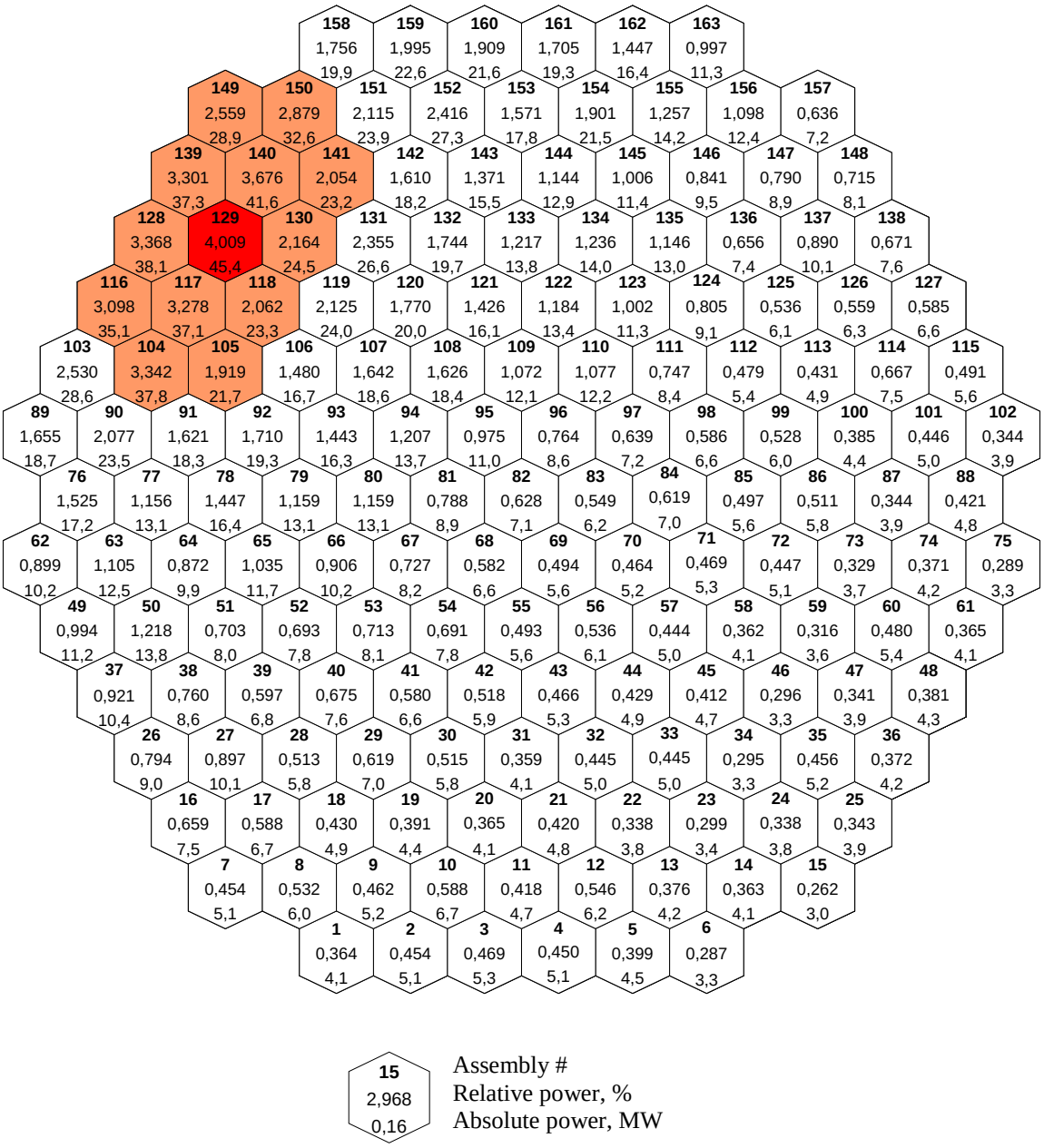


**Figure 5.65: Scenario 2 with stuck rods in #117&#140. Snapshot of the HEXTRAN/SMABRE computed assembly powers at 69s**

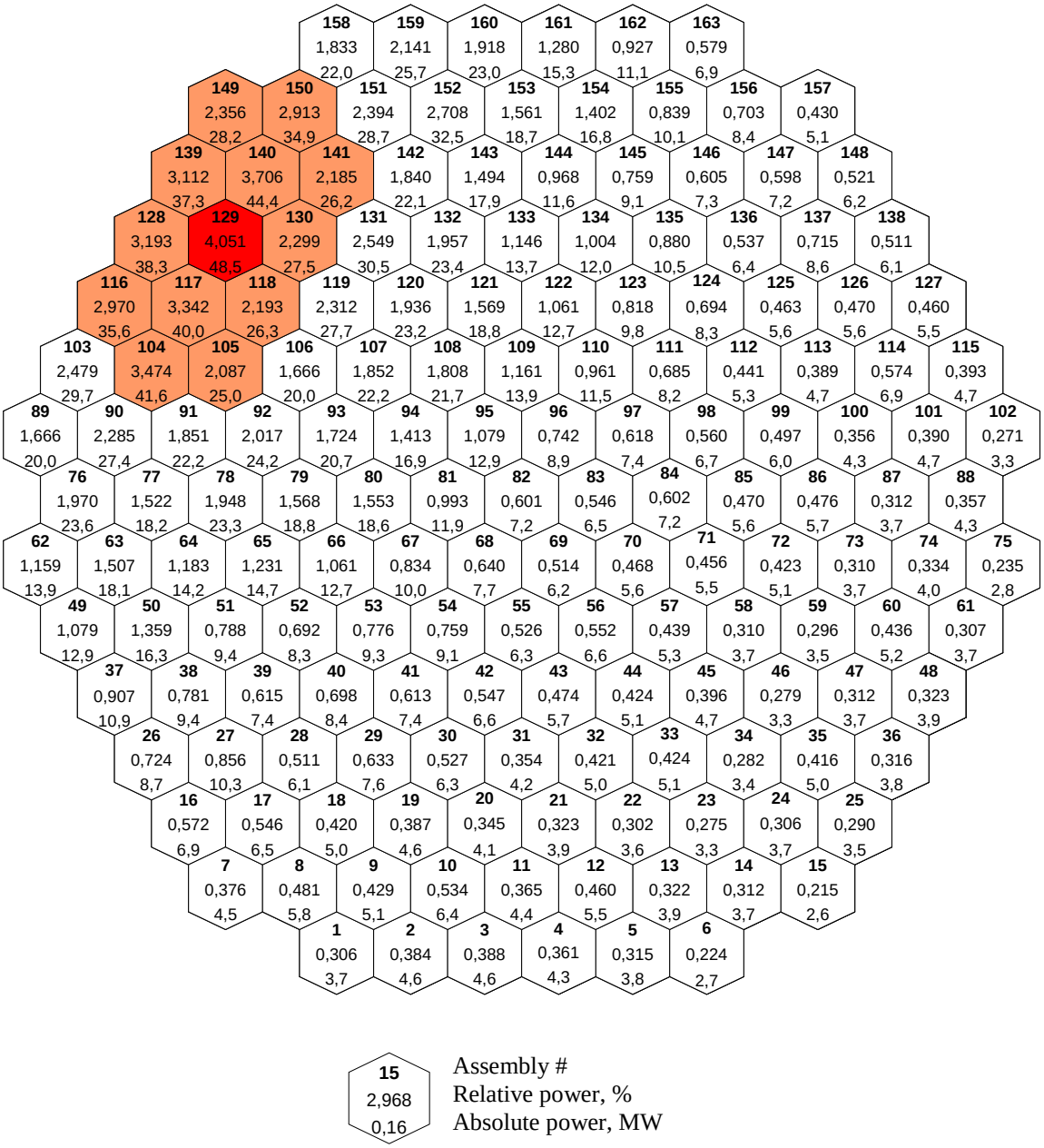


**Figure 5.66: Scenario2 with stuck rods in #117&#140. Snapshot of the DYN3D/ATHLET computed assembly powers at 69s**

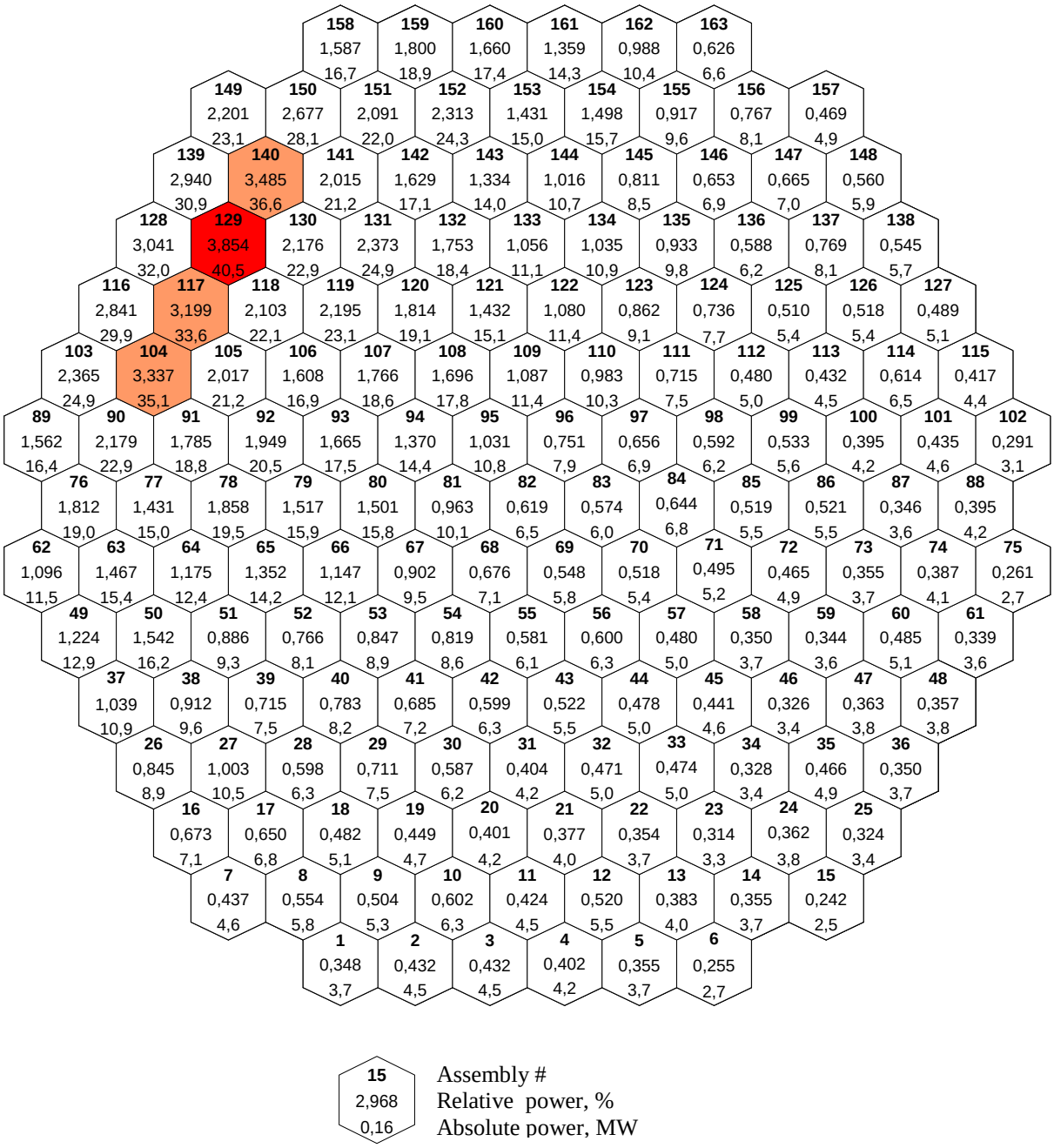


**Figure 5.67: Scenario2 with stuck rods in #117&#140, and 12-sector model computed core BC. Snapshot of COBAYA3/COBRA3 predicted assembly powers at 69s**

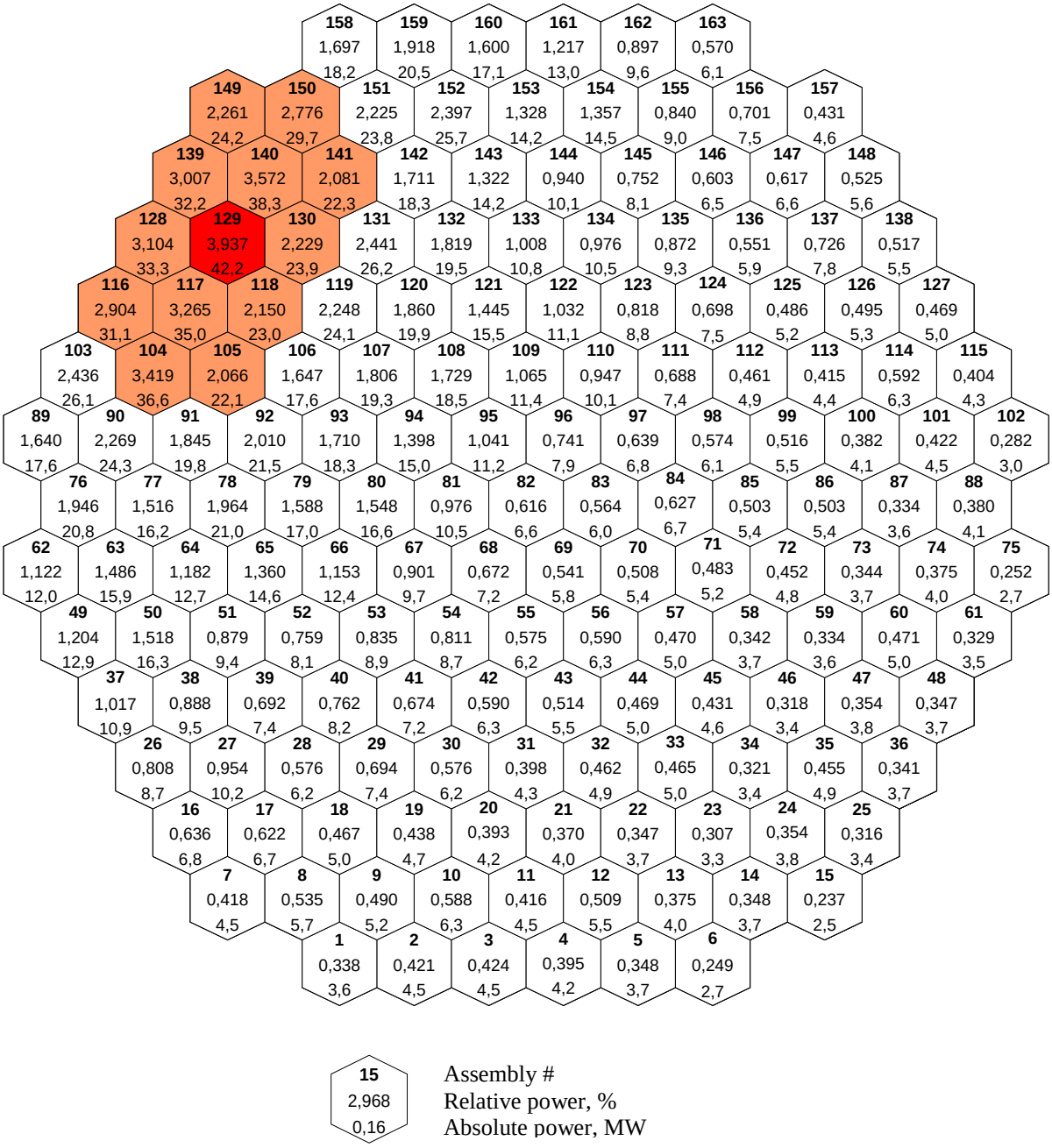


**Figure 5.68: Scenario2 with stuck rods in #117&#140, and 24-sector model computed core BC. Snapshot of the COBAYA3/COBRA3 predicted assembly powers at 69s**

# Chapter 6: Results of Exercise 3

The objective of Exercise 3 is to test the core-vessel-plant coupling in a full plant simulation. The integrated codes employ improved component and circuit models, already tested in the V1000CT-2 Benchmark Exercises 1 and 2, and the MCP start up transient of V1000CT-1 benchmark. A specific objective of this exercise is to test the VVER-1000 secondary circuit model in MSLB calculations.

The results in this Chapter provide a code-to-code comparison of participants' solutions. Since the BIPR8/ATHLET plant model of VVER-1000 is well validated, the BIPR8/ATHLET solution for Scenario 2 serves as a support solution for the secondary circuit and especially for the controllers. In order to eliminate the uncertainty in modeling of the SG feed-water flow controllers, an option with ATHLET calculated feed-water flow boundary conditions is provided in the specification (Kolev et al, 2010a).

In the analysis to follow, we focus on Scenario 2 results. Scenario 1 results are given in Appendix E and are briefly discussed below.

## 6.1 Scenario 1 results

The objective is to analyze the impact of the improved vessel thermal-hydraulic modeling in a core-plant simulation of a coolant transient involving asymmetric loop cool-down and pump trip. A specific objective is to test the user models of the VVER-1000 secondary circuit in system codes.

The results in Appendix E graphically illustrate the agreement or disagreement of the solutions in code-to-code comparison. The analysis shows a reasonable qualitative agreement of the time histories, and unacceptable quantitative differences in important parameters. As the reactor power is at the decay heat level, the discrepancies are mainly due to secondary circuit modeling which requires further attention.

Because of an error in the BIPR8/ATHLET user input file, the check valve in the broken line has been completely closed (actually it allows up to 50 kg/s flow rate in reverse direction). In consequence, the intact steam generators pressure is incorrect. Please note that a second MCP trips on secondary circuit pressure signal at ~ 200s, and comparison with BIPR8/ATHLET results is possible only in the initial part of the transient.

## 6.2 Scenario 2 results

For the purposes of this analysis, we consider the MSLB Scenario 2 with stuck rods in assemblies #117 and #140. This scenario is of special interest because of the return to power phenomenon enforced by decreasing the tripped rods reactivity worth, which is a very good test case for the coupled codes.

During the transient, all MCP remain in operation. The control rods in assemblies #117 and #140 remain stuck out of the core after scram. A return to power occurs, reaching a maximum of about 50% nominal rated power at about 69 s from the beginning of the transient.

Three participants have submitted integrated code solutions of Exercise 3 - GRS/KI (BIPR8/ATHLET), VTT (HEXTRAN/SMABRE) and UNIPI (NEM/RELAP3D). The BIPR8 code has used its native cross-section library. A supplementary CATHARE2 solution with point kinetics is also compared to evaluate the secondary circuit model vs. the validated BIPR8/ATHLET user model.

The available solutions are insufficient for statistical treatment. In the discussion to follow, the agreement or disagreement of the results is only graphically illustrated.

We focus on the testing of the secondary circuit and the full plant model. Parameter distributions have been considered in Exercise 2 and are not analyzed here. The analysis comprises 39 time histories.

### 6.3 Time histories

*Break flow rate*

Figure 6.1 shows the computed total break flow rates. All participants use direct solution for the break flow with the code thermal-hydraulic model. The significant difference in maximal values in the first seconds predicted with ATHLET is due to the specific ATHLET modeling of the liquid fraction of the break flow, based on empirical information (S. Nikonov, 2004).

Figure 6.2 shows the computed total integrated break flow. The flows computed by GRS/KI and UNIPI show a relatively good agreement after the initial phase of the transient where the impact of the liquid break flow is strong.

Figure 6.3 displays a wide spread in the predicted liquid break flows. The CATHARE2 predicted integrated liquid flow (Kolev et al, 2004), (Kolev et al, 2005) is 22000 kg.

*BRU-K and BRU-SN steam dump flows*

The modeling of the steam dump flows and MSH pressure are important for the correct simulation of the MSLB transient.

The results in Figures 6.4 and 6.5 show a generally good agreement between the ATHLET and CATHARE2 predicted steam dump to condenser (BRU-K) flow rates and integrated flows. In the CATHARE2 VVER-1000 model, the BRU-K and BRU-SN controllers are similar to those in the ATHLET input model. The steam dump to house needs (BRU-SN) model is somewhat simplified, as described in the specification (Kolev et al, 2010a). Correspondingly, the ATHLET and CATHARE2 predicted MSH pressure and BRU-SN flows are in generally good agreement.

The results in Figures 6.6 and 6.7 show significant differences in the VTT and UNIPI computed flow rates of the steam dump to house consumption (BRU-SN), mainly due to oversimplified controller modeling. In this comparison, the GRS/KI ATHLET solution serves as reference.

*Pressures*

Figures 6.8-6.12 show the predicted secondary circuit pressures. Good agreement of the BIPR8/ATHLET, CATHARE2 and HEXTRAN/SMABRE results is displayed. The RELAP3D results in Figures 6.8 and 6.9 show a discrepancy due to incorrect modeling of the MSH pressure controller.

Figures 6.13-6.17 show the computed time histories of primary circuit pressures. There is a spread in the results reflecting the impact of different mixing models and power dynamics. The significant discrepancy in the VTT results is related with the modeling of the secondary circuit dynamics, including steam dump controllers (see Figures 6.32-6.39).

*Temperatures*

Figures 6.18-6.26 show the computed time histories of primary circuit temperatures at the reactor inlet and outlet nozzles and the core average coolant temperature. The results of BIPR8/ATHLET and CATHARE2 are in generally good agreement. The discrepancy in the RELAP3D results reflects the impact of wrong MSH pressure calculation due to the BRU-K pressure controller modeling, and the use of one-channel upper plenum model which lumps the flow parameters above the core. The difference in the HEXTRAN/SMABRE computed temperature in the faulted loop #4 seems to be a combined effect of the computed pressure and mass inventory in the intact SG.

The differences in the core average coolant density and Doppler temperatures, seen in Figures 6.27 and 6.29, influence the total power dynamics as shown in Figures 6.30-6.31.

*Total power*

Figures 6.30 and 6.31 illustrate the time history of the total fission and thermal reactor power. The predicted maximum total power after scram is smaller than that in Exercise 2 obtained with more conservative vessel thermal hydraulic boundary conditions.

For the considered solutions, the major contributions to the observed differences come from the modeling of the secondary pressure and steam flow, along with the spatial coupling and fuel modeling.

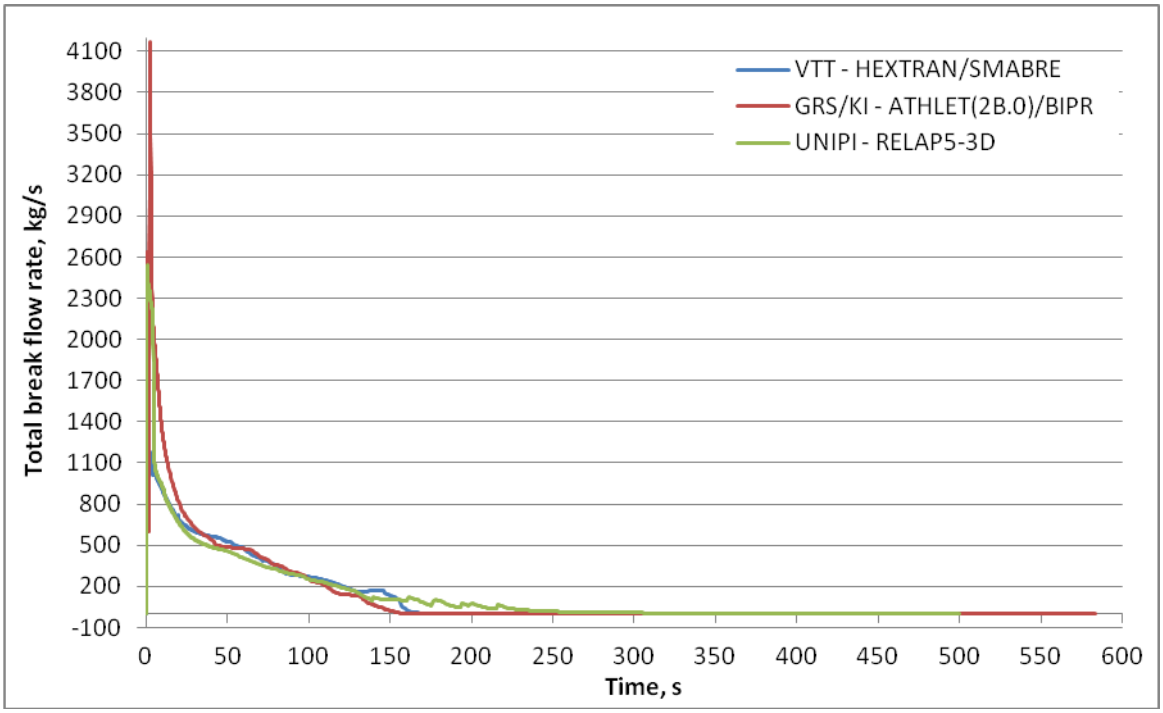


**Figure 6.1: Total break flow rate (Scenario 2)**

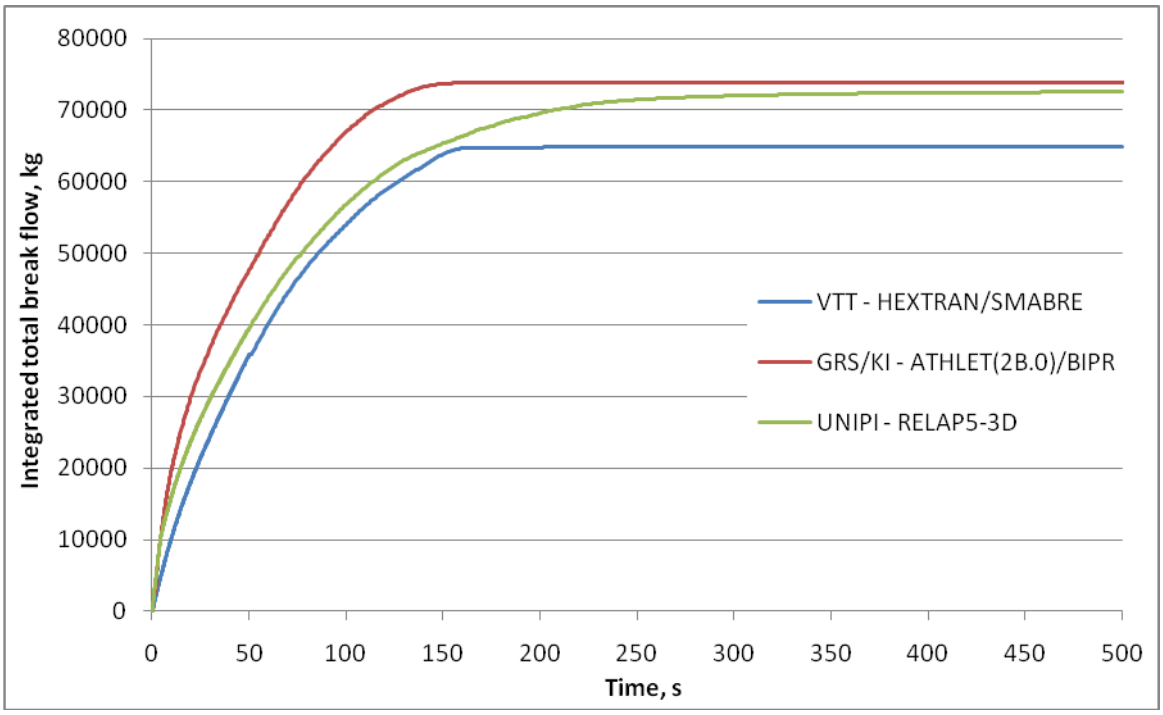


**Figure 6.2: Integrated total break flow rate (Scenario 2)**

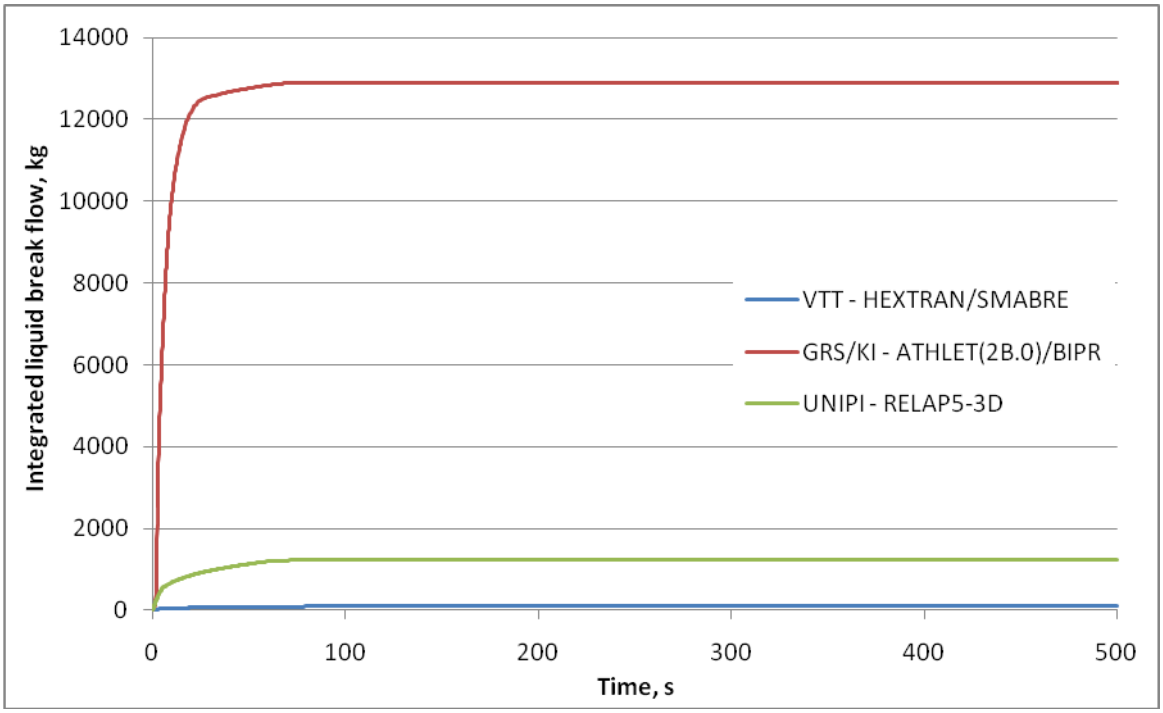


**Figure 6.3: Integrated liquid break flow rate (Scenario 2)**

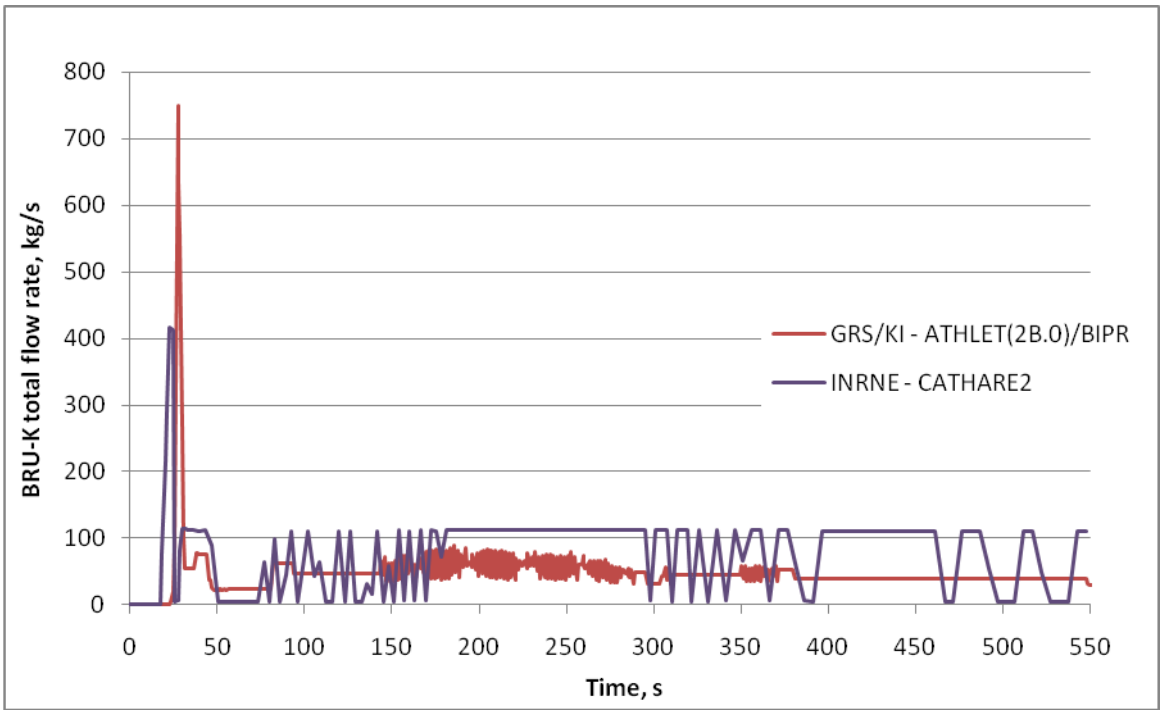


**Figure 6.4: BRU-K flow rate (Scenario 2)**

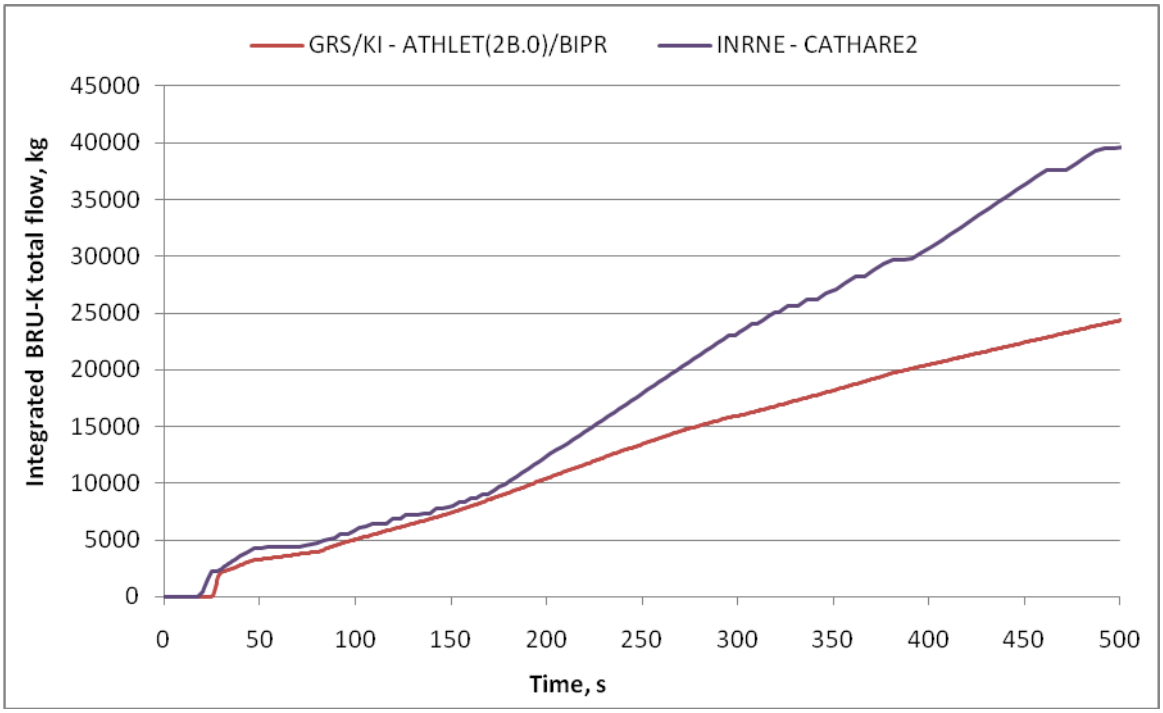


**Figure 6.5: Integrated BRU-K flow rate (Scenario 2)**

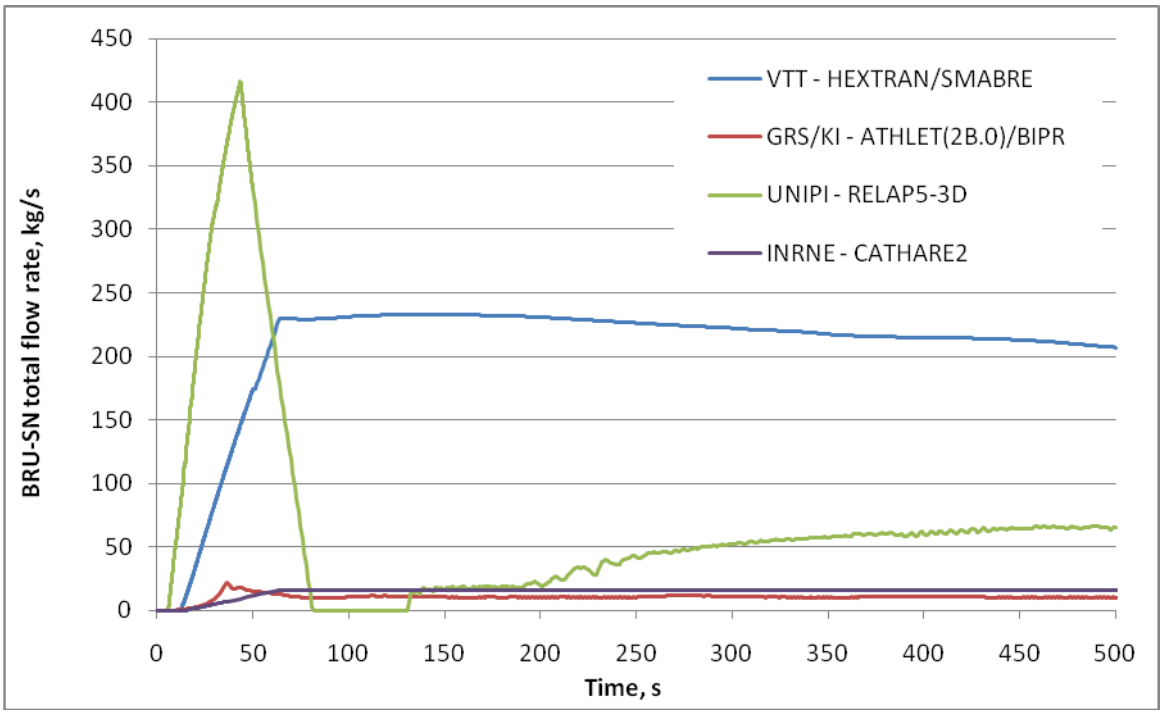


**Figure 6.6: BRU-SN total flow rate (Scenario 2)**

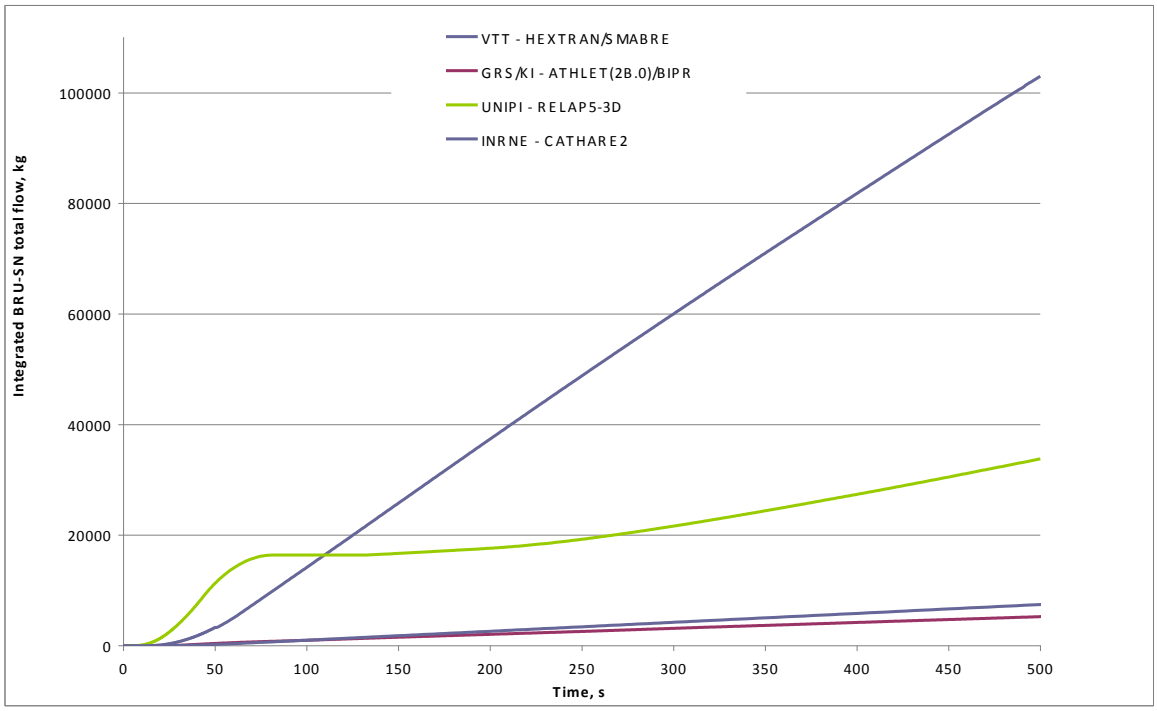


**Figure 6.7: Integrated total BRU-SN flow (Scenario 2)**

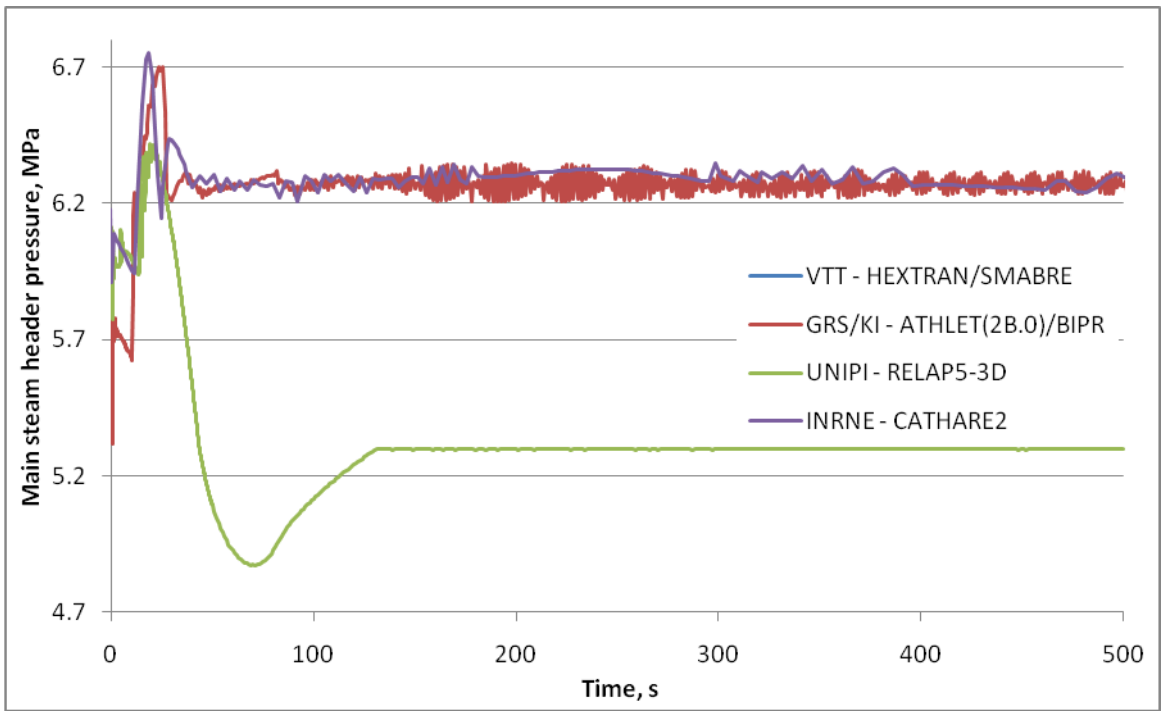


**Figure 6.8: Main steam header pressure (Scenario 2)**

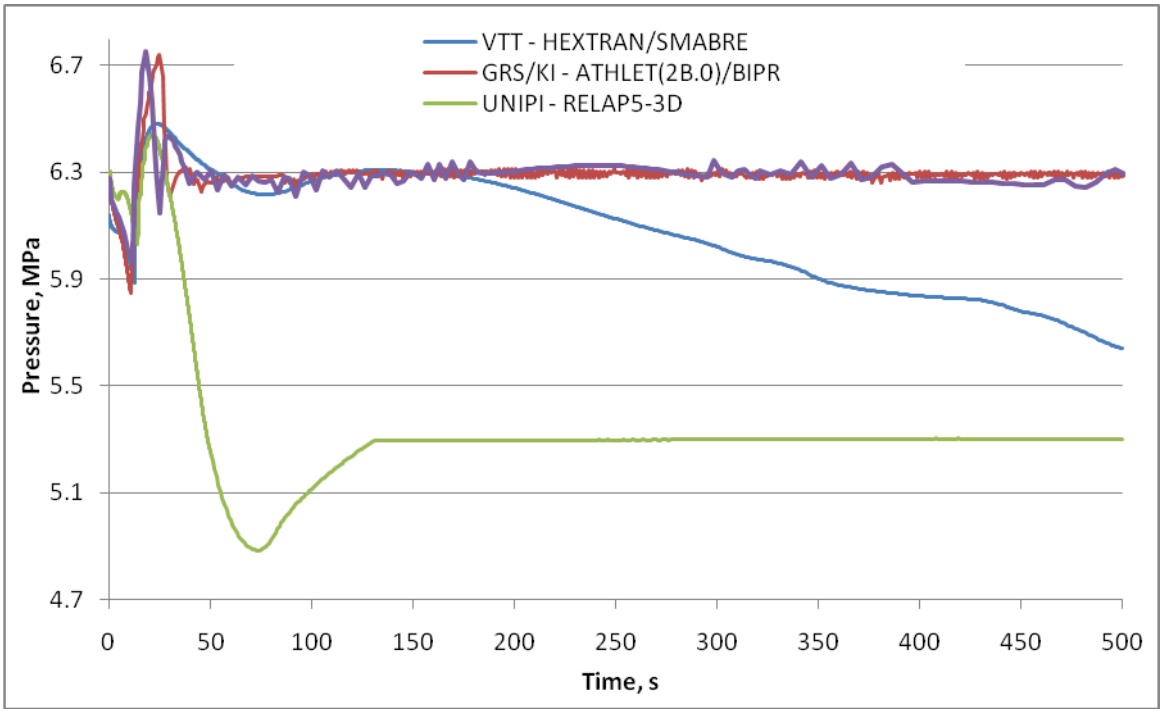


**Figure 6.9: SG1 pressure (Scenario 2)**

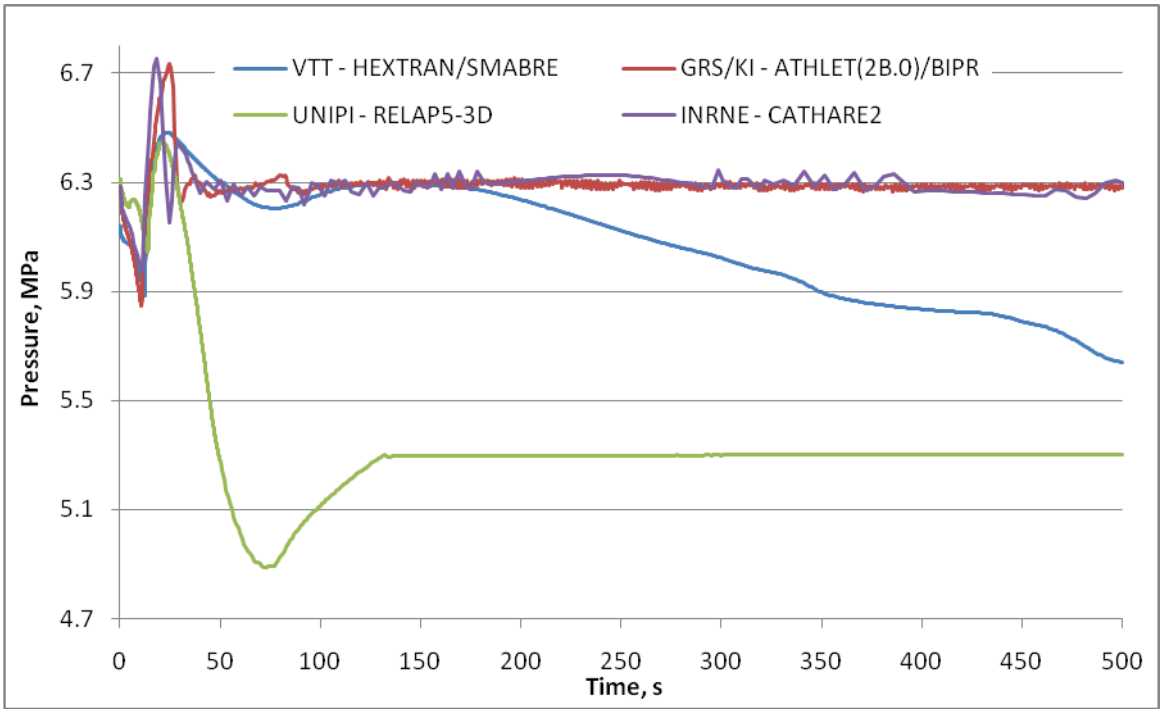


**Figure 6.10: SG2 pressure (Scenario 2)**

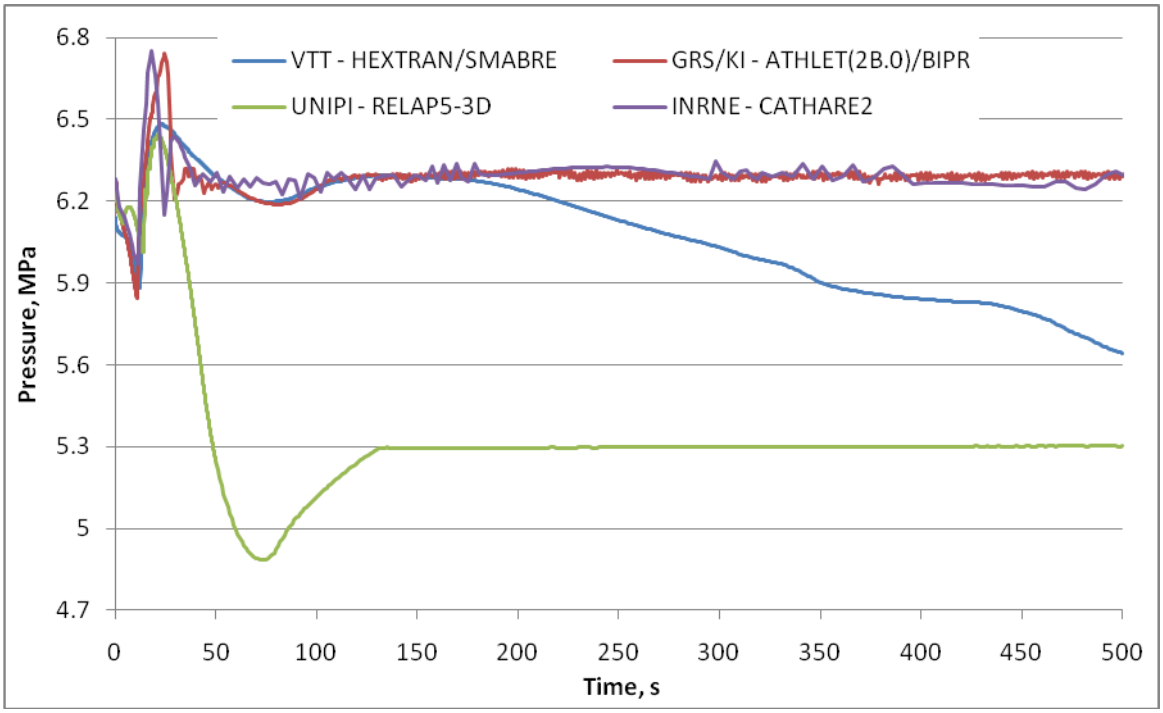


**Figure 6.11: SG3 pressure (Scenario 2)**

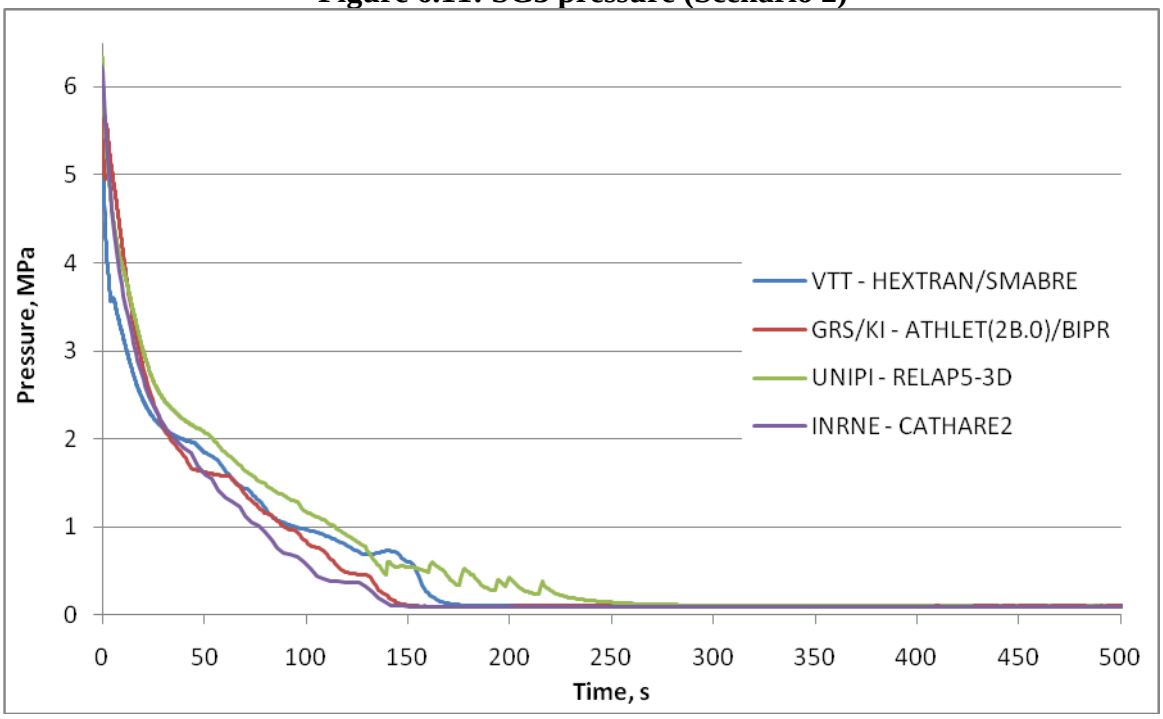


**Figure 6.12: SG4 pressure (Scenario 2)**

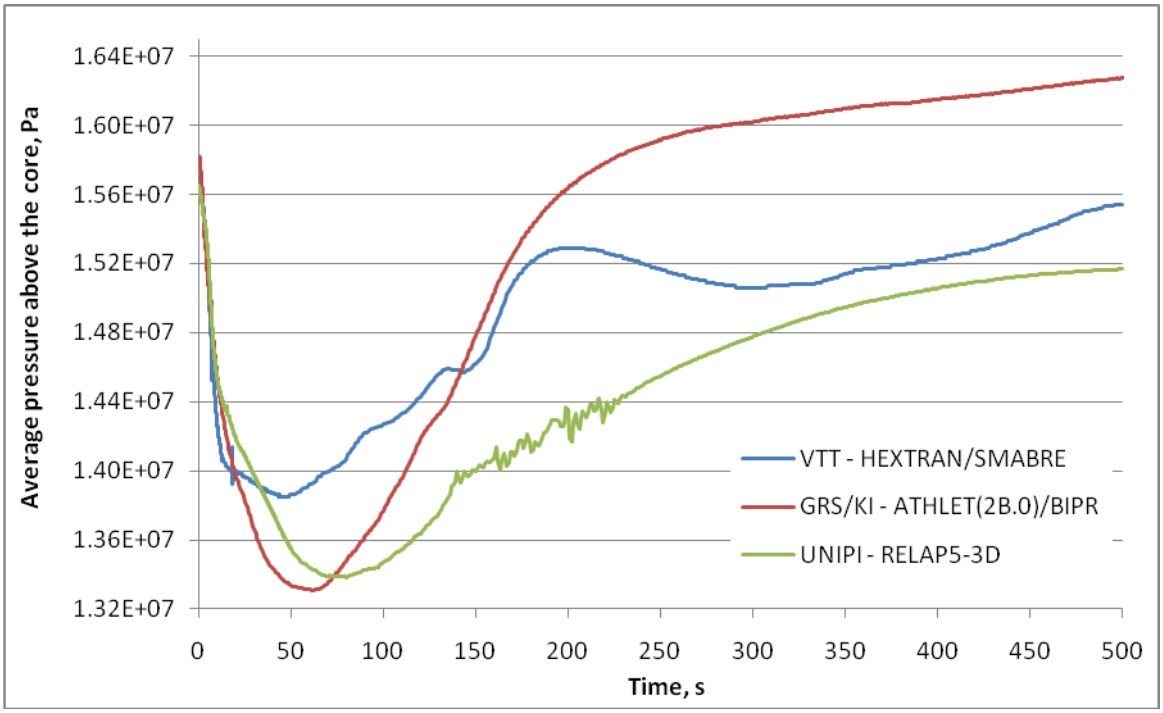


**Figure 6.13: Average pressure above the core (Scenario 2)**

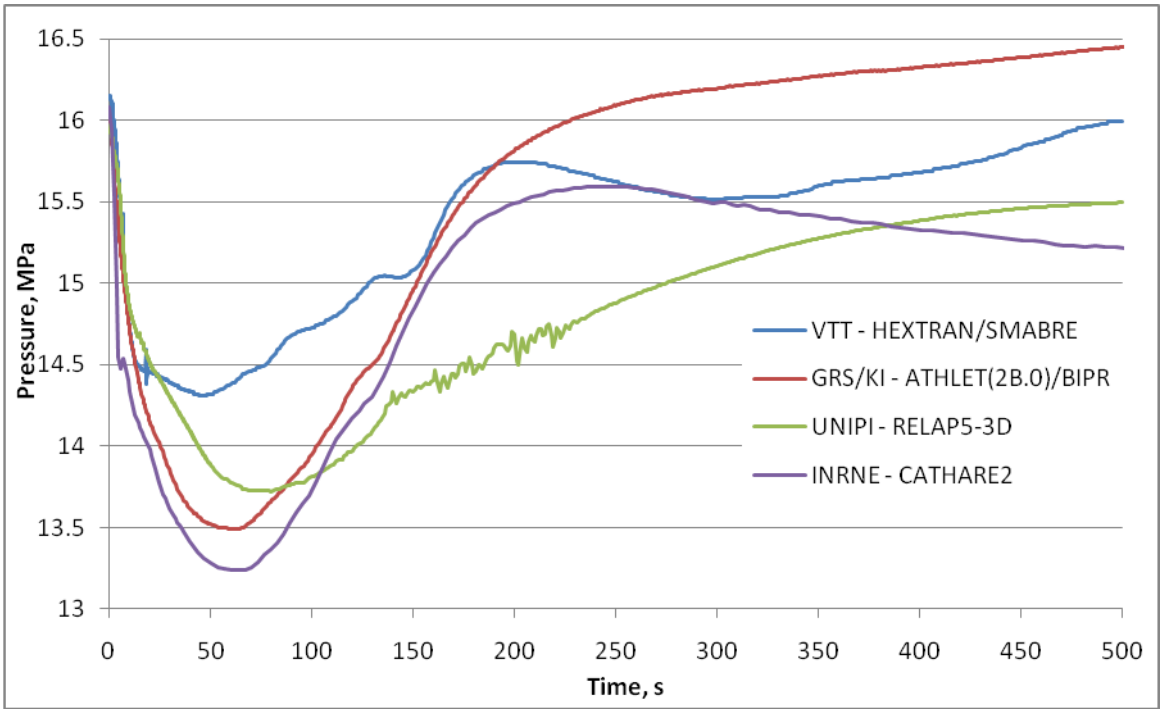


**Figure 6.14: Cold leg 1 pressure (Scenario 2)**

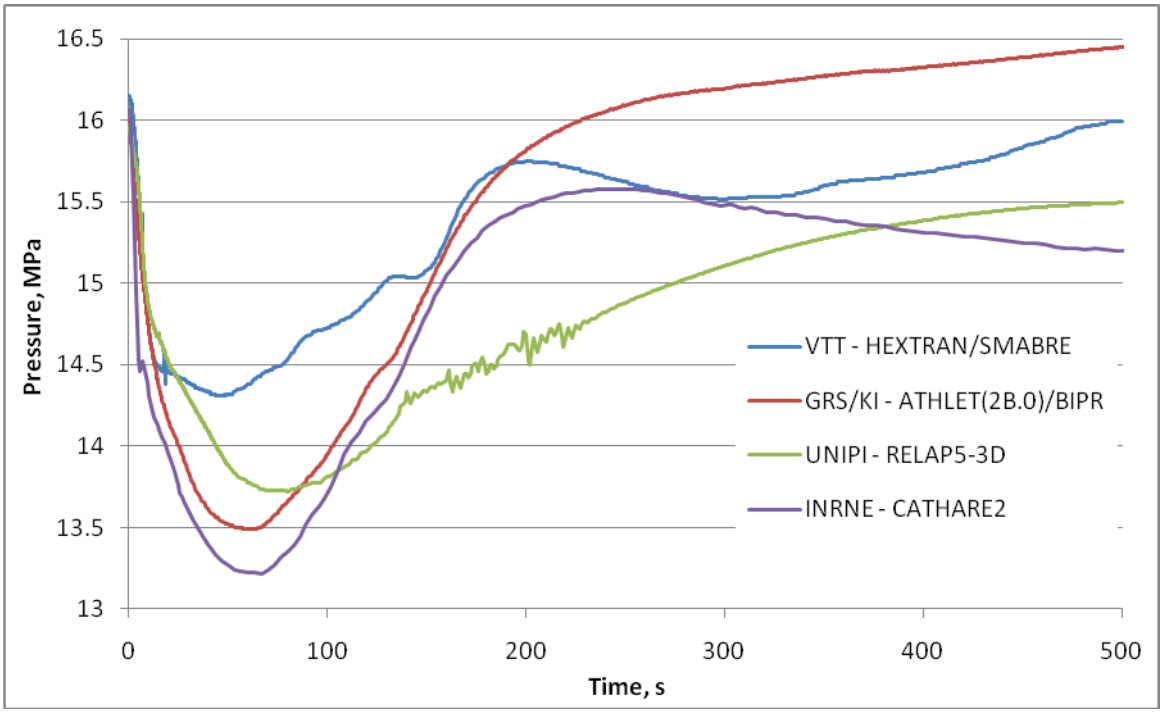


**Figure 6.15: Cold leg 2 pressure (Scenario 2)**

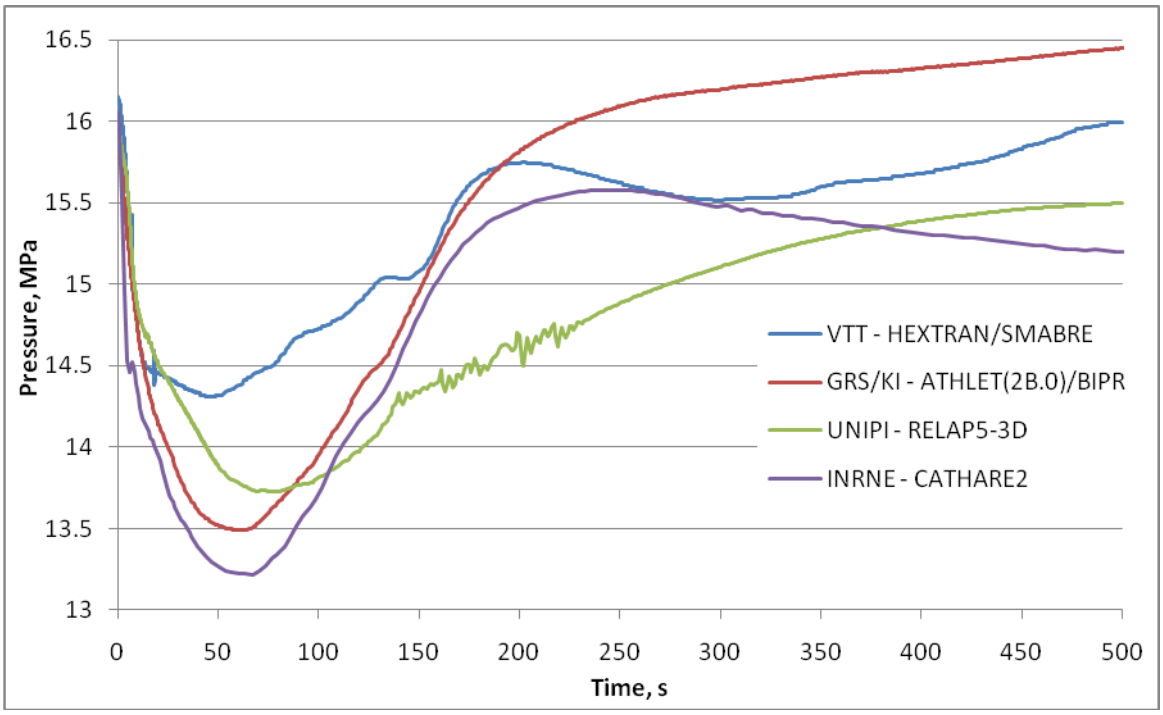


**Figure 6.16: Cold leg 3 pressure (Scenario 2)**

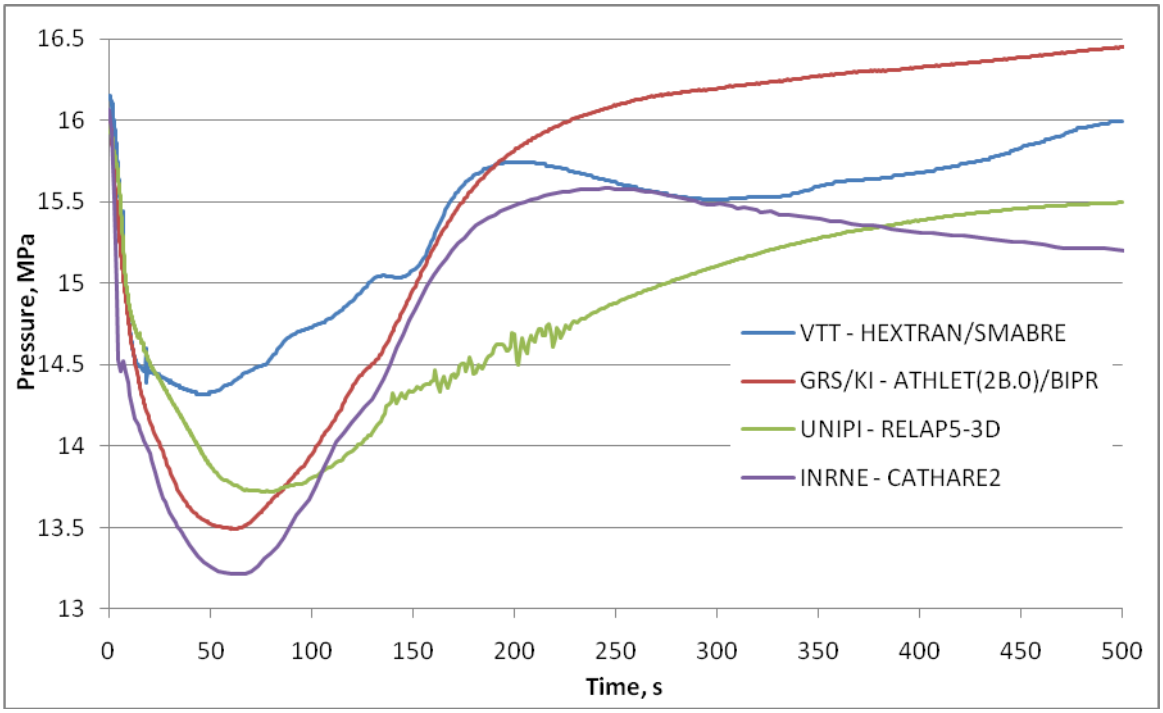


**Figure 6.17: Cold leg 4 pressure (Scenario 2)**

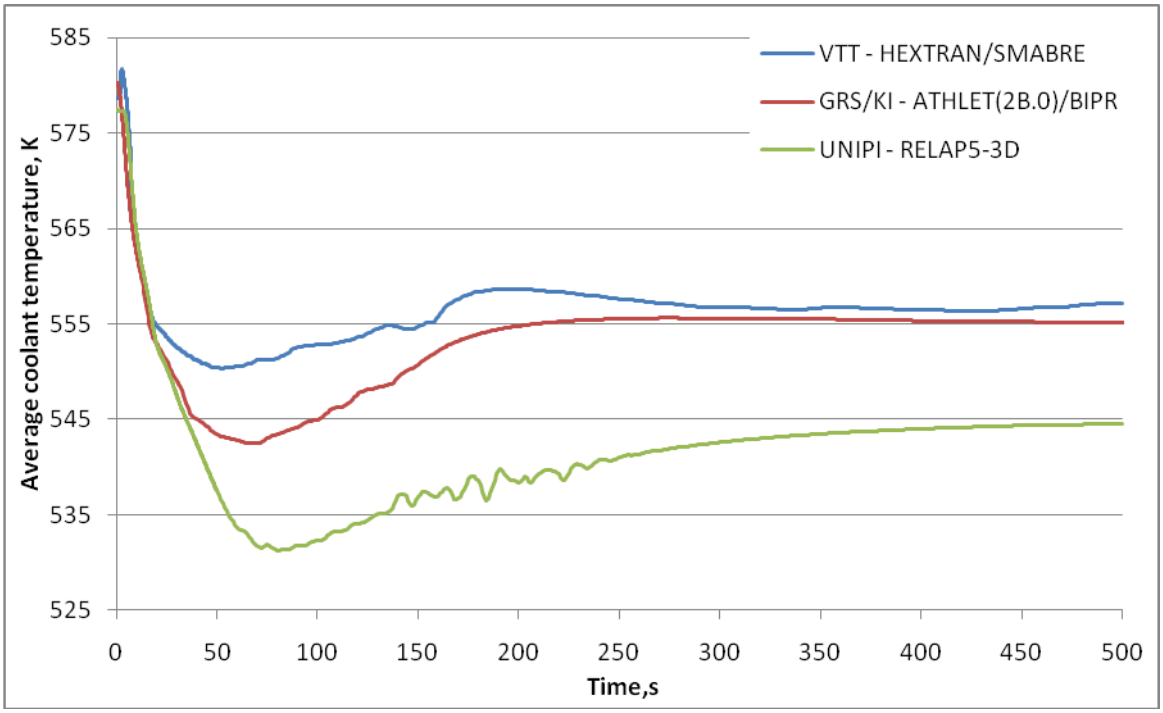


**Figure 6.8: Average core coolant temperature (Scenario 2)**

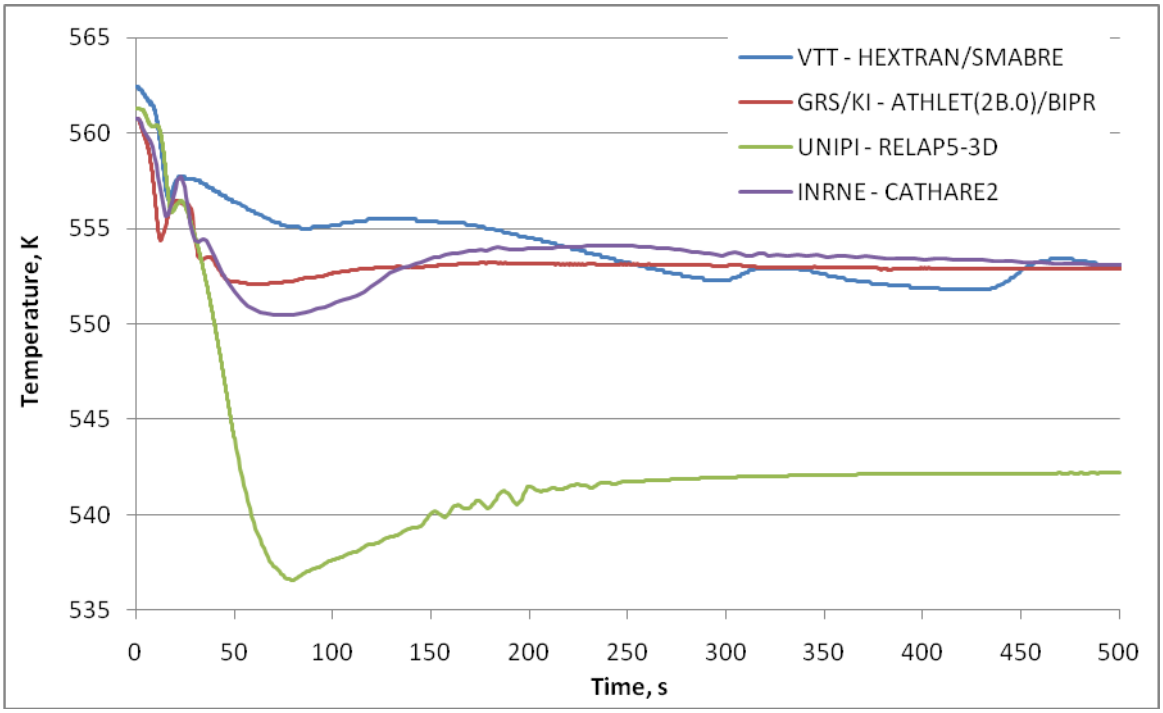


**Figure 6.9: Cold leg 1 temperature (Scenario 2)**

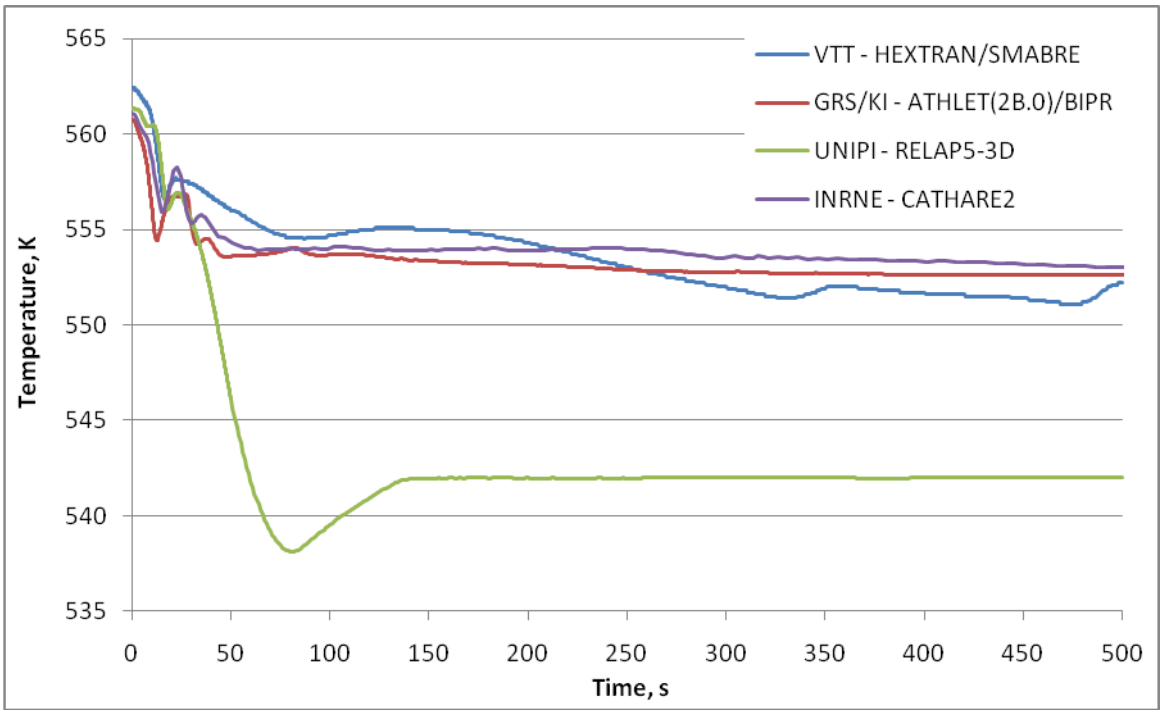


**Figure 6.10: Cold leg 2 temperature (Scenario 2)**

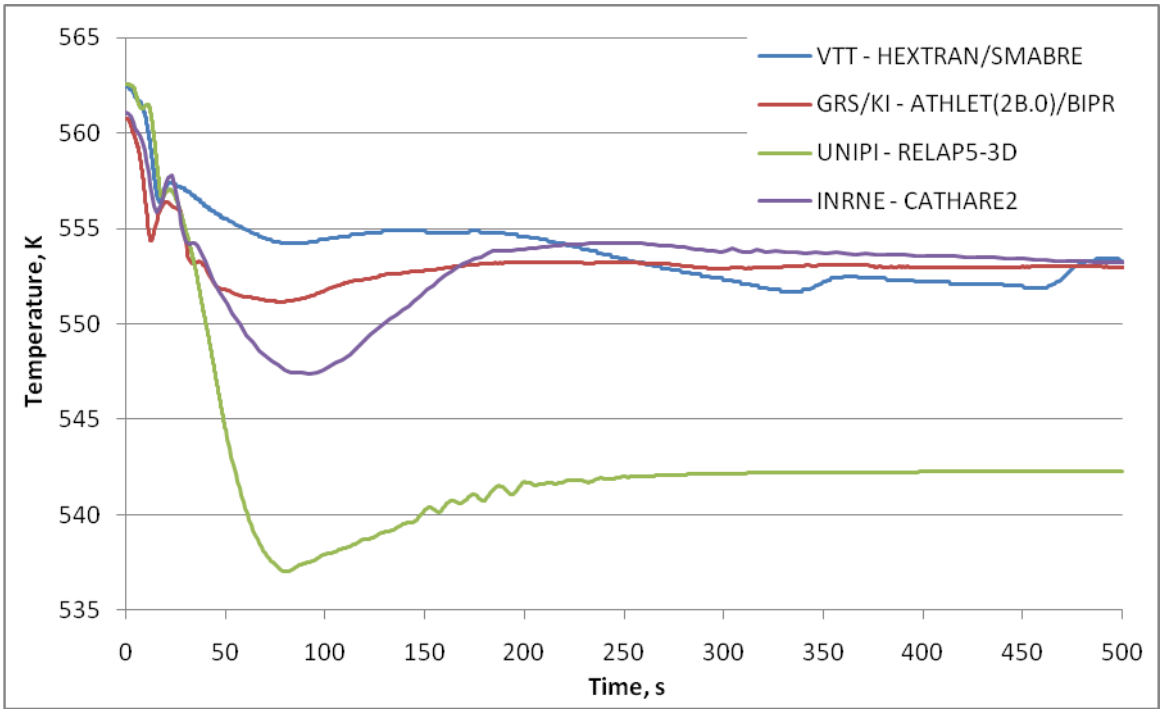


**Figure 6.11: Cold leg 3 temperature (Scenario 2)**

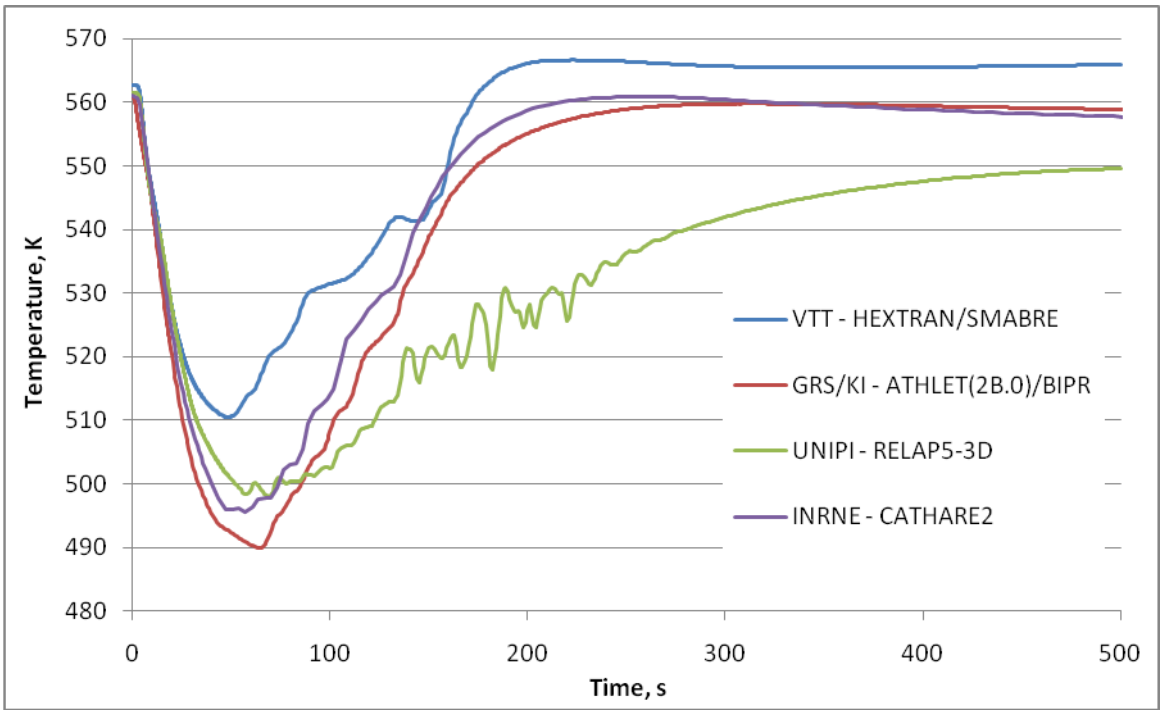


**Figure 6.12: Cold leg 4 temperature (Scenario 2)**

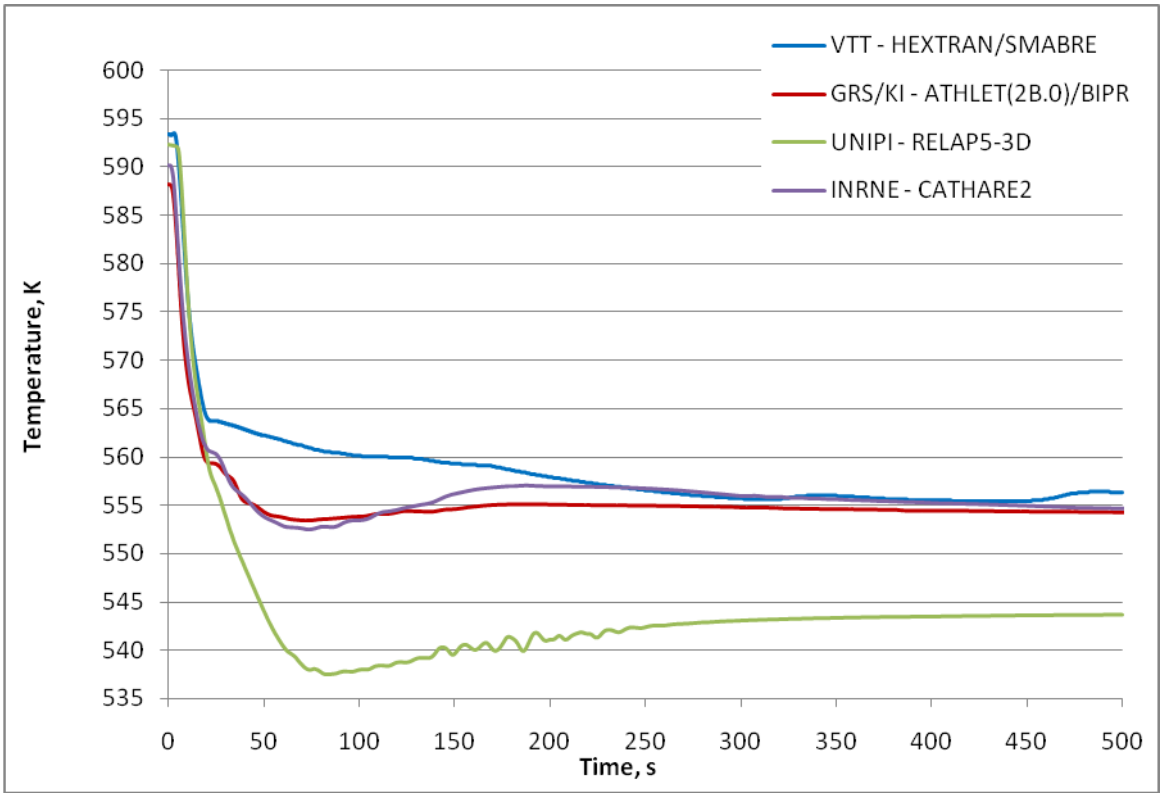


**Figure 6.13: Hot leg 1 temperature (Scenario 2)**

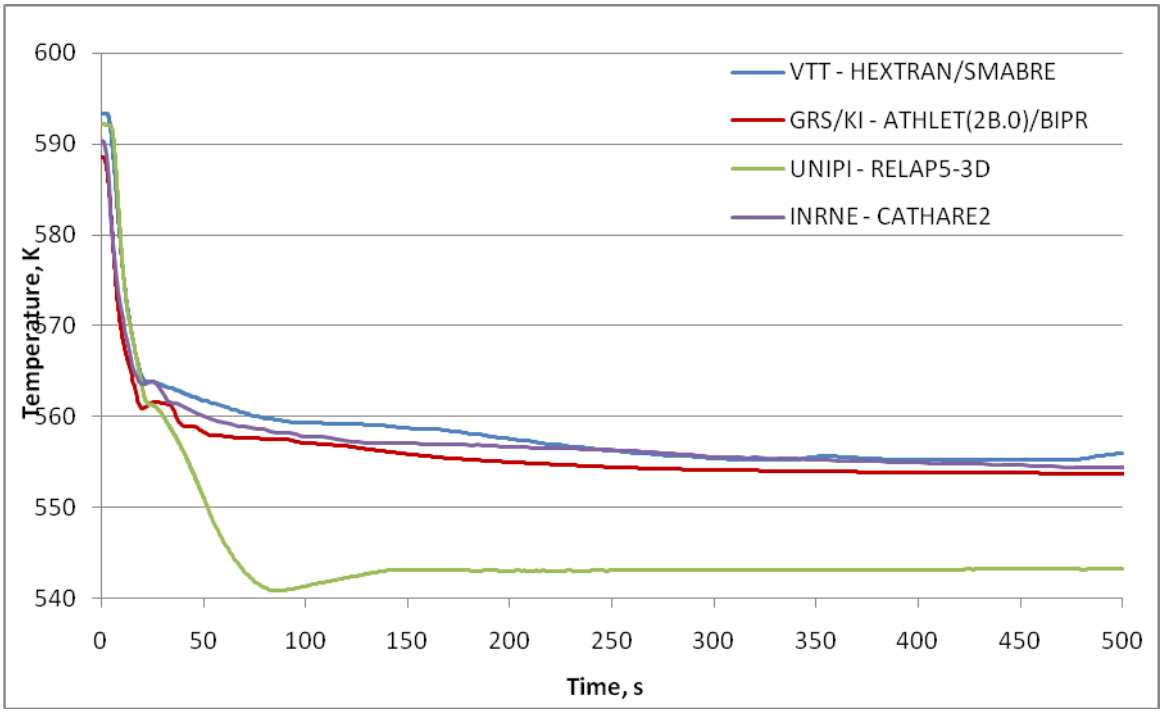


**Figure 6.14: Hot leg 2 temperature (Scenario 2)**

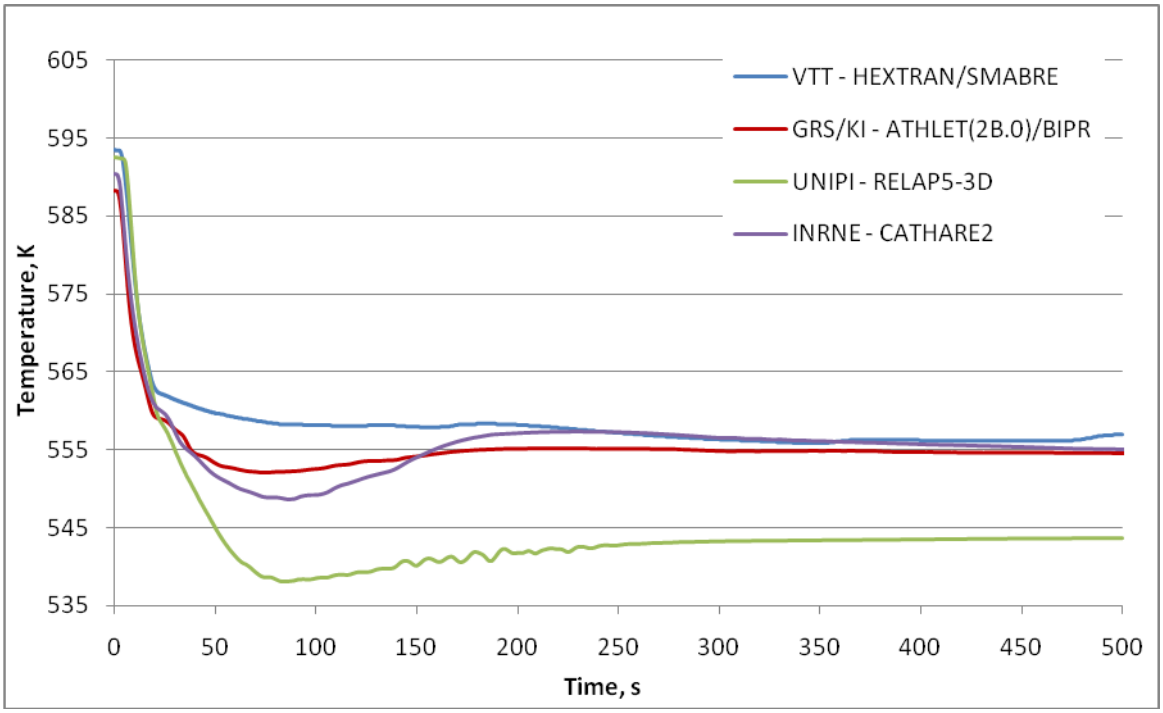


**Figure 6.15: Hot leg 3 temperature (Scenario 2)**

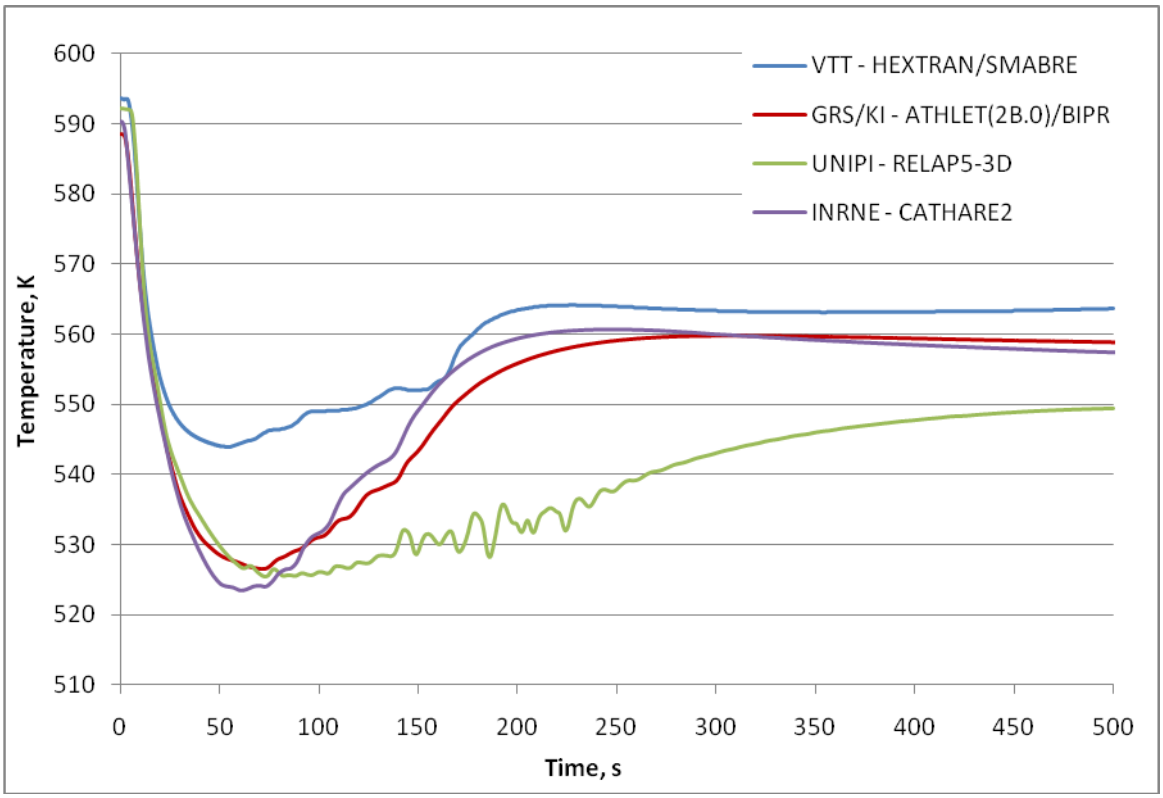


**Figure 6.16: Hot leg 4 temperature (Scenario 2)**

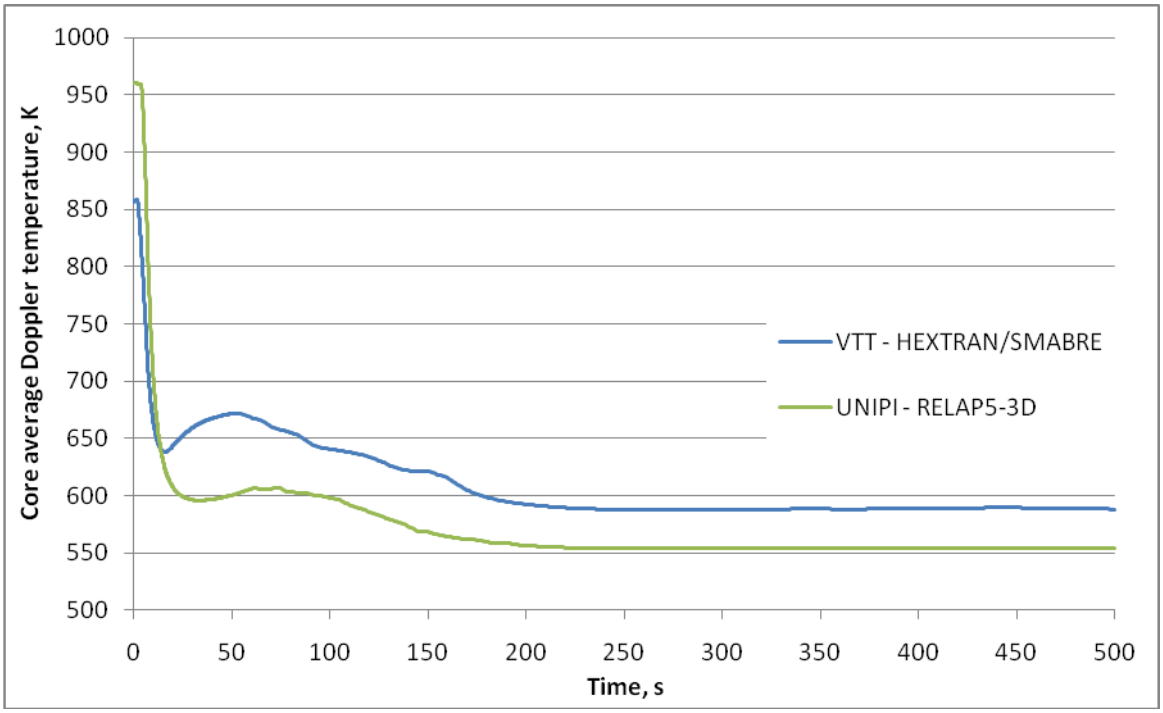


**Figure 6.17: Core average Doppler temperature (Scenario 2)**

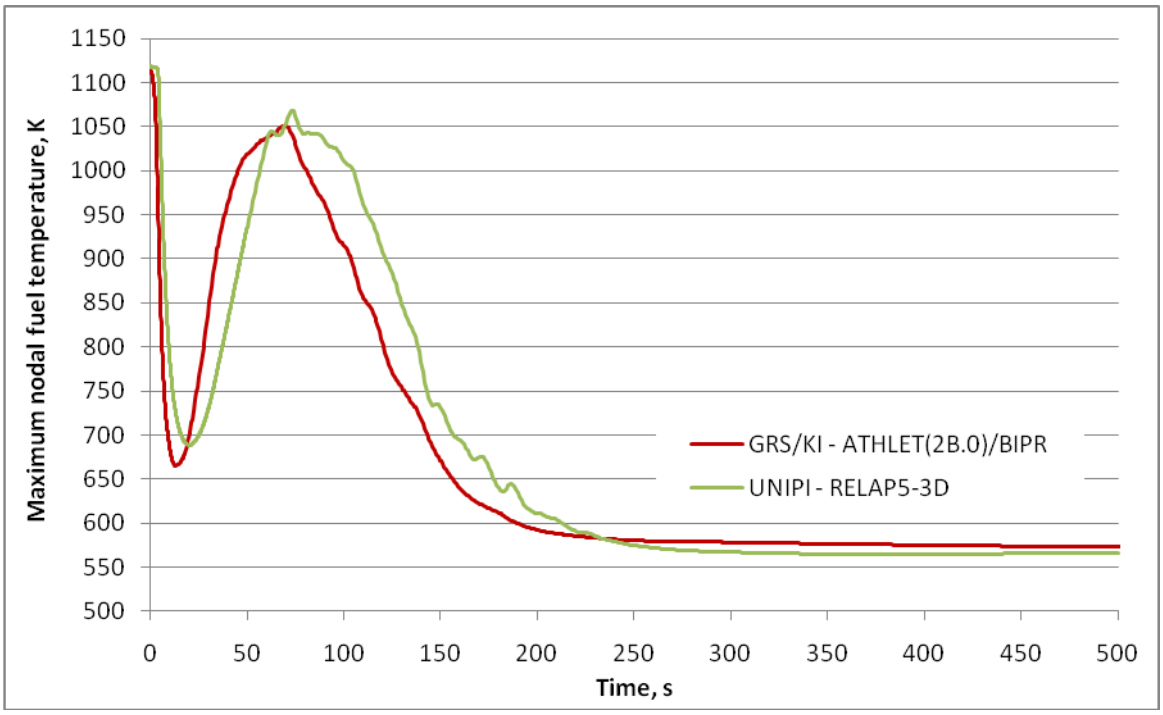


**Figure 6.18: Maximum nodal fuel temperature (Scenario 2)**

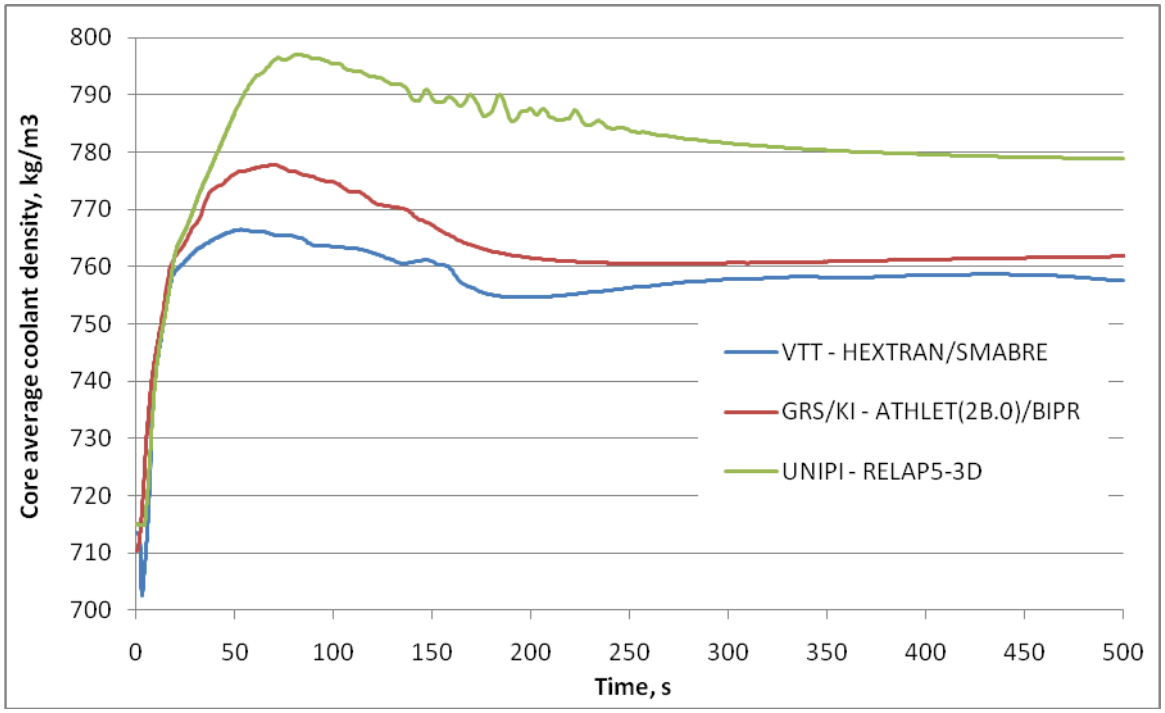


**Figure 6.19: Core average coolant density (Scenario 2)**

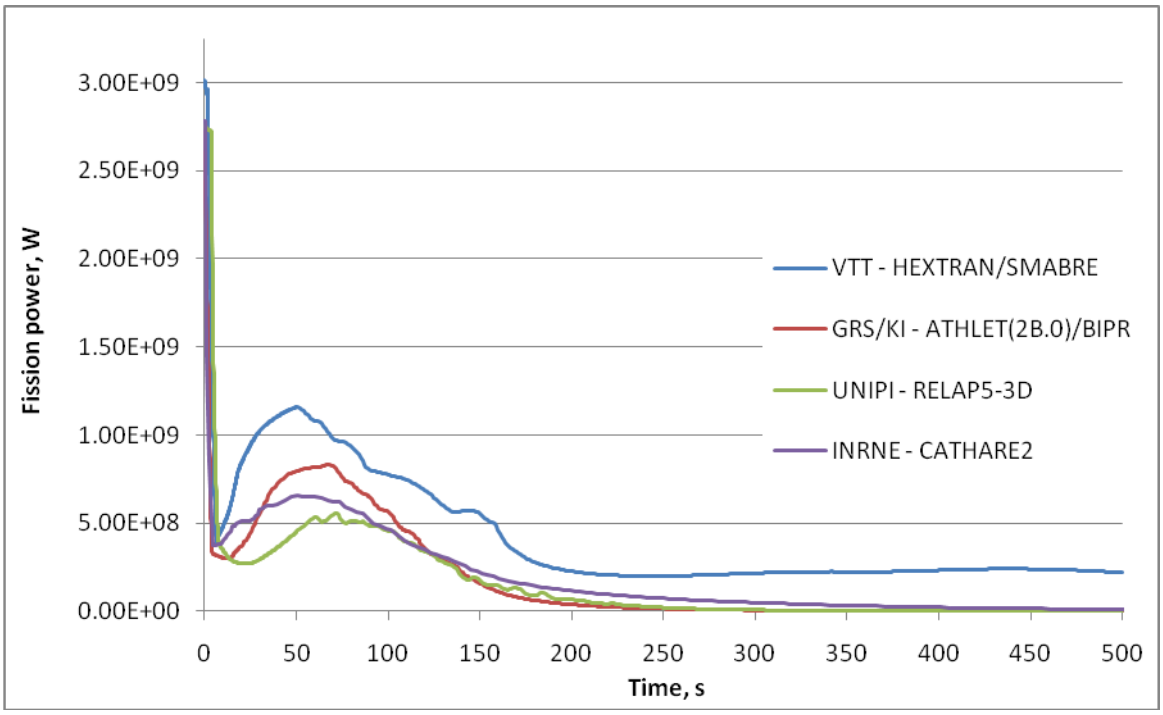


**Figure 6.20: Fission power**

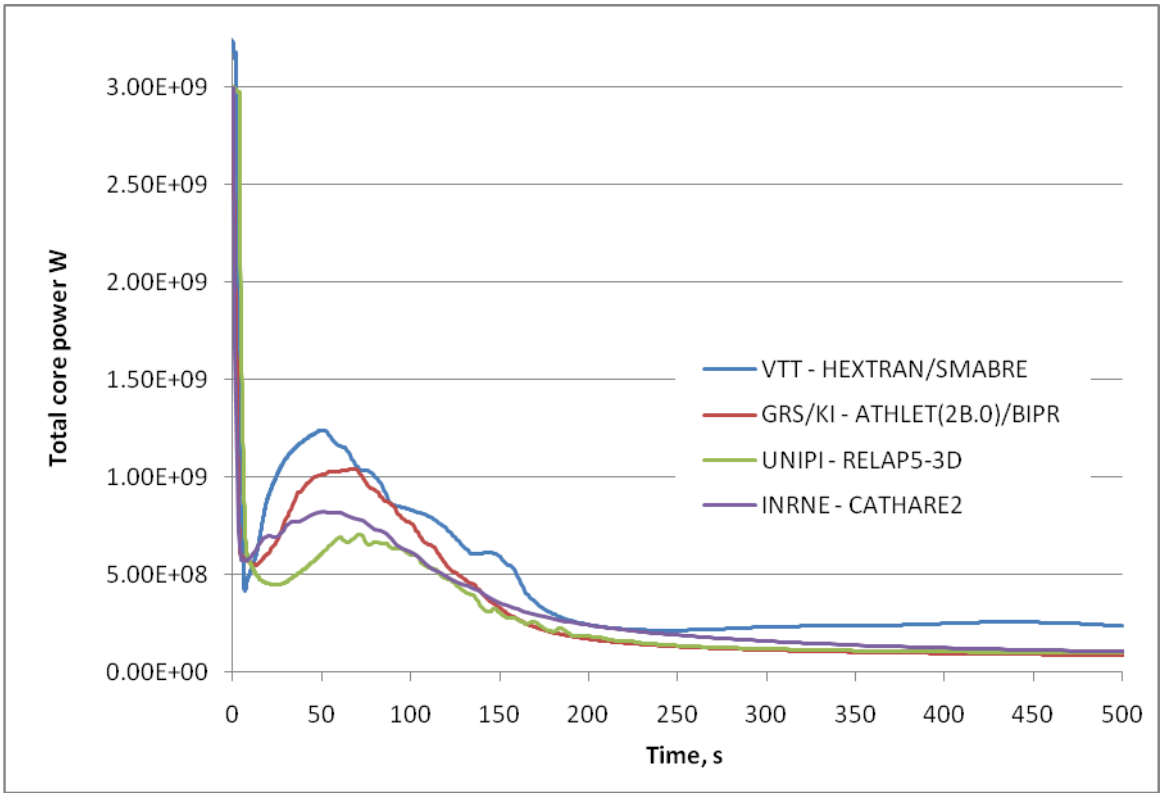


**Figure 6.21: Total core power**

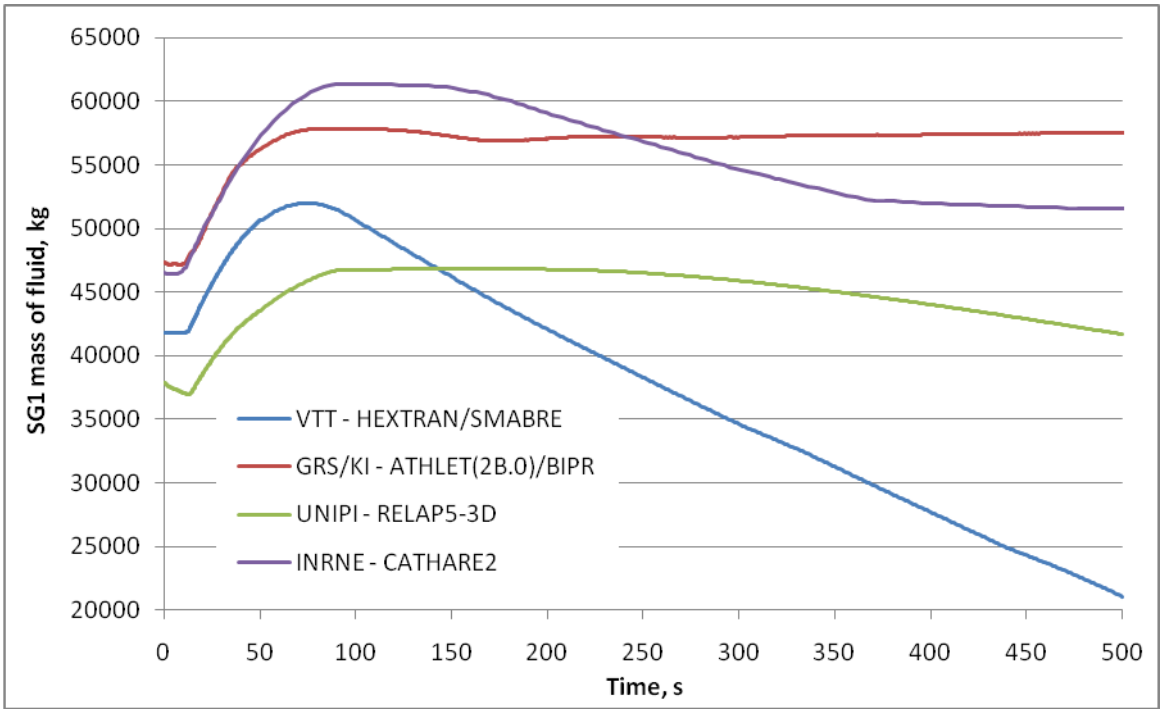


**Figure 6.22: SG1 mass of fluid (Scenario 2)**

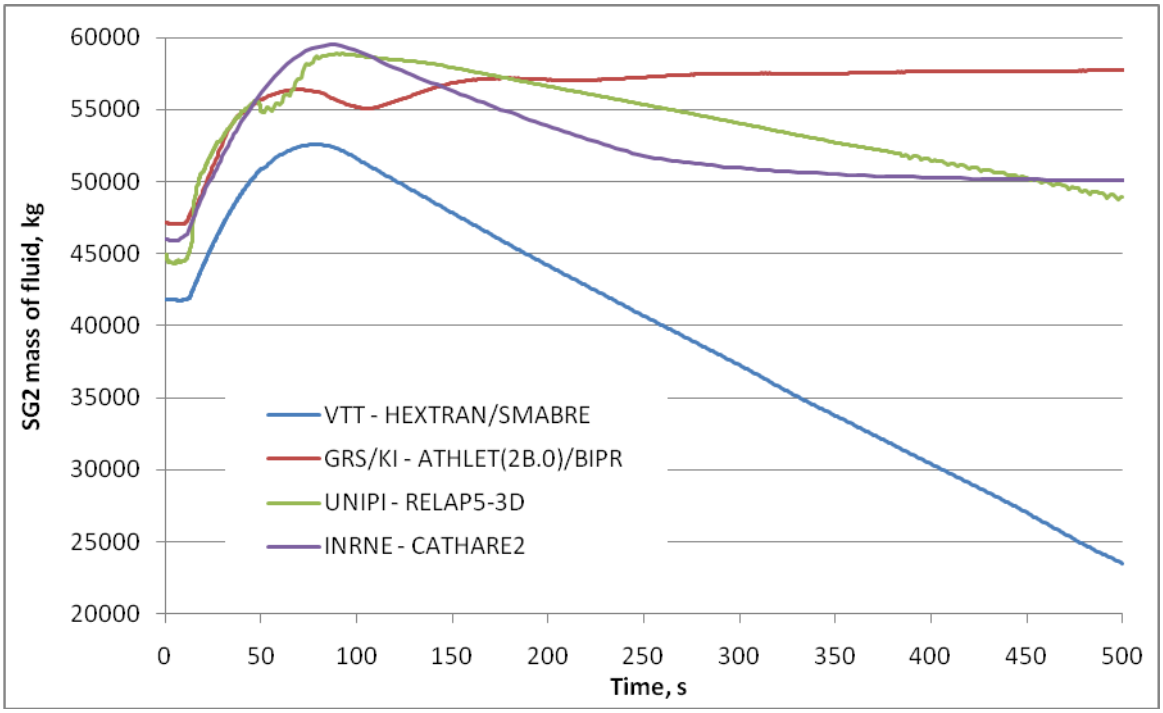


**Figure 6.23: SG2 mass of fluid (Scenario 2)**

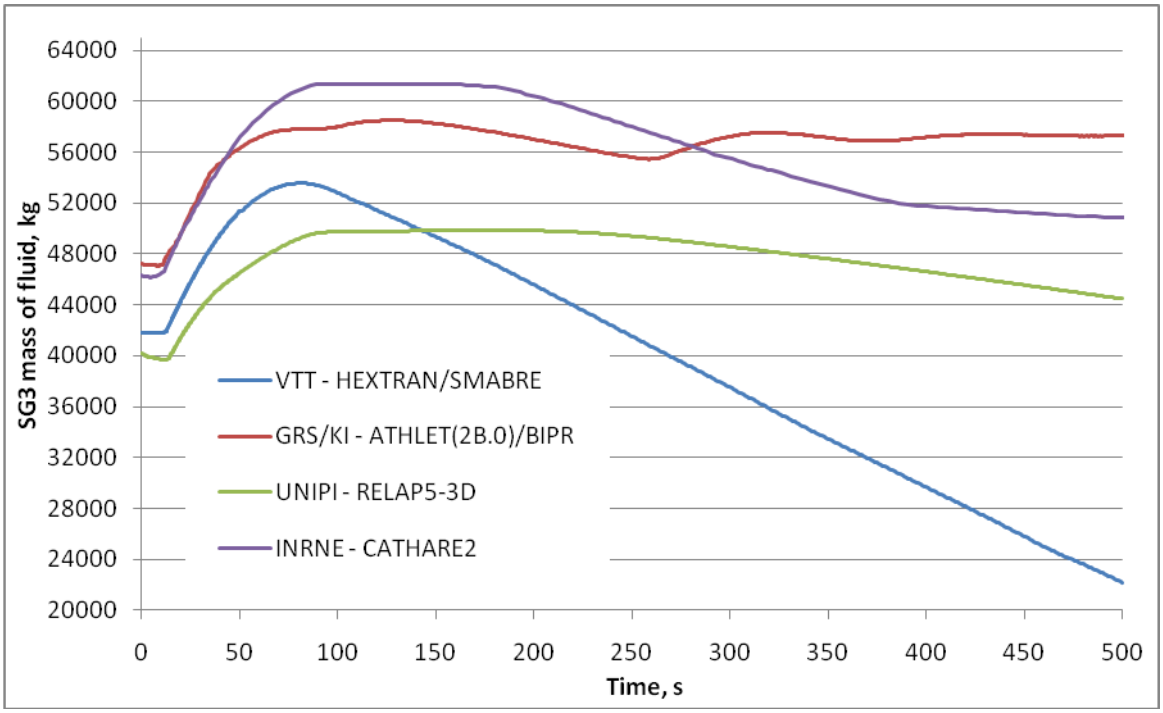


**Figure 6.24: SG3 mass of fluid (Scenario 2)**

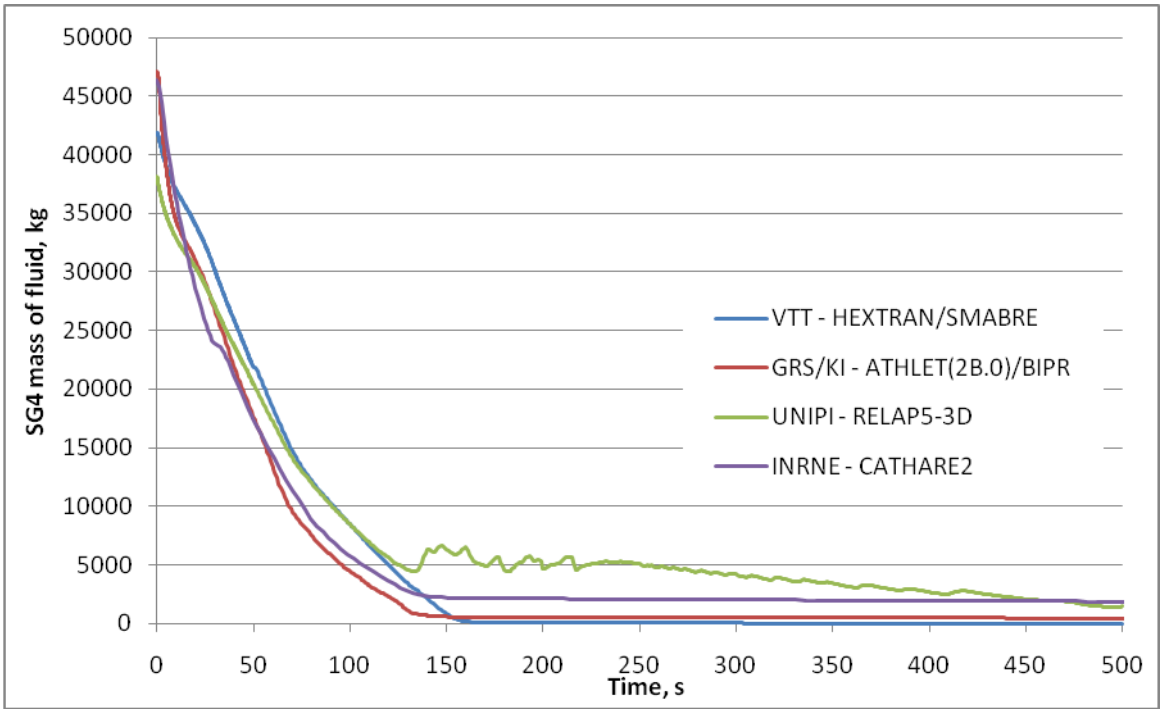


**Figure 6.25: SG4 mass of fluid (Scenario 2)**

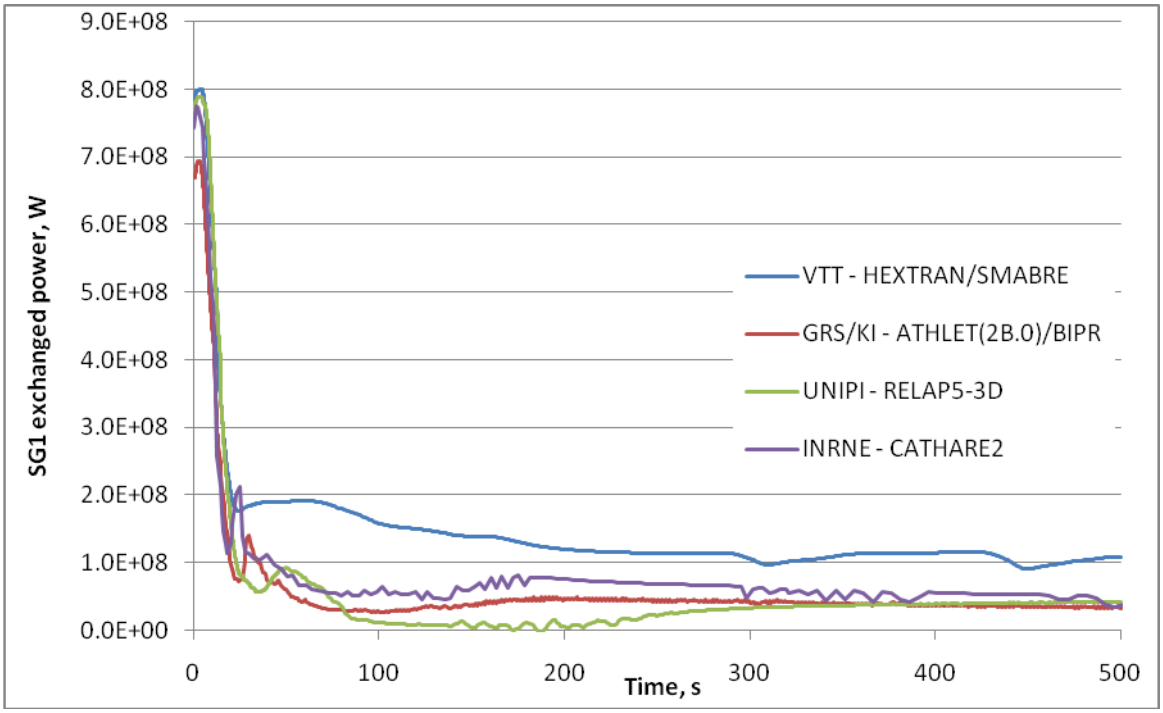


**Figure 6.26: SG1 exchanged power (Scenario 2)**

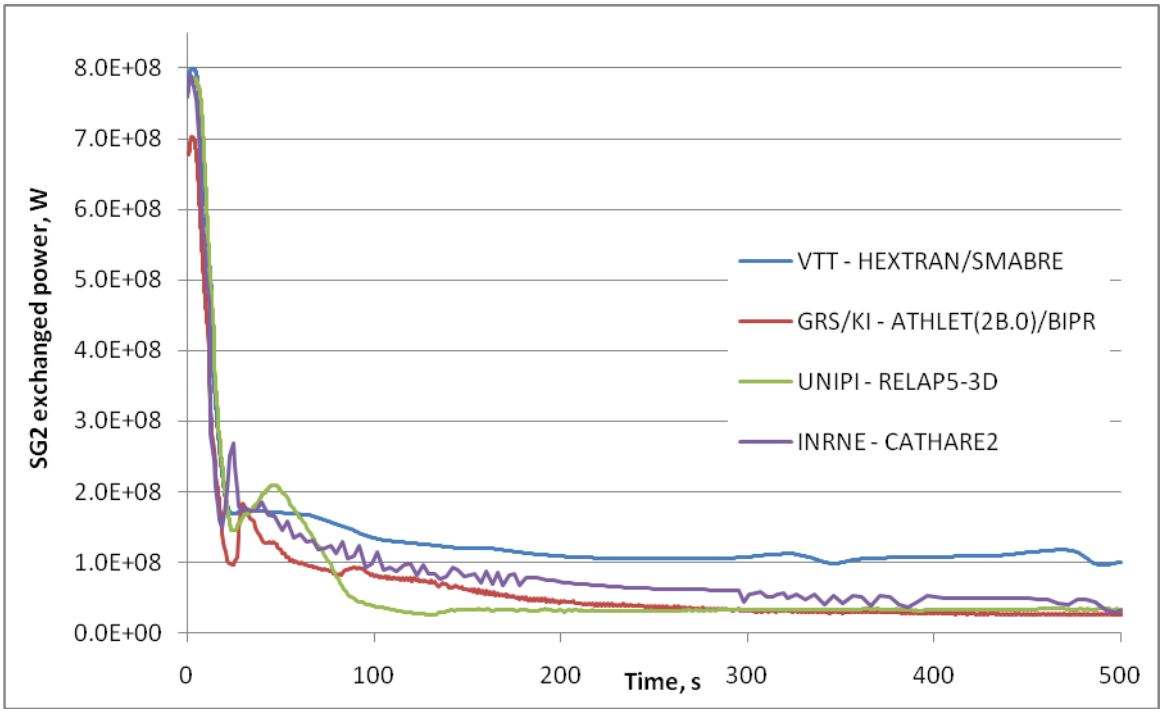


**Figure 6.27: SG2 exchanged power (Scenario 2)**

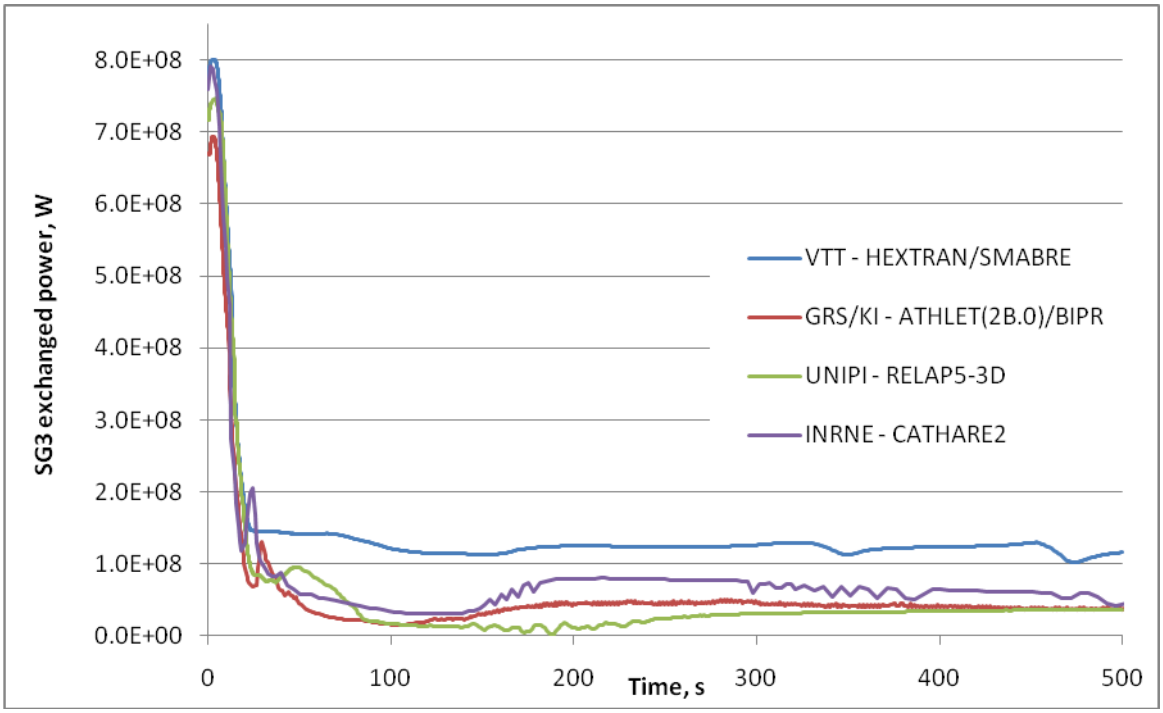


**Figure 6.28: SG3 exchanged power (Scenario 2)**

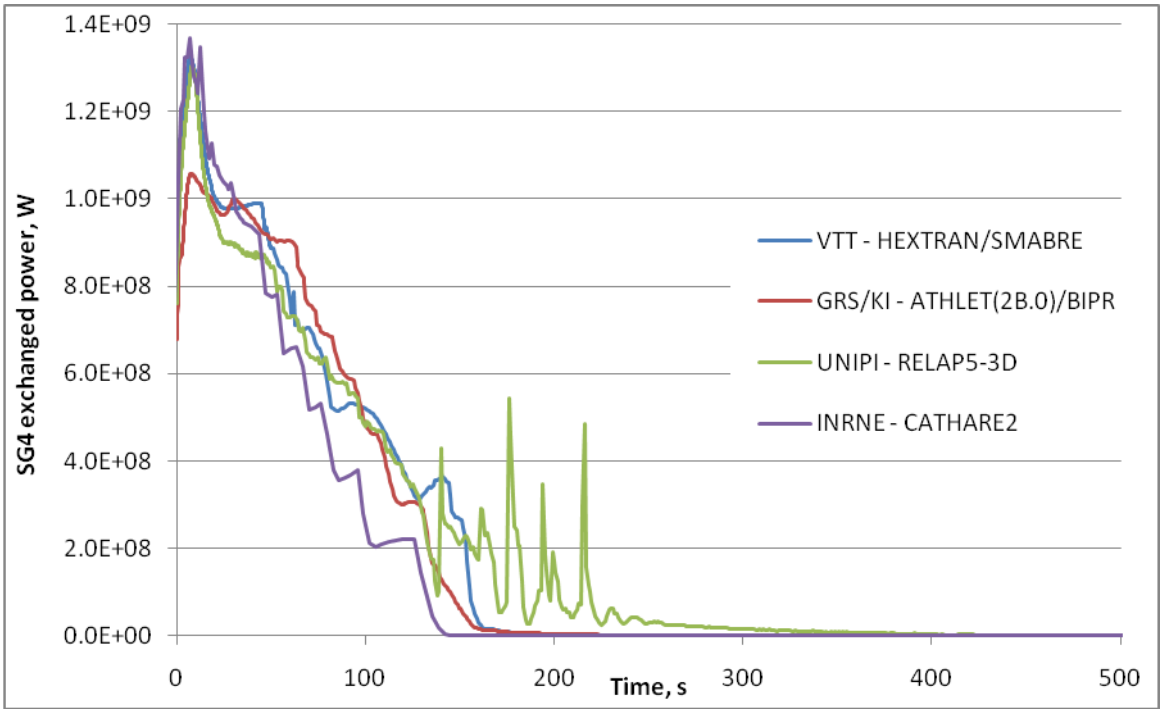


**Figure 6.29: SG4 exchanged power (Scenario 2)**

# Chapter 7: Summary and conclusions

In this volume, the results of the OECD/CEA VVER-1000 MSLB benchmark were analyzed. The results submitted by the participants were used to make code-to-code comparisons and subsequent statistical analysis. A coarse-mesh to CFD comparison of single-phase vessel mixing calculations with MSLB boundary conditions was also analyzed.

At the start of the VVER-1000 Coolant Transient Benchmarks (V1000CT) the coolant mixing was an unresolved issue in the analysis of complex plant transients with reactivity insertion. In order to support the necessary development work, Phase 2 of the benchmarks (V1000CT-2) was launched. The V1000CT-2 coolant mixing and MSLB benchmark was designed to provide a validation framework for the new generation best-estimate codes equipped with 3D neutron kinetics and improved vessel thermal-hydraulic models. A specific objective was to assess the performance of single-phase vessel mixing models (CFD and coarse-mesh), and the impact of thermal-hydraulic model refinement. For a consistent step-by-step validation, the multi-level methodology was employed and three exercises were defined.

In Exercise 1, which is a pure thermal-hydraulic problem, the participants validated their CFD or coarse-mesh vessel thermal-hydraulic models against plant data, on different scales:

- separate effects (mixing in the down-comer and lower plenum)
- vessel component
- plant system (optional)

A validated LES solution with the TRIO_U code served as reference for the separate effects. The results show that the accuracy attained in both CFD and improved coarse-mesh thermal-hydraulic models can be acceptable for industrial applications. The codes still have limitations but the development work for single-phase mixing is on the right way. The quality of the results depends on the experience of the user and the compliance with the Best Practice Guidelines.

The mixing models validated in Exercise 1 have been used in the other V1000CT-2 exercises for coupled core-vessel and core-system MSLB simulation to assess the applicability of best-estimate codes to VVER-1000 MSLB analysis.

In Exercise 2, which is a coupled core-vessel MSLB simulation with imposed vessel boundary conditions, standalone and coupled codes were tested step-by-step. The solutions were compared code-to-code and against fine-mesh solutions, where possible. The results show that:

- HZP solutions of COBAYA3, DYN3D, CRONOS and PARCS agree well with each other and with fine-mesh solutions. The respective nodal solvers yield converged solutions
- the NEM and HEXTRAN solvers need some improvements to produce spatially converged solutions for large hexagonal nodes and in regions of steep gradients

- the steady-state core-vessel solutions at HFP with DYN3D/ATHLET, CRONOS/FLICA, COBAYA/COBRA3, NEM/RELAP3D and HEXTRAN/ SMABRE are in reasonable overall agreement. The observed discrepancies can be explained with differences in the flux solvers, fuel and hydraulics modeling, and the spatial coupling
- the time histories of total power and reactivity of DYN3D/ATHLET, COBAYA/COBRA3 and HEXTRAN/SMABRE are in good agreement, despite some differences in the fuel Doppler temperature, which indicates some compensation effects due to coarse-mesh N/TH overlays in the radial plane
- the transient total power is sensitive to the core inlet distributions and the spatial coupling, due to local effects and transient 3D flux re-distribution, as illustrated in Chapter 5
- in this type of transient, the refinement of the neutronics model in the radial plane does not really impact the total power evolution. The neutronics scheme refinement impacts the local power distributions but not to the extent of the thermal-hydraulics meshing
- the local effects are sensitive to the azimuthal spatial resolution and accuracy of the core inlet TH conditions, as illustrated by a sensitivity study in Chapter 5. This sensitivity is stronger in case of steep flux gradients
- the axial distributions are sensitive to the core inlet distributions and the decay heat distribution during the transient, as illustrated in Chapter 5
- the vessel thermal-hydraulic models used in this study are applicable to VVER MSLB analysis. For an acceptable resolution at the core inlet, at least 16 - 24 angular meshes in the vessel are recommended

In Exercise 3, the performance of the integrated codes was evaluated in code-to-code comparison. It should be noted that the solutions submitted by the participants were ‘first calculation’ results, without feedback and recalculation. Because of this, and of certain declines from the secondary circuit specification in some user models of the steam dump controllers and the check valve, a relatively wide scatter of the core-system results is displayed. The comparison shows that the user models of the secondary circuit of VVER-1000 require further attention.

In the overall, for the prediction of the system behavior in this benchmark, key parameters were the SG fluid masses, the break flow rates, the secondary pressure, as well as the coolant and fuel temperatures, and the powers. Other parameters were important to analyze because they help to determine what was causing the behavior of the key parameters. In particular, it was proven that the refinement of the vessel mixing model has a great effect on the 3D core and core-vessel dynamics.

The following sources of modeling uncertainties were identified:

- Thermal-hydraulic modeling issues: vessel mixing modeling; vessel meshing; turbine bypass controllers modeling; liquid break flow modeling for horizontal steam generators
- Thermal-hydraulic key parameters: core inlet temperatures; core inlet mass flow rates; core outlet pressure; gas gap conductance

- Cross-section modeling: spectral history dependencies; instantaneous cross-section dependences, cross-term effects; ADF modeling; refinement of the cross-section library
- Neutronics and coupling modeling: different flux solvers; spatial N/TH coupling in terms of the number of thermal-hydraulic channels and spatial mesh overlays at the core inlet; direct moderator heating; temporal coupling schemes

The comparative study allows a conclusion that the considered vessel mixing models and coupled codes are applicable to the analysis of asymmetric coolant transients characterized by sector formation, such as MSLB.

The lessons learned from the VVER vessel mixing and MSLB benchmarks will have a significant impact on the future coupled code analysis of reactivity transients.

# References


Bieder, U., S.Betin, G.Fauchet, N.P.Kolev (2004), "Preparation of the V1000CT-2 Exercise 1 thermal-hydraulic benchmark", 2nd Workshop on the OECD VVER-1000 Coolant Transient Benchmarks, Sofia, April 5-6

Frisani, A., C.Parisi , F.D'Auria (2006), "The use of RELAP5-3D code in the OECD/NEA VVER-1000 CT-1 and CT-2 Benchmark" RELAP5-3D Users Seminar Holiday Inn Sun-Spree Resort – West Yellowstone, USA, 16-18 August 2006

Hoehne, T. (2007), "CFX-5 calculated transient down-comer core inlet TH parameters for the OECD VVER-1000 MSLB benchmark", Invited contribution to the V1000CT-2 benchmark

Ivanov B., K.Ivanov, N.Kolev (2006a), "Cross-section library 2.0 for VVER-1000 MSLB", Ad-hoc meeting-Workshop on the V1000CT-2 benchmark, Vancouver, Canada, 12 September, 2006

Ivanov, B., S.Aniel, P.Siltanen, E.Royer, K.Ivanov (2006b), "Impact of cross-section generation procedures on the simulation of the VVER-1000 pump startup experiment in the OECD/DOE/CEA V1000CT benchmark by coupled 3D N/TH models", Progress In Nuclear Energy, Vol.48, No.8, pp. 746-763

Kolev, N.P., D.Popov, S.Aniel, E.Royer (2004), "Specifications of the V1000CT-2 Exercise 1 thermal-hydraulic benchmark", 2nd Workshop on the OECD VVER-1000 Coolant Transient Benchmarks, Sofia, April 5-6

Kolev, N.P., N.Petrov, D. Angelova, J.Donov, Y.Dinkov, D.Popov, S.Nikonov (2005), *VVER-1000 Main Steam Line Break Analysis*, INRNE Report for CEA, Saclay

Kolev N.P. et al (2009), "VVER-1000 Coolant Transient Benchmark Phase 2 (V1000CT-2), Volume1: Specifications of the VVER-1000 vessel mixing problem", NEA/NSC/DOC (2007)22, OECD/NEA, Paris

Kolev N.P. et al (2010a), "VVER-1000 Coolant Transient Benchmark (V1000CT-2), Volume 2: Final specifications of the MSLB problem", NEA/NSC/DOC(2006)6, OECD/NEA, Paris

Kolev N.P. et al (2010b), "VVER-1000 Coolant Transient Benchmark (V1000CT-2), Volume 3: Summary results of Exercise 1 on vessel mixing simulation", NEA/NSC/DOC (2010)10, OECD/NEA, Paris

Mahaffy, J., B. Chung, F. Dubois, F. Ducros, E. Graffard, M. Heitsch, M. Henriksson, E. Komen, F. Moretti, T. Morii, P. Mühlbauer, U. Rohde, M. Scheuerer, B. L. Smith, C. Song, T. Watanabe, G.Zigh (2007), "*Best Practice Guidelines for the use of CFD in Nuclear Reactor Safety Applications",* OECD NEA/CSNI/R (2007)5

Nikonov, S., M.Lizorkin, A.Kotsarev, S.Langenbuch and K.Velkov, "Optimal Nodalization Schemes of VVER-1000 Reactor Pressure Vessel for the Coupled Code ATHLET-BIPR8KN", Proc. 16th AER Symposium on VVER Reactor Physics and Safety, Bratislava, 25-29 September 2006

Nikonov, S., Private communication, 2004

Ts.Topalov, D.Popov (2004), "Overview of the Kozloduy-6 vessel mixing tests", 2nd Workshop on the OECD VVER-1000 Coolant Transient Benchmarks, Sofia, April 5-6

Spasov, I., J. Jimenez, J.A. Lozano, J.J. Herrero (2009), "V1000CT2-EXT2 benchmark solutions with COBAYA3/COBRA3", Internal Report, Universidad Politecnica de Madrid

Spasov, I., J. Jimenez, J.A. Lozano, J.J. Herrero, N.P.Kolev, (2010), "COBAYA3 vs. CRONOS solutions of the V1000-MSLB benchmark", to appear

U.Bieder, G. Fauchet, S.Betin, N.Kolev and D.Popov (2005), "Calculation of coolant mixing in VVER-1000", 11th Int. Conf. on Nuclear Reactor Thermal-Hydraulics (NURETH-11), Avignon, France, October 2-6, Paper: 201

## References (codes)

Aniel S. et al, (2005),"FLICA4: Status of numerical and physical models and overview of the applications", Proc. of NURETH11, Avignon, 2-6 October

ANSYS CFX10 Manuals (2006)

Bergeron A., Caruge D., Clement P. (1999), "Assessment of the 3-D Thermal-hydraulic Nuclear Computer Code FLICA4 on Rod Bundle Experiments", NURETH-6, San Francisco, 3-8 October 1999

CEA (2007), CATHARE 2.5 User's Manual

Downar, T., et al (2004), "PARCS v2.6 US NRC Core Neutronics Simulator Theory Manual"https://engineering.purdue.edu/PARCS/Code/Manual/Theory/PDF/PARCS_TheoryManual.pdf (2004)

Grundmann, U. (1999), "HEXNEM: A nodal method for the solution of the neutron diffusion equation in hexagonal geometry", Proc. M&C 1999, Madrid, 27-30 September, pp. 1086-1095

Grundmann, U., F.Holstein (1999), "A 2D intra-nodal flux expansion method for hexagonal geometry", Nucl. Sci. Eng., 133, 201-212

Hämäläinen, A. (2004) "Applying thermal hydraulics modeling in coupled processes of nuclear power plants", VTT Publication 578

Idaho Nuclear Laboratory (INL) (2001), INEEL-EXT-98-00834, Revision 1.3a, February 2001

Jackson J.W., N.E.Todreas (1981), "COBRA-IIIc/MIT-2: A Computer Program for Steady State and Transient Thermo-Hydraulic Analysis of Rod Bundle Nuclear Fuel Elements", MIT report

Jiménez, J., D. Cuervo, J.M. Aragonés (2007), "Multi-Scale and Multi-Physics Coupling in COBAYA3", Proc. NURETH-12, Paper: 48, Pittsburgh, Pennsylvania, Sept 30-Oct 4

Kaloinen, E. et al (1981), "HEXBU-3D: A 3D PWR simulator program for hexagonal fuel assemblies", VTT Research report 7/1981, Helsinki

Kyrki-Rajamaki, R. (1991), "HEXTRAN: VVER reactor dynamics code for 3D transients", Proc. 1st AER Symp. on VVER reactor physics and safety, Rez, 23-28 September

Lautard, J. et al. (1990), “CRONOS – A Modular Computational System for Neutronic Core Calculation”, Proc. IAEA Meeting, Cadarache, France

Lautard J., D.Schneider, A.M. Baudron (1999), “Mixed dual methods for neutronics reactor core calculations in the CRONOS system”, Proc. of M&C, Madrid, 27-30 September

Lizorkin, M., S.Nikonov, S.Langenbuch, K.Velkov (2006) “Development and Application of the Coupled Thermal-Hydraulics and Neutron-Kinetics Code ATHLET/BIPR-VVER for Safety Analysis”, Proc. EUROSAFE 2006, Paris, 13-14 November

Lozano, J.A., J.Jimenez, N.García-Herranz and J.M.Aragonés (2009), “Development and performance of the ANDES/COBRAIII coupled system in hexagonal-Z geometry” , Proc. M&C 2009, Saratoga Springs, NY, May 3-7; Annals of Nuclear Energy, 2010

Magnaud, C. (1999), “Pin-by-pin transport calculation with the CRONOS reactor code”, Proc. of M&C, Madrid, 27-30 September

Miettinen, J. (1985), “Development and assessment of the SBLOCA code SMABRE”, Proc. of the Specialists meeting on Small Break LOCA analysis in LWR, Pisa, Italy, Vol.2, pp. 481-495

Odar, F., C.Murray et al (2003), TRACE V4.0 User’s Manual, May

Teschendorf, V., H.Austregesilo, G.Lerchl (1996), “Methodology, status and plans for development and assessment of the code ATHLET“, Proc. of the OECD/CSNI Workshop on transient thermal-hydraulic and neutronics codes requirements, Annapolis, USA, 5-8 Nov 1996, NUREG/CP-0159, NEA/CSNI/R(97)4

Toumi I., Bergeron A., Gallo D. Royer E., Caruge D. (2000), “FLICA4: A Three-dimensional Two-phase Flow Computer Code with Advanced Numerical Methods for Nuclear Applications”, Nuclear Engineering and Design, 200, 139-155

Syrjälahti, E., A. Hämäläinen (2006), “HEXTRAN-SMABRE calculation of the VVER-1000 coolant transient-1 benchmark”, Progress in Nuclear Energy 48, 849-864

UPM, Madrid (2009), The COBAYA3 neutronic code – “Quick Guide”

# Appendix A: Two-dimensional radial power distributions in the steady states

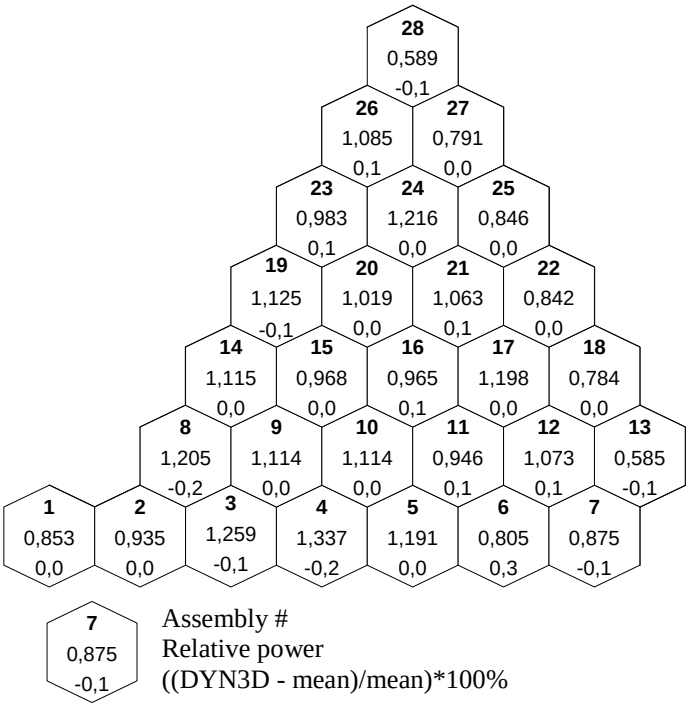


**Figure A.1: HZP state 0. DYN3D computed assembly powers vs. mean of DYN3D, CRONOS, COBAYA and PARCS results**

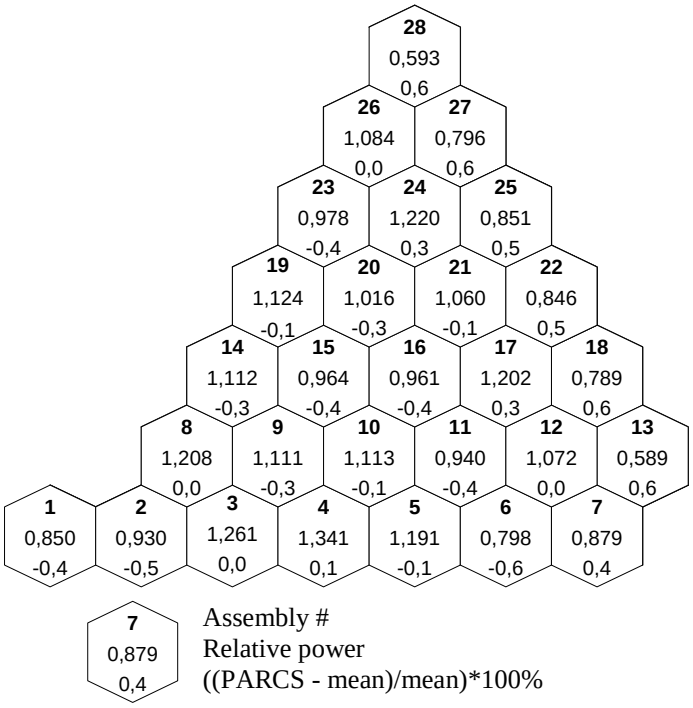


**Figure A.2: HZP state 0. PARCS computed assembly powers vs. mean of DYN3D, CRONOS, COBAYA and PARCS results**

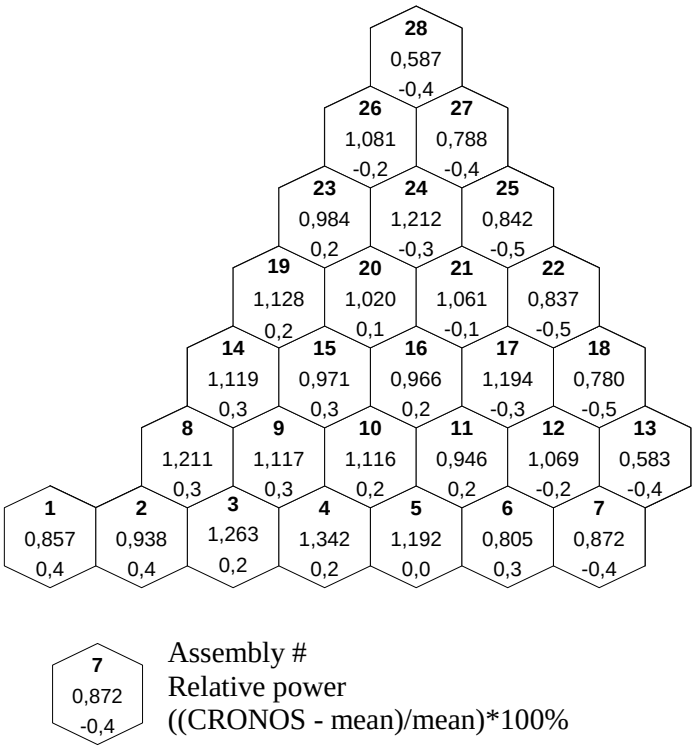


**Figure A.3: HZP state 0. CRONOS computed assembly powers vs. mean of DYN3D, CRONOS, COBAYA and PARCS results**

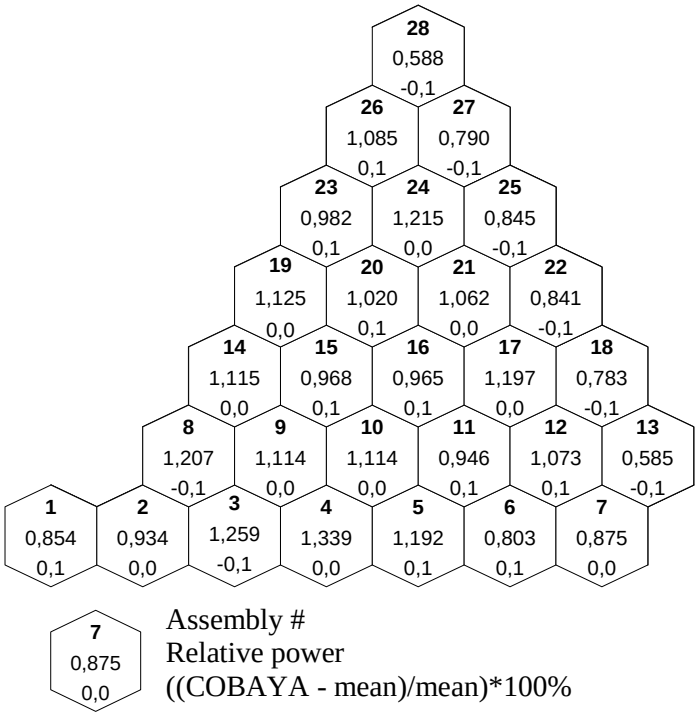


**Figure A.4: HZP state 0. COBAYA computed assembly powers vs. mean of DYN3D, CRONOS, COBAYA and PARCS results**

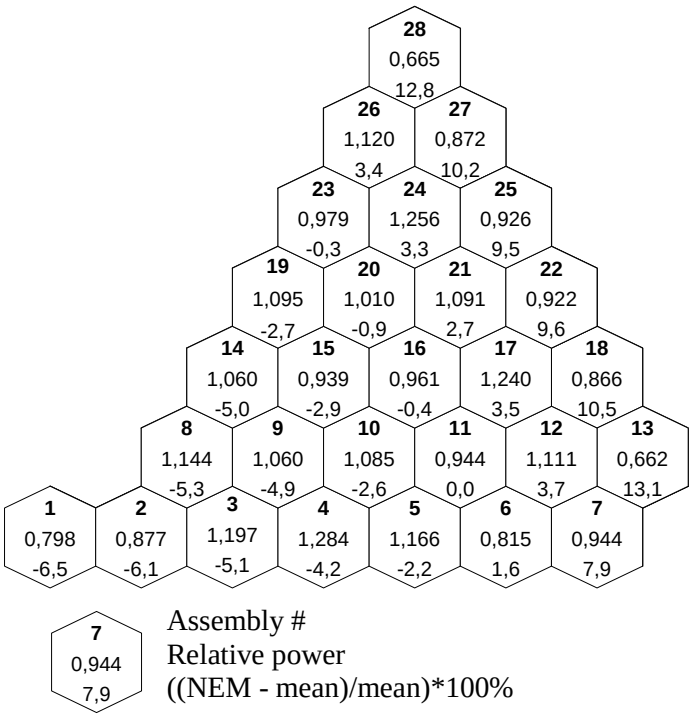


**Figure A.5: HZP state 0. NEM computed assembly powers vs. mean of DYN3D, CRONOS, COBAYA and PARCS results**

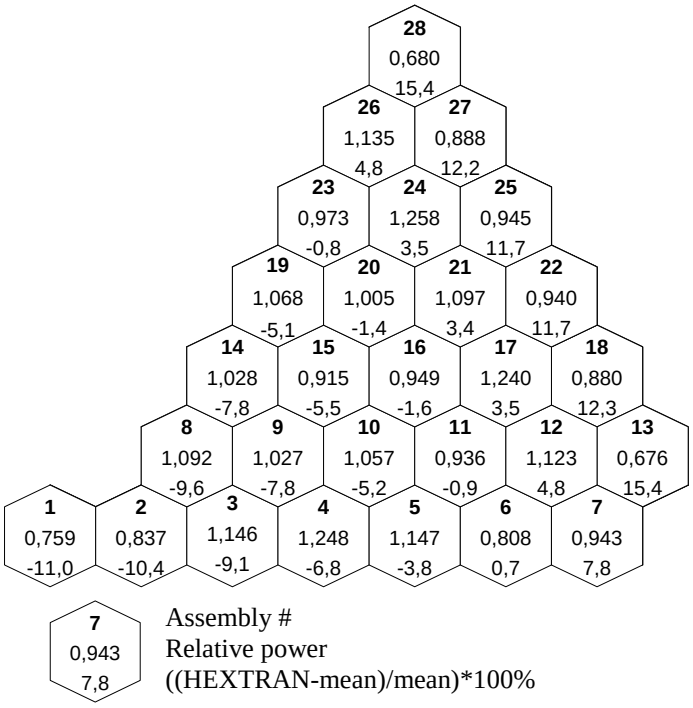


**Figure A.6: HZP state 0. HEXTRAN computed assembly powers vs. mean of DYN3D, CRONOS, COBAYA and PARCS results**

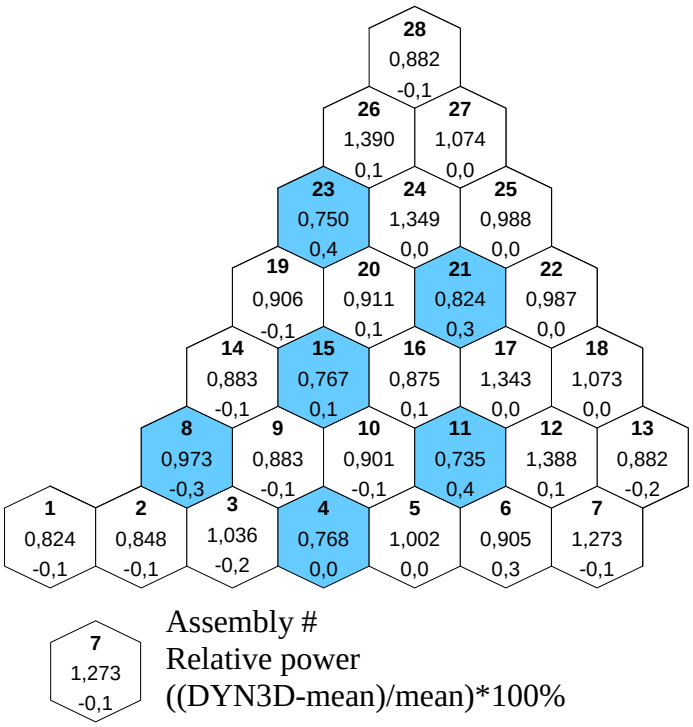


**Figure A.7: HZP state 1a. DYN3D computed assembly powers vs. mean of DYN3D, CRONOS, COBAYA and PARCS results. Blue color marks inserted rods**

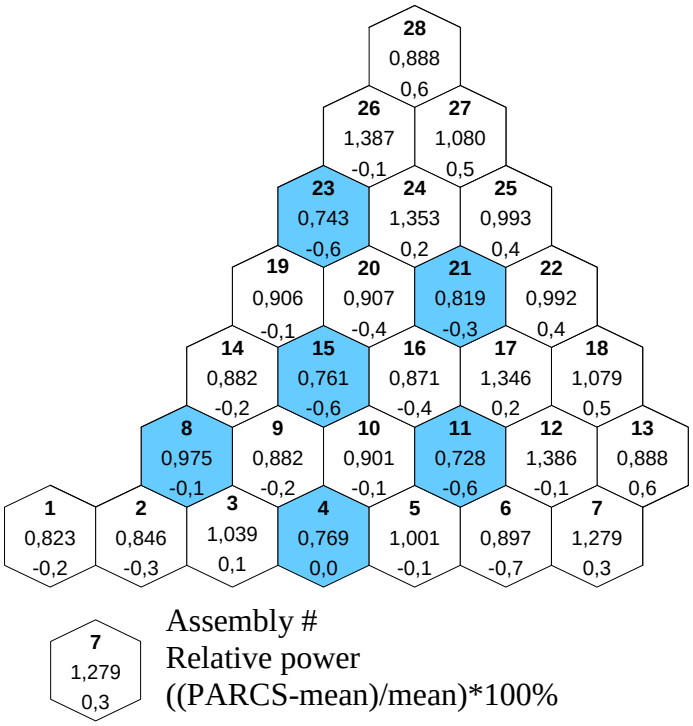


**Figure A.8: HZP state 1a. PARCS computed assembly powers vs. mean of DYN3D, CRONOS, COBAYA and PARCS results**

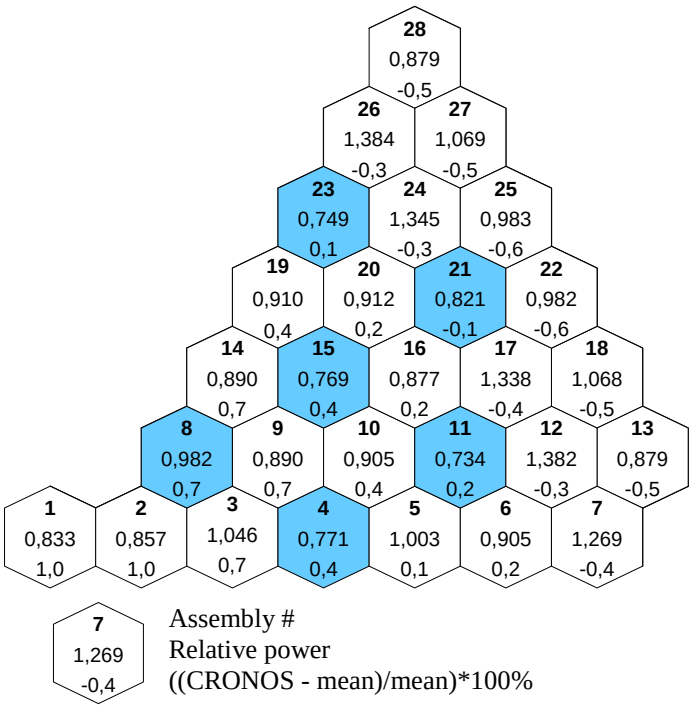


**Figure A.9: HZP state 1a. CRONOS computed assembly powers vs. mean of DYN3D, CRONOS, COBAYA and PARCS results**

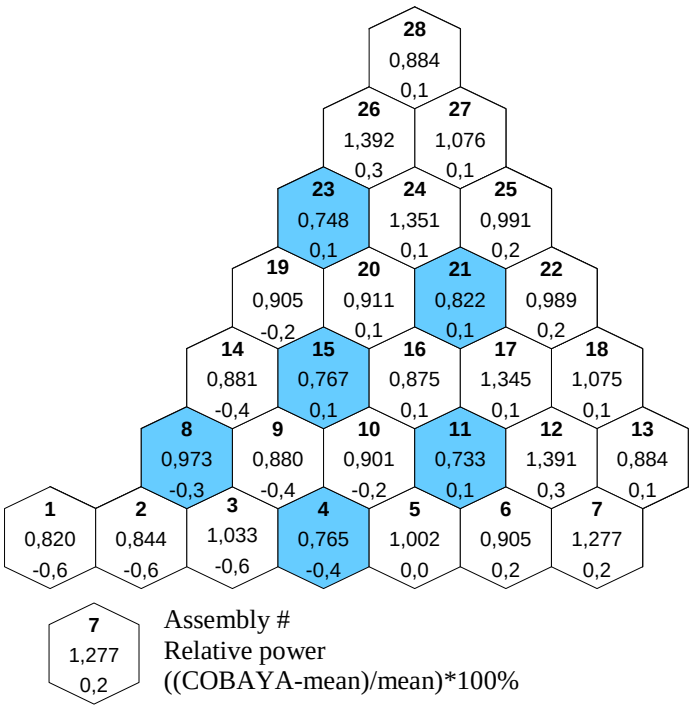


**Figure A.10: HZP state 1a. COBAYA computed assembly powers vs. mean of DYN3D, CRONOS, COBAYA and PARCS results**

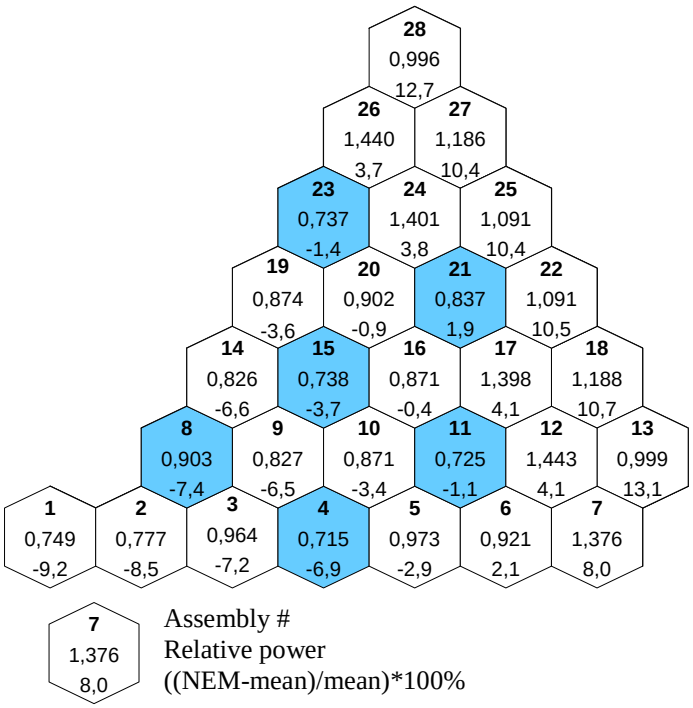


**Figure A.11: HZP state 1a. NEM computed assembly powers vs. mean of DYN3D, CRONOS, COBAYA and PARCS results**

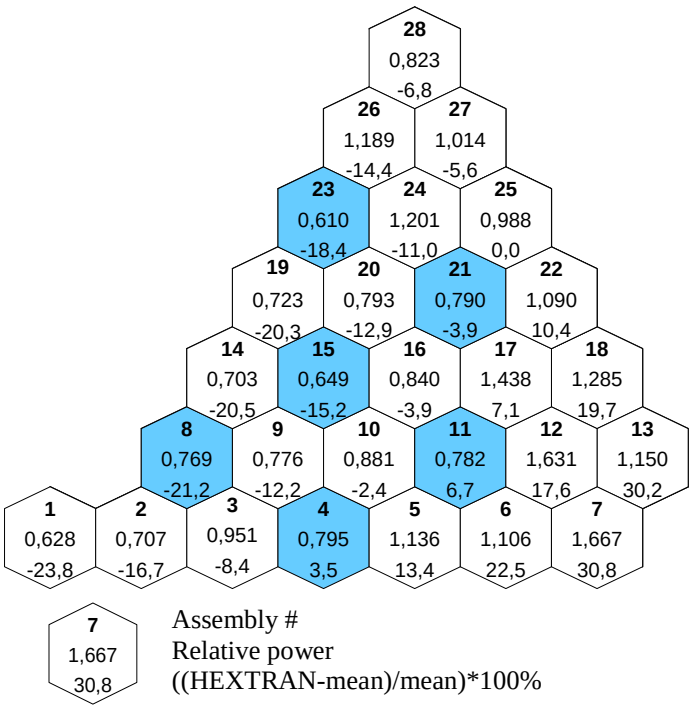


**Figure A.12: HZP state 1a. HEXTRAN computed assembly powers vs. mean of DYN3D, CRONOS, COBAYA and PARCS results**

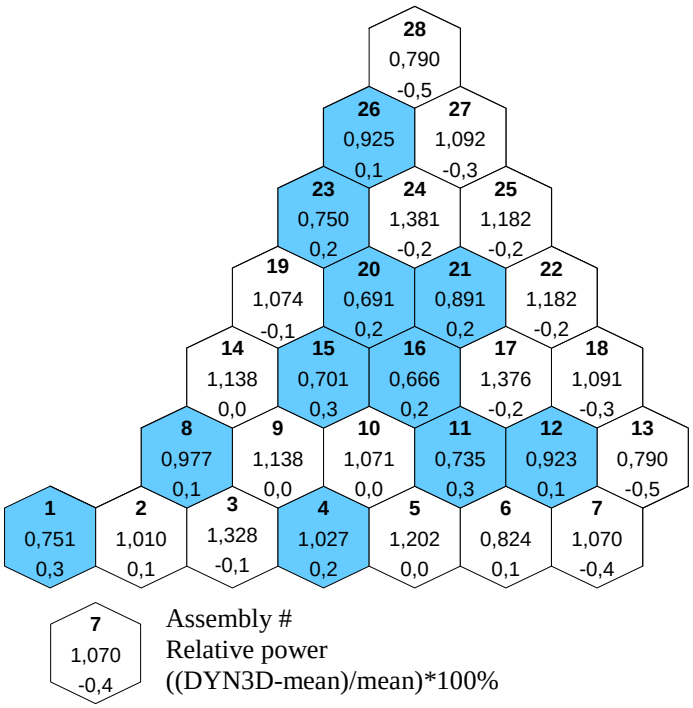


**Figure A.13: HZP state 1b. DYN3D computed assembly powers vs. mean of DYN3D, CRONOS, COBAYA and PARCS results**

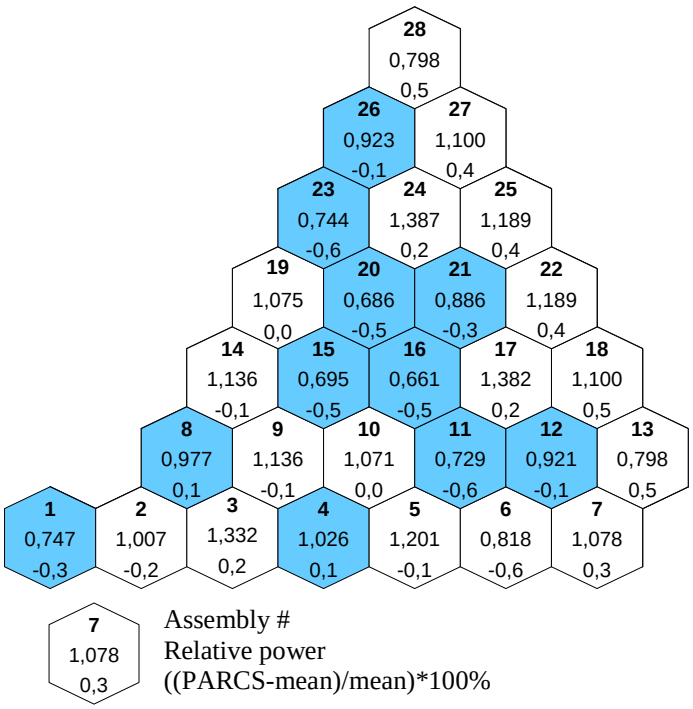


**Figure A.14: HZP state 1b. PARCS computed assembly powers vs. mean of DYN3D, CRONOS, COBAYA and PARCS results**

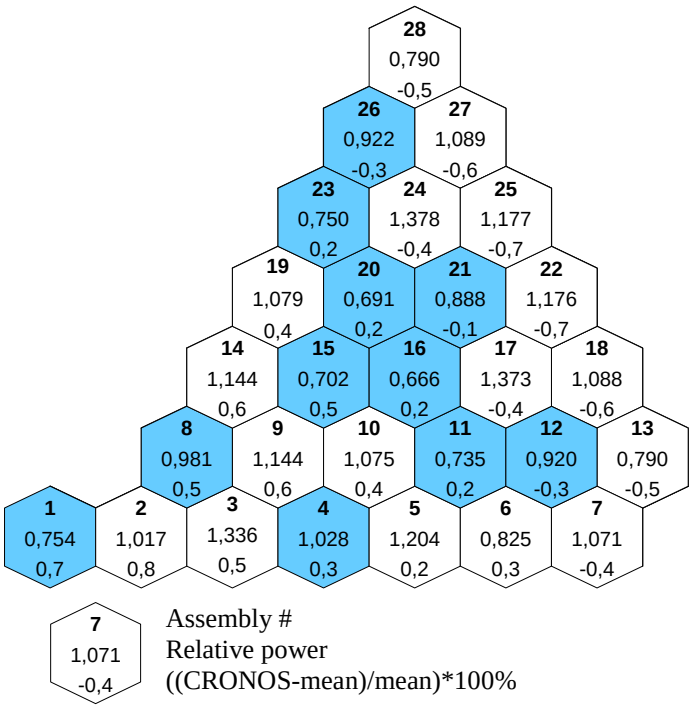


**Figure A.15: HZP state 1b. CRONOS computed assembly powers vs. mean of DYN3D, CRONOS, COBAYA and PARCS results**

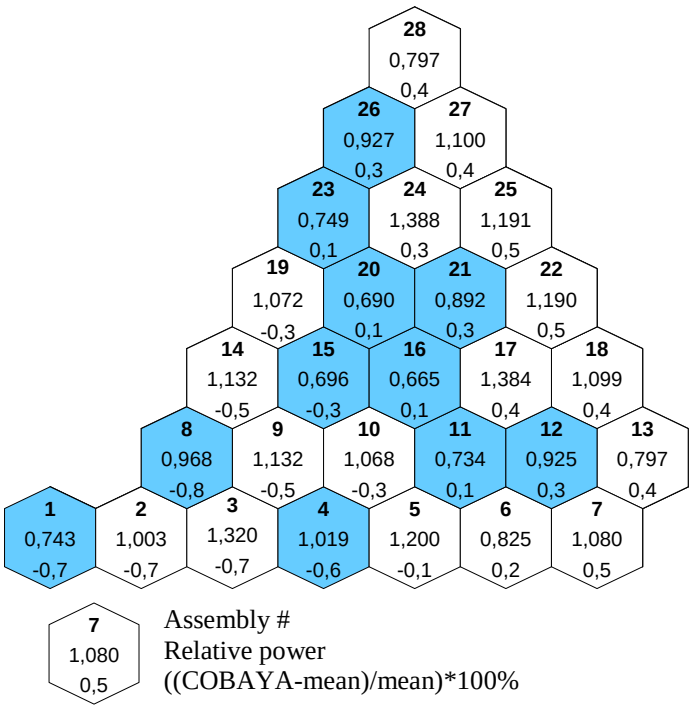


**Figure A.16: HZP state 1b. COBAYA computed assembly powers vs. mean of DYN3D, CRONOS, COBAYA and PARCS results**

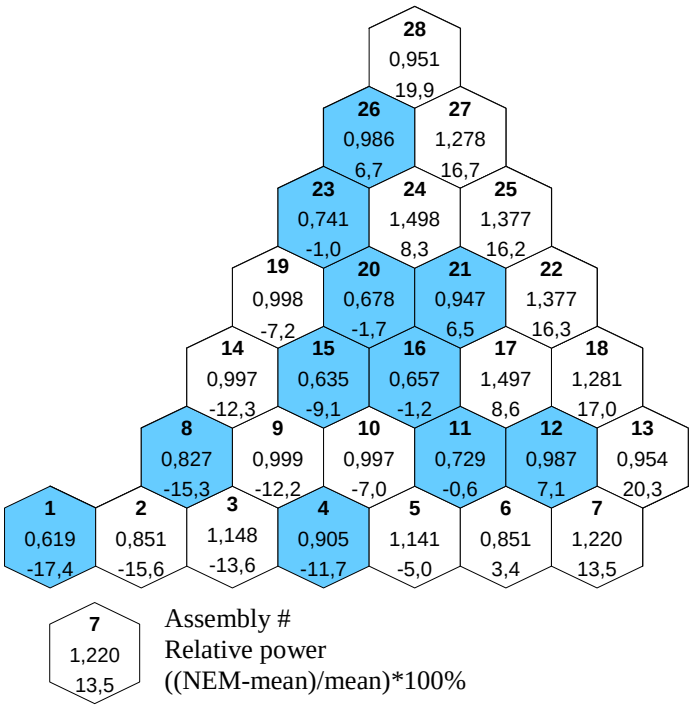


**Figure A.17: HZP state 1b. NEM computed assembly powers vs. mean of DYN3D, CRONOS, COBAYA and PARCS results**

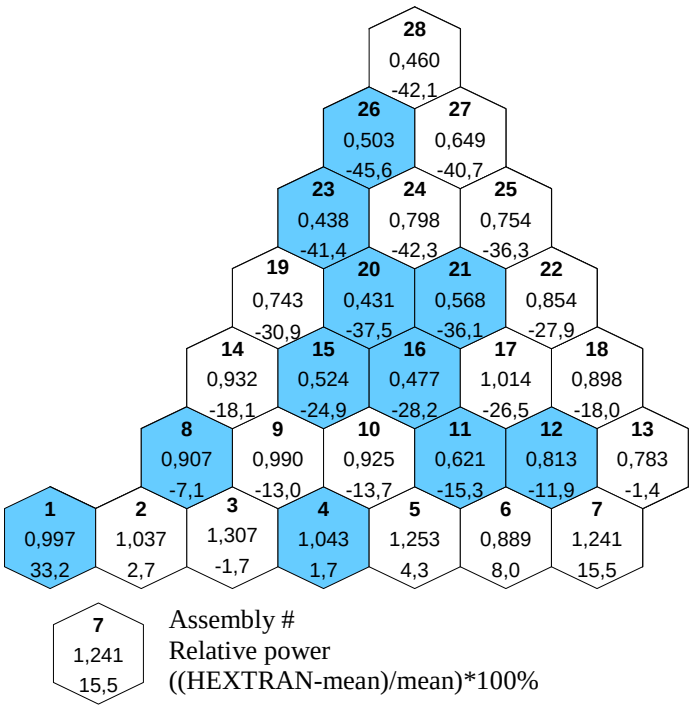


**Figure A.18: HZP state 1b. HEXTRAN computed assembly powers vs. mean of DYN3D, CRONOS, COBAYA and PARCS results**

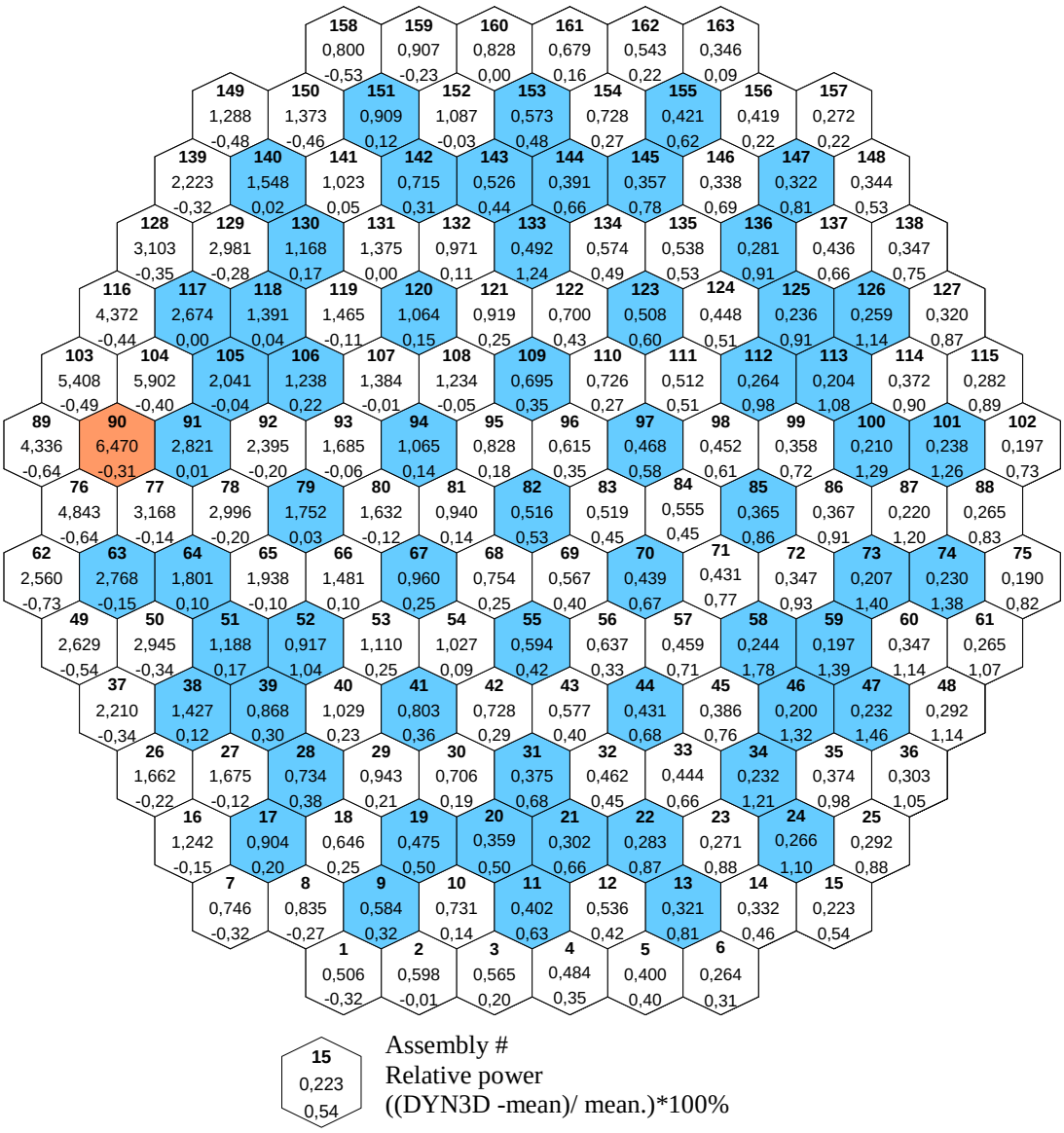


**Figure A.19: HZP state 3. DYN3D computed assembly powers vs. mean of DYN3D, CRONOS, COBAYA and PARCS results**

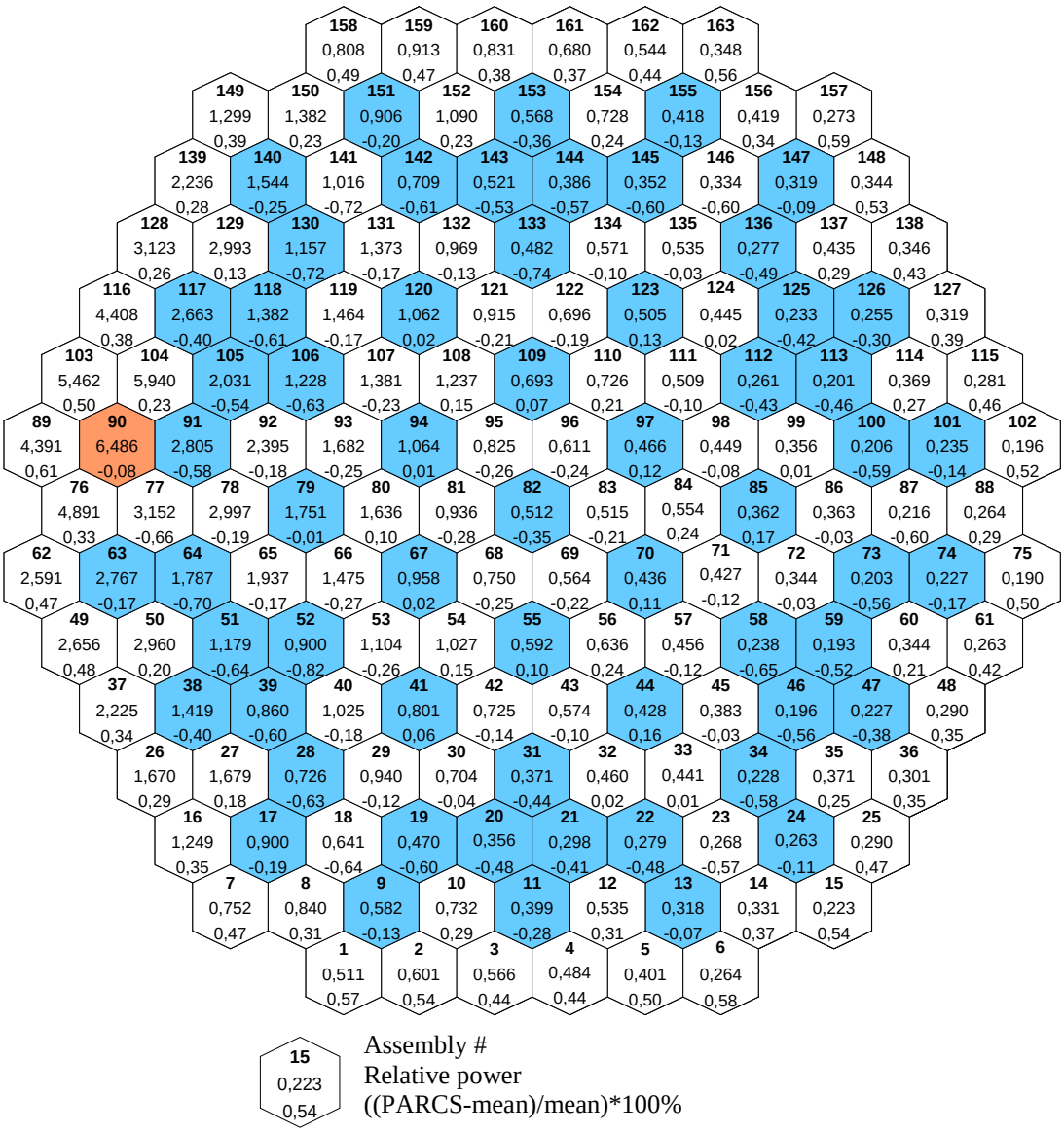


**Figure A.20: HZP state 3. PARCS computed assembly powers vs. mean of DYN3D, CRONOS, COBAYA and PARCS results**

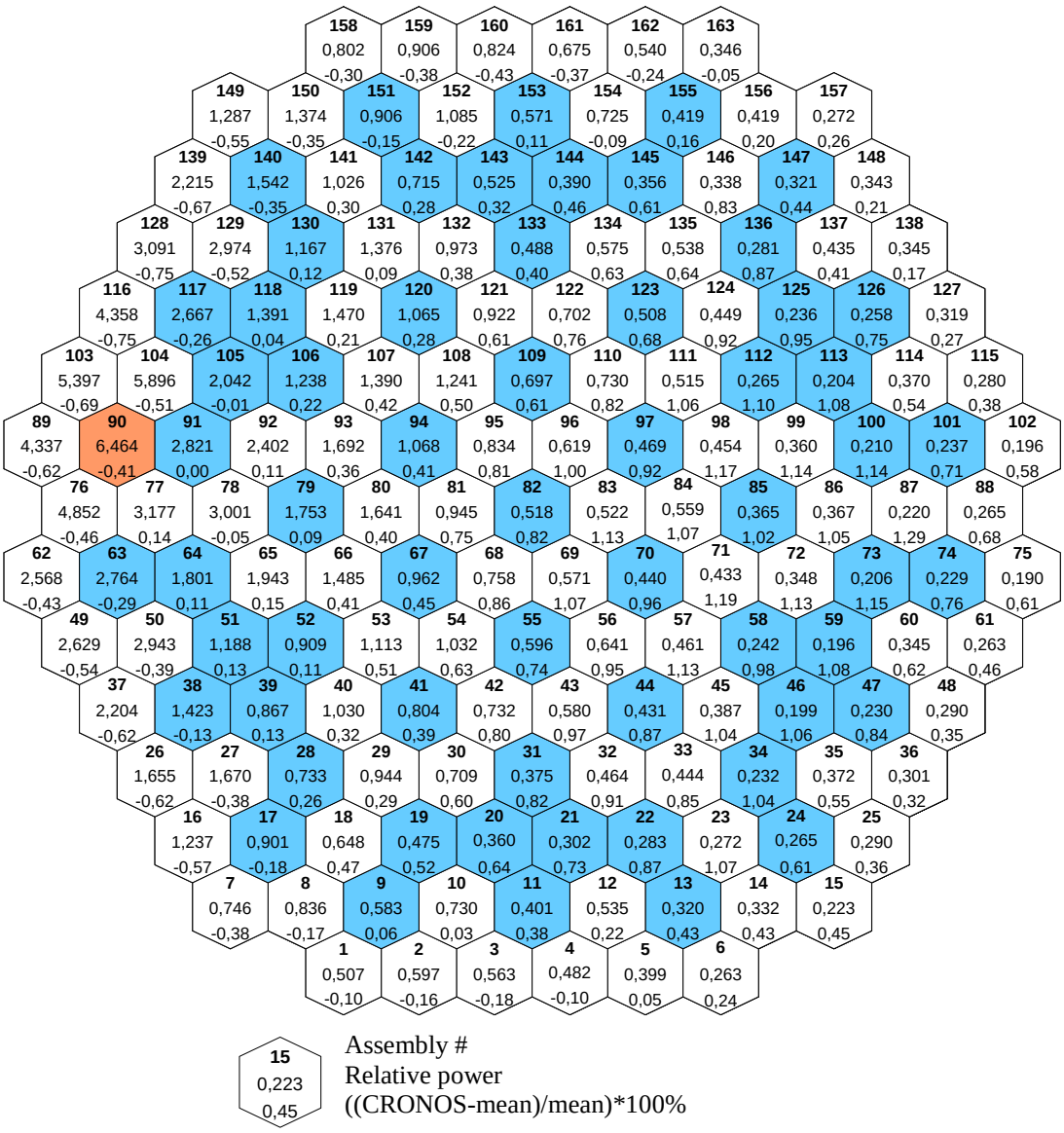


**Figure A.21: HZP state 3. CRONOS computed radial power distribution vs. mean of DYN3D, CRONOS, COBAYA and PARCS results**

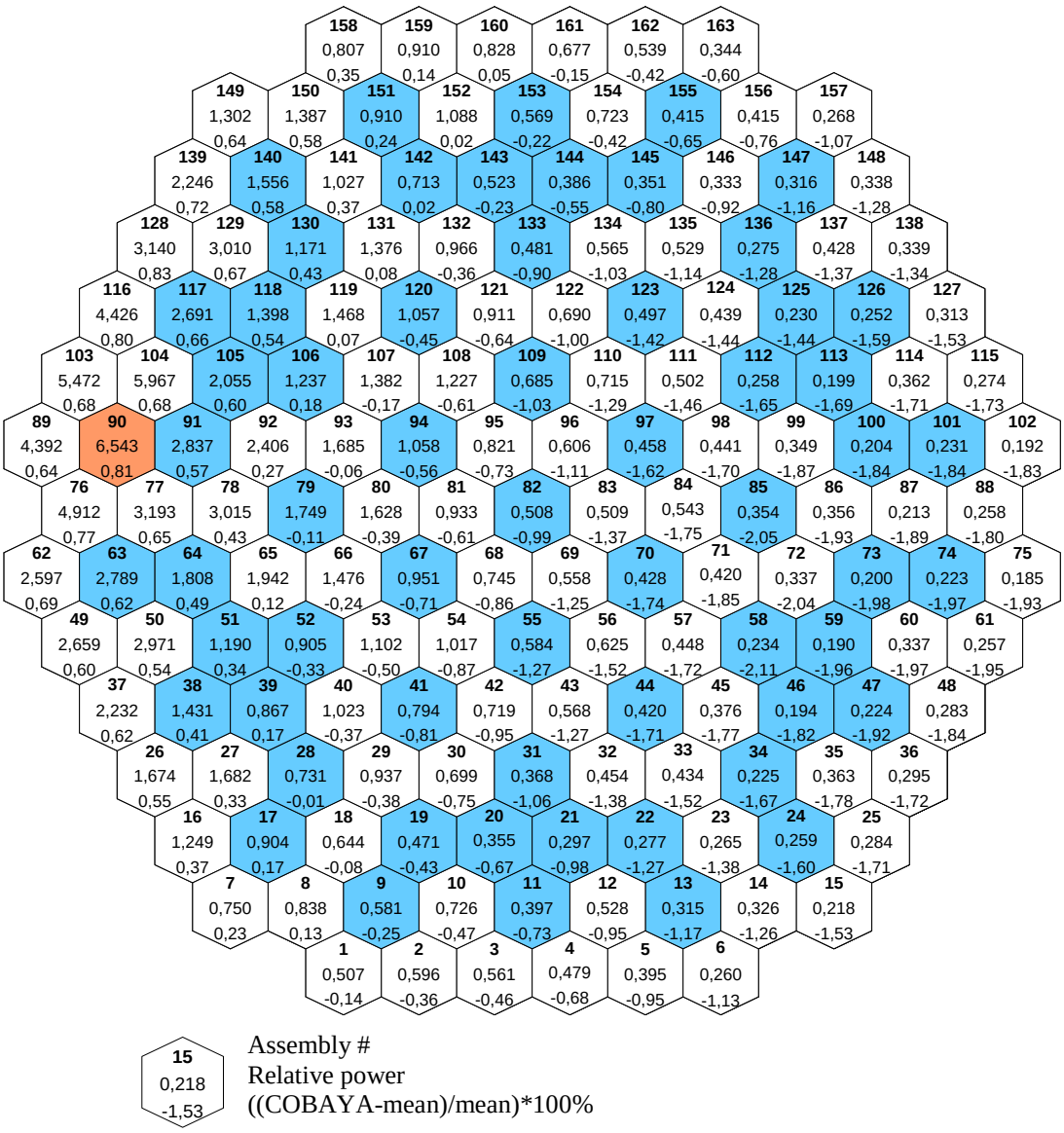


**Figure A.22: HZP state 3. COBAYA computed radial power distribution vs. mean of DYN3D, CRONOS, COBAYA and PARCS results**

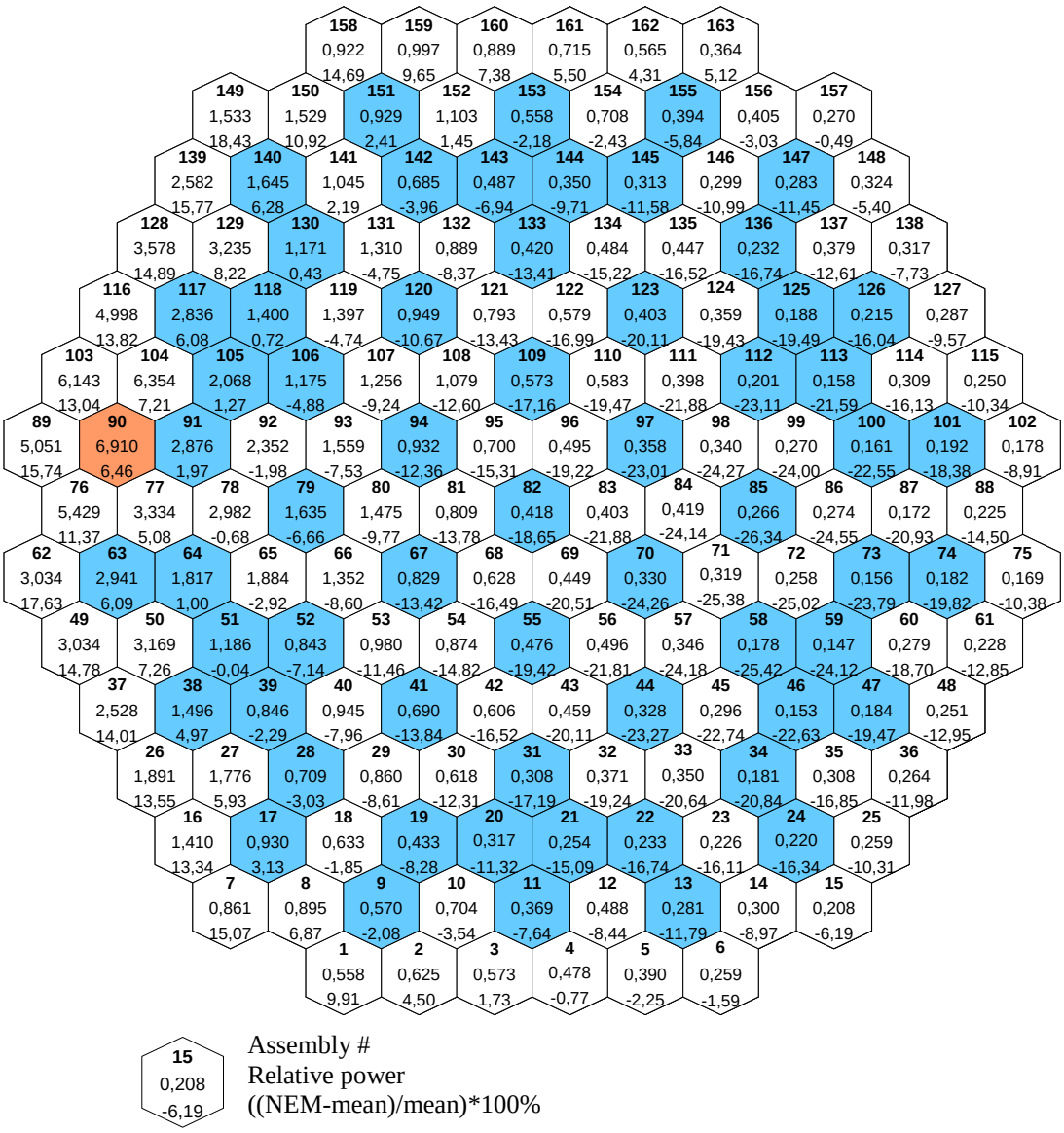


**Figure A.23: HZP state 3. NEM computed radial power distribution vs. mean of DYN3D, CRONOS, COBAYA and PARCS results**

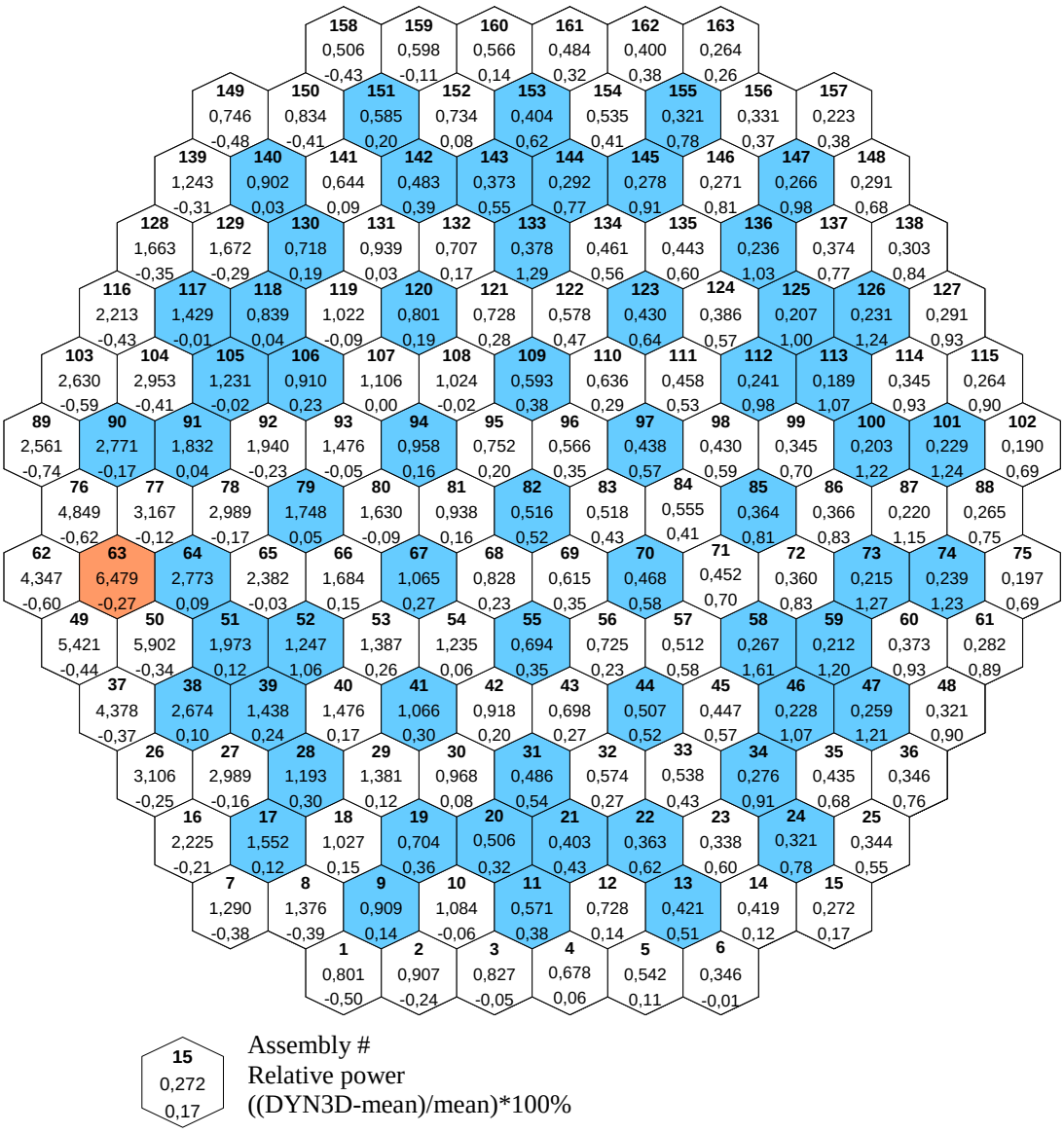


**Figure A.24: HZP state 4. DYN3D computed radial power distribution vs. mean of DYN3D, CRONOS, COBAYA and PARCS results**

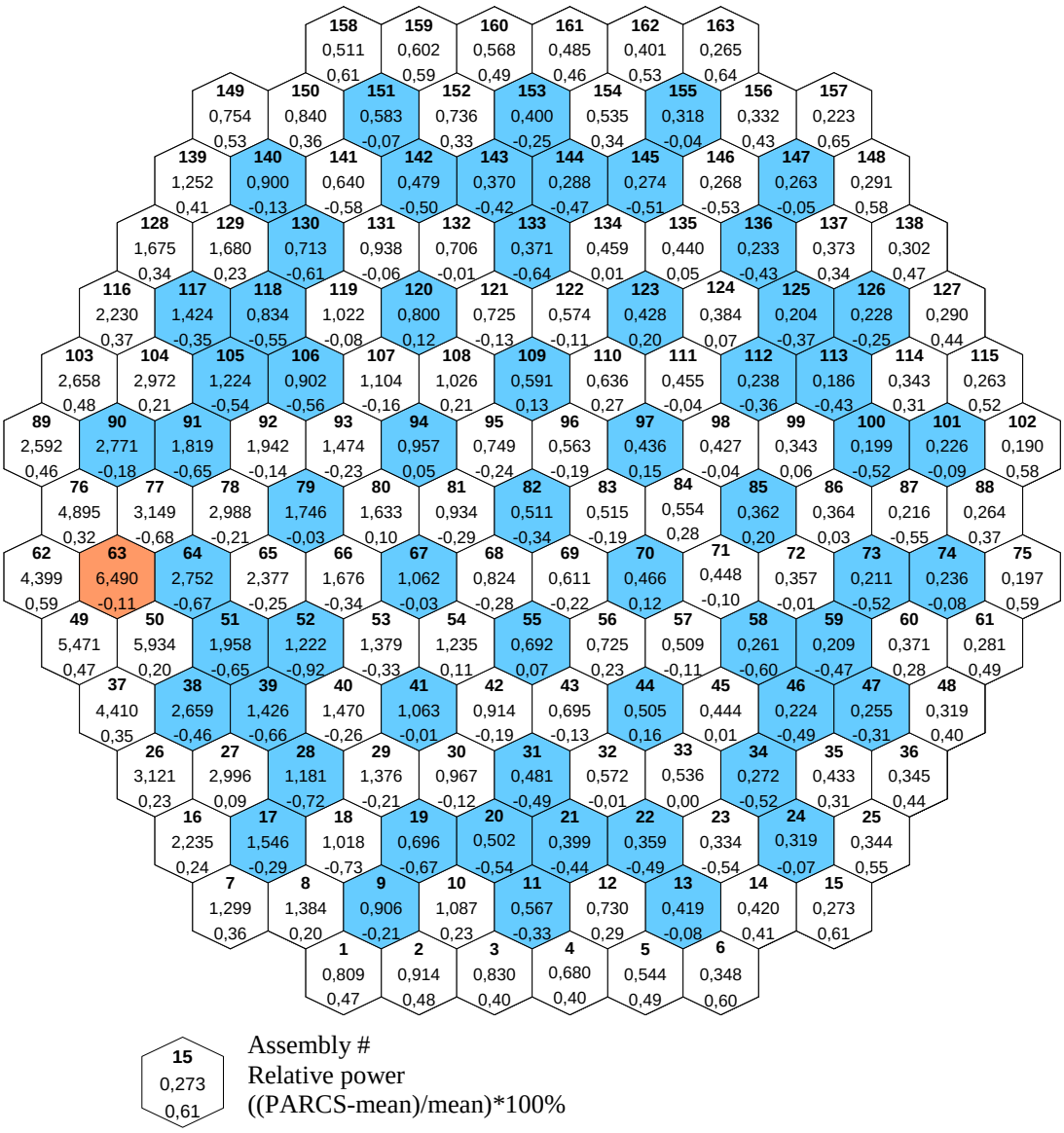


**Figure A.25: HZP state 4. PARCS computed radial power distribution vs. mean of DYN3D, CRONOS, COBAYA and PARCS results**

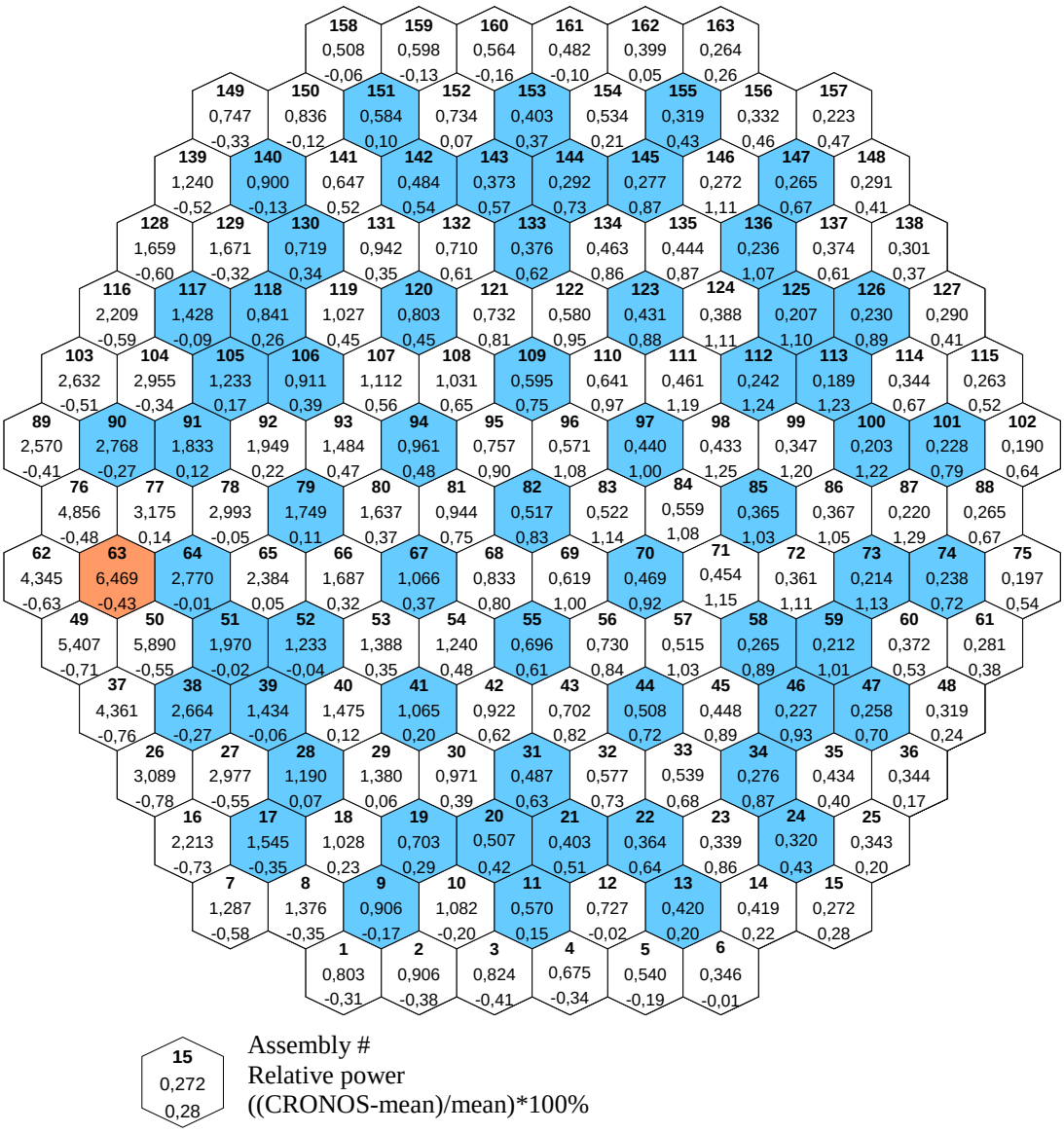


**Figure A.26: HZP state 4. CRONOS computed radial power distribution vs. mean of DYN3D, CRONOS, COBAYA and PARCS results**

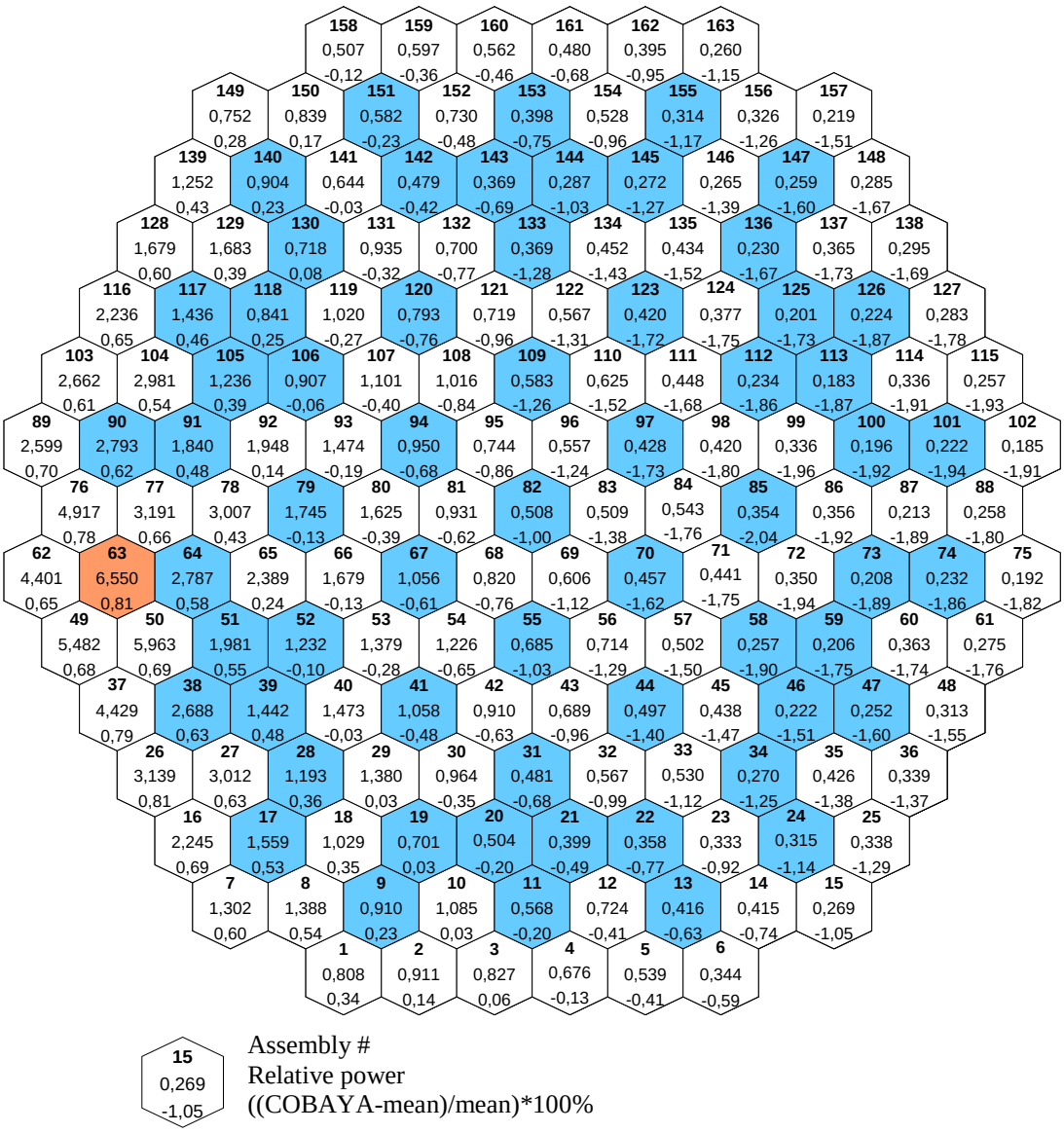


**Figure A. 27: HZP state 4. COBAYA computed radial power distribution vs. mean of DYN3D, CRONOS, COBAYA and PARCS results**

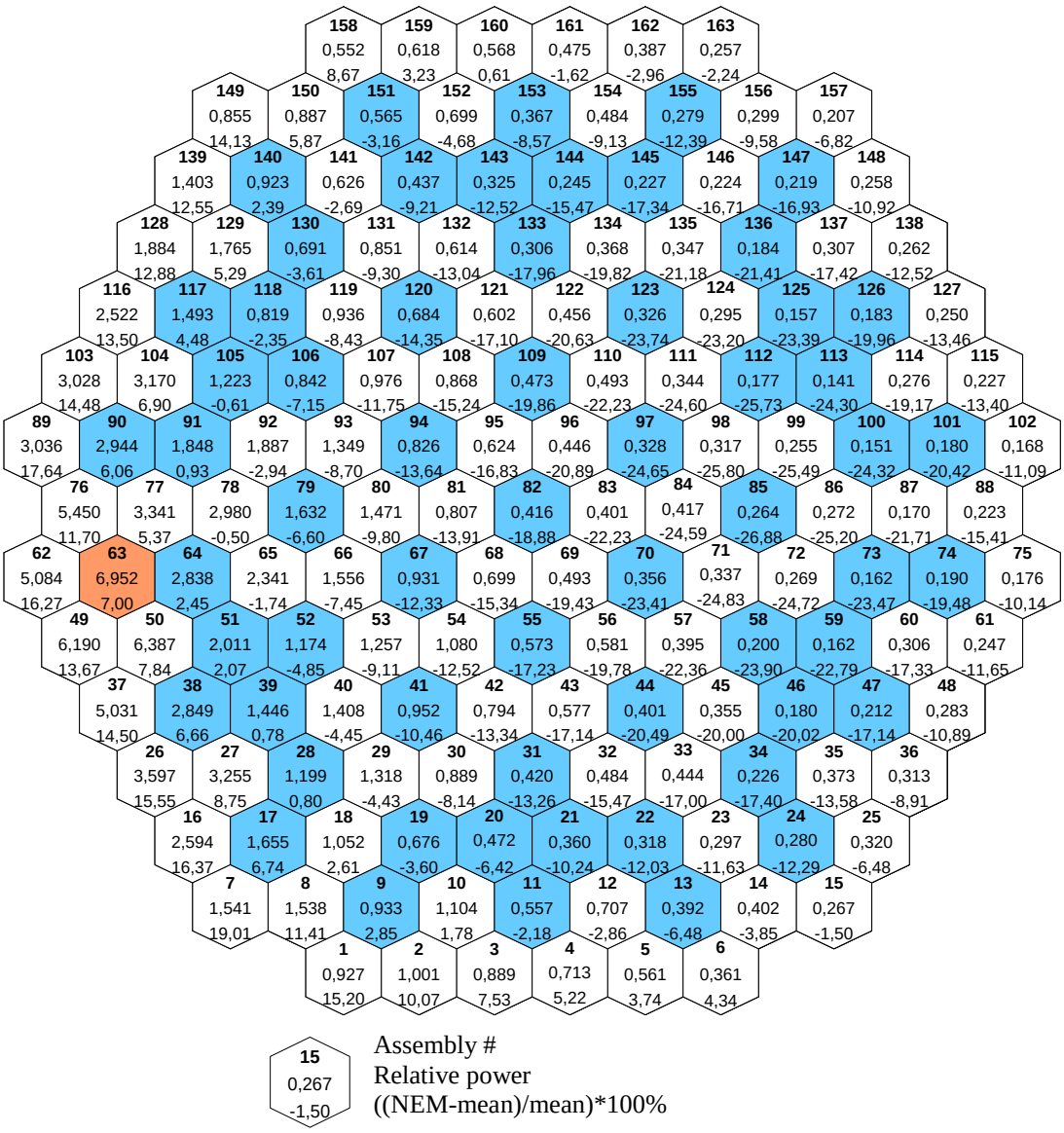


**Figure A.28: HZP state 4. NEM computed radial power distribution vs. mean of DYN3D, CRONOS, COBAYA and PARCS results**

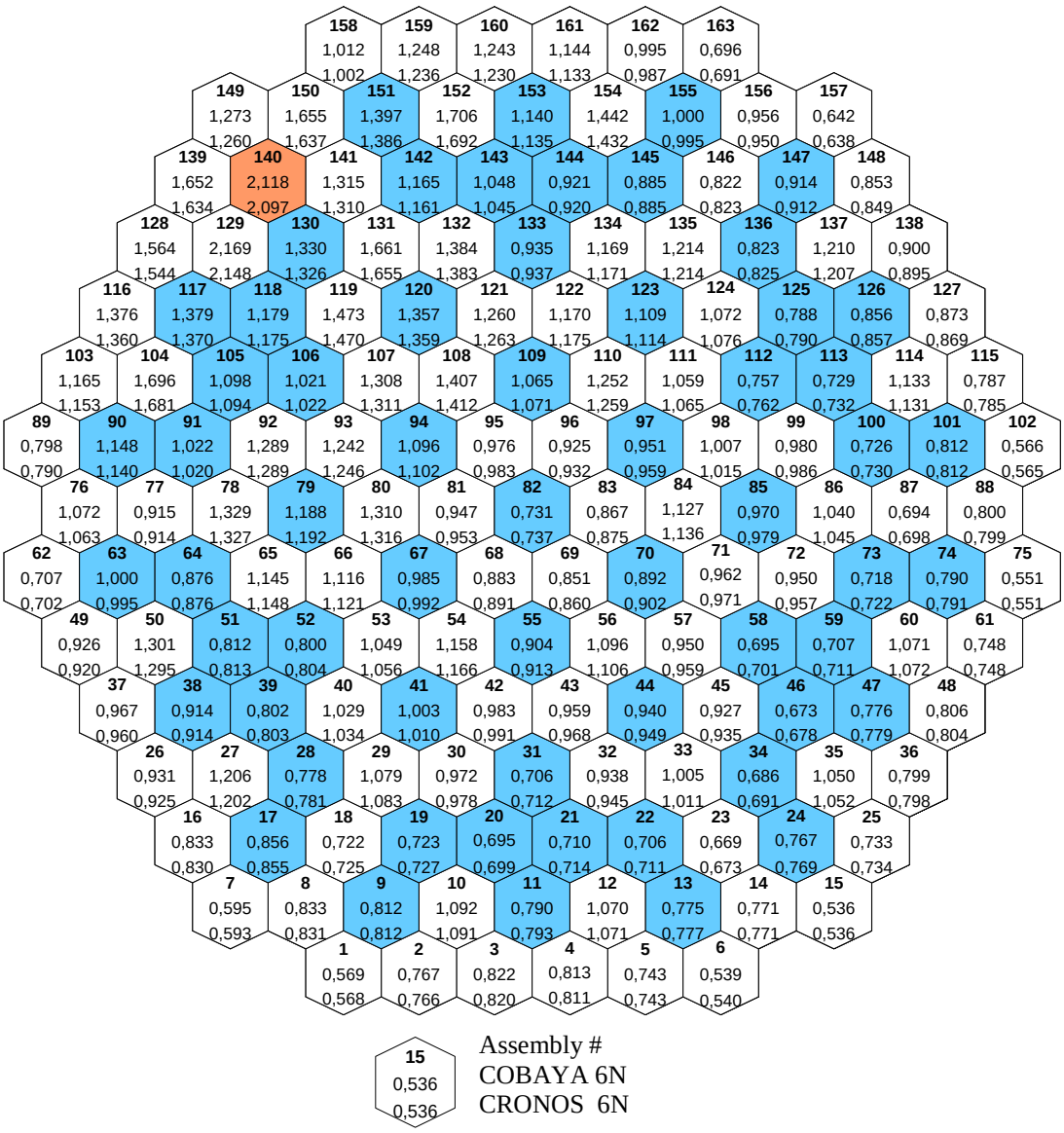


**Figure A.29: HZP state 5. COBAYA and CRONOS computed radial power distribution (XS library for Scenario 2)**

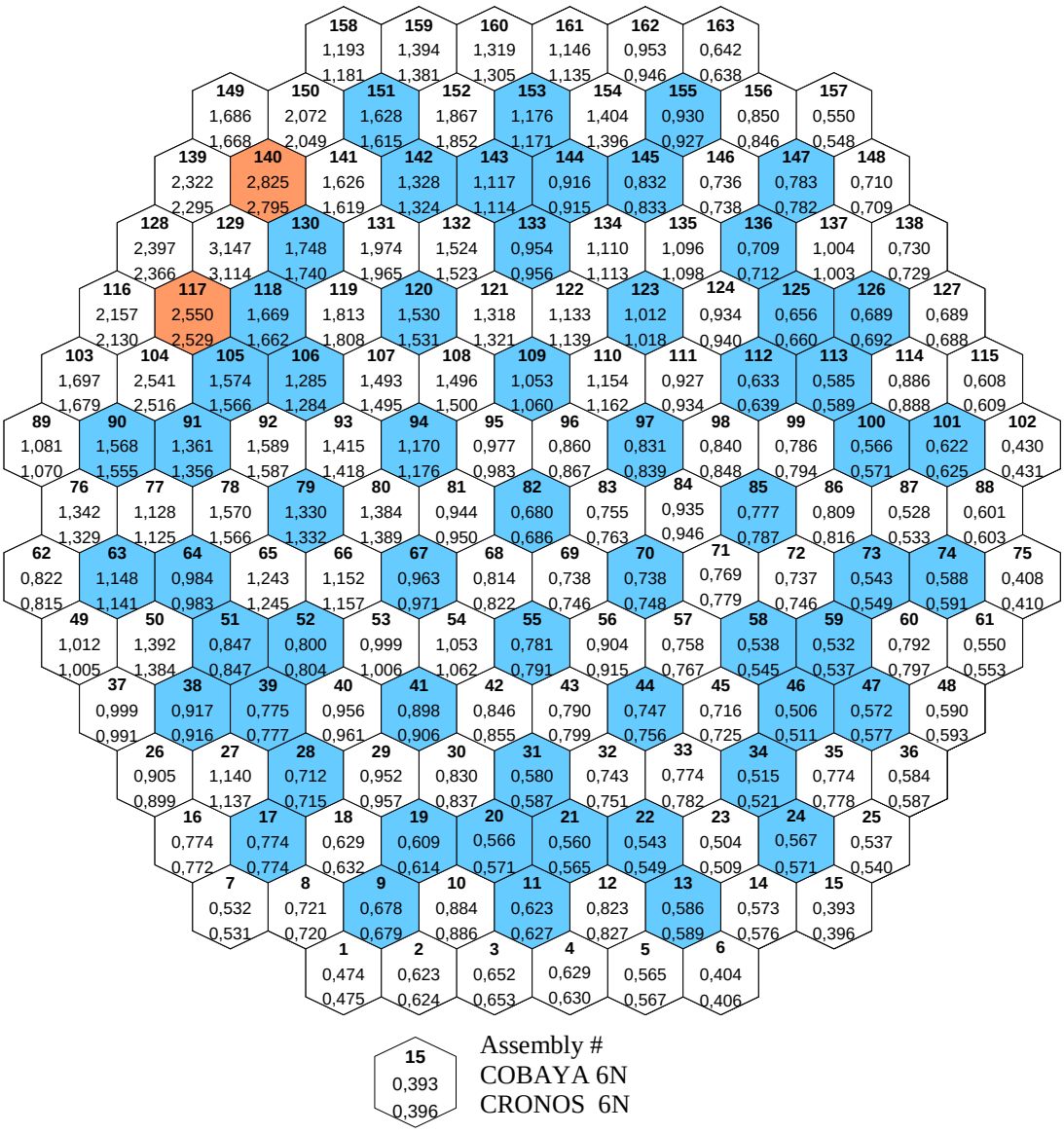


**Figure A.30: HZP state 6. COBAYA and CRONOS computed radial power distribution (XS library for Scenario 2)**

# Appendix B: Initial HFP results of Exercise 2

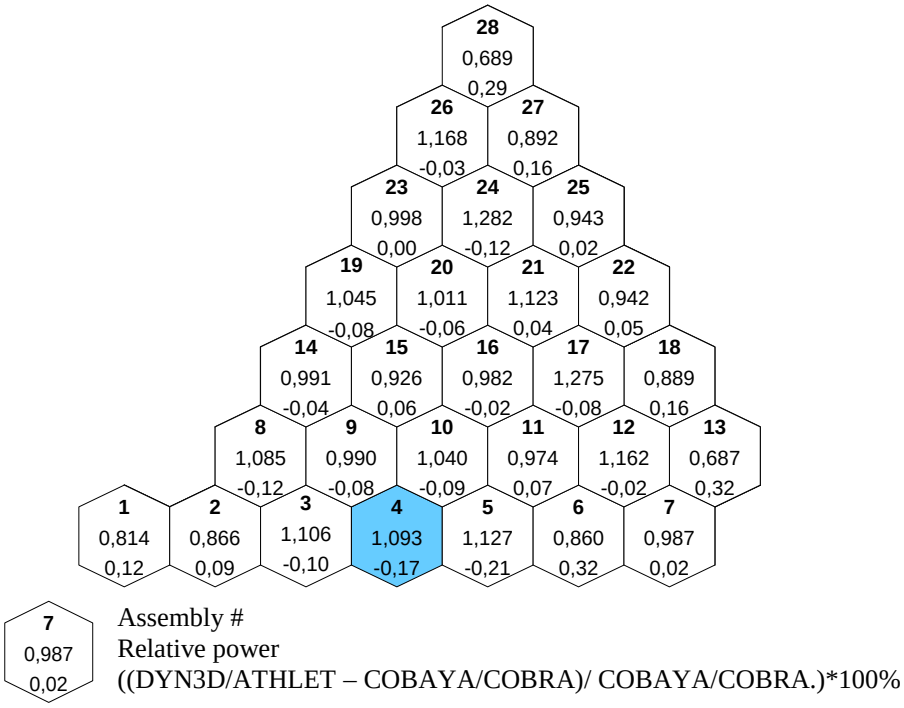


**Figure B.1: HFP steady state. DYN3D/ATHLET vs. COBAYA3/COBRA3 computed assembly powers. COBAYA/COBRA used ATHLET calculated core BCs**

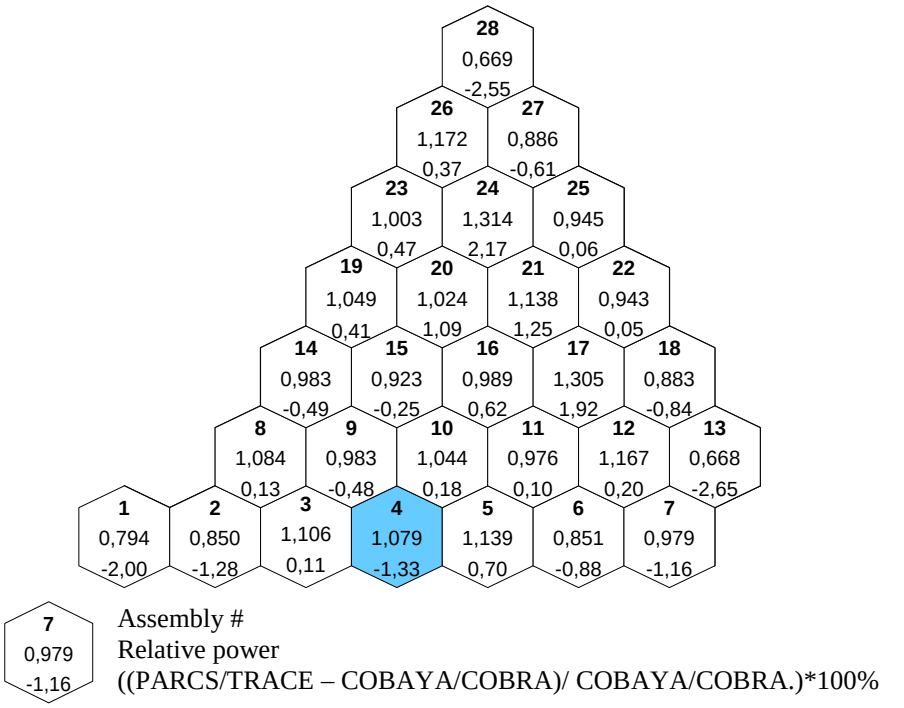


**Figure B.2: HFP steady state. PARCS/TRACE vs. COBAYA3/COBRA3 computed assembly powers. COBAYA/COBRA used TRACE calculated core BCs**

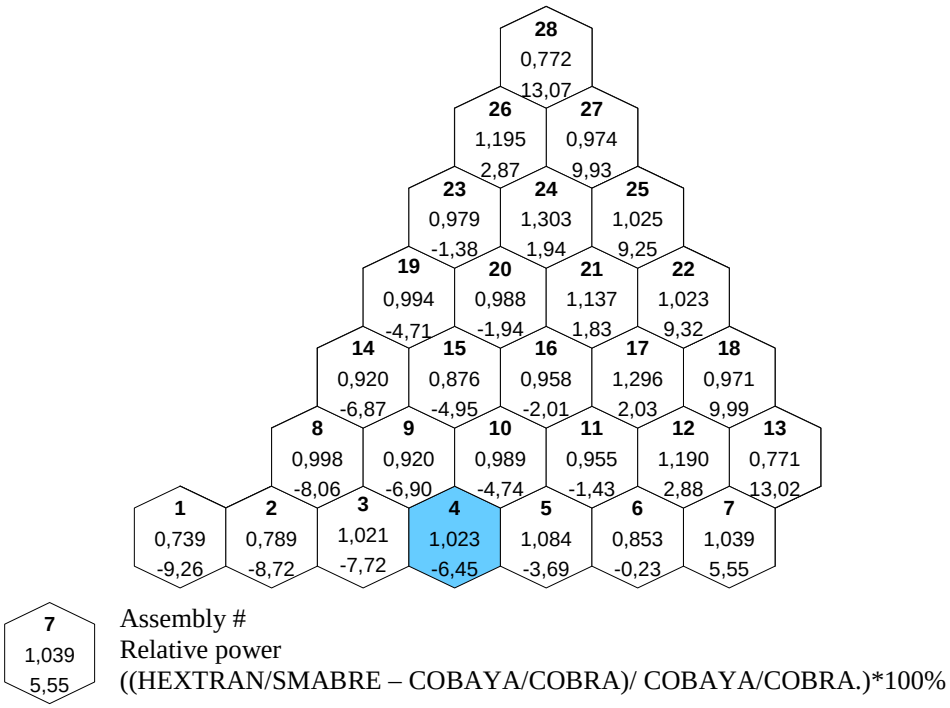


**Figure B.3: HFP steady state. HEXTRAN/SMABRE vs. COBAYA3/COBRA3 computed assembly powers. COBAYA/COBRA used SMABRE calculated core BCs**

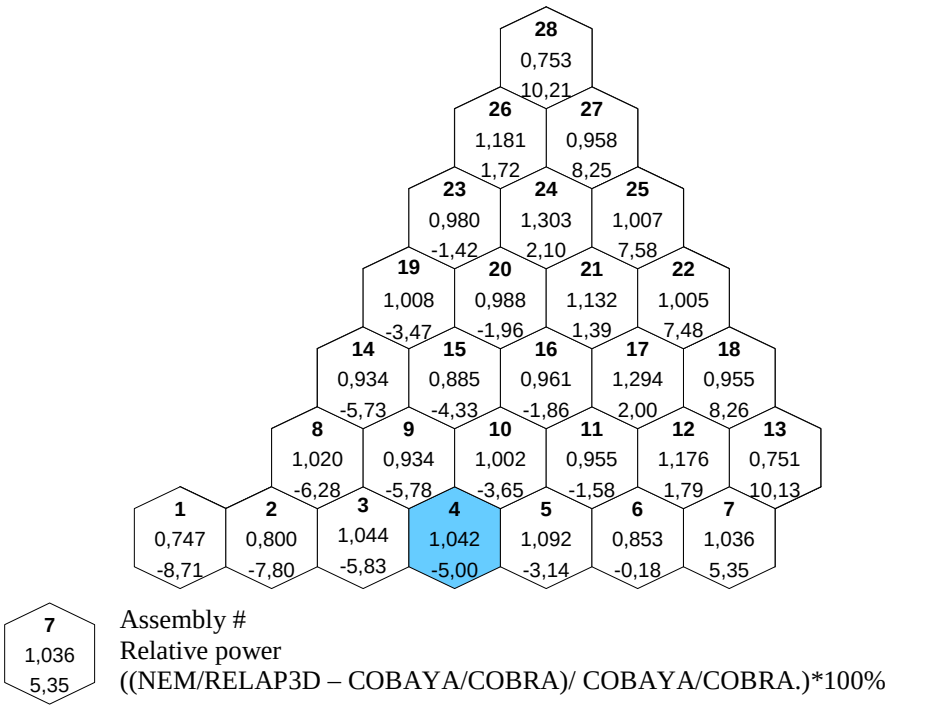


**Figure B.4: HFP steady state. NEM/RELAP5-3D vs. COBAYA3/COBRA3 computed assembly powers. COBAYA/COBRA used RELAP5-3D calculated core BCs**

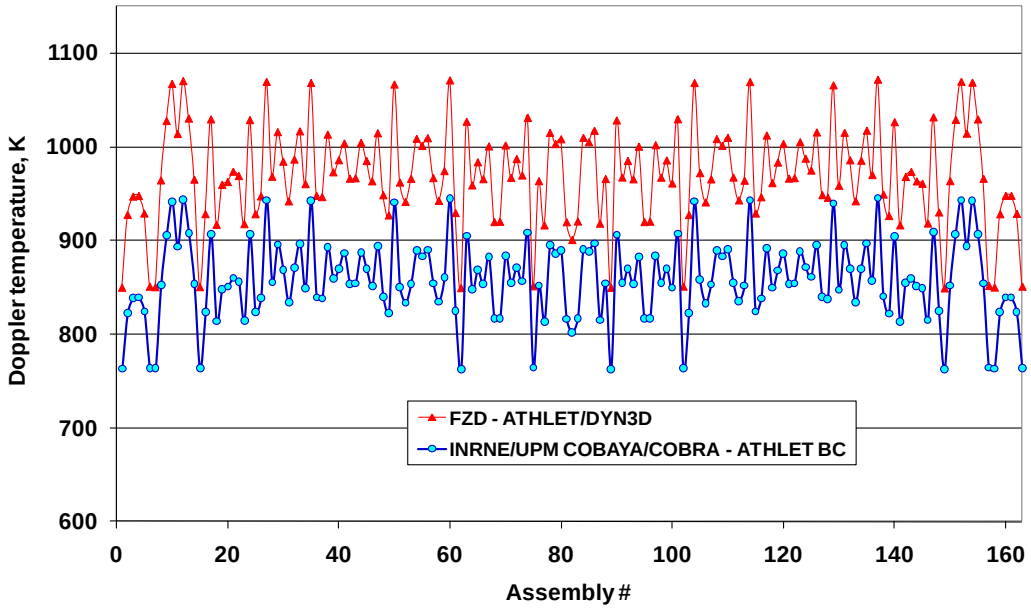


**Figure B.5: HFP steady state. DYN3D/ATHLET vs. COBAYA3/COBRA3 computed FA Doppler temperatures. COBAYA/COBRA used ATHLET calculated core BCs**

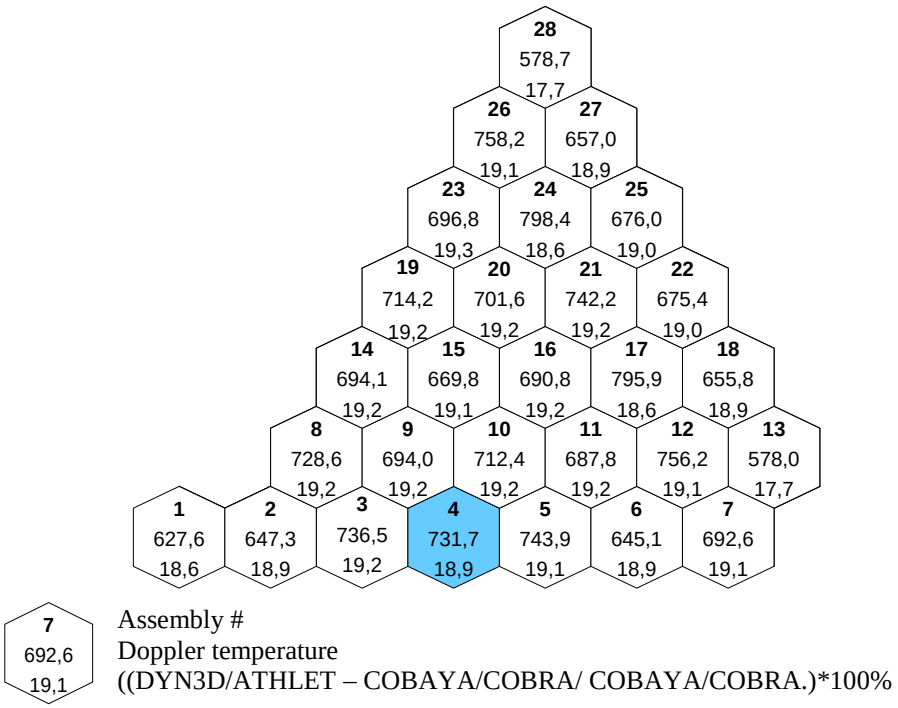


**Figure B.6: HFP steady state. DYN3D/ATHLET vs. COBAYA3/COBRA3 computed FA Doppler temperatures. COBAYA/COBRA used ATHLET calculated core BCs**

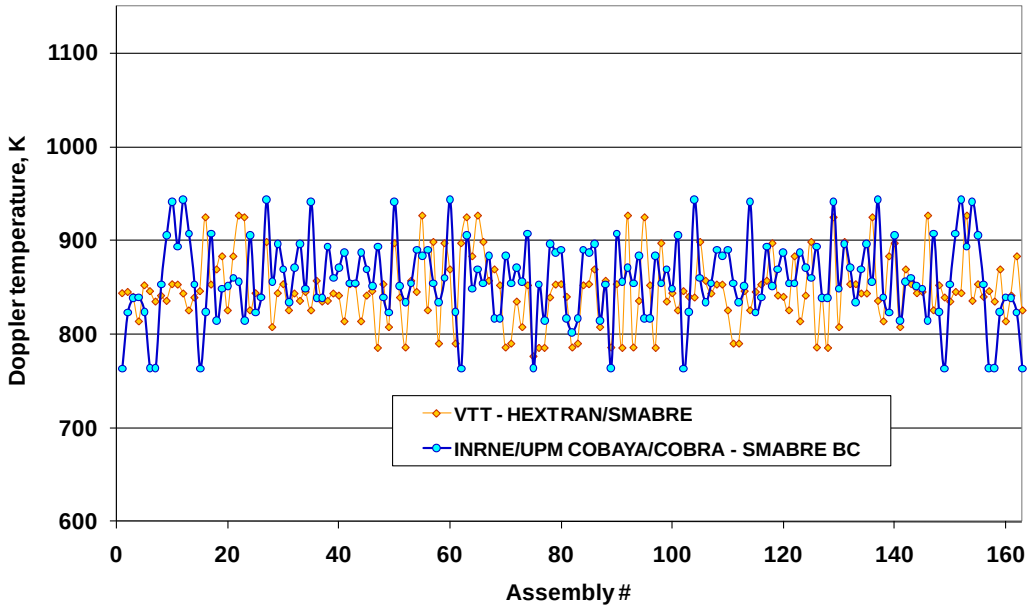


**Figure B.7: HFP state. HEXTRAN/SMABRE vs. COBAYA3/COBRA3 computed Doppler temperatures. COBAYA/COBRA used SMABRE calculated core BCs**

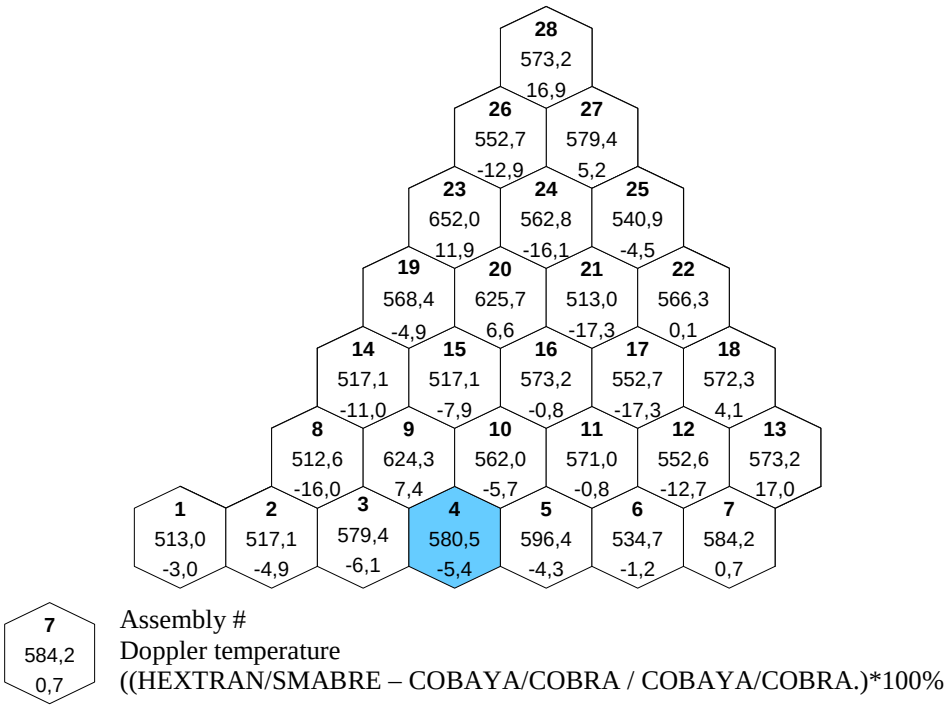


**Figure B.8: HFP state. HEXTRAN/SMABRE vs. COBAYA3/COBRA3 computed FA Doppler temperatures. COBAYA/COBRA used SMABRE calculated core BCs**

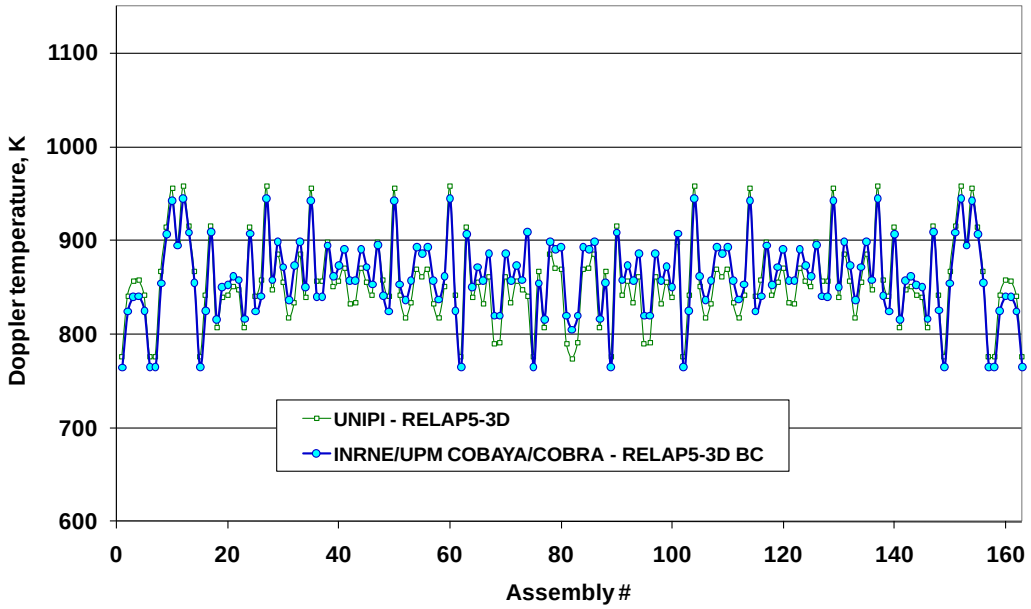


**Figure B.9: HFP steady state. NEM/RELAP3D vs. COBAYA3/COBRA3 computed FA Doppler temperatures. COBAYA/COBRA used RELAP3D calculated core BCs**

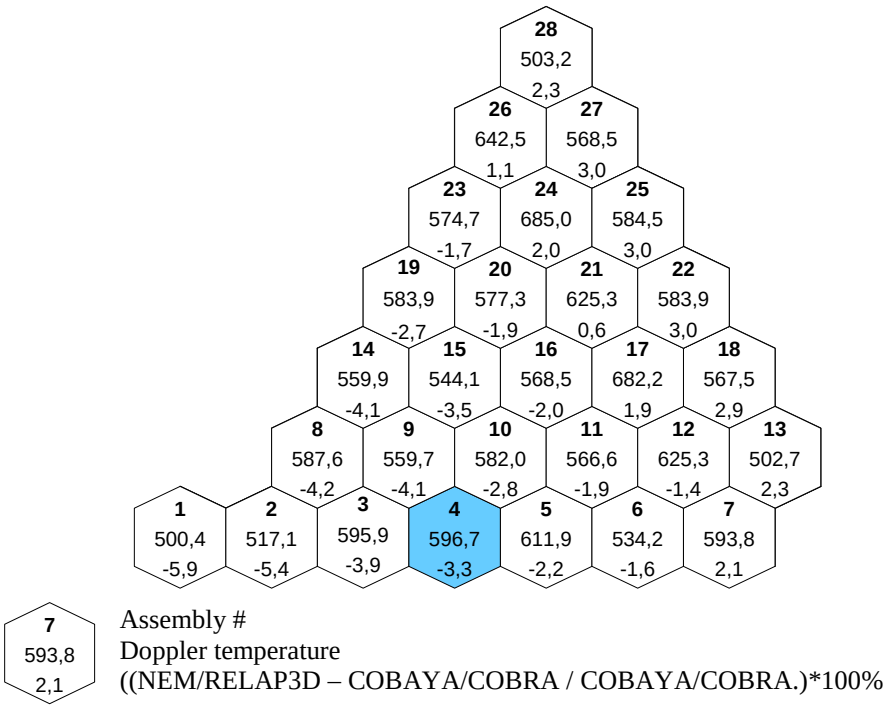


**Figure B.10: HFP steady state. NEM/RELAP3D vs. COBAYA3/COBRA3 computed FA Doppler temperature. COBAYA/COBRA used RELAP3D calculated core BCs**

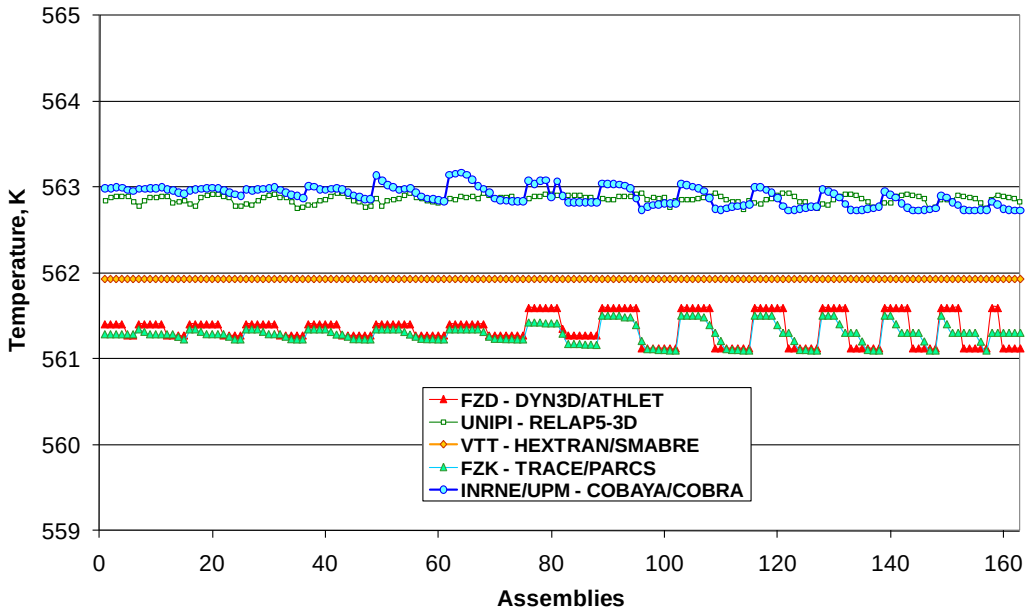


**Figure B.11: Assembly-by-assembly core inlet temperature in the initial HFP state**

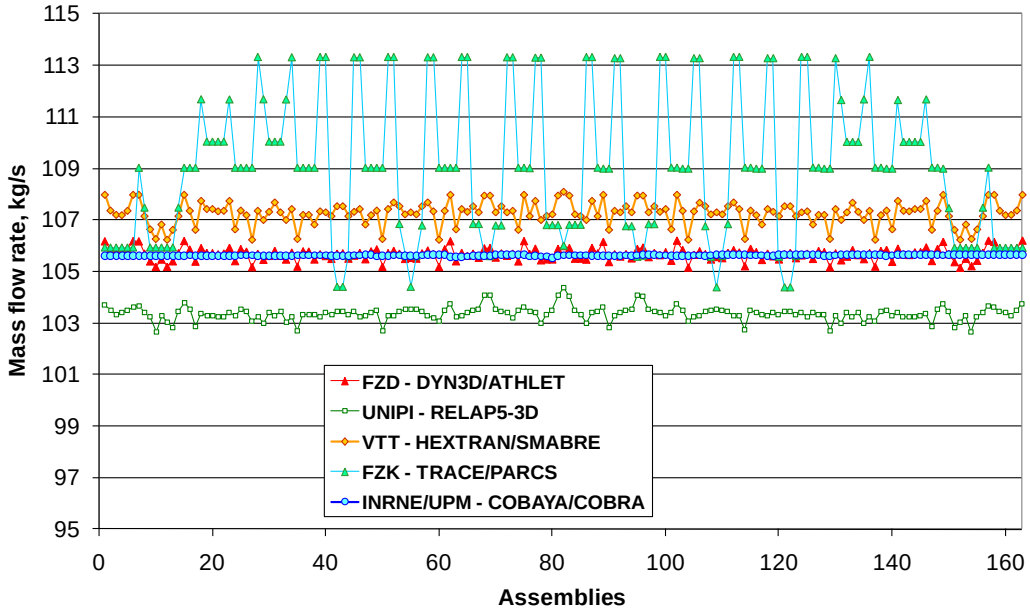


**Figure B.12: Assembly-by-assembly core inlet mass flow rate in the initial HFP state**

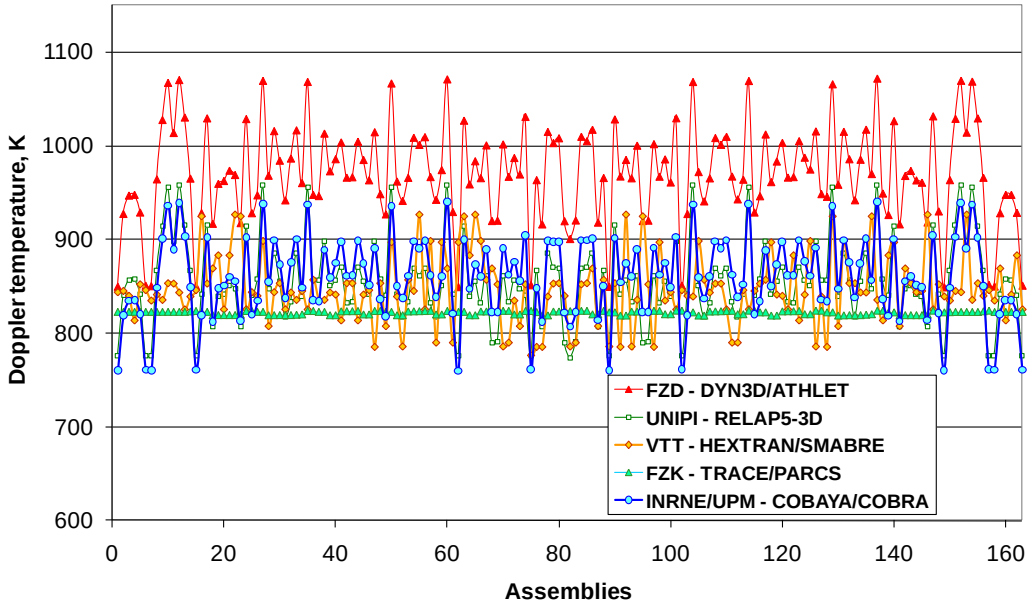


**Figure B.13: Assembly-by-assembly Doppler temperature in the initial HFP state**

# Appendix C: Exercise 2, Scenario 1 results

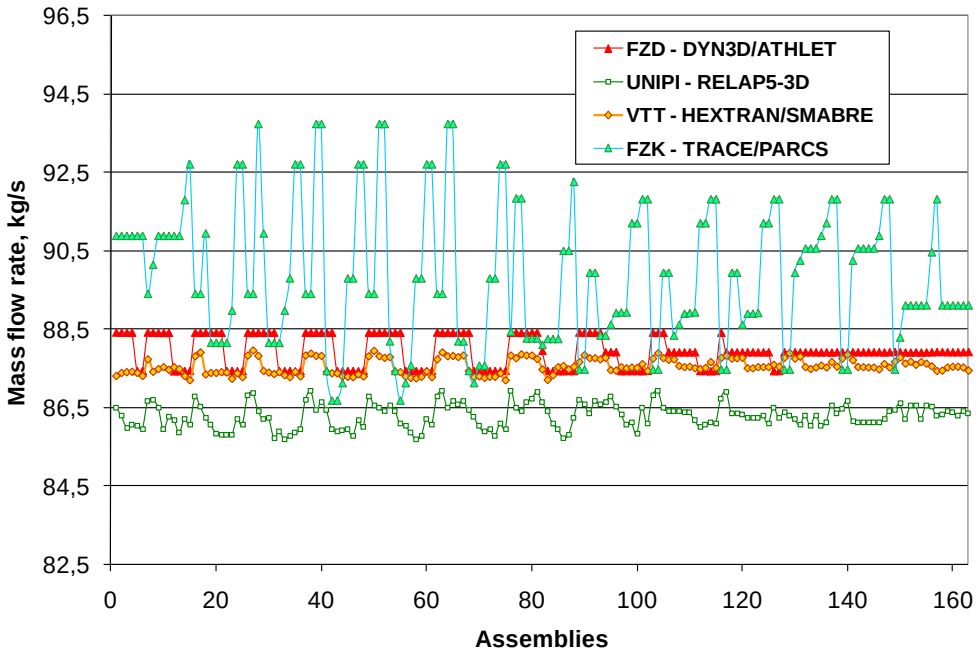


**Figure C.1: Scenario 1: Assembly-by-assembly core inlet mass flow rates at time of maximum overcooling (166s)**

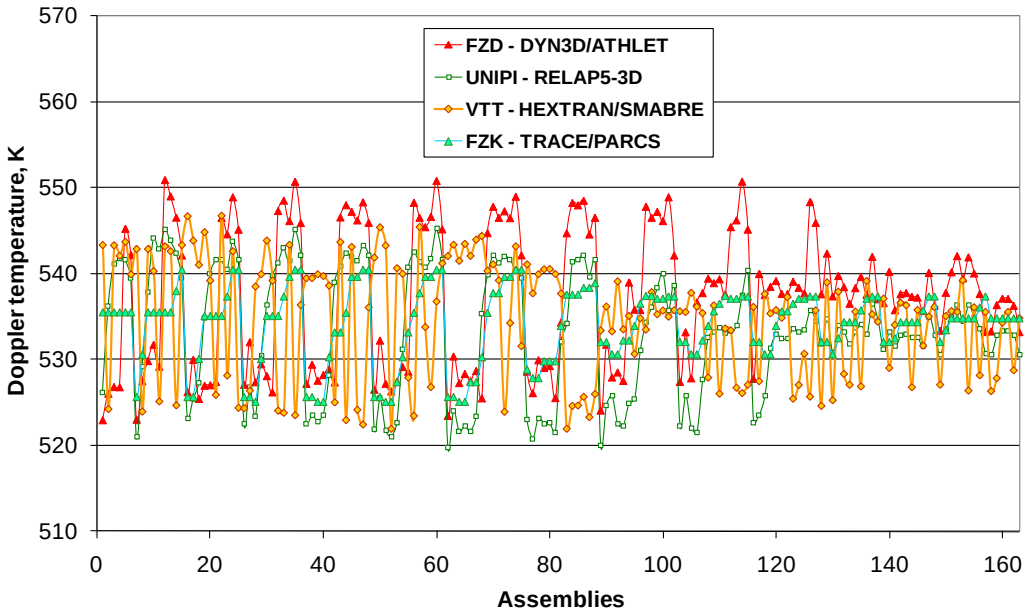


**Figure C.2: Scenario 1: Assembly-by-assembly Doppler temperatures at time of maximum overcooling (166s)**

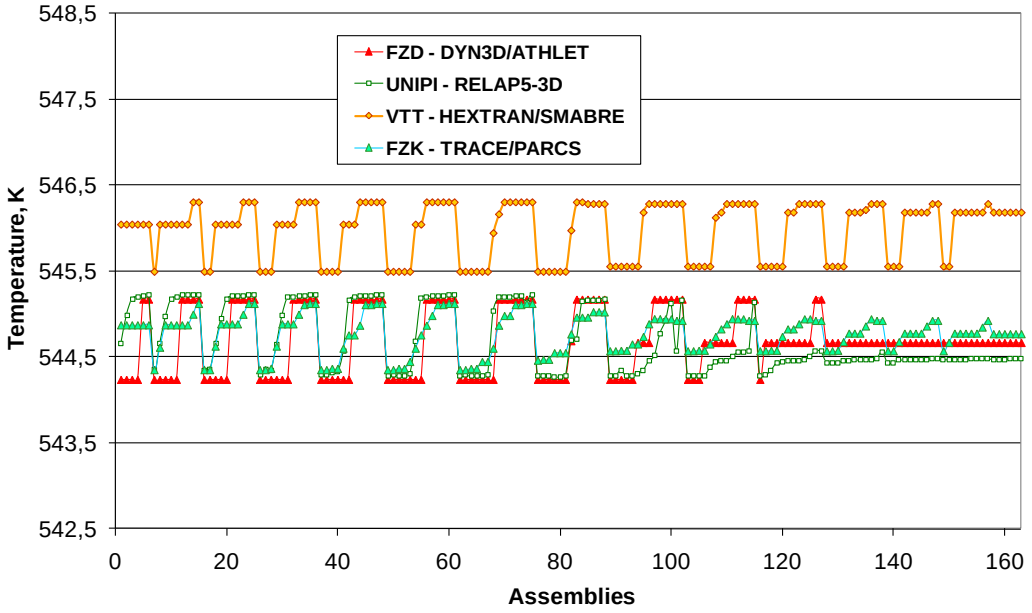


**Figure C.3: Scenario 1: Assembly-by-assembly core inlet temperatures at 600s**

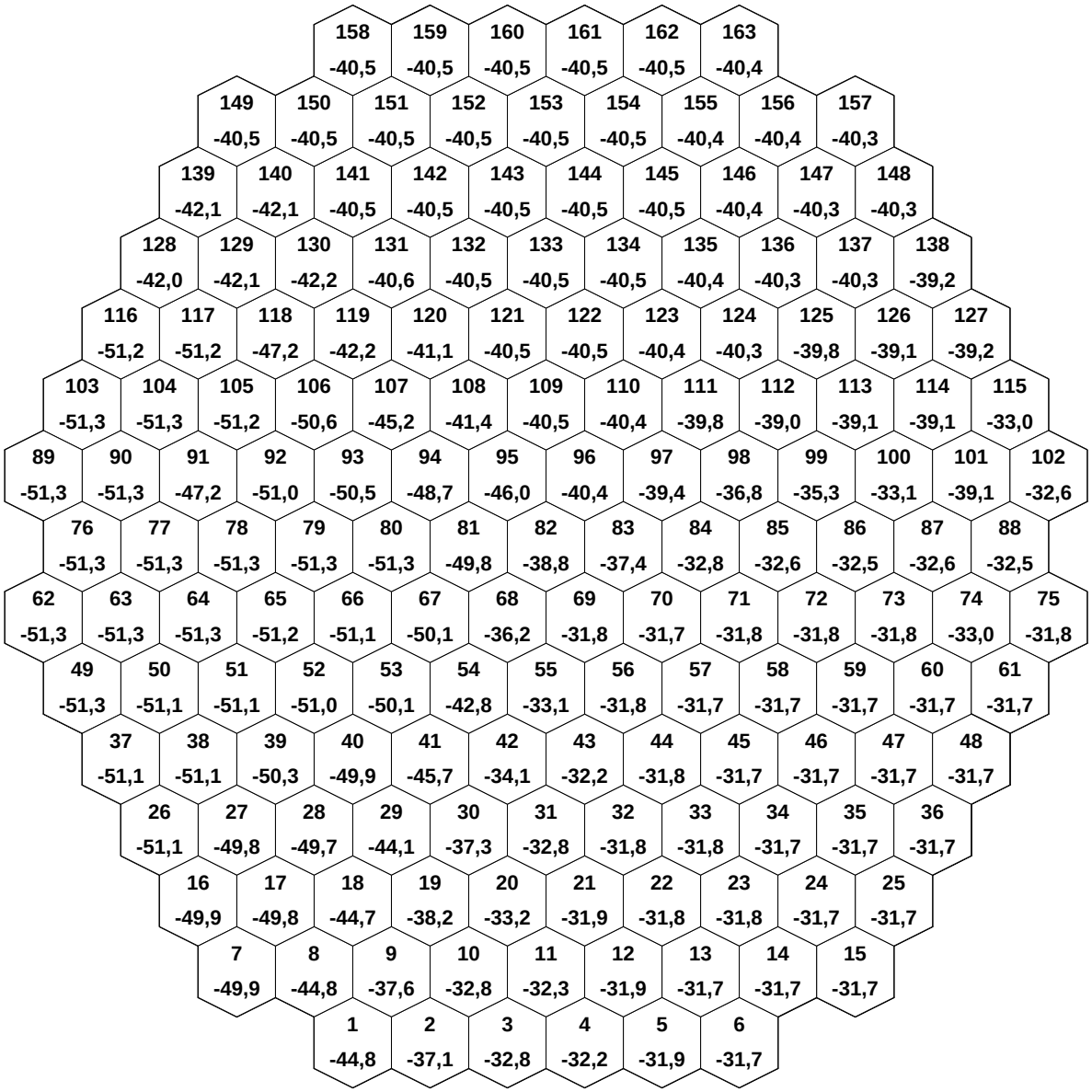


**Figure C.4: Scenario 1, RELAP3D/NEM results at time of max overcooling (166s): Core inlet temperature deviations from the initial HFP state**

# Appendix D: Exercise 2, Scenario 2 results

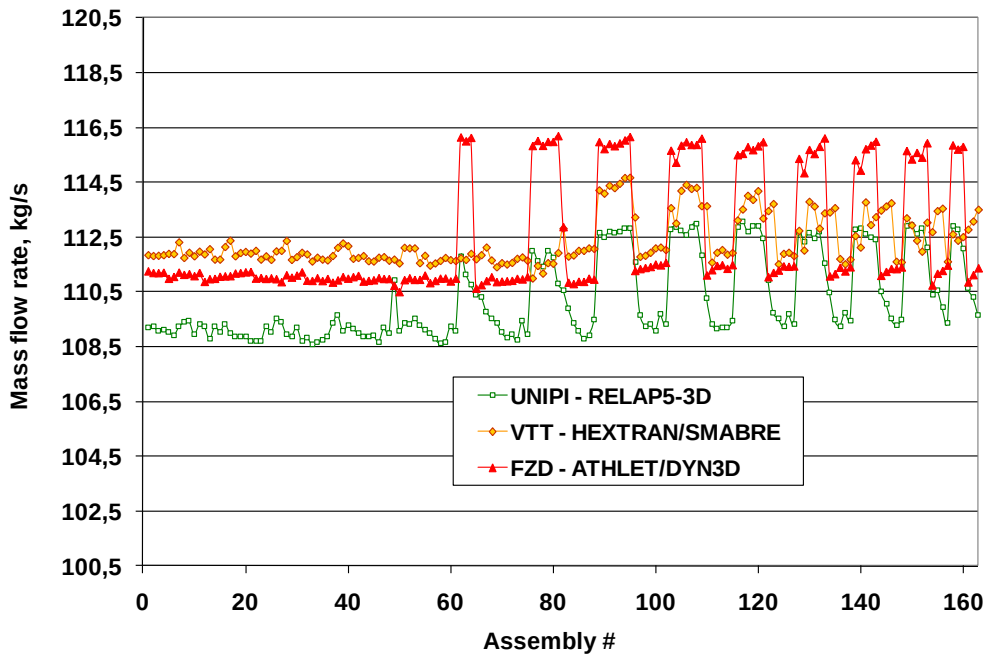


**Figure D.1: Scenario 2: Assembly-by-assembly core inlet mass flow rates at time of maximum overcooling (69s)**

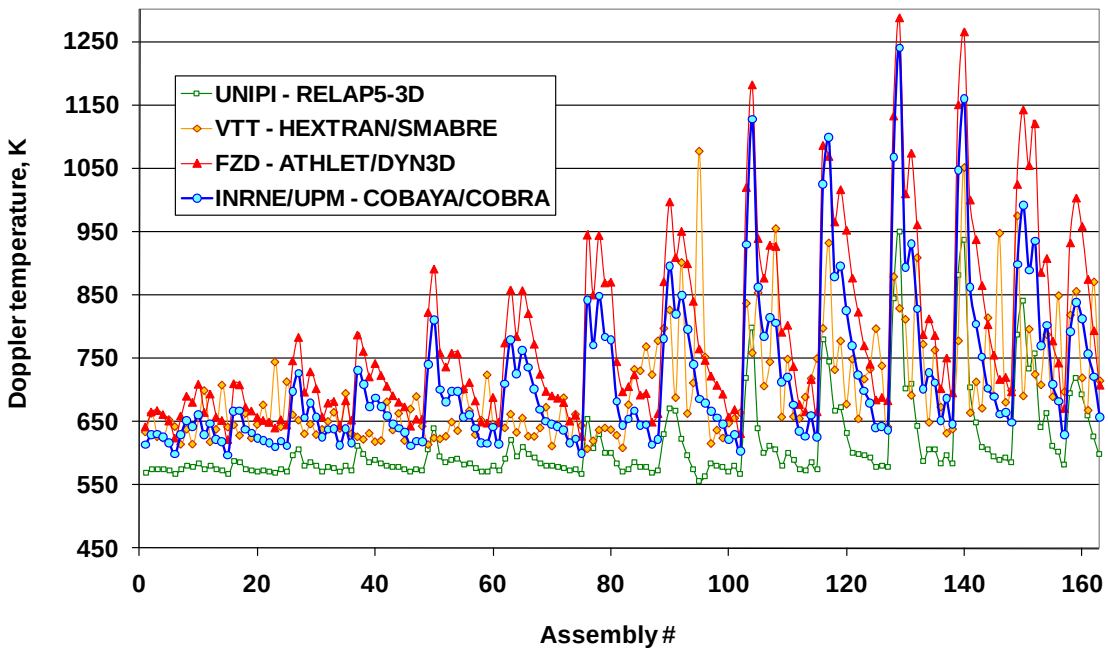


**Figure D.2: Scenario 2: Assembly-by-assembly Doppler temperatures at time of maximum overcooling (69s)**

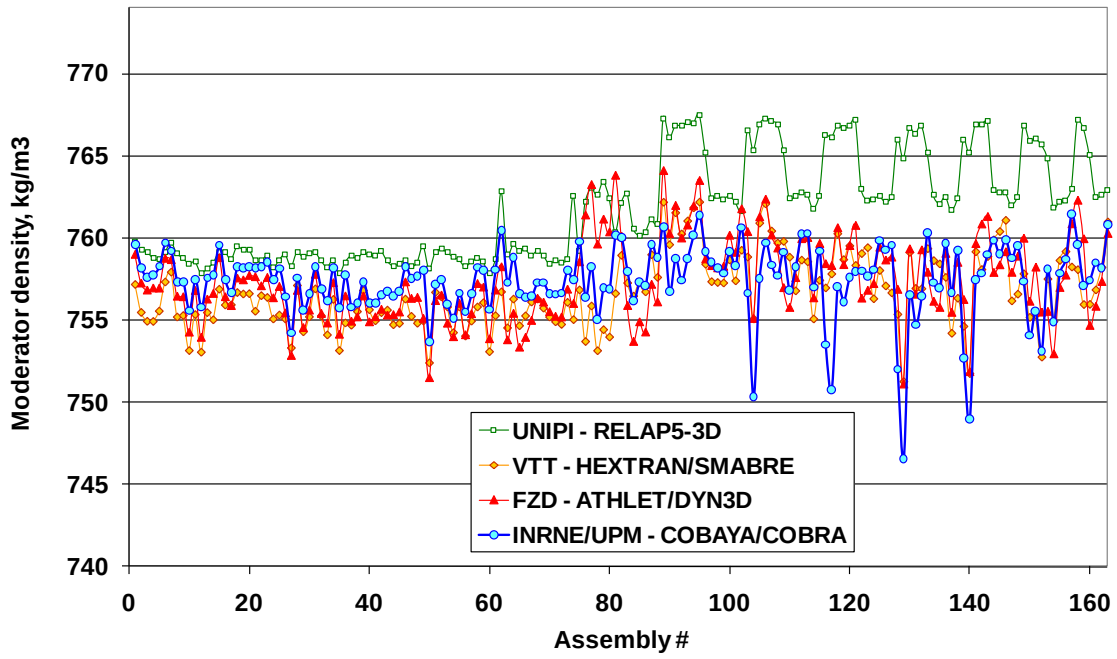


**Figure D.3: Scenario 2: Assembly-by-assembly core outlet coolant density at 200s**

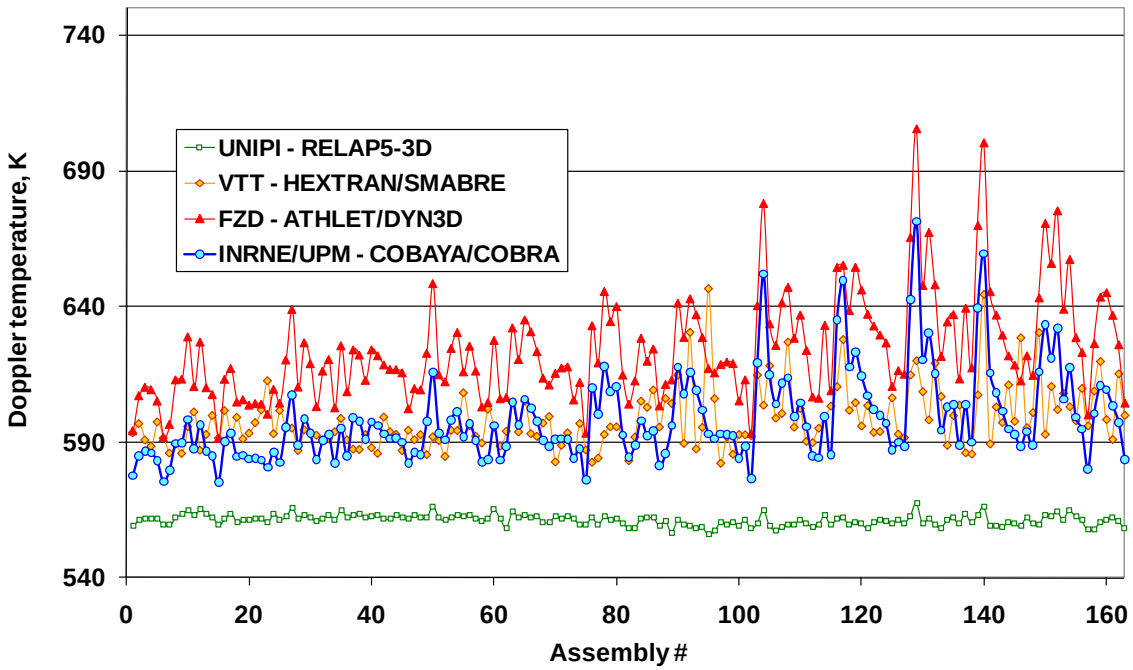


**Figure D.4: Scenario 2: Assembly-by-assembly Doppler temperatures at 200s**

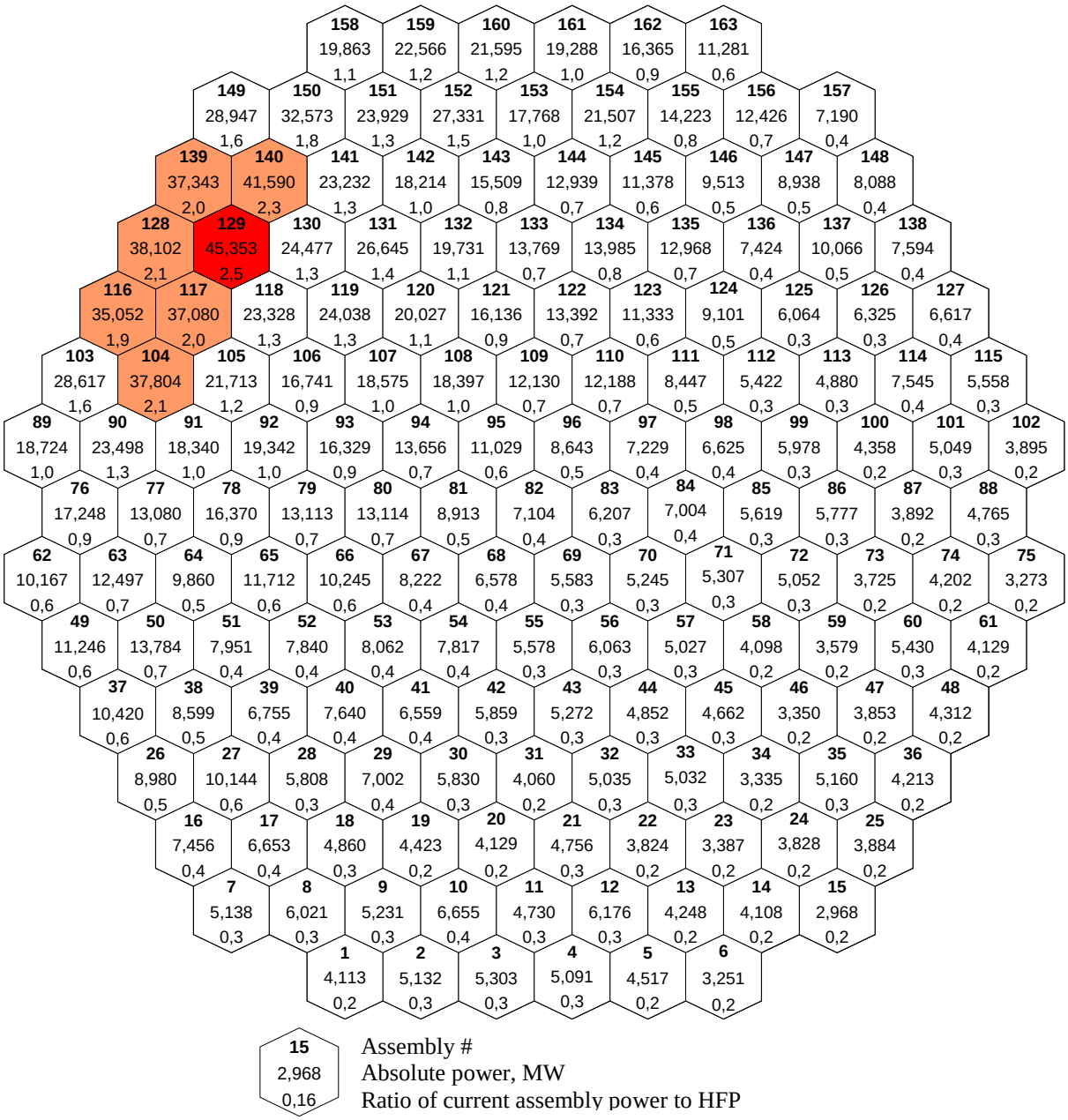


**Figure D.5: Scenario2, stuck rods in #117&#140. HEXTRAN/SMABRE computed radial power distribution (abs. powers) and ratio of current assembly power/HFP at 69 s**

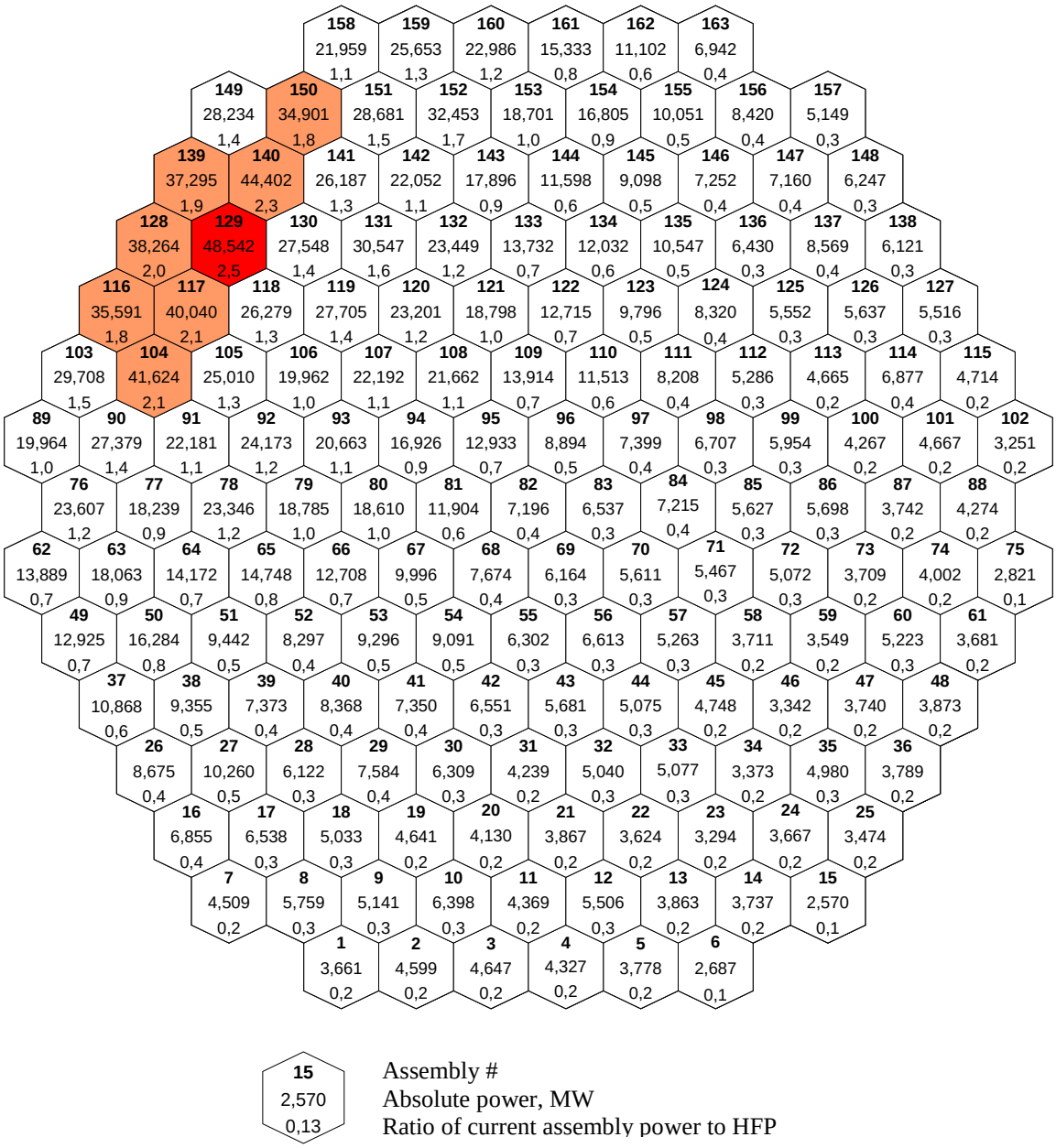


**Figure D.6: Scenario2, #117&#140. DYN3D/ATHLET computed radial power distribution (abs. powers) and ratio of current assembly power/HFP at 69 s**

# Appendix E: Exercise 3, Scenario 1 results

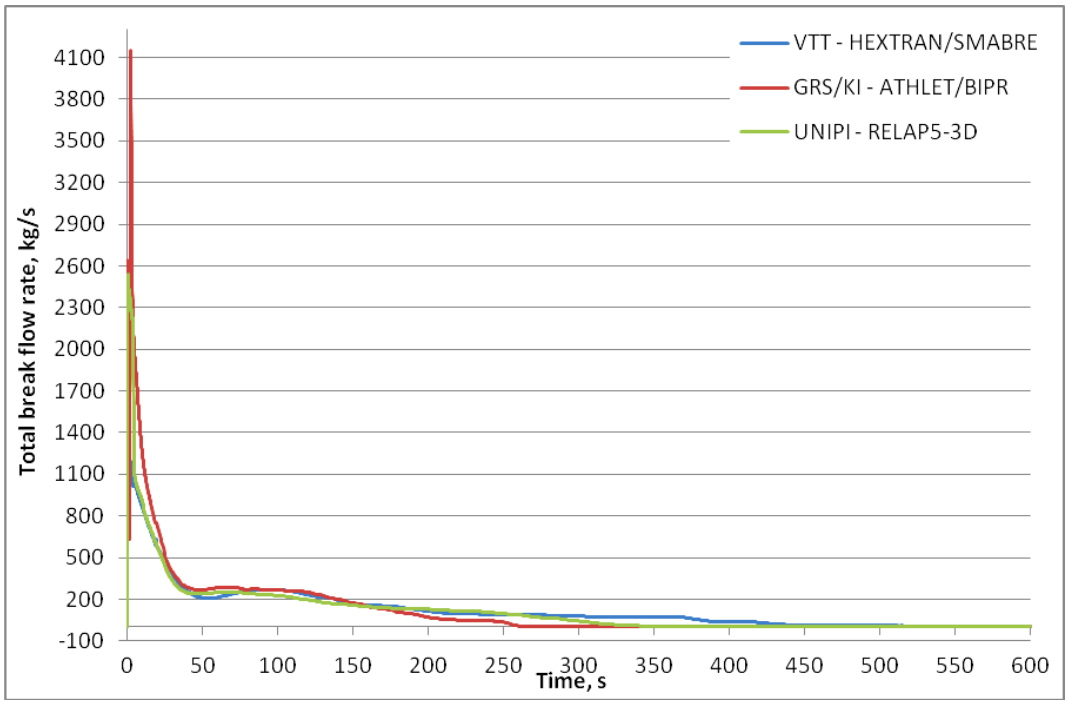


**Figure E.1: Total break flow rate**

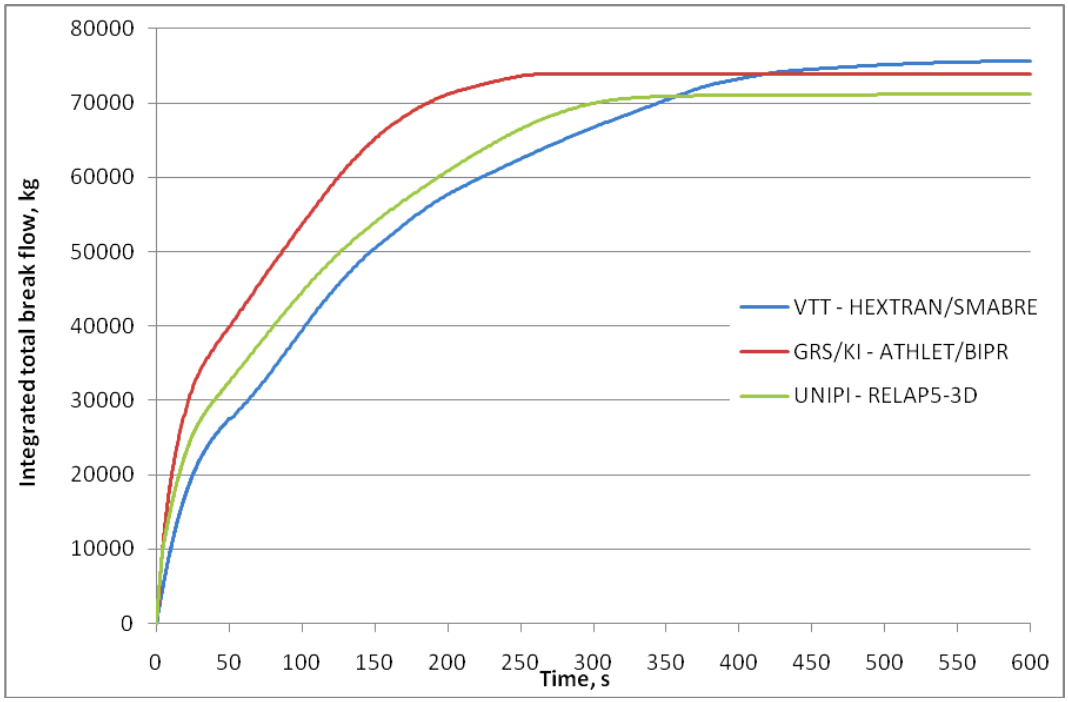


**Figure E.2: Integrated total break flow rate**

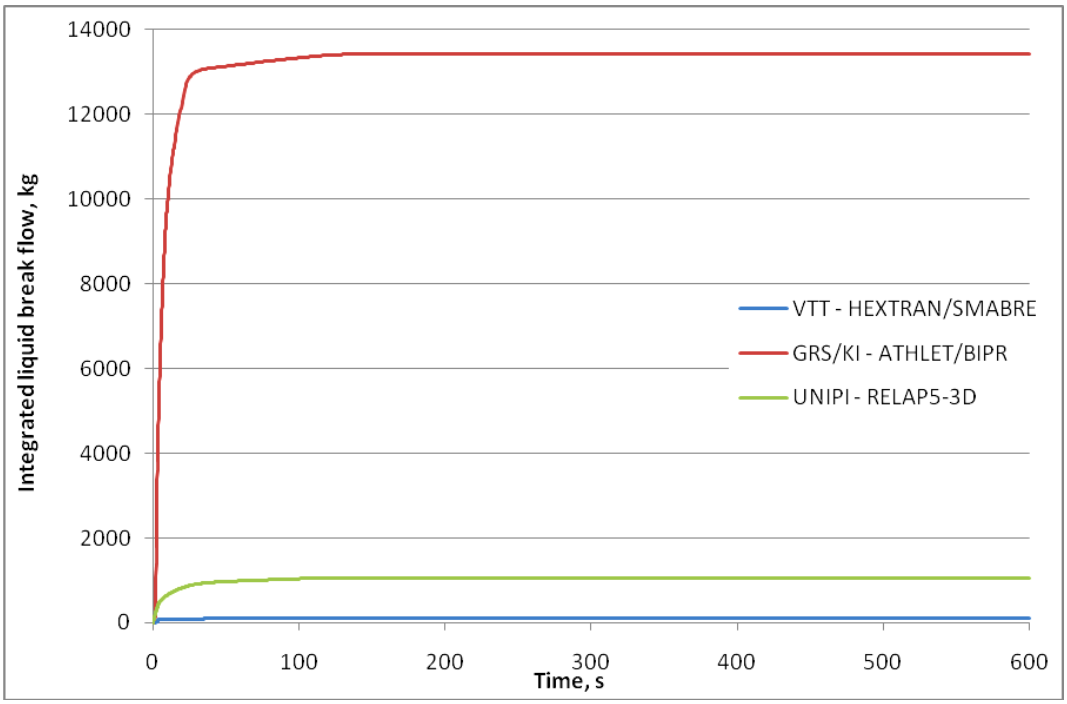


**Figure E.3: Integrated liquid break flow rate**

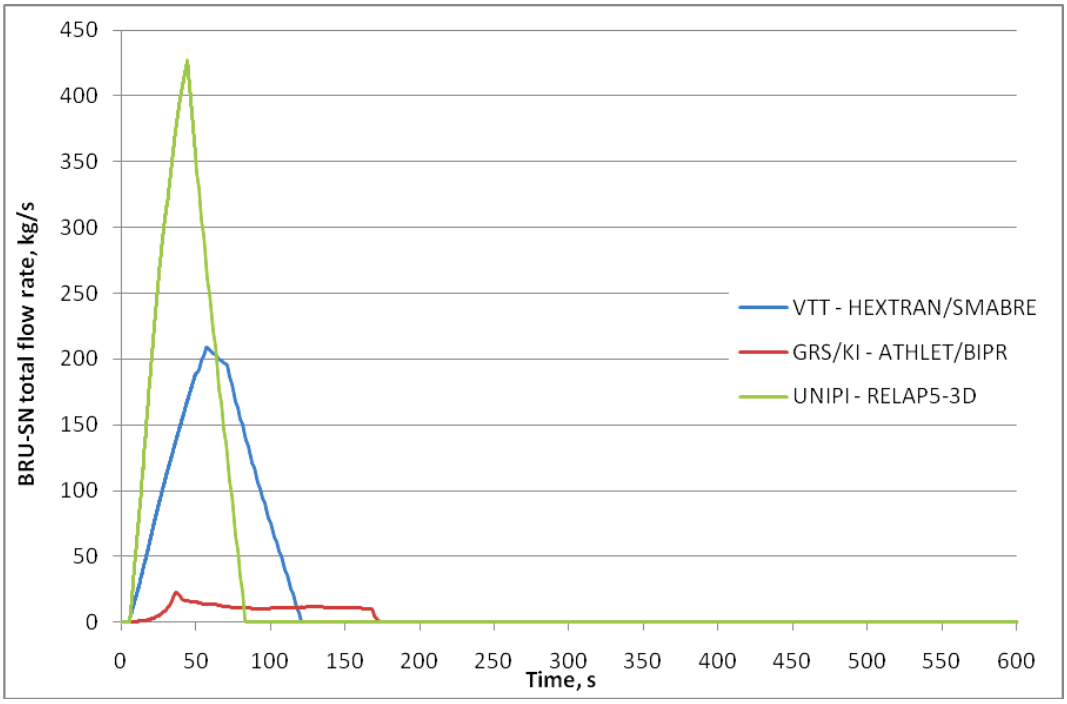


**Figure E.4: BRU-SN (steam dump to house needs) total flow rate**

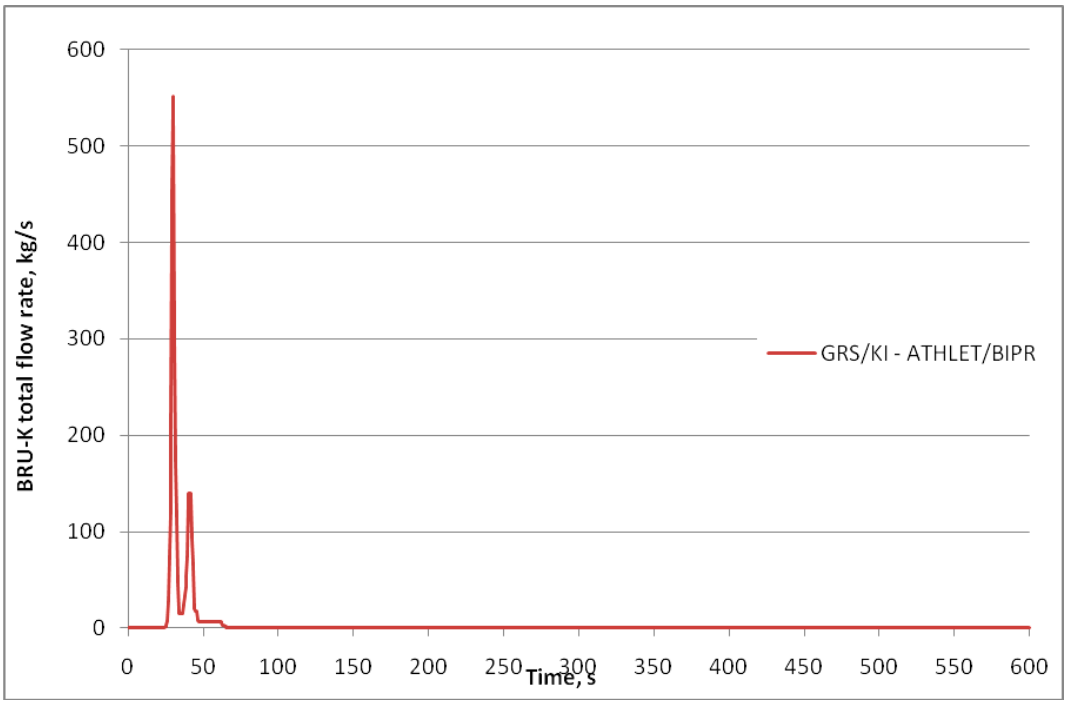


**Figure E.5: BRU-K (steam dump to condenser) total flow rate**

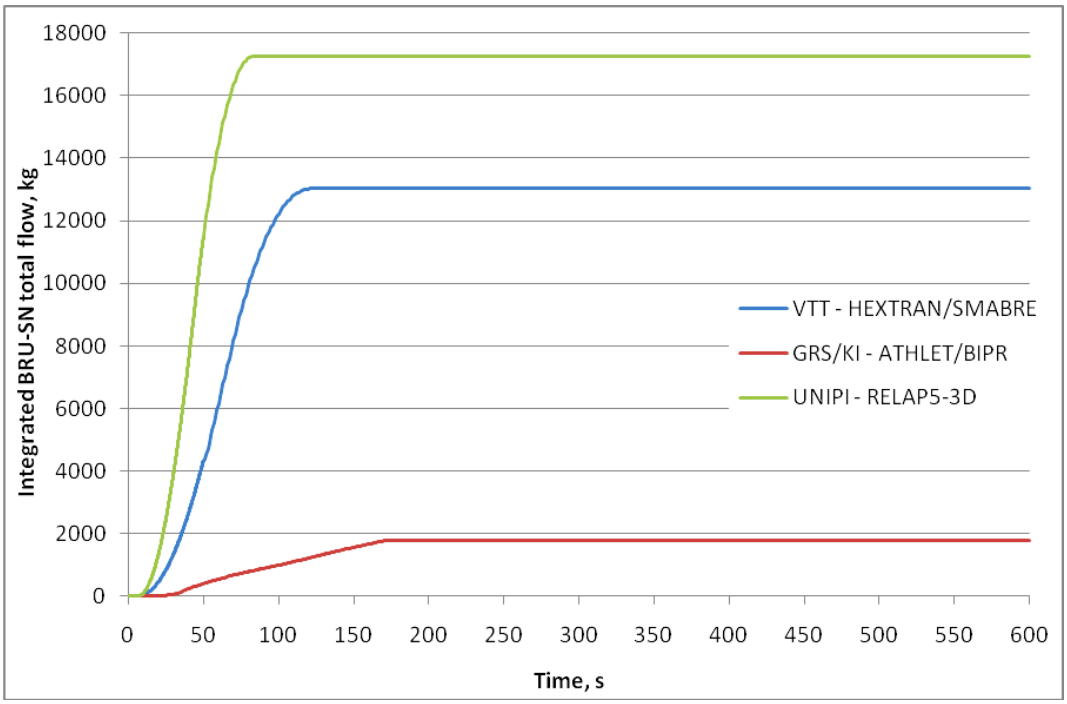


**Figure E.6: Integrated BRU-SN (steam dump to house needs) total flow rate**

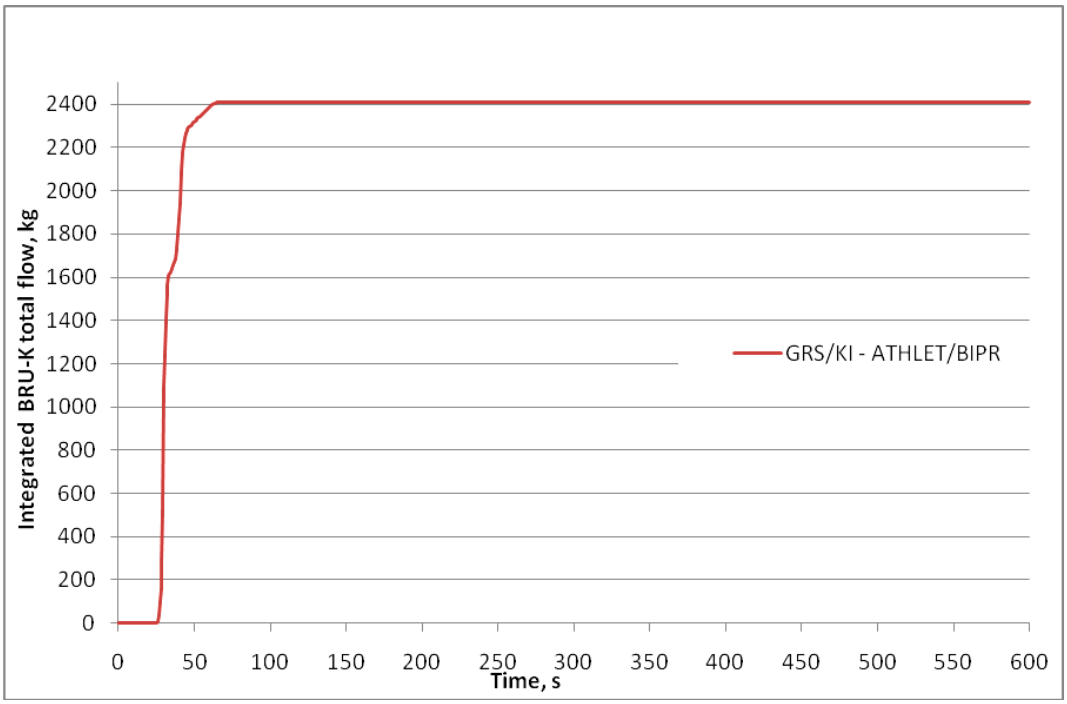


**Figure E.7: Integrated BRU-K (steam dump to condenser) total flow rate**

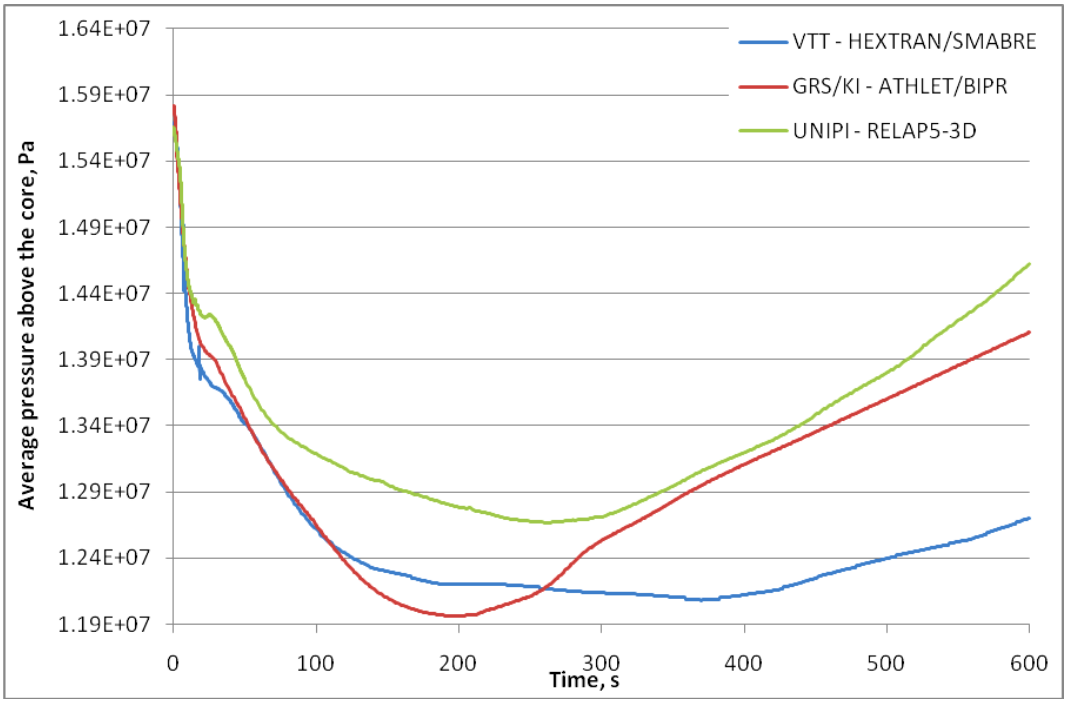


**Figure E.8: Average pressure above the core**

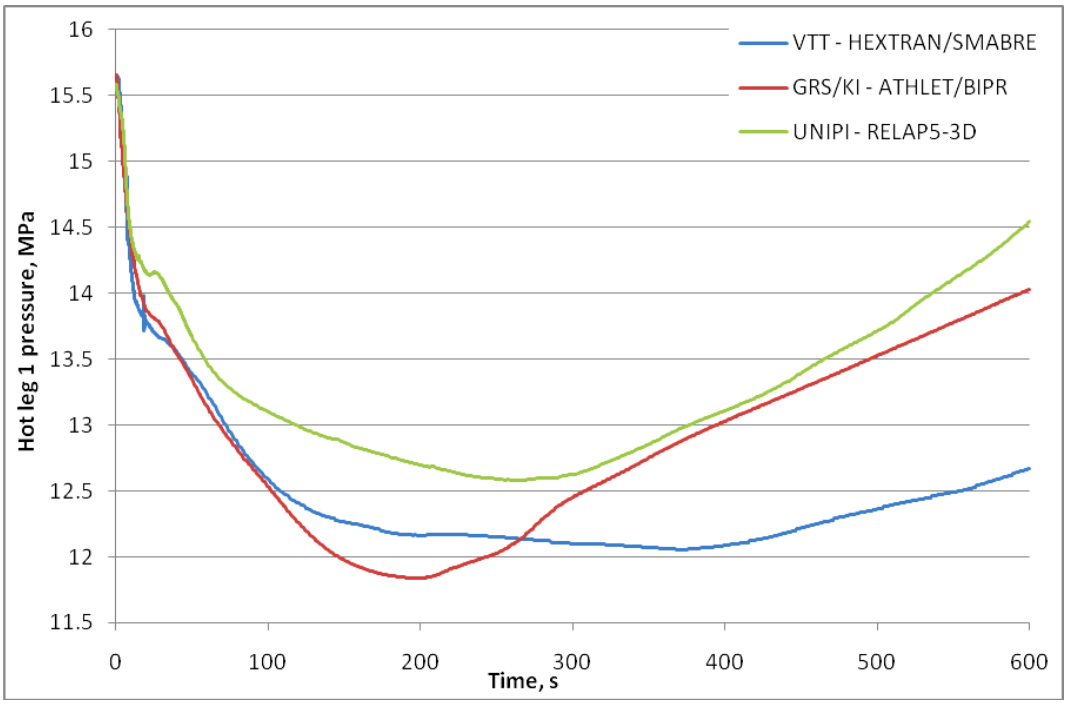


**Figure E.9: Hot leg 1 pressure**

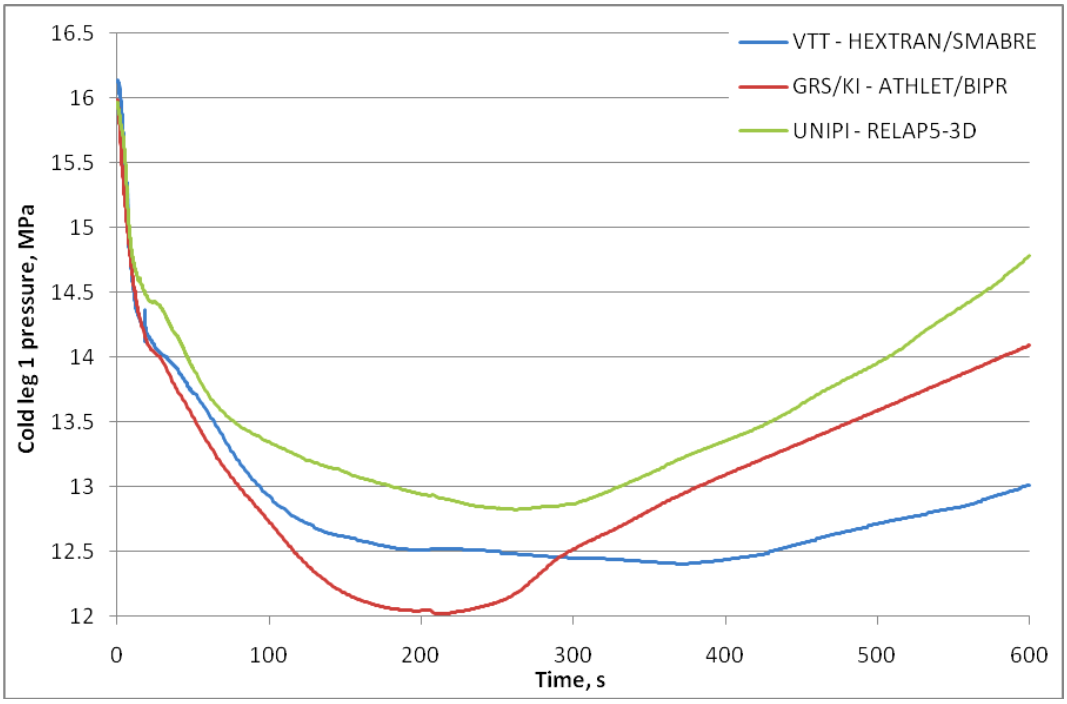


**Figure E.10: Cold leg 1 pressure**

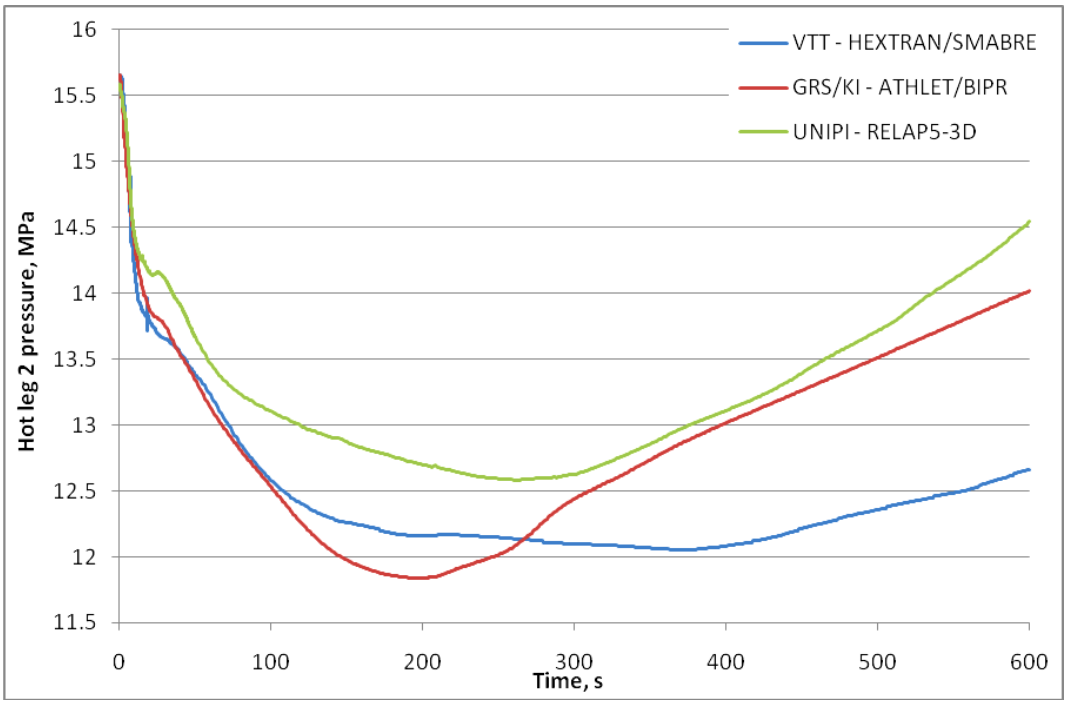


**Figure E.11: Hot leg 2 pressure**

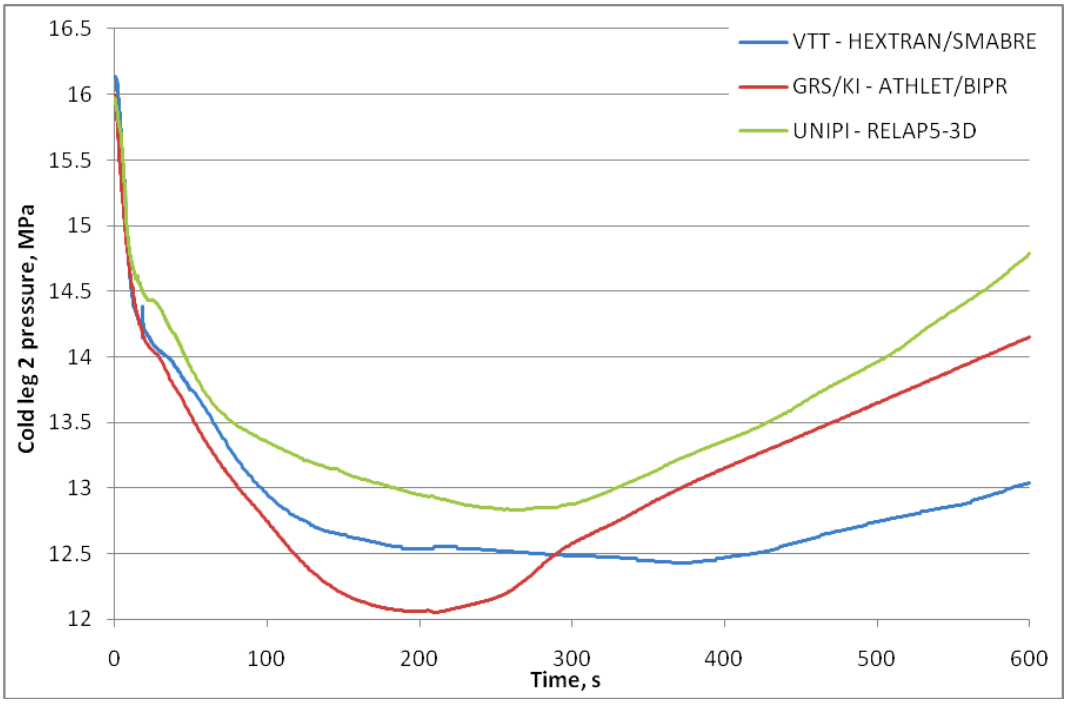


**Figure E.12: Cold leg 2 pressure**

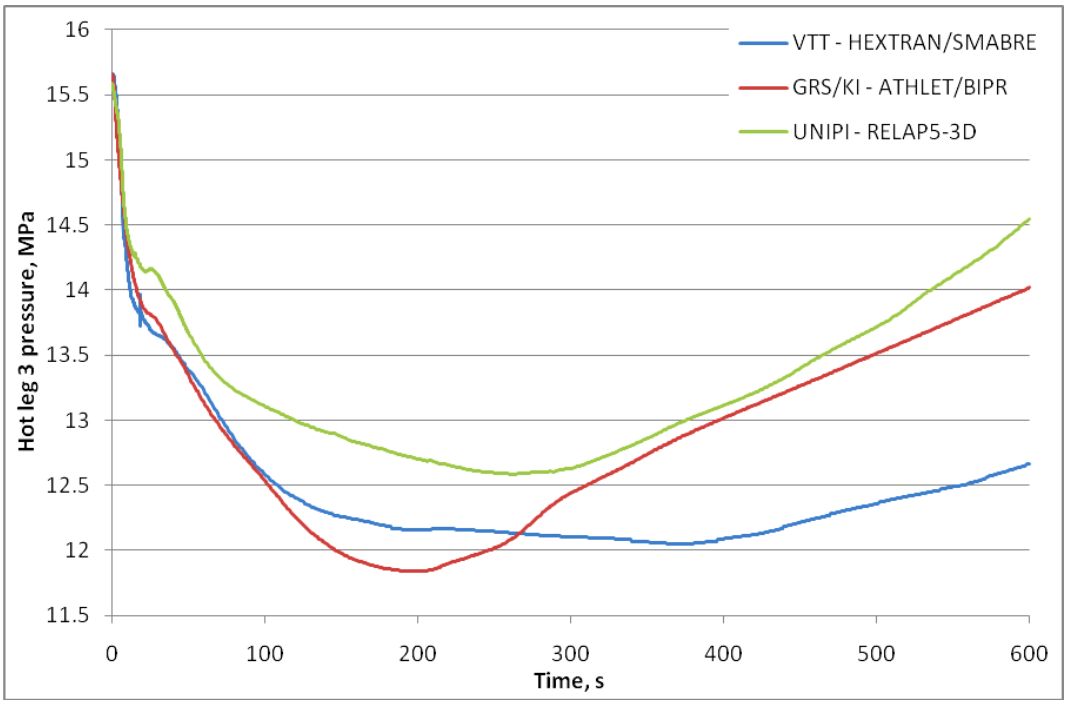


**Figure E.13: Hot leg 3 pressure**

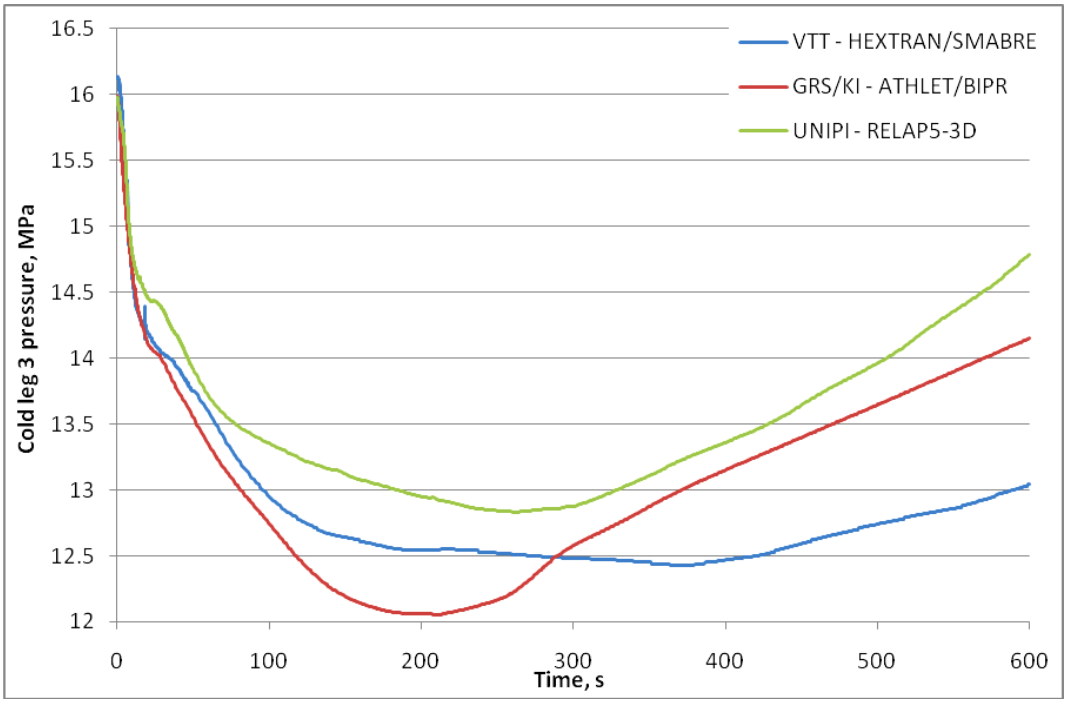


**Figure E.14: Cold leg 3 pressure**

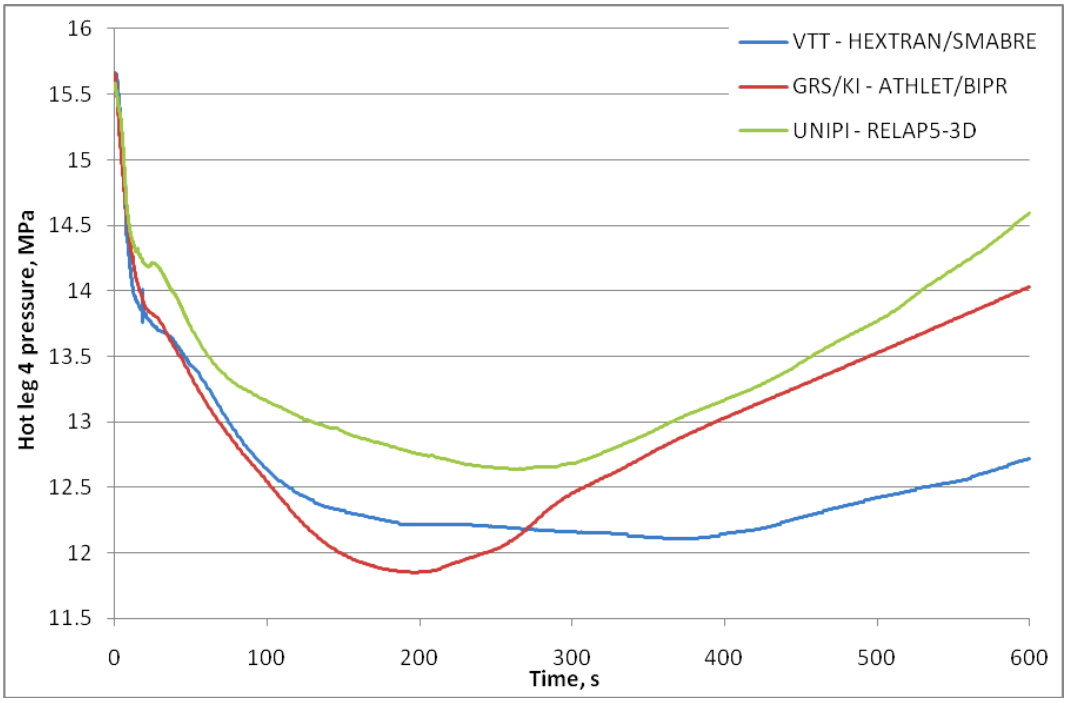


**Figure E.15: Hot leg 4 pressure**

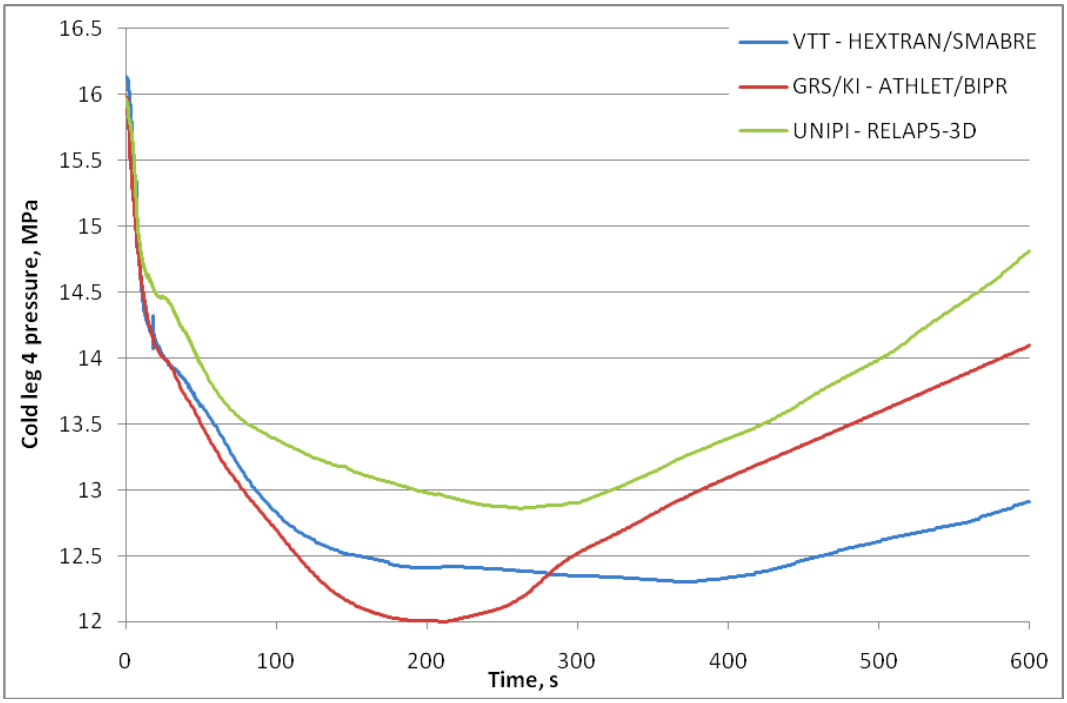


**Figure E.16: Cold leg 4 pressure**

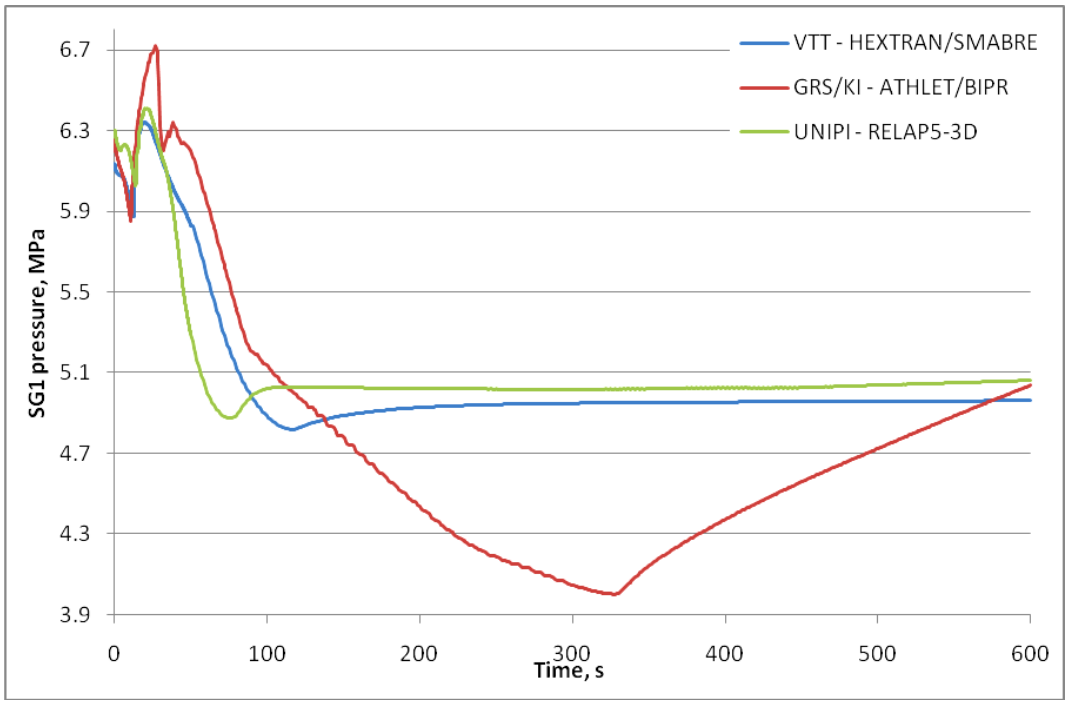


**Figure E.17: SG 1 pressure**

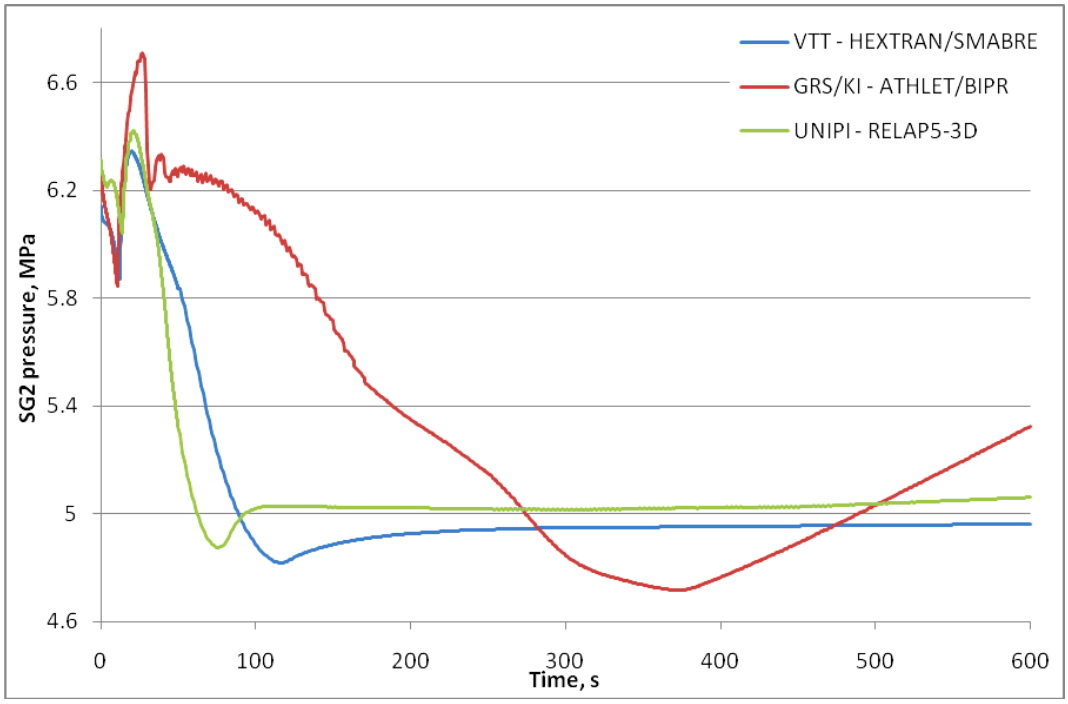


**Figure E.18: SG 2 pressure**

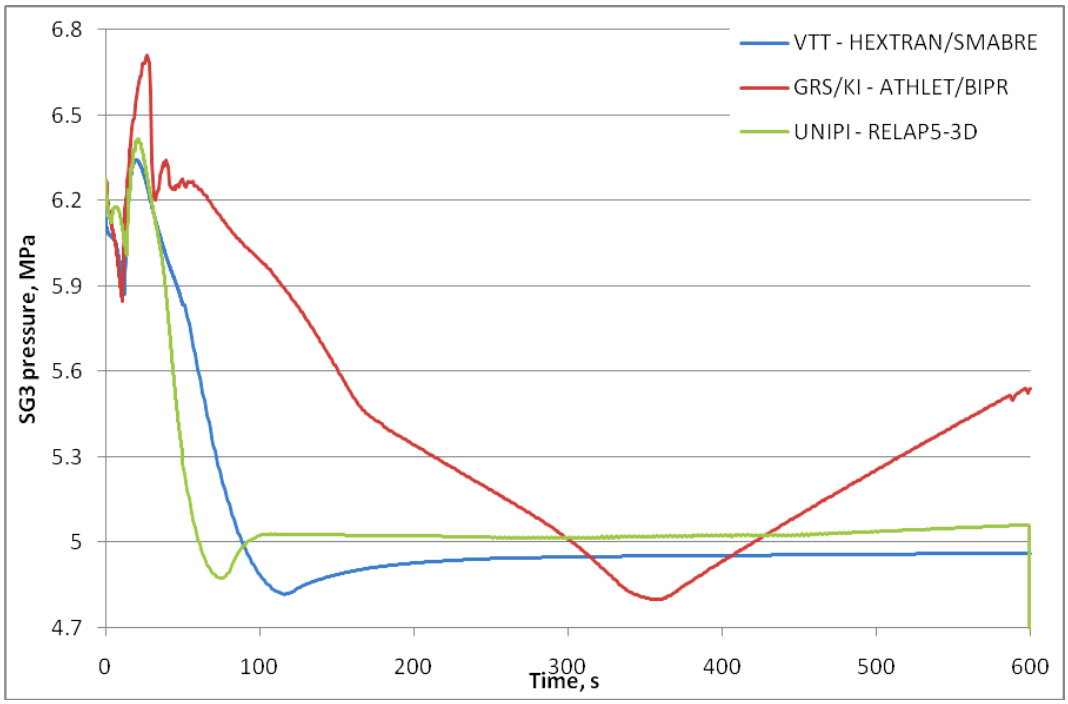


**Figure E.19: SG3 pressure**

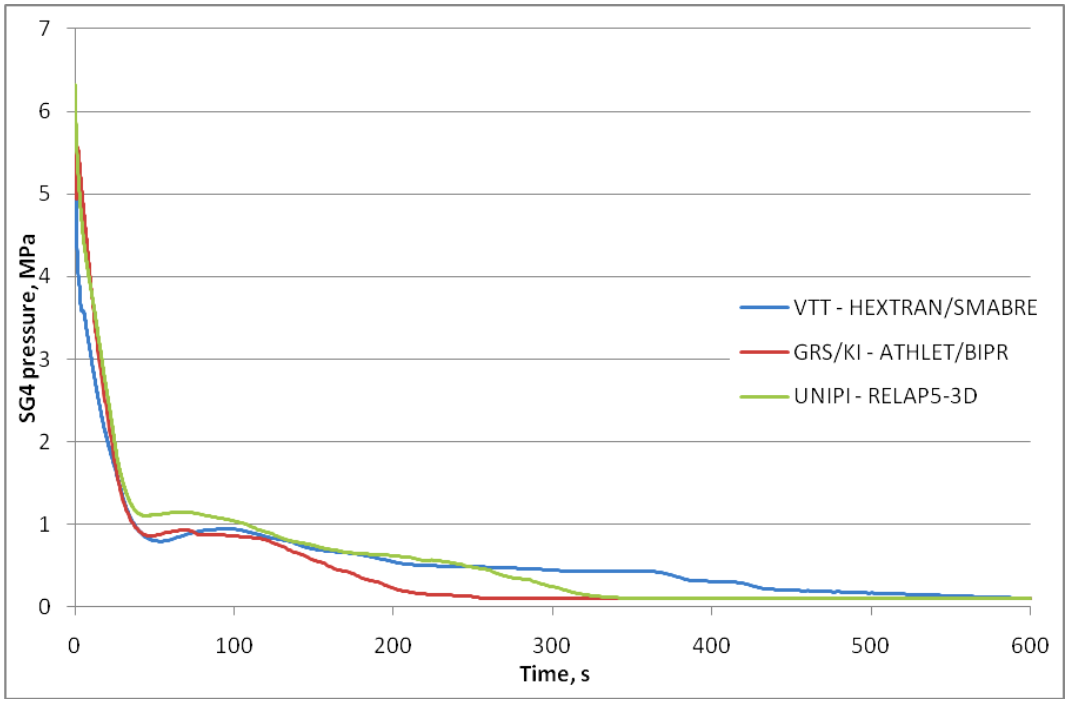


**Figure E.20: SG4 pressure, MPa**

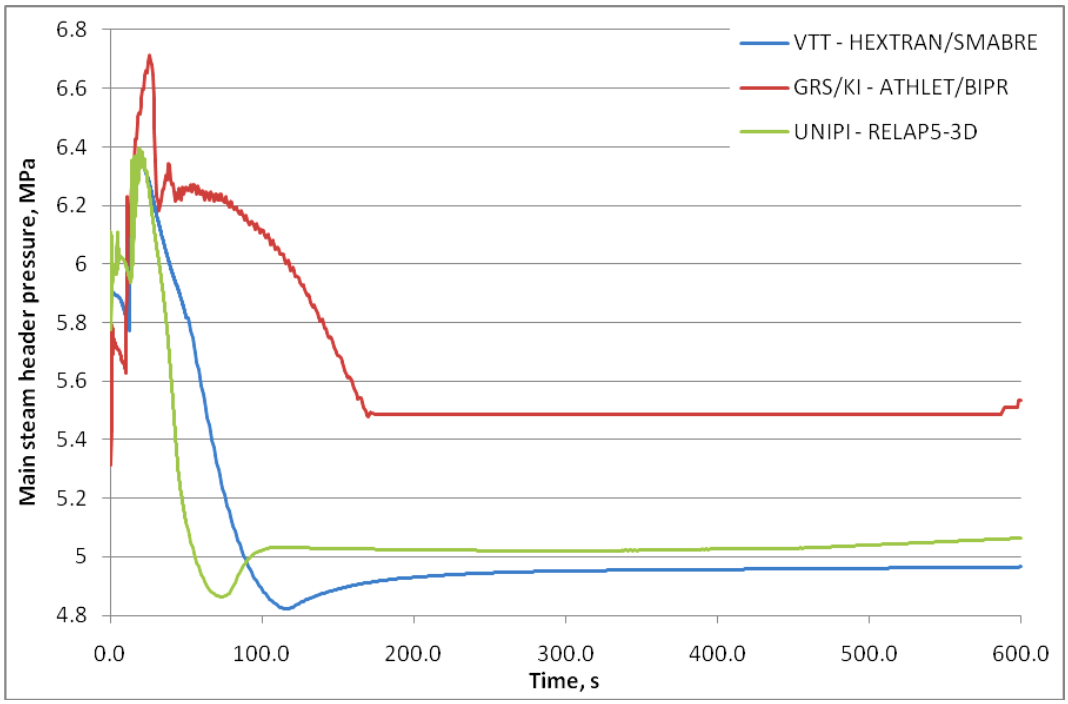


**Figure E.21: Main steam header pressure**

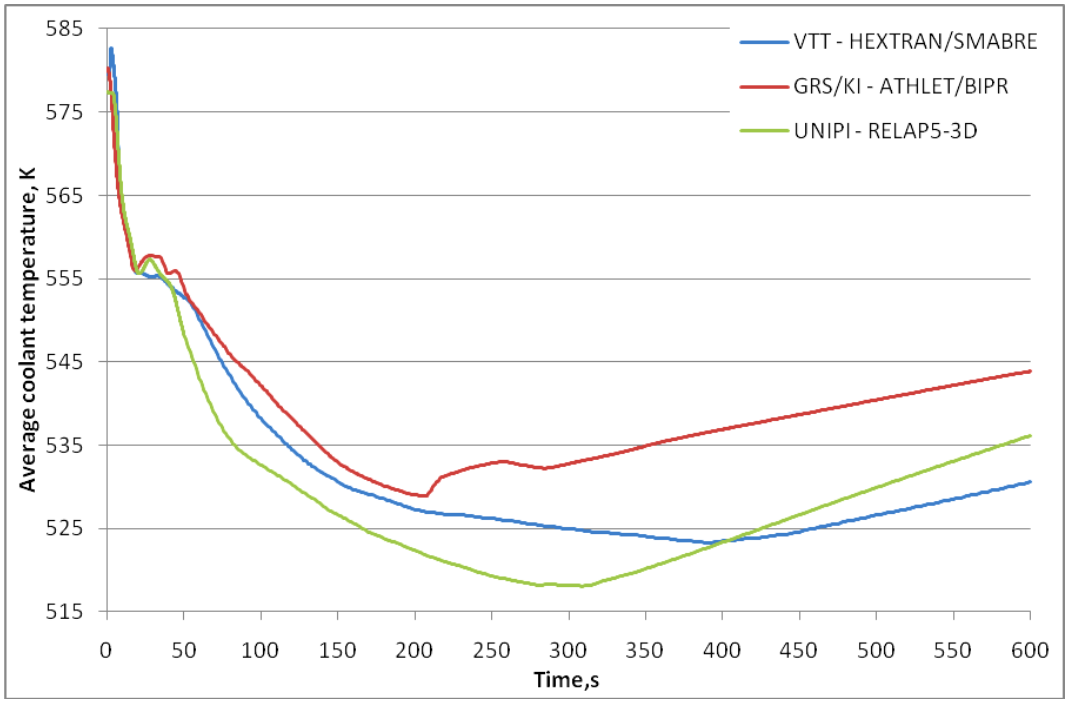


**Figure E.22: Average core coolant temperature**

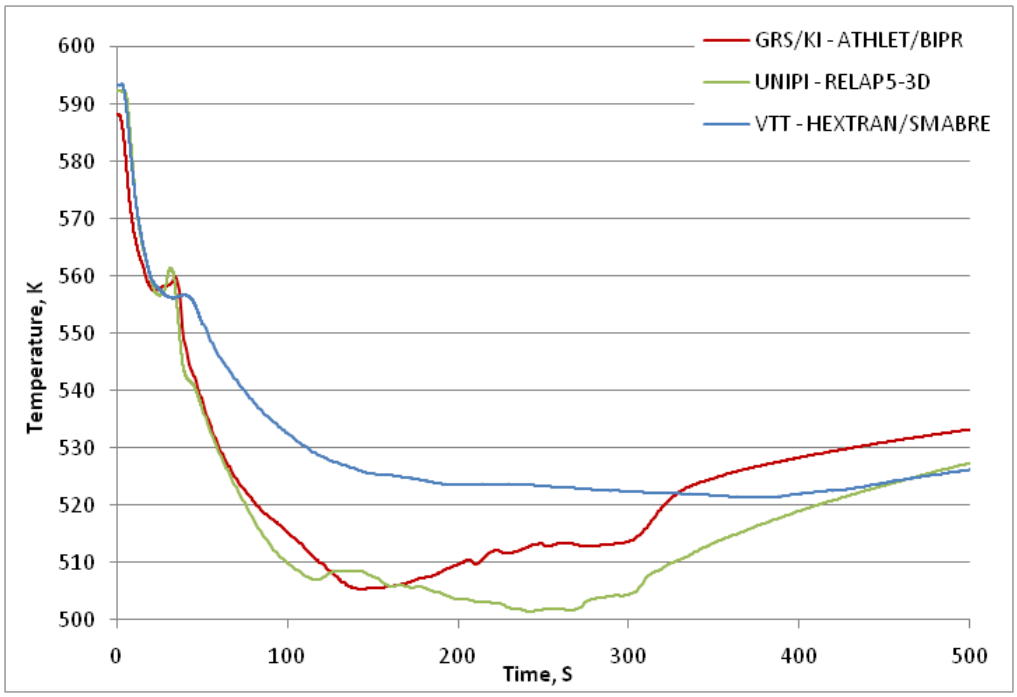


**Figure E.23: Hot leg 1 temperature**

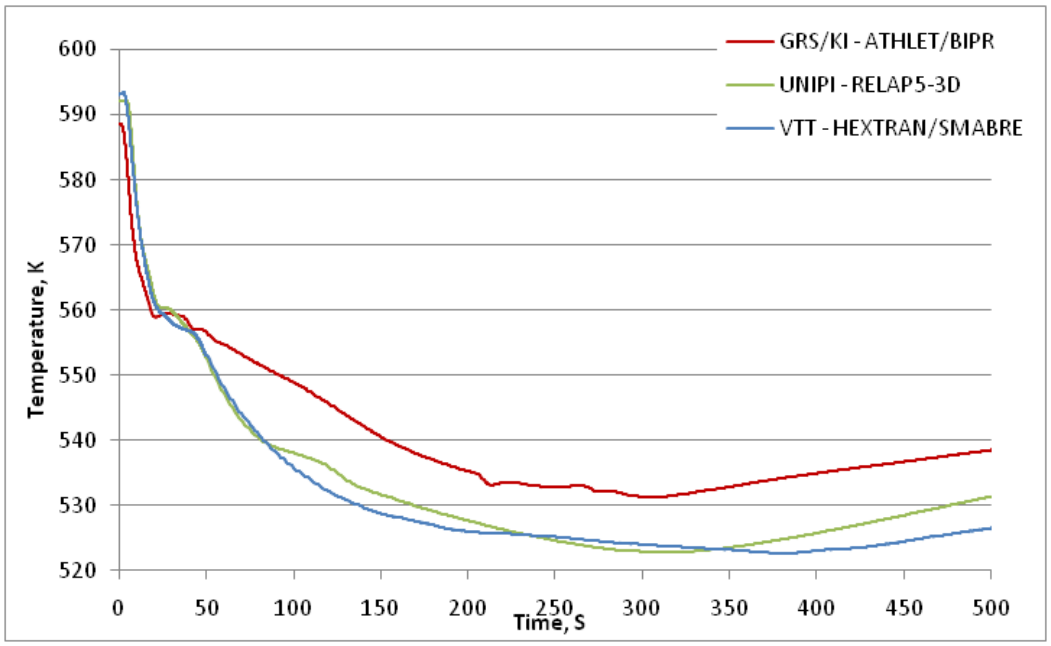


**Figure E.24: Hot leg 2 temperature**

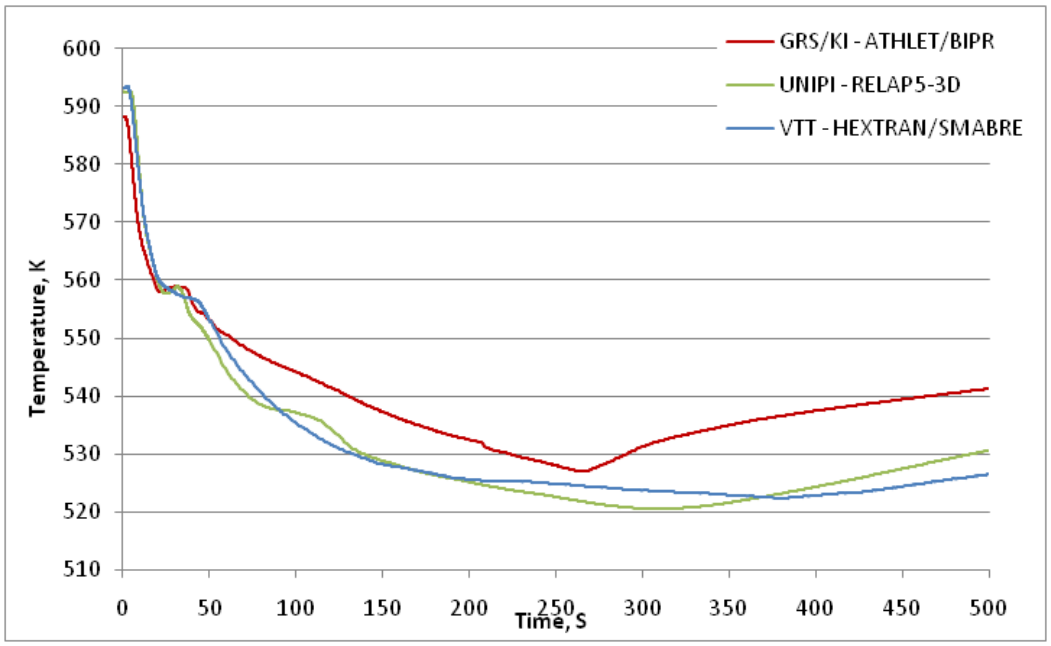


**Figure E.25: Hot leg 3 temperature**

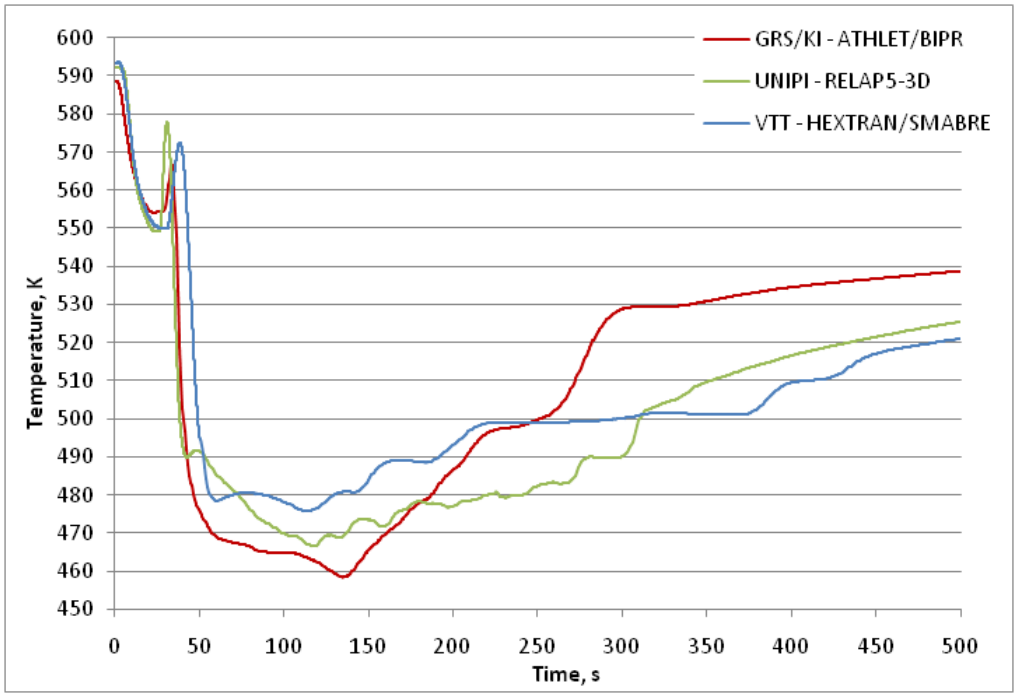


**Figure E.26: Hot leg 4 temperature**

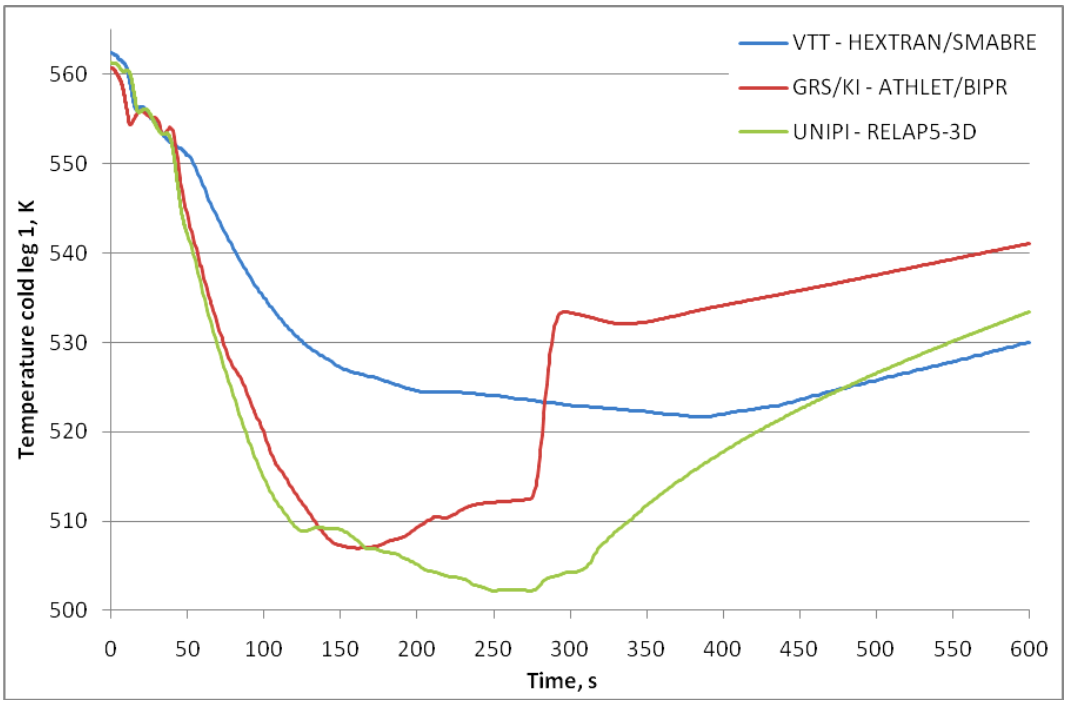


**Figure E.27: Cold leg 1 temperature**

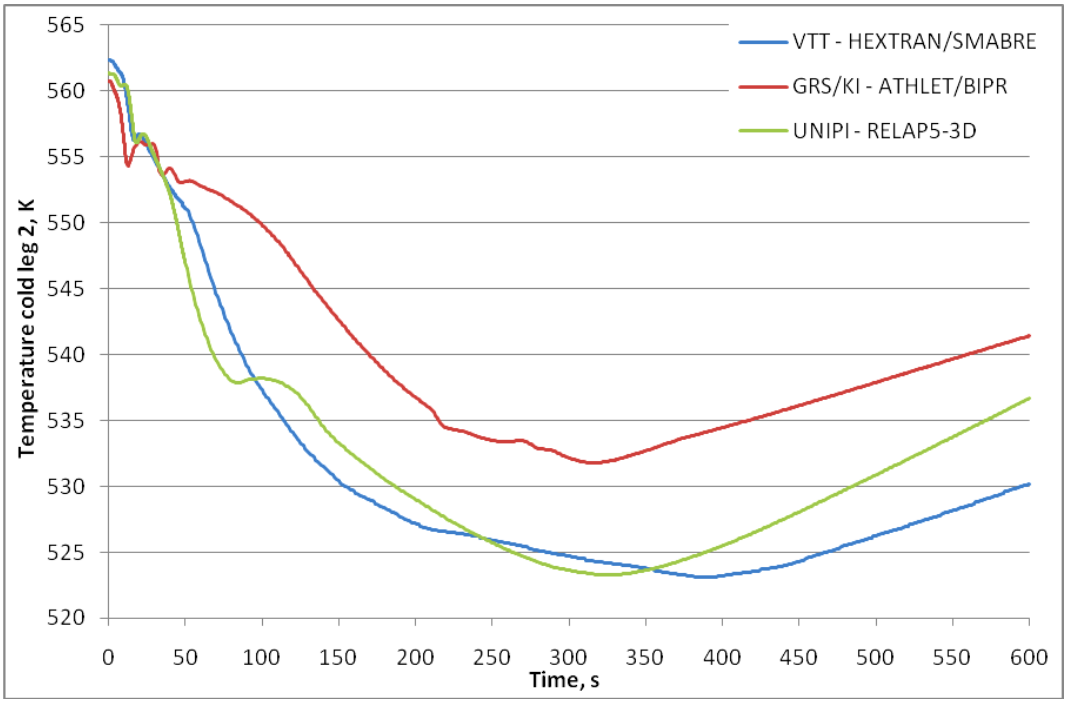


**Figure E.28: Cold leg 2 temperature**

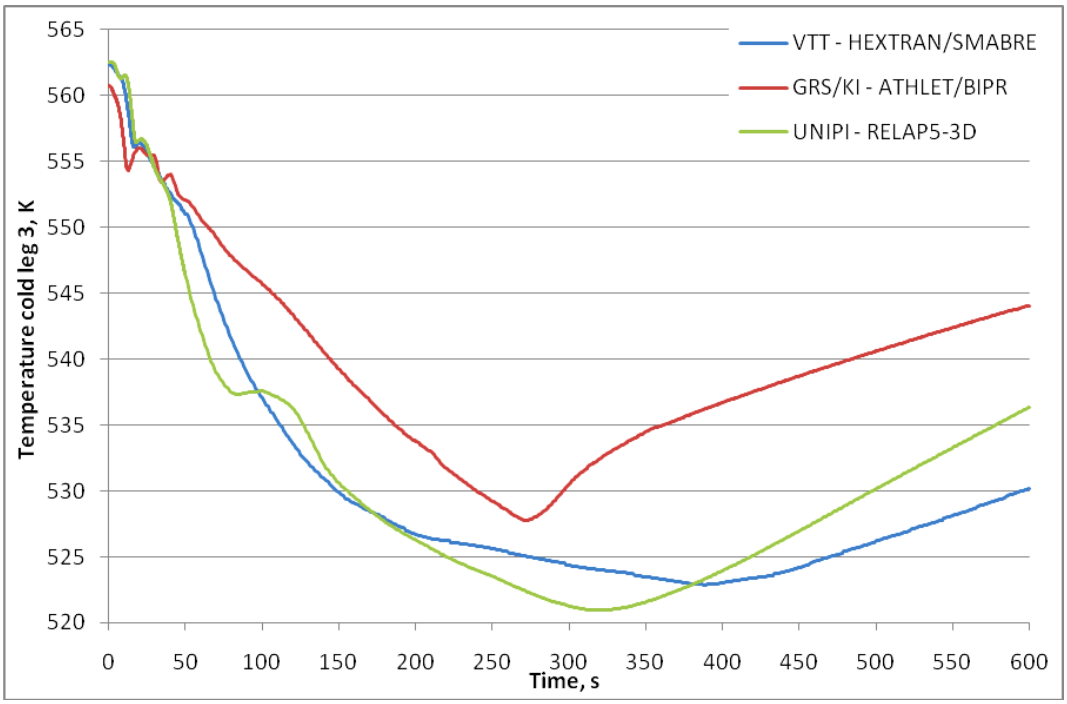


**Figure E.29: Cold leg 3 temperature**

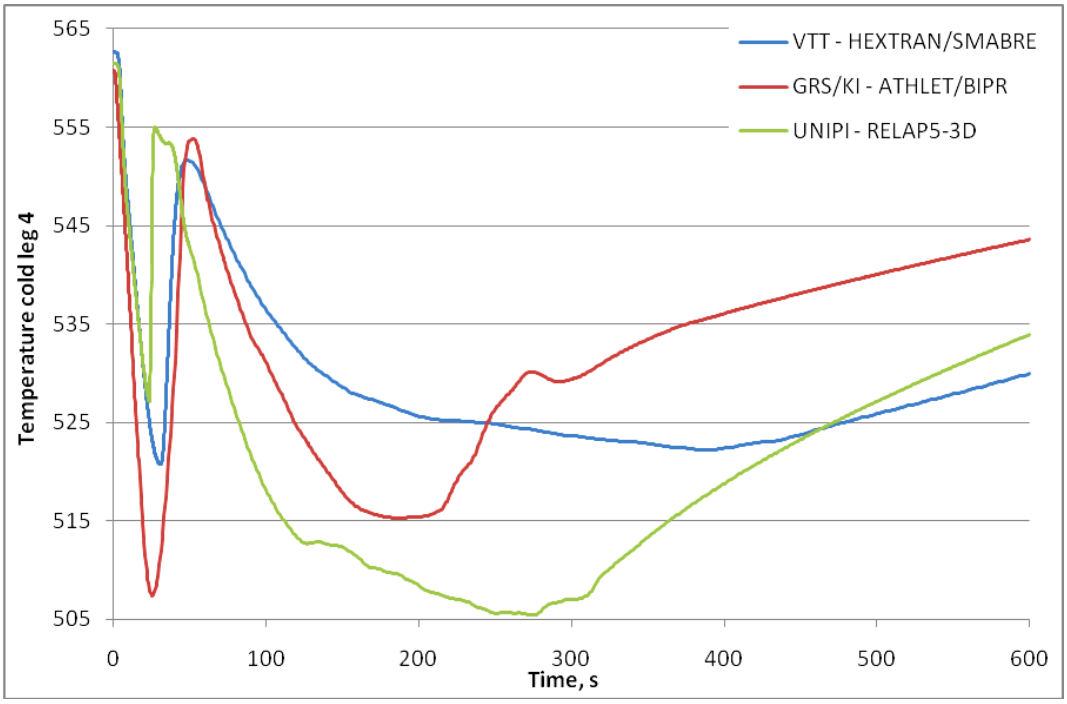


**Figure E.30: Cold leg 4 temperature**

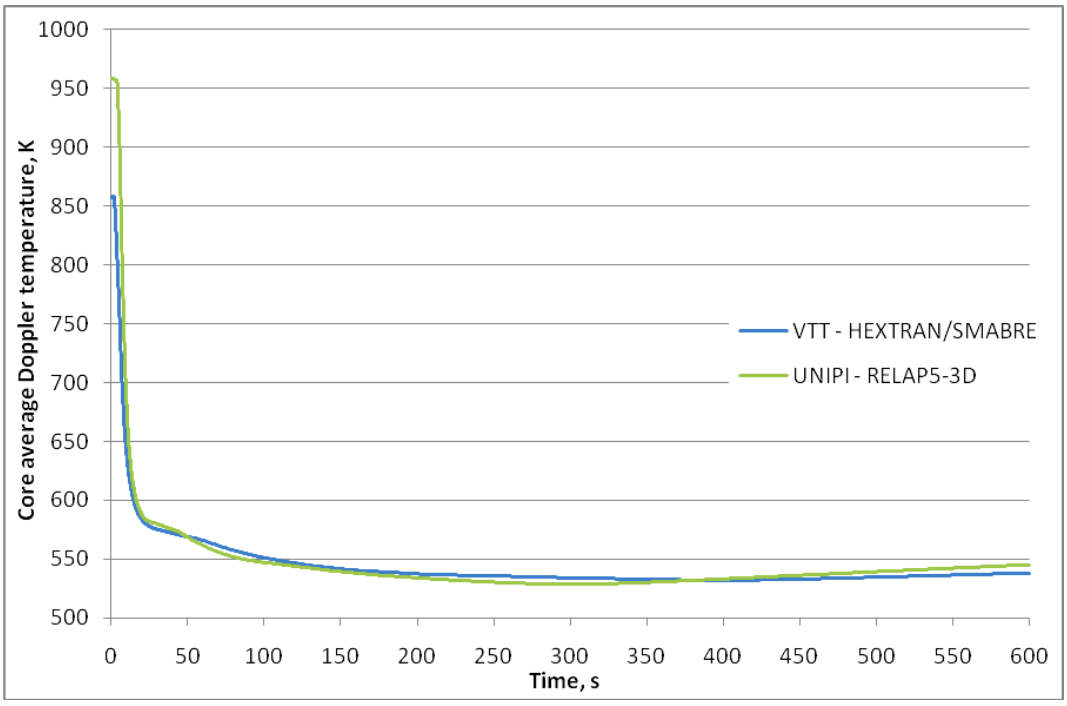


**Figure E.31: Core average fuel Doppler temperature**

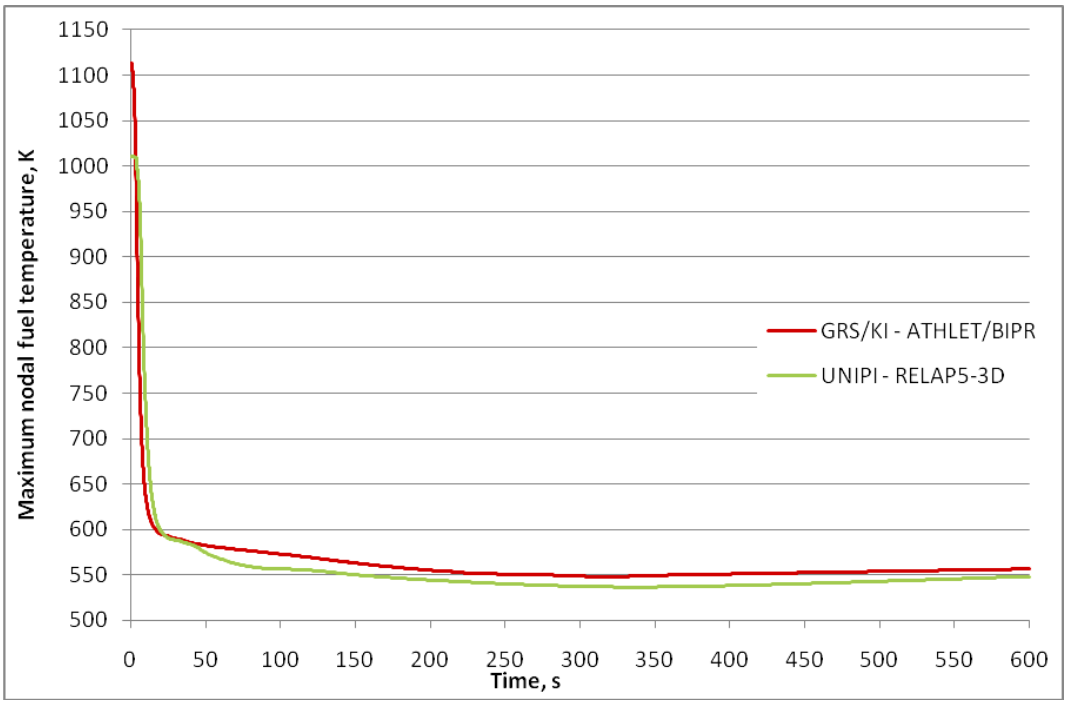


**Figure E.32: Maximum nodal fuel temperature**

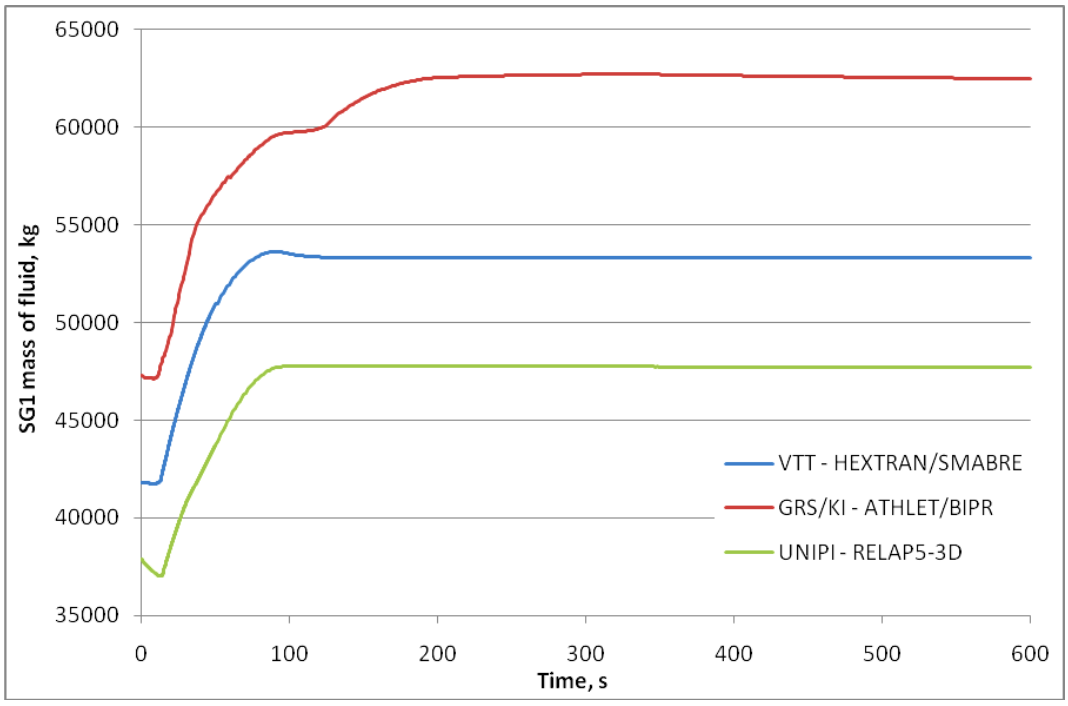


**Figure E.33: SG1 mass of fluid**

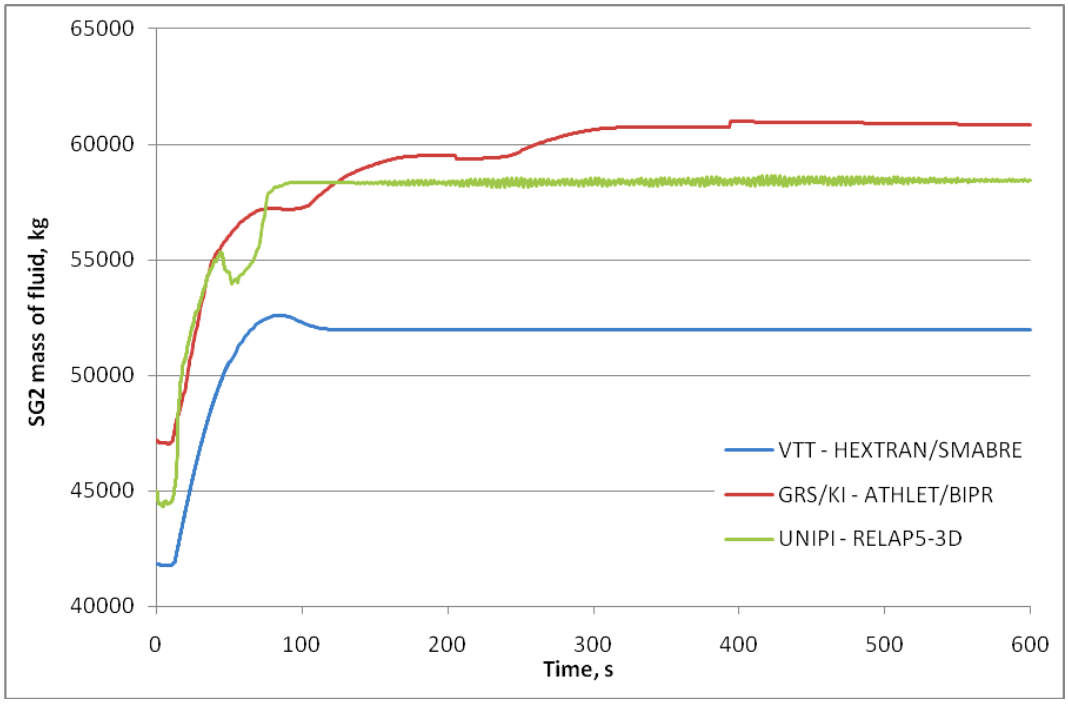


**Figure E.34: SG2 mass of fluid**

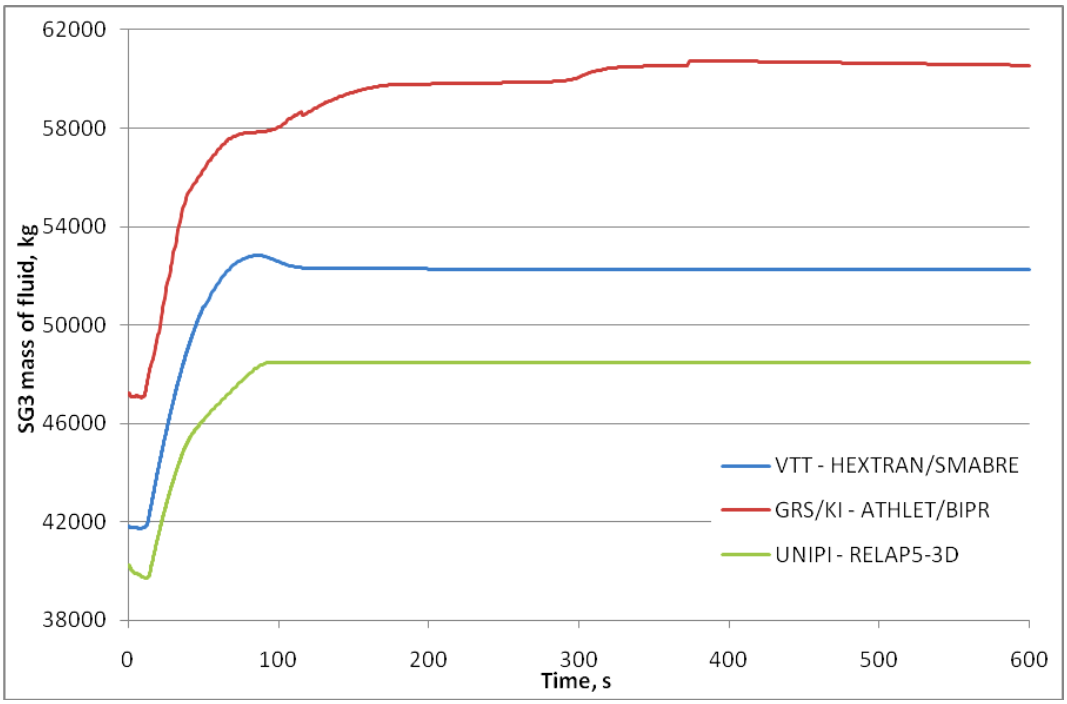


**Figure E.35: SG3 mass of fluid**

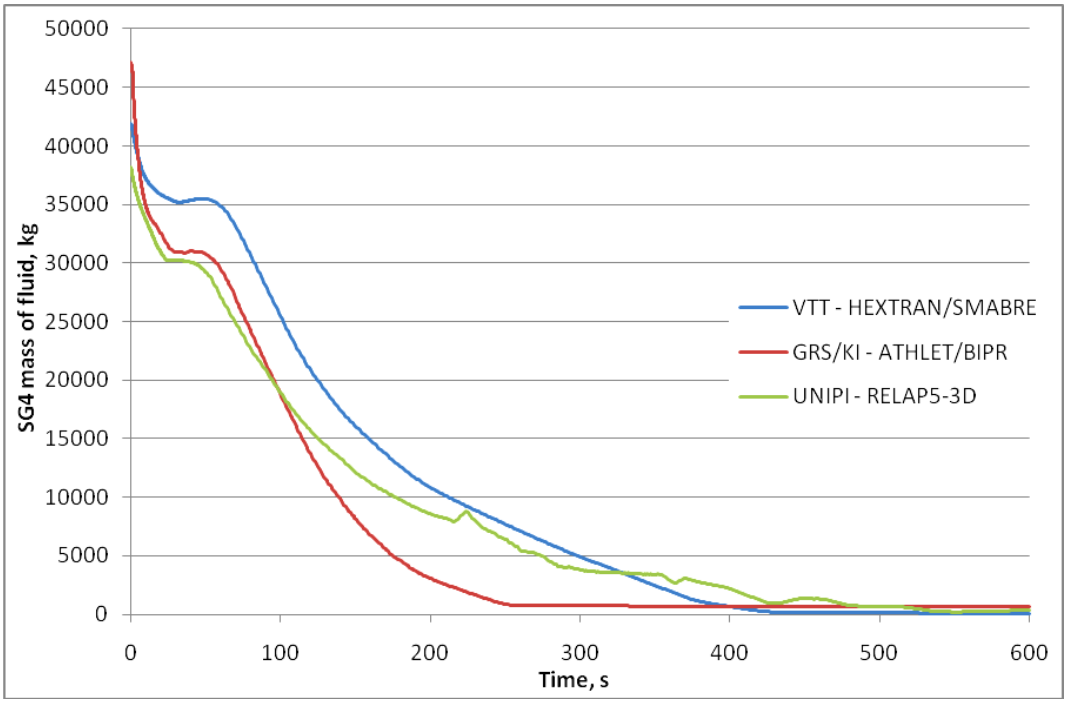


**Figure E.36: SG4 mass of fluid**

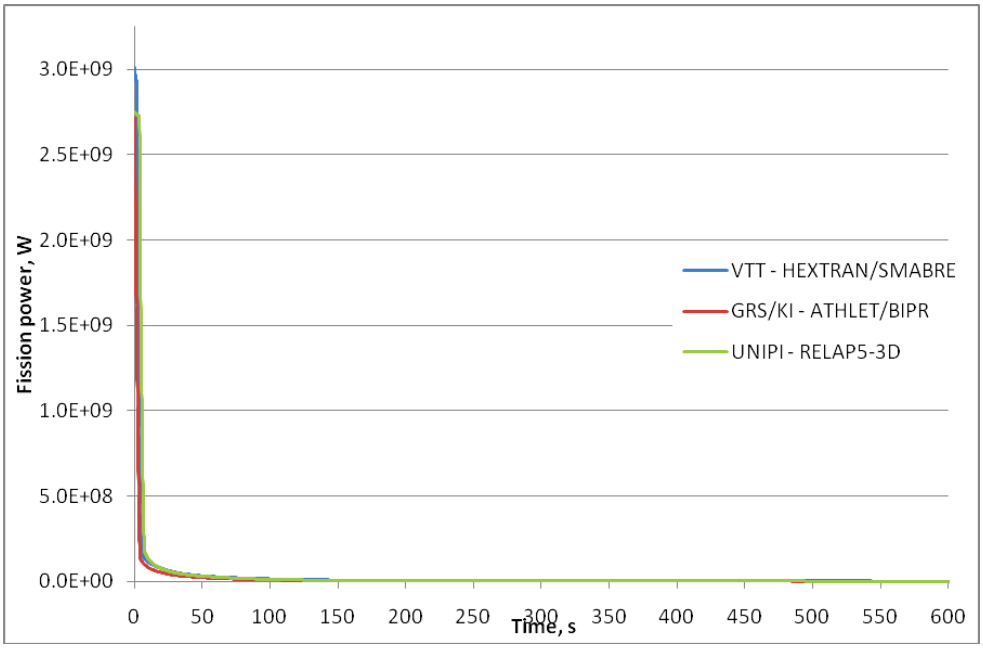


**Figure E.37: Fission power**

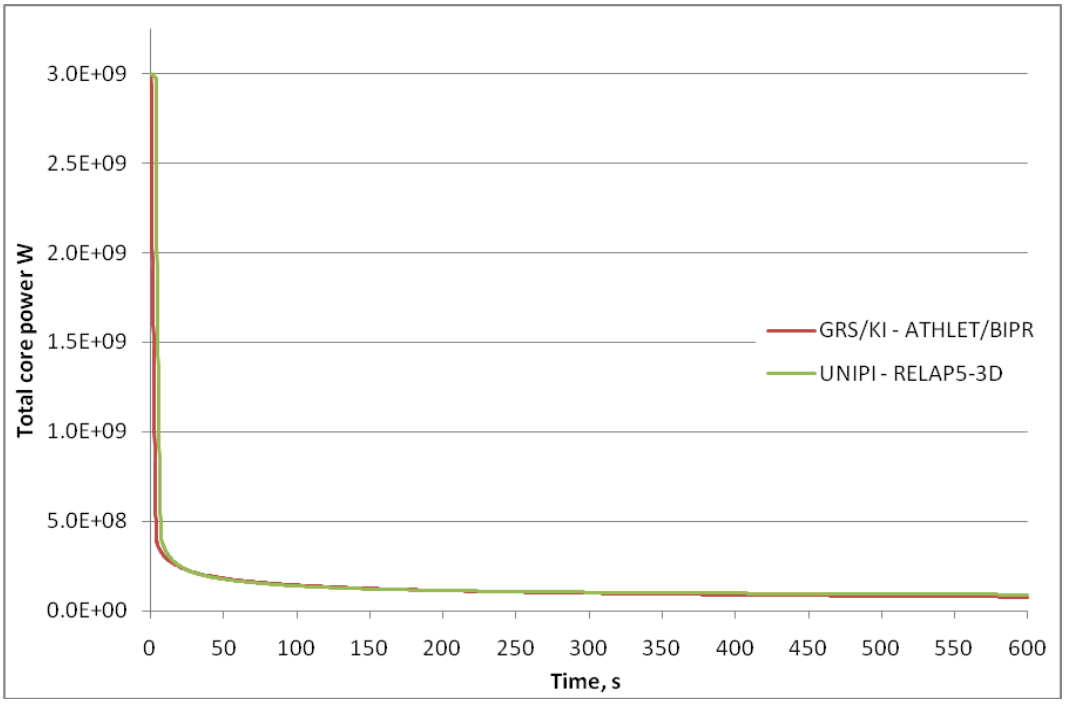


**Figure E.38: Total core power**

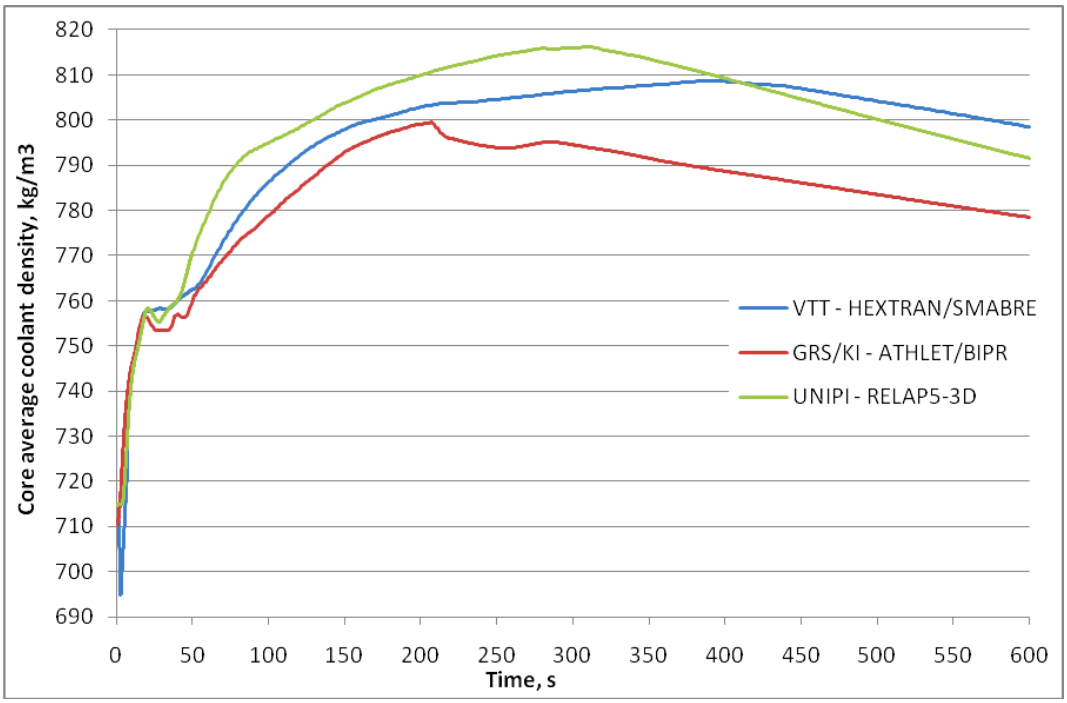


**Figure E.39: Core average coolant density**

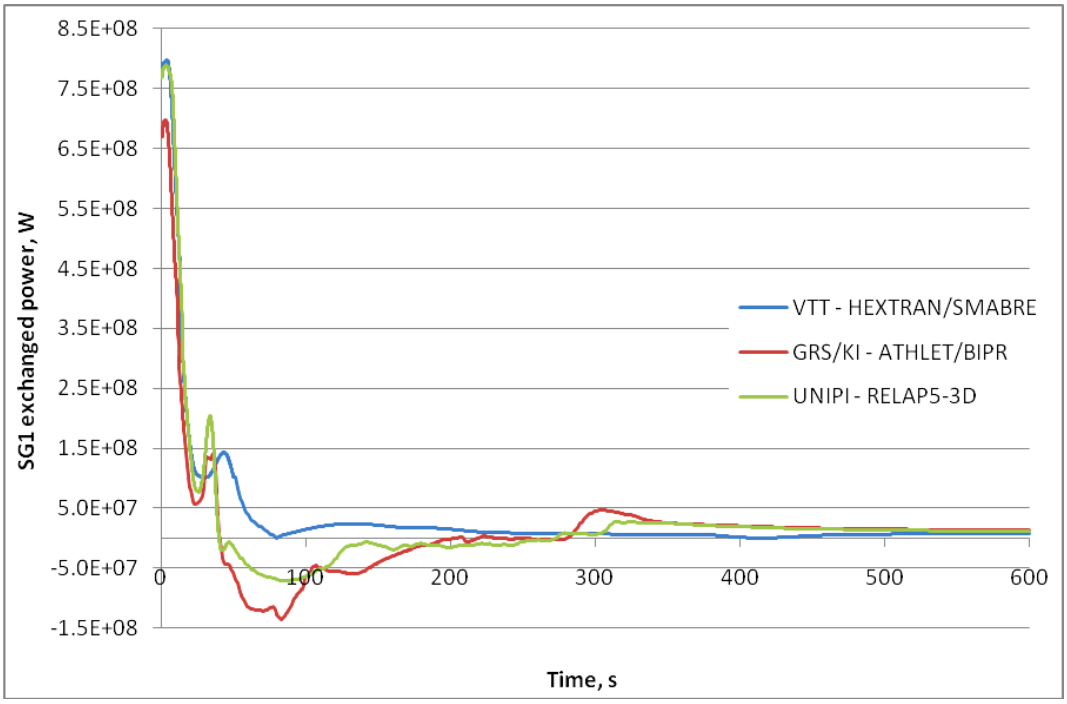


**Figure E.40: SG1 exchanged power**

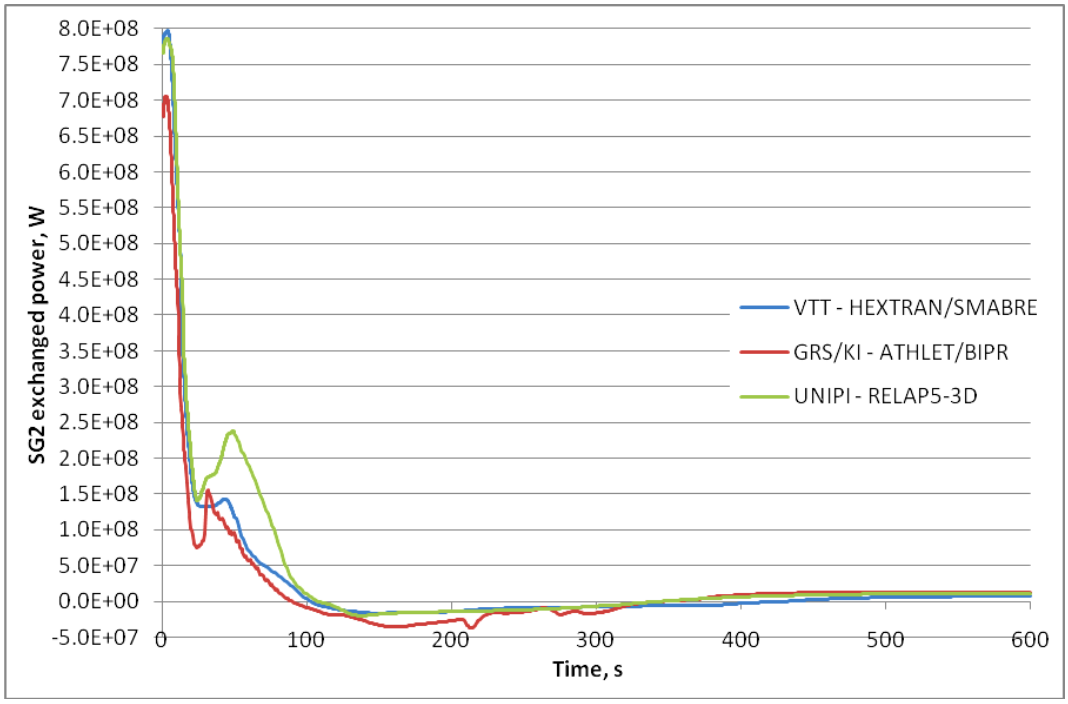


**Figure E.41: SG2 exchanged power**

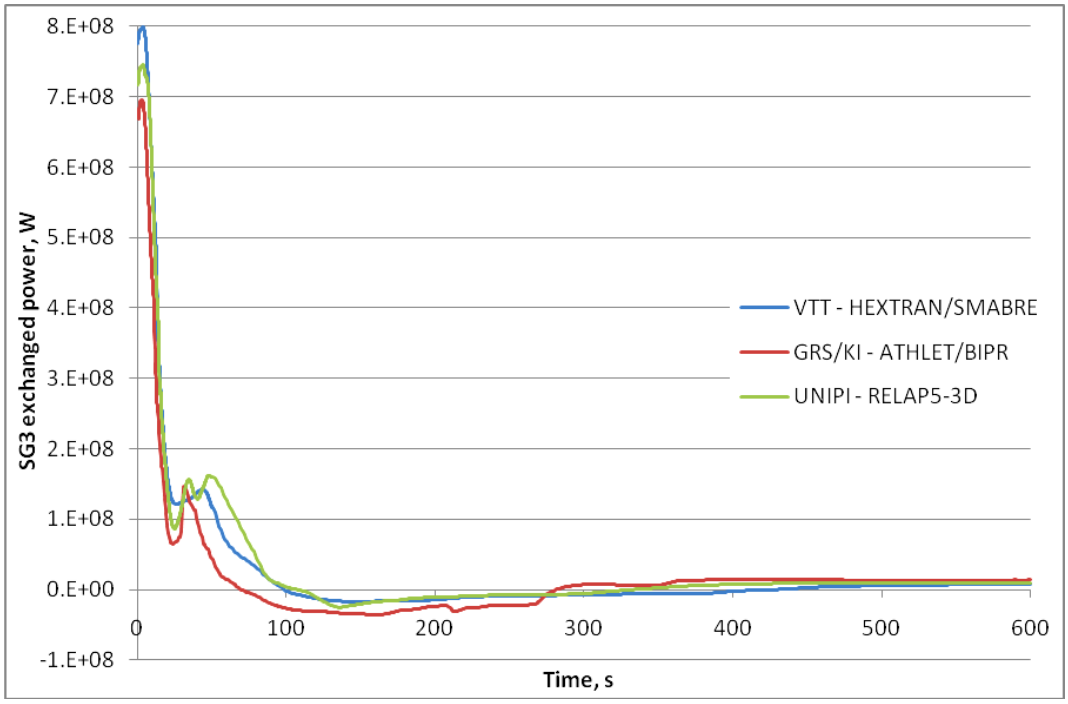


**Figure E.42: SG3 exchanged power**

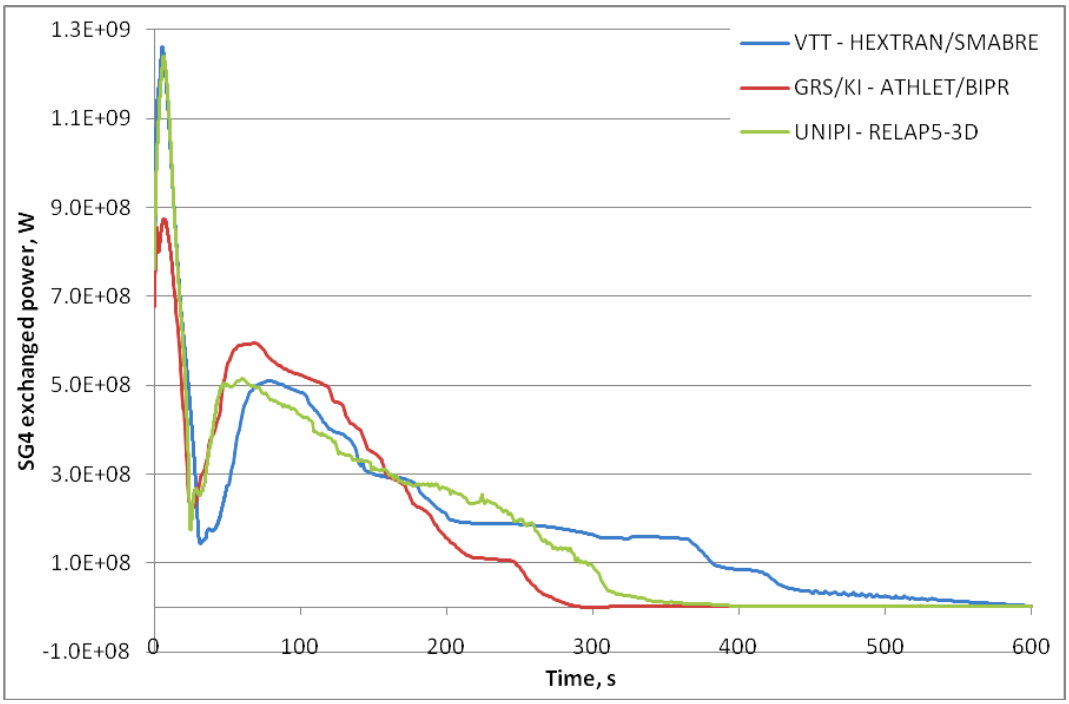


**Figure E.43: SG 4 exchanged power**

# Appendix F: Description of computer codes used for analysis of the VVER-1000 MSLB benchmark

## CFD CODES

### CFX 10 (FZD)

ANSYS CFX software (CFX10 Manuals, 2006) delivers powerful computational fluid dynamics (CFD) technology for simulations of all levels of complexity.

As one of the many computer-aided engineering (CAE) tools available within the ANSYS Workbench platform, ANSYS CFX takes advantage of data and information common to many simulations. This begins with common geometry: Users can link to existing native computer-aided design (CAD) packages as well as create and/or modify CAD models in an intuitive solid modeling environment. Complementing the common geometry model is a suite of meshing tools, designed to ensure easy generation of the most appropriate mesh for the given application. ANSYS CFX tools then guide the user through the setup of operating conditions, selection of materials and definition of models.

The ANSYS CFX solver uses the most modern solution technology with a coupled algebraic multi-grid solver and extremely efficient parallelization to help ensure that solutions are ready for analysis quickly and reliably. Solution analysis with the ANSYS CFX post-processor then gives users the power to extract any desired quantitative data from the solution; it also provides a comprehensive set of flow visualization options. Animations of flow simulations can be easily generated and 3D images are directly created and shared with any colleagues or clients using the freely distributable 3D viewer from ANSYS CFX.

The next-generation physics pre-processor, ANSYS CFX-Pre, allows multiple meshes to be imported, allowing each section of complex geometries to use the most appropriate mesh. ANSYS CFX includes the following features:

- An advanced coupled solver which is both reliable and robust
- Full integration of problem definition, analysis and results presentation
- An intuitive and interactive setup process, using menus and advanced graphics

ANSYS CFX is capable of modeling:

- Steady-state and transient flows
- Laminar and turbulent flows
- Subsonic, transonic and supersonic flows
- Heat transfer and thermal radiation
- Buoyancy
- Non-Newtonian flows
- Transport of non-reacting scalar components
- Multiphase flows
- Combustion
- Flows in multiple frames of reference
- Particle tracking

*ANSYS Interaction*

The coupling of CFX and ANSYS software continues to improve in both user workflow and simulation capabilities. This release introduces a full two-way Fluid Structure Interaction capability coupling the ANSYS and CFX solvers, and the ability to run ANSYS CFX within the Workbench engineering simulation environment is extended to a number of Unix platforms.

*Transient Analysis*

Analysis of fully transient situations continues to be a growing trend in CFD simulation, and ANSYS CFX introduces both new transient physical models (such as Transient Particle Tracking and Kinetic Theory for Fluidized Beds), as well as algorithmic and transient efficiency improvements (Adaptive Time-stepping and Extrapolated Initial Solutions).

Some of the new features of ANSYS CFX 10 are described below:

*ANSYS FSI Coupling*

ANSYS CFX now has full two-way transient coupling with the ANSYS multi-physics solver to allow the simulation of Fluid-Structure Interaction. The ANSYS and ANSYS CFX solvers run simultaneously with Force, Displacement and/or Thermal data shared implicitly at each time-step. The communication between the solvers uses a native ANSYS CFX IPC library, and the solvers can be run on the same or different computers, in serial or parallel.

*Porosity*

To complement the various momentum porous loss models available in CFX-5.7 and earlier, ANSYS CFX has added a true volume porosity model. This porous domain model uses a unique 'double-node' approach at the porous interface, to ensure sharp capture of the pressure and velocity discontinuities that occur at that location. The interface treatment conserves total pressure and supports significantly greater pressure losses than the previous sub-domain based models in previous versions of ANSYS CFX.

*Turbulence Modeling*

A significant capability in ANSYS CFX is the first-ever commercial release of a predictive laminar to turbulent transition capability, the Menter-Langtry model. The transition model in ANSYS CFX has been highly validated and can be used to determine the location and extent of transition in both aerospace and turbo machinery applications. The model requires no special provisions for geometry or grid topology. For expert users, ANSYS CFX also provides user control of turbulent wall functions, including heat transfer.

*Transient Improvements*

Computing resources needed for a transient calculation can be optimized through the use of time step Adaption & Extrapolated Initial Guess for transient calculations in ANSYS CFX. Time step Adaption allows the solver to automatically adjust the physical time step in a transient solution based on user-specified criteria including target number of coefficient loops or Courant Number. The Extrapolated Initial Guess extends the solution from previous time steps as the initial guess for the current time step, providing a better

starting condition and minimizing the required number of coefficient loops to reach time step convergence. Key numerical transient improvements have also been made, which makes it possible to achieve 2nd order transient calculation with one iteration per time step, for time steps in the explicit range.

## DESCRIPTION OF SYSTEM CODES

### DYN3D/ATHLET (FZD)

DYN3D (Grundmann, 1999), (Grundmann and Holstein, 1999) is a three-dimensional core model for dynamic and depletion calculations in LWR cores with quadratic or hexagonal fuel assembly geometry. The neutron-kinetic model is based on the solution of the three-dimensional, two-group neutron diffusion equations by nodal expansion methods. Different methods are used for quadratic and hexagonal fuel assembly geometry. In the case of Cartesian geometry, the three-dimensional diffusion equation of each node is transformed into three one-dimensional equations for each direction (x, y, z) by transversal integrations. The equations are coupled by the transversal leakage term. In each energy group, the one-dimensional equations are solved with the help of flux expansions in polynomials up to second order and exponential functions are the solutions of the homogeneous equation. The fission source in the fast group and the scattering source in the thermal group as well as the leakage terms are approximated by the polynomials. In the case of hexagonal fuel assemblies, the diffusion equation in the node is transformed into a two-dimensional equation in the hexagonal plane and a one-dimensional equation in the axial direction. The two equations are coupled by the transverse leakage terms that are approximated by polynomials up to the second order. Considering the two-dimensional equation in the hexagonal plane, the side-averaged values (HEXNEM1) or the side-averaged + corner-point values (HEXNEM2) of flux and current are used for the approximate solution of the diffusion equation.

The thermal-hydraulic system code ATHLET (Teschendorf et al, 1996) was developed by the Gesellschaft für Anlagen- und Reaktorsicherheit (GRS) for the analysis of anticipated and abnormal plant transients, small and intermediate leaks as well as large breaks in light water reactors. It is intended to cover the whole spectrum of design basis and beyond design basis accidents (without core degradation) for PWRs and BWRs with only one code. The code features advanced thermal-hydraulics, modular code architecture, separation between physical models and numerical methods, pre- and post-processing tools and portability.

The code development is accompanied by a systematic and comprehensive validation program. A large number of integral experiments and separate effect tests, including the major International Standard Problems, have been calculated by GRS and by independent organizations. The range of applicability has been extended to the Russian reactor types VVER and RBMK in co-operation with foreign partner organizations.

ATHLET is being applied by numerous institutions in Germany and abroad; its development and validation are sponsored by the German Federal Ministry of Economics and Labour (BMWA).

**BIPR8/ATHLET (GRS/KI)**

The computer code for 3D neutron kinetics BIPR8-KN (Lisorkin et al, 2006) has been developed in the Department of Physics in the RRC KI. A two-group, 3D hexagonal coarse-mesh nodal approximation for neutron flux is applied. The static branch of this code permits to simulate VVER core burn-up and refueling, including the calculation of the multiplication factor and reactivity coefficients for different core states. BIPR-8KN uses its native nuclear data libraries, prepared by a Russian code. The cross-section libraries include the burn-up dependence and instantaneous dependencies of TH parameters, as well as Xe and Sm poisoning corrections. Simplified cross-section corrections are used instead of ADF. The kinetic branch of BIPR-8KN calculates the transient core power and 3D neutron flux distribution, taking into account two prompt neutron energy groups and six delayed neutron groups and feedback effects.

The thermal-hydraulic system code ATHLET (Teschendorf et al, 1996) is being developed by GRS for the analysis of the whole spectrum of leaks and transients in PWR and BWR. The code is applicable to western LWR designs as well as for Russian VVER and RBMK reactors. The main code features are the advanced thermal hydraulics, the modular code architecture, especially the separation between physical models and numerical methods, the pre- and post-processing tools, and the portability to the prevalent computer platforms.

The code is based on a five-equation model (mixture momentum equation with drift) as well as on a six-equation two-fluid model, additionally enabling the simulation of several non-condensable gases, dissolved nitrogen and boron transport. The piping network of the reactor coolant system is modeled by connecting basic fluid dynamic elements, called thermo-fluid objects, allowing for cross flow between parallel channels.

**HEXTRAN/SMABRE (VTT)**

The 3D core N/TH solution method of the HEXTRAN code (Kyrki-Rajamaki, R., 1991), is based on coupling and extension of the 3D steady-state hexagonal core simulator HEXBU-3D (Kaloinen, 1981) and a 1D thermal-hydraulics code.

HEXTRAN solves the two-group neutron diffusion equations by a nodal expansion method in x-y-z geometry. A basic feature of the method is decoupling of the two-group equations into separate equations for two spatial modes and reconstruction of group fluxes from characteristic solutions to these equations. The two solutions are called the fundamental or asymptotic mode (with a smooth behavior within a homogenized node), and the transient mode, which deviates significantly from zero only near material discontinuities. The nodal equations are solved with a two-level iteration scheme where only one unknown per node - the average of fundamental mode, is determined in inner iterations. The nodal flux shapes are improved in outer iterations by recalculation of the coupling coefficients.

The thermal-hydraulic calculation of the reactor core is performed in parallel one-dimensional hydraulic channels, each channel usually coupled with one fuel assembly. The channels can be further divided into axial sub-regions. Parallel to the heated channels, several unheated bypass channels can be modeled. Channel hydraulics is based on conservation equations for steam and water mass, total enthalpy and total momentum, and on a selection of optional correlations describing, for example, slip, non-equilibrium evaporation and condensation and one- and two-phase friction. The phase velocities are related by an algebraic slip ratio or by the drift flux formalism. The thermal-hydraulic solution methods are the same as in the one-dimensional code TRAB. During the

hydraulic iterations, a one-dimensional heat transfer calculation is made for an average fuel rod of each assembly. The radial heat conduction of the fuel rod is solved according to Fourier's law. The fission power is divided into prompt and delayed power parts and a fraction of the power can be dissipated directly in the coolant. Decay heat is included in the thermal power.

Advanced time integration methods are applied in the dynamic calculation. The numerical technique can vary between the standard fully implicit theta method and the central-difference theta method both in the heat conduction calculation for fuel rods and in the solution of thermal-hydraulic conservation equations for cooling channels.

For the analysis of core-system transients, HEXTRAN is coupled with the SMABRE system code.

SMABRE (Miettinen, 1985) is a 1D system thermal-hydraulics code, developed by VTT. The code is able to model 3D thermal hydraulic effects using parallel channels (multi-1D mode) combined with the turbulent mixing mode. SMABRE contains a five-equation two-phase thermal hydraulic model, using the drift flux model. The numerical solution method used in SMABRE is a predictor-corrector type non-iterative solution.

**RELAP3D (UNIPI)**

NESTLE, the multi-dimensional neutron kinetics model in RELAP5-3D (INL, 2001) allows the user to model reactor transients where the spatial distribution of the neutron flux changes with time. The neutron kinetics model uses the Nodal Expansion Method (NEM) to solve the few-group neutron diffusion equations. The number of energy groups can be two or four. Up scattering is explicitly taken into account, if desired.

Core geometries modeled include Cartesian and hexagonal. Three-, two- and one-dimensional models can be utilized. Various core symmetry options are available, including quarter, half and full core for Cartesian geometry and one-sixth, one-third and full core for hexagonal geometry. The boundary conditions can be zero flux, non-re-entrant current, reflective and cyclic. The NEM method uses quartic or quadratic polynomial expansions for the transverse integrated fluxes in Cartesian or hexagonal geometries, respectively. Transverse leakage terms are represented by a quadratic polynomial or constant for Cartesian or hexagonal geometry, respectively. Assembly discontinuity factors (ADF) are utilized to correct for homogenization errors. The number of delayed neutron precursor groups is user-specified. The neutron kinetics subroutines require input regarding the neutron cross-sections in the computational nodes of the kinetics mesh. A neutron cross-section model is implemented which allows the instantaneous dependencies of the neutron cross-sections to be parameterized as functions of heat structure temperatures, fluid void fraction or fluid density, poison concentration and fluid temperatures.

A flexible coupling scheme between the neutron kinetics mesh and the thermal-hydraulics mesh is used to minimize the input data needed to specify the neutron cross-sections in terms of thermal-hydraulic variables. A control rod model has been implemented so that the effect of the initial position and subsequent movement of the control rods during transients may be taken into account in the computation of the neutron cross-sections.

RELAP5-3D (INL, 2001) has a 3D reactor vessel component, which allows coarse-3D simulation of the vessel thermal hydraulics, coupled to the 3D neutron kinetics.

**PARCS/TRACE (FZK)**

PARCS: The Purdue Advanced Reactor Core Simulator (Downar et al, 2004) is a 3D neutronic code, which solves the steady state and transient multi-group diffusion and $SP_3$ transport equations in orthogonal and non-orthogonal geometries. The highlights of PARCS features can be summarized as follows (Downar, 2004):

- PARCS has the ability to perform eigenvalue calculations, transient (kinetic) calculations, xenon transient calculations, decay heat calculations, pin power calculations and adjoint calculations for LWR
- The Triangular Polynomial Expansion (TPEN) method is employed to solve for the neutron fluxes in the homogenized hexagonal nodes
- A transient fixed source problem is solved at each time point of the transient
- PARCS is coupled directly (internal coupling) to the thermal-hydraulic system code TRACE (Odar, 2003) which provides the temperature and flow field information to PARCS during the transient via the few-group cross sections.

TRACE: The TRAC/RELAP Advanced Computational Engine (Odar et al, 2003) is a modernized NRC thermal-hydraulic code designed to consolidate and extend the capabilities of NRC's 3 legacy safety codes - TRAC-P, TRAC-B and RELAP. It is able to analyze large/small break LOCAs and system transients in both pressurized and boiling reactors. The code was developed by the Los Alamos National Laboratory (LANL), the Information Systems Laboratory (ISL), and the Penn State University (PSU) for use in best-estimate analysis of light water reactors and Generation IV systems. To meet these challenges TRACE uses many new features like multi-dimensional flow modeling and 2D heat conduction. TRACE is able to use different coolant types like H2O, D2O, He, Na and PbBi as well. The partial differential equations that describe two-phase flow and heat transfer are solved with finite-difference numerical methods. This is the NRC flagship thermal-hydraulic analysis tool.

**CATHARE (INRNE)**

CATHARE2 (CEA, 2007) is a system thermal-hydraulic code developed by CEA, EDF, IRSN and AREVA for reactor safety analysis. It is applicable for different types of reactors – PWR, VVER, BWR and gas-cooled reactors, and covers the domain of large/small break LOCAs and transients. The code is modular (component modules) and is based on a six-equation two-fluid model. The current version V2.5_2 includes a 3D coarse-mesh module. CATHARE provides a set of physical closure laws validated against a large experimental database.

The code has been tested for VVER in a series of computational benchmarks and standard problems. The qualification matrix includes experiments relative to VVER such as horizontal SG, vessel mixing tests, CCFL and re-flooding. All the existing integral test facilities with horizontal steam generators (PACTEL, PMK and PSB) have been used for the assessment.

**CRONOS/FLICA4 (INRNE/CEA)**

CRONOS2 (Lautard et al.,1990), (Lautard et al, 1999), (Magnaud, 1999) is a 3D neutronics code designed to provide all the computational means needed for diffusion and transport core calculations, including design, fuel management, operation and accidents. It allows steady-state, burn-up and kinetic multi-group calculations of power distribution

taking into account the thermal-hydraulic feedback effects (performed either by FLICA4 or by a simplified multi-1D model). It has also generalized perturbation theory capabilities. Either eigenvalue or source calculations can be performed.

CRONOS is coupled with FLICA4 for 3D core dynamics simulation. The mode of coupling is external.

FLICA4 (Toumi et al, 2000), (Aniel et al, 2005) is a 3D thermal-hydraulic code used for several reactor types (PWR, VVER, BWR, experimental reactors, gas-cooled reactors). The two-phase compressible flow is modeled by a set of four equations: mass, momentum, and energy conservation for the two-phase mixture, and mass conservation for the vapour. The velocity disequilibrium is taken into account by a drift flux correlation. A 1D thermal module is used to solve the conduction in solids (fuel).

FLICA4 includes an object-oriented pre-processor to define the geometry and the boundary conditions. Radial unstructured meshes are available, without any limitation on the number of cells. Zooming on a specific radial zone can be performed by a second calculation using a finer mesh (for instance a sub-channel calculation of the hot assembly). The fully implicit numerical scheme uses the finite volume approximation and a Roe solver. This kind of method is particularly accurate, with a low numerical diffusion.

For neutronics, coupling with 3D core simulators such as CRONOS2 or internal point kinetics can be used.

**COBAYA/COBRA3 (INRNE/UPM)**

COBAYA3 (UPM, 2009; Lozano et al, 2009) is a multi-scale, multi-group 3D neutronics code for LWR based on the diffusion approximation. The code has a nodal and a pin scale solver, which can be used separately or together, and both can handle kinetics and thermal-hydraulic feedbacks for the cross sections libraries.

The nodal solver is called ANDES (Analytical Nodal Diffusion Equation Solver). It solves the neutron multi-group diffusion equations in 3D geometry and allows calculation of a variety of cases. The capability to treat nodes with rectangular and triangular-Z geometry permits the simulation of cores based not only on rectangular fuel assemblies (PWR, BWR), but also on hexagonal assemblies (VVER, SFR, VHTR).

In both geometries, the code allows transient calculations by coupling the neutronics code with the COBRA-III and COBRA-TF thermal-hydraulic codes, or using a simplified model (SIMULA-TH).

The N/TH coupling allows the application of ANDES/COBAYA3 code to a great variety of steady state and transient problems:

- Steady state eigenvalue calculation at any power level.
- Steady state calculation with critical boron search at any power level.
- Transient calculations (fixed source problem) from an initial steady state

The COBAYA3 lattice solver allows steady state and transient pin-by-pin calculations in multi-group diffusion approximation, for orthogonal and hexagonal cell geometries. The orthogonal geometry solver is coupled with the COBRA sub-channel code.

COBRA-III-C/MIT-2 (Jackson, 1981) is a public code for thermal-hydraulics sub-channel calculations, with implicit cross-flows and homogeneous two-phase flow fluids. The code is used worldwide for DNBR analysis in PWR sub-channels, and also for 3D whole core simulation with one or more channels per fuel assembly. COBRA uses direct

inversion at each plane of the axial flow equations, with cross flows updated over an outer iteration loop, for the homogeneous model single-phase coolant , and finite-element direct solution of the fuel rod radial temperatures.

The 3D core N/TH coupling is internal, through a semi-implicit scheme using a staggered alternate time mesh.

# APPENDIX G: Participants' provided computational details

**Organization: FZD (Forchung Zentrum Dresden)**

Code: DYN3D/ATHLET

## I. Vessel thermal-hydraulic model

1. *Type of model*

Multi-1D

2. *Vessel thermal-hydraulic nodalization. How are the channels/T-H cells chosen?*

3. *Vessel mixing model?*

An empirical model called SATM (Self Adapting Turbulent Mixing) was developed and implemented into the interface between ATHLET and DYN3D, which distributes the enthalpy flow from the single loops between the different fuel assemblies and simulates the coolant mixing inside the reactor pressure vessel.

This empirical model is based on the following assumptions:

- Inside the pressure vessel, there is an azimuthal equalization of the flow rates from the single loops.
- The flow shifts from the loop position to the sector position.
- The described sector formation is present in the vessel until the core inlet plane.

At each time step in the coupled code calculation, the position of the sectors and the fuel assemblies belonging to each of the sectors are recalculated. In this way, the dynamics of the sector widening and reduction during pump start up and coast –down as well as the azimuthal moving of the different sectors in the core plane during the operation of different numbers of MCPs is inherently considered by the model.

Further, in the model a coolant exchange rate between neighboring sectors is implemented simulating the turbulent mixing in the vessel. Coefficients for the exchange rate can be input. The exchange is realized on enthalpy flow basis.

4. *How are the inlet ring and down-comer modeled?*

4 parallel channels

5. *How is the lower plenum modeled?*

4 thermal hydraulic volumes + above mentioned SATM model

6. *How are the upper plenum and upper head modeled?*

4 thermal hydraulic volumes; no mixing between them

## II. Core thermal-hydraulic model

7. *Core thermal hydraulic model (multi-1D, 3D) and nodalization: How are the channels/TH cells chosen?*

Multi-1D; 163 independent thermal hydraulic channels

8. *Number of heat structures (fuel rods) modeled?*

1 average fuel rod per fuel assembly (hydraulic channel), i.e. 163 fuel rods

9. *Radial fuel rod nodalization?* 5 nodes (equal area)

10. *Relation used for Doppler temperature?* According to the specification

**III. Core neutronics model**

11. *Number of radial nodes per assembly?* one

12. *Axial nodalization?* 30 nodes in the heated part

13. *Radial and axial reflector modeling?*

One node for lower and for upper axial reflector; one row of reflector assemblies around the core (altogether 48)

14. *Spatial decay heat distribution modeling?*

Distribution is based on infinite operation at the given power level

15. *Cross-sections and interpolation procedure used?*

Provided cross-section data and interpolation routine

**IV. Coupling schemes**

16. *Hydraulics/heat structure spatial mesh overlays (mapping schemes in radial and axial plane)?*

Both meshes are identical

17. *Hydraulics/neutronics spatial mesh overlays (mapping schemes in radial and axial plane)?*

Both meshes are identical

18. *Heat structure/neutronics spatial mesh overlays (mapping schemes in radial and axial plane)?*

Both meshes are identical

19. *Coupling numerics –explicit, semi-implicit or implicit?*

Implicit

20. *Coupling method – external or internal?*

External

21. *Coupling design – serial integration or parallel processing?*

Serial integration

22. *Temporal coupling scheme?*

Implicit

**V. General**

23. *Deviations from the specifications?* no

24. *User assumptions?* no

25. *Specific features of the used codes?*

Dynamic model for determination of gas gap heat transfer coefficients

26. *Are you using the core outlet pressure boundary conditions?* yes

27. *Have you used plant specific initial loop flows?* yes

28. *Neutron kinetics model?*

HEXNEM2 option of DYN3D; 2D solution with 12 unknowns in radial plane (sides and corner points); 1D solution in axial plane; coupling via transverse leakage

**Organization: VTT (Technical Research Centre of Finland)**

Code: HEXTRAN/SMABRE

**I. Vessel thermal-hydraulic model**

1. *Type of model*

Multi-1D

2. *Vessel thermal-hydraulic nodalization. How are the channels/T-H cells chosen?*

6 sectors in the vessel all the way from the inlet to the outlet

3. *Vessel mixing model?*

Multi-1D model with approximate turbulence modeling

4. *How are the inlet ring and down-comer modeled?*

6 azimuthal meshes and one axial mesh in the inlet ring

5. *How is the lower plenum modeled?*

6 azimuthal and 2 axial meshes

6. *How are the upper plenum and upper head modeled?*

6 azimuthal and 3 axial meshes in the upper plenum

**II. Core thermal-hydraulic model**

7. *Core thermal hydraulic model (multi-1D, 3D) and nodalization: How are the channels/TH cells chosen?*

Multi-1D, 163 channels.

8. *Number of heat structures (fuel rods) modeled?* 163.

9. *Radial fuel rod nodalization?* 6 radial meshes.

10. *Relation used for Doppler temperature?* As provided in the specification.

**III. Core neutronics model**

11. *Number of radial nodes per assembly?* One.

*Axial nodalization?* 30 nodes in the heated part

12. *Radial and axial reflector modeling?*

One node for each axial reflector and one row of reflector assemblies around the core.

13. *Spatial decay heat distribution modeling?*

Proportional to the initial 3D power distribution.

14. *Cross-sections and interpolation procedure used*?

As provided in the specification.

## IV. Coupling schemes

15. *Hydraulics/heat structure spatial mesh overlays (mapping schemes in radial and axial plane)?*

Both meshes are identical.

16. *Hydraulics/neutronics spatial mesh overlays (mapping schemes in radial and axial plane)?*

Both meshes are identical.

17. *Heat structure/neutronics spatial mesh overlays (mapping schemes in radial and axial plane)?*

Both meshes are identical.

18. *Coupling numerics –explicit, semi-implicit or implicit?*

Explicit.

19. *Coupling method – external or internal?*

Internal.

20. *Coupling design – serial integration or parallel processing?*

Serial integration.

21. *Temporal coupling scheme?*

## V. General

22. *Deviations from the specifications?* No
23. *User assumptions?* No
24. *Specific features of the used codes?*
25. *Are you using the core outlet pressure boundary conditions?* Yes
26. *Have you used plant specific initial loop flows?* Yes
27. *Neutron kinetics model?* Two-group nodal flux solver using modal representation (asymptotic and transient modes) and high-order polynomial nodal expansion method

**Organization: FZK (Forchung Zentrum Karlsruhe)**

Code: PARCS V7/TRACE V230

**I. Vessel thermal-hydraulic model**

1. *Type of model:* Coarse 3D
2. *Vessel thermal-hydraulic nodalization. How are the channels/TH cells chosen?* Six sectors and 5 radial meshes in the radial plane.
3. *Vessel mixing model?* Coarse 3D without turbulence.
4. *How are the inlet ring and down-comer modeled?* 3D modeling.
5. *How is the lower plenum modeled?* 3D modeling.
6. *How are the upper plenum and upper head modeled?* 3D modeling.

**II. Core thermal-hydraulic model**

7. *Core thermal hydraulic model (multi-1D, 3D) and nodalization: How are the channels/TH cells chosen?*

Coarse 3D with 6 sectors and 3 radial meshes in the radial plane (18 cells).

8. *Number of heat structures (fuel rods) modeled?* 18
9. *Radial fuel rod nodalization?* 6 radial meshes
10. *Relation used for Doppler temperature?* As provided in the specification.

**III. Core neutronics model**

11. *Number of radial nodes per assembly?* One
12. *Axial nodalization?* 30 nodes
13. *Radial and axial reflector modeling?*

One node for each axial reflector and one row of reflector assemblies around the core

14. *Spatial decay heat distribution modeling?*
15. *Cross-sections and interpolation procedure used?* As provided in the specification

**IV. Coupling schemes**

16. *Hydraulics/heat structure spatial mesh overlays (mapping schemes in radial and axial plane)?*

Both meshes are identical.

17. *Hydraulics/neutronics spatial mesh overlays (mapping schemes in radial and axial plane)?*

18 hydraulic cells and 163 neutronics cells in the radial plane.

Identical axial meshes in the heated core.

18. *Heat structure/neutronics spatial mesh overlays (mapping schemes in radial and axial plane)?*

18 heat structures and 163 neutronics cells in the radial plane.

Identical axial meshes in the heated core.

19. *Coupling numerics –explicit, semi-implicit or implicit?* Semi-implicit.
20. *Coupling method – external or internal?* Internal.
21. *Coupling design – serial integration or parallel processing?* Serial integration.
22. *Temporal coupling scheme?* Semi-implicit.

**V. General**

23. *Deviations from the specifications?* No
24. *User assumptions?* No
25. *Specific features of the used codes?*
26. *Are you using the core outlet pressure boundary condition?* Yes
27. *Have you used plant specific initial loop flows?* Yes
28. *Neutron kinetics model?* Using the TPEN method

**Organization: University of Pisa (UNIPI)**

Code: NESTLE (NEM) / RELAP5-3D mod3.2.6

**I. Vessel thermal-hydraulic model**

1. *Type of model* – Coarse 3D
2. *Vessel thermal-hydraulic nodalization. How are the channels/T-H cells chosen?*

60 sectors x 9 radial nodes in the upper part of the lower plenum,

1D upper plenum model (one channel),

6 axial nodes outside the core, in the upward flow part,

30 axial nodes in the heated core

3. *Vessel mixing model?* Coarse 3D without turbulence.
4. *How are the inlet ring and down-comer modeled?*

Coarse-3D with 20 azimuth meshes, one radial mesh and 20 axial meshes

5. *How is the lower plenum modeled?*

Coarse 3D with 4 axial layers:

Number of azimuth nodes: 20, 20, 20, 60.

Number of radial nodes: 4, 4. 8, 9

Number of axial nodes: 1,1,1,1

6. *How are the upper plenum and upper head modeled?*

1D upper plenum model

**II. Core thermal-hydraulic model**

7. *Core thermal hydraulic model (multi-1D, 3D) and nodalization: How are the channels/TH cells chosen?* 163
8. *Number of heat structures (fuel rods) modeled?* 163
9. *Radial fuel rod nodalization?* 6 radial meshes

10. *Relation used for Doppler temperature?* As defined in the specification

**III. Core neutronics model**

11. *Number of radial nodes per assembly?* One
12. *Axial nodalization?* 30 nodes in the active core
13. *Radial and axial reflector modeling?*

One node for each of the top and bottom reflectors and one additional row of reflector assemblies for the radial reflector.

14. *Spatial decay heat distribution modeling?* Proportional to the 3D power distribution.
15. *Cross-sections and interpolation procedure used?*

As provided in the specification.

**IV. Coupling schemes**

16. *Hydraulics/heat structure spatial mesh overlays (mapping schemes in radial and axial plane)?*

163 TH channels.

17. *Hydraulics/neutronics spatial mesh overlays (mapping schemes in radial and axial plane)?*

Both meshes are identical.

18. *Heat structure/neutronics spatial mesh overlays (mapping schemes in radial and axial plane)?* N/A
19. *Coupling numerics –explicit, semi-implicit or implicit?* Semi-implicit.
20. *Coupling method – external or internal?* Internal.
21. *Coupling design – serial integration or parallel processing?* Serial integration.
22. *Temporal coupling scheme?*

**V. General**

23. *Deviations from the specifications?* No
24. *User assumptions?* No
25. *Specific features of the used codes?*
26. *Are you using the core outlet pressure boundary conditions?* Yes
27. *Have you used plant specific initial loop flows?* Yes
28. *Neutron kinetics model?* Nodal Expansion Method (NEM)

**Organization: INRNE (Institute for Nuclear Research and Nuclear Energy), Sofia**

Code: CATHARE 2.5/Point kinetics

**I. Vessel thermal-hydraulic model**

1. *Type of model*

Multi-1D

2. *Vessel thermal-hydraulic nodalization. How are the channels/T-H cells chosen?*

The vessel model is multi-1D with cross-flow, 24 sectors from the vessel inlet to the core outlet and 12 sectors in the upper plenum.

3. *Vessel mixing model?*

The model is multi-1D with cross flow governed by local pressure drops. The cross-flow was modeled with horizontal junctions and vertical (diagonal) junctions connecting donor cells at a given elevation to receptor cells in the neighboring sectors, at a higher elevation. Vertical junctions were used to a limited extent, with small flow area and in the lower and upper plenums only.

4. *How are the inlet ring and the down-comer modeled?*

Multi-1D modeling without turbulence.

24 volume elements in the inlet ring corresponding to 24 azimuth sectors,
24 volume elements in the upper part of the down-comer,
24 axial elements in the lower down-comer.

5. *How is the lower plenum modeled?*

2 axial layers of 24 volumes each

6. *How are the upper plenum and upper head modeled?*

3 axial layers x 12 volumes each in the upper plenum,

12 volumes in the outlet ring

## II. Core thermal-hydraulic model

7. *Core thermal hydraulic model (multi-1D, 3D) and nodalization: How are the channels/TH cells chosen?*

24 channels and 24 bypass channels

8. *Number of heat structures (fuel rods) modeled?* 24

9. *Radial fuel rod nodalization?* 6 radial meshes

10. *Relation used for Doppler temperature?* As defined in the specification

## III. Core neutronics model

Point kinetics with equivalent parameters

11. *Spatial decay heat distribution?* Uniform

## IV. Temporal integration scheme

12. *Temporal integration –explicit, semi-implicit or implicit?* Implicit

## V. General

13. *Deviations from the specifications?* Point kinetics

14. *User assumptions?* No

15. *Specific features of the used codes?* 11-group decay heat model

16. *Are you using the core outlet pressure boundary conditions?* Yes

17. *Have you used plant specific initial loop flows?* Yes

18. *Neutron kinetics model?* Point kinetics model

**Organization: INRNE/CEA**

Code: CRONOS2/FLICA4

**I. Core thermal-hydraulics model**

*1. Core thermal hydraulic model (multi-1D, 3D) and nodalization: How are the channels/TH cells chosen?*

3D FLICA4 model with one point per hexagon in the radial plane,

30 axial nodes in the heated core.

*2. Number of heat structures (fuel rods) modeled?* 163 x 30

*3. Radial fuel rod nodalization?* 6 radial meshes

*4. Relation used for Doppler temperature?* As defined in the specification.

**II. Core neutronics model**

*5. Number of radial nodes per assembly?* One

*6. Axial nodalization?* 30 nodes in the active core.

*7. Radial and axial reflector modeling?*

One node for each of the top and bottom reflectors and one additional row of reflector assemblies for the radial reflector.

*8. Spatial decay heat distribution modeling?* Proportional to the initial 3D power distribution.

*9. Cross-sections and interpolation procedure used?* As provided in the specification.

**III. Coupling schemes**

*10. Hydraulics/heat structure spatial mesh overlays (mapping schemes in radial and axial plane)?*

Both meshes are identical.

*11. Hydraulics/neutronics spatial mesh overlays (mapping schemes in radial and axial plane)?*

Both meshes are identical.

*12. Heat structure/neutronics spatial mesh overlays (mapping schemes in radial and axial plane)?*

Both meshes are identical.

*13. Coupling numerics –explicit, semi-implicit or implicit?*

*14. Coupling method – external or internal?* External.

*15. Coupling design – serial integration or parallel processing?* Serial integration.

*16. Temporal coupling scheme?* Explicit.

**IV. General**

*17. Deviations from the specifications?* No

*18. User assumptions?* No

*19. Specific features of the used codes?*

*20. Are you using the core outlet pressure boundary conditions?* Yes

21. *Have you used plant specific initial loop flows?* Yes
22. *Neutron kinetics model? Coarse 3D,* CRONOS2 2nd-order super-convergent FEM with 6 triangles per hexagon.

**Organization: INRNE/UPM**

Code: COBAYA3/COBRA3

**I. Core thermal-hydraulics model**

*1. Core thermal hydraulic model (multi-1D, 3D) and nodalization: How are the channels/TH cells chosen?*

Multi-1D COBRA3c model with one point per hexagon in the radial plane.

30 axial nodes in the heated core.

*2. Number of heat structures (fuel rods) modeled?* 163 x 30

*3. Radial fuel rod nodalization?* 6 radial meshes

*4. Relation used for Doppler temperature?* As defined in the specification.

**II. Core neutronics model**

*5. Number of radial nodes per assembly?* 6 nodes (triangular-Z prisms).

*6. Axial nodalization?* 30 nodes in the active core.

*7. Radial and axial reflector modeling?*

One axial node for each of the top and bottom reflectors and one additional row of reflector assemblies for the radial reflector.

*8. Spatial decay heat distribution modeling?* Proportional to the initial 3D power distribution.

*9. Cross-sections and interpolation procedure used?* As provided in the specification.

**III. Coupling schemes**

*10. Hydraulics/heat structure spatial mesh overlays (mapping schemes in radial and axial plane)?*

Both meshes are identical.

*11. Hydraulics/neutronics spatial mesh overlays (mapping schemes in radial and axial plane)?*

One hydraulic node/6 neutronic nodes per hexagon in the radial plane.

Identical axial meshes.

*12. Heat structure/neutronics spatial mesh overlays (mapping schemes in radial and axial plane)?*

One heat structure/6 neutronic nodes per hexagon in the radial plane.

*13. Coupling numerics –explicit, semi-implicit or implicit?* Semi-implicit.

*14. Coupling method – external or internal?* Internal.

*15. Coupling design – serial integration or parallel processing?* Serial integration.

*16. Temporal coupling scheme?* Semi-implicit with staggered mesh.

## IV. General

*17. Deviations from the specifications?* No

*18. User assumptions?* No

*19. Specific features of the used codes?*

*20. Are you using the core outlet pressure boundary conditions?* Yes

*21. Have you used plant specific initial loop flows?* Yes

*22. Neutron kinetics model? Coarse 3D,* CRONOS2 2$^{nd}$-order super-convergent FEM with 6 triangles per hexagon.